THE UNIVERSITY OF TEXAS AT AUSTIN
CENTER FOR TRANSPORTATION RESEARCH

TECHNICAL REPORT 0-7088-1
TxDOT PROJECT NUMBER 0-7088

Develop Closure Joint Materials Specification and Evaluate Performance for Side-by-Side Accelerated Bridge Construction (ABC) Superstructure Systems

Justin Lam
Michelle Sabers
Niyam Shah
Thanos Drimalas
Kevin Folliard
Oguzhan Bayrak
H.C. Dennis Wang
Elias Saqan

June 2024

Published April 2025

https://library.ctr.utexas.edu/ctr-publications/0-7088-1.pdf

Technical Report Documentation Page

1. Report No. FHWA/TX-25/0-7088-1	2. Government Accession No.	3. Recipient's Catalog No.
4. Title and Subtitle Develop Closure Joint Materials Specification and Evaluate Performance for Side-by-Side Accelerated Bridge Construction (ABC) Superstructure Systems		5. Report Date Submitted: June 2024 6. Performing Organization Code
7. Author(s) Justin Lam, Michelle Sabers, Niyam Shah, Thanos Drimalas, Kevin Folliard, Oguzhan Bayrak, H.C. Dennis Wang, and Elias Saqan		8. Performing Organization Report No. 0-7088-1
9. Performing Organization Name and Address Center for Transportation Research The University of Texas at Austin 3925 W. Braker Lane, 4th Floor Austin, TX 78759		10. Work Unit No. (TRAIS) 11. Contract or Grant No. 0-7088
12. Sponsoring Agency Name and Address Texas Department of Transportation Research and Technology Implementation Division 125 E. 11th Street Austin, TX, 78701		13. Type of Report and Period Covered Technical Report May 2019 – May 2024 14. Sponsoring Agency Code
15. Supplementary Notes Project performed in cooperation with the Texas Department of Transportation.		

16. Abstract

The goal of this project was to develop, investigate, and implement optimized concrete mixtures to be used in closure pour connections between precast elements in side-by-side accelerated bridge construction (ABC) superstructure systems. This project involves the use of innovative materials and mixture proportions that are intended to provide high early strengths to facilitate accelerated bridge construction, while ensuring that good long-term durability is also achieved. Mixtures including rapid-setting, fiber-reinforced concrete (RSFRC) and ultra-high-performance concrete (UHPC) were developed by the Performing Agency and evaluated in the laboratory (materials and full-scale structural testing) and on outdoor exposures to fully characterize the critical fresh, hardened, structural, and durability properties that are need for closure pour connections. Based on the findings of the literature review and laboratory/exposure site tests, candidate UHPC mixtures were selected for full-scale structural testing. By developing a wide range of mixtures with varying rheological properties, strength gain characteristics, and toughness values, the Performing Agency developed a suite of mixtures from which TxDOT may select for any given closure pour connection, thereby increasing the potential reach and impact of this project's findings. Lastly, ABC projects in Amarillo and Bryan districts were evaluated and monitored during the course of the project.

17. Key Words	18. Distribution Statement
UHPC, Steel Fiber, Fiber-Reinforced Concrete, Closure Pour, Accelerated Bridge Construction	No restrictions. This document is available to the public through the National Technical Information Service, Springfield, Virginia 22161; www.ntis.gov.

19. Security Classif. (of report)	20. Security Classif. (of this page)	21. No. of pages	22. Price
Unclassified	Unclassified	196	

Form DOT F 1700.7 (8-72) Reproduction of completed page authorized

THE UNIVERSITY OF TEXAS AT AUSTIN
CENTER FOR TRANSPORTATION RESEARCH

Develop Closure Joint Materials Specification and Evaluate Performance for Side-by-Side Accelerated Bridge Construction (ABC) Superstructure Systems

Justin Lam
Michelle Sabers
Niyam Shah
Thanos Drimalas
Kevin Folliard
Oguzhan Bayrak
Elias Saqan
H.C. Dennis Wang

CTR Technical Report:	0-7088-1
Report Date:	Submitted: June 2024
Project:	0-7088
Project Title:	Develop Closure Joint Materials Specification and Evaluate Performance for Side-by-Side Accelerated Bridge Construction (ABC) Superstructure Systems
Sponsoring Agency:	Texas Department of Transportation
Performing Agency:	Center for Transportation Research at The University of Texas at Austin

Project performed in cooperation with the Texas Department of Transportation and the Federal Highway Administration.

Center for Transportation Research
The University of Texas at Austin
3925 W. Braker Lane, 4th floor
Austin, TX 78759

http://ctr.utexas.edu/

Disclaimers

Author's Disclaimer: The contents of this report reflect the views of the authors, who are responsible for the facts and the accuracy of the data presented herein. The contents do not necessarily reflect the official view or policies of the Federal Highway Administration or the Texas Department of Transportation (TxDOT). This report does not constitute a standard, specification, or regulation.

Patent Disclaimer: There was no invention or discovery conceived or first actually reduced to practice in the course of or under this contract, including any art, method, process, machine manufacture, design or composition of matter, or any new useful improvement thereof, or any variety of plant, which is or may be patentable under the patent laws of the United States of America or any foreign country.

Engineering Disclaimer

NOT INTENDED FOR CONSTRUCTION, BIDDING, OR PERMIT PURPOSES.

Acknowledgments

The authors extend sincere gratitude to the Texas Department of Transportation (TxDOT) for generously funding and supporting this research study. The invaluable contributions of the project manager, Martin Dassi, and the dedicated members of the Project Monitoring Team, significantly enhanced the overall success and impact of this project.

Table of Contents

List of Tables

List of Figures

Chapter 1. Introduction

1.1. Overview

The need for faster rates of infrastructure construction and repair continues to increase as population growth (especially in Texas) in large, urban areas continues, bringing with it more traffic congestion and driver delays. The help to address these concerns, accelerated bridge construction (ABC) has become increasingly popular in recent years. Although large structural components can be fabricated or cast off-site and lifted into place, there is still a critical need to connect these components on-site, and to do so in an expedition manner that is consistent with the goals of ABC technologies. This project focuses solely on the development of specialized concrete mixtures used in closure pours that are designed to gain strength rapidly, thus maintaining the strict construction schedule (and early opening to traffic) essential to bridges constructed or partially replaced using ABC techniques.

1.2. Scopes and Objectives

The goals of this project were to develop, investigate, and implement optimized concrete mixtures to be used in closure pour connections between precast elements in side-by-side accelerated bridge construction (ABC) superstructure systems. This project involved the use of innovative materials and mixture proportions that are intended to provide high early strengths to facilitate accelerated bridge construction, while ensuring that good long-term durability is also achieved. Mixtures including rapid-setting, fiber-reinforced concrete (RSFRC) and ultra-high-performance concrete (UHPC) were developed by the Performing Agency and evaluated in the laboratory (materials and full-scale structural testing) and on outdoor exposures to fully characterize the critical fresh, hardened, structural, and durability properties that are need for closure pour connections. Based on the findings of the literature review and laboratory/exposure site tests, candidate UHPC mixtures were selected for full-scale structural testing. By developing a wide range of mixtures with varying rheological properties, strength gain characteristics, and toughness values, the Performing Agency investigated a suite of mixtures from which TxDOT may select for any given closure pour connection, thereby increasing the potential reach and impact of this project's findings. Lastly, ABC projects in Amarillo and Bryan districts were evaluated and monitored during the course of the project.

1.3. Organization of Report

The research project was structured into distinct chapters, encompassing, literature review, experimental investigation, and analysis. Each chapter of this report systematically presents the outcomes and key findings derived from these respective tasks.

- Chapter 2 – Literature Review: General overview of previous research related to the background and history of UHPC, mixture proportions and properties of UHPC, UHPC as a closure pour between structural elements, and case studies of UHPC applications on UHPC
- Chapter 3 – Laboratory Evaluation of Proprietary and Non-Proprietary UHPC Mixes: A comprehensive laboratory evaluation on materials and mix proportions, mixing procedures, and the fresh, hardened, and durability properties of UHPC
- Chapter 4 – Large Scale Structural Testing: A comprehensive laboratory investigation on the usage and performance of propetiary and non-proprietary UHPC mixes as closure joint material for large scale bridge decks
- Chapter 5 – Field Trials: A comprehensive evaluation of instrumentation and monitoring activities conducted on the Navasota River and Farwell Creek ABC projects constructed by TxDOT
- Chapter 6 – Conclusions and Recommendations: The previous chapters' findings and conclusions are summarized along with recommendations

Chapter 2. Literature Review

In accordance with the scope of TxDOT Project 0-7088: Develop Closure Joint Materials Specification and Evaluate Performance for Side-by-Side Accelerated Bridge Construction (ABC) Superstructure Systems, the Research Team at the University of Texas at Austin has carried out a literature review to examine the state-of-the-art of UHPC mixtures, properties, and its application on ABC projects. The literature review summarized in this chapter has been grouped into the following four main sections: background and history of UHPC, mixture proportions and properties of UHPC, UHPC as a closure pour between structural elements, and case studies of UHPC applications on ABC.

2.1. Background & History of UHPC

Ultra-high-performance concrete (UHPC) is an emerging material with enhanced mechanical and durability properties as compared to conventional concrete. UHPC is sometimes referred to as Engineered Cementitious Composites (ECC), a term introduced in the early 1990s to emphasize the engineered nature of this unique material (Li, 1993). For simplicity and consistency, the term UHPC will be used in this report, with the understanding that it is an umbrella term that includes any other material with unusually high strength and ductility. The improved properties of UHPC include higher compressive and tensile strengths, higher toughness, increased durability, as well as disconnected pore structure and reduced porosity.

In the last two decades, UHPC solutions have been developed and implemented for transportation structures in the United States. In the last 10-20 years, proprietary and non-proprietary UHPC mixtures have been introduced. Applications of UHPC have been have mainly focused on thin overlays, bridge connections (closure pours) and impact resistance structures. The high compressive and post-peak tensile strengths of UHPC allow for reduced rebar development and lap splice lengths as compared to conventional concrete, which can result in shorter and simpler lap-splice connections for precast deck panels (Graybeal, 2014a). The use of UHPC to construct entire members (e.g., bridge girders) can significantly reduce the reinforcing steel and sectional dimensions, and thus self-weight, although the cost of casting full structural elements from UHPC is typically cost prohibitive.

2.2. UHPC Mixture Proportions & Properties

UHPC is a cementitious composite material made of cement, fine aggregates, supplementary cementitious materials, 2% fibers (usually short fibers), high-range water reducer, and water. UHPC mixtures are specifically designed to achieve

enhanced mechanical and durability properties. Currently, there are a number of proprietary UHPC mixtures in the construction market (Graybeal, 2014a). Non-proprietary mixtures have also been developed in a number of research studies (e.g., Wille and Boisvert-Cotulio 2013, Hernandez 2016). While the exact composition of these mixtures varies, they present a number of common characteristics. UHPC mixtures have a very low water-to-cementitious materials ratio (w/cm values between 0.16 and 0.20 have been reported) and a high content of silica fume of about 25% of the weight of cement. Most UHPC mixtures do not contain coarse aggregates although some may use much smaller coarse aggregate than typical concrete. Steel fibers in the amount of about 2% by volume are typically used to achieve post-peak toughness, although polymeric fibers have also been used, particularly PVA fibers. High-range water reducing admixtures (HRWR), specifically polycarboxylates, are essential components of UHPC, especially due its typically high cementitious materials content, reduced w/cm, small maximum aggregate size, and high fiber content. Although the standard composition of UHPC mixtures vary, Table 2.1 shows a typical proprietary UHPC mixture composition (Graybeal, 2014a).

Table 2.1 Typical Composition of UHPC

Material	lb/yd^3	Percentage by Weight
Portland Cement	1200	28.5
Fine Sand	1720	40.8
Silica Fume	390	9.3
Ground Quartz	355	8.4
HRWR	51.8	1.2
Accelerator	50.5	1.2
Steel Fibers	263	6.2
Water	184	4.4

Some proprietary UHPC mixtures require specialized mixers to adequately and efficiently mix and achieve target rheological properties, and even using such equipment, mixing times can be excessive, especially when compared to typical mixing times for central mixers used at precast plants. Hernandez (2016) demonstrated that locally available materials could be used to produce UHPC type mixtures, using conventional mixers and mixing time, and it was further shown that quartz sand could be eliminated from such mixtures, thus eliminating the associated health and safety issues related to this material. Because of the small size and amorphous nature of quartz sand, special respirators and clothing are required to safely use the material in the laboratory and in the field. Self-leveling UHPC can be produced, if material selection and mixture proportioning are optimized. The key is adequately mixing the UHPC to ensure adequate fiber dispersion and to

achieve the desired workability (e.g., initial slump, slump retention, stability, final finish, etc.) for a given application.

Proprietary UHPC mixes typically produces concrete compressive strengths that are significantly higher than conventional concrete. Graybeal (2006a) conducted uniaxial compression tests using on proprietary mixes under different curing conditions. Very high compressive strengths were obtained regardless of the curing treatment applied. The average compressive strength at 28 days of specimens cured under laboratory conditions (73 ℉ and ambient humidity) was 18.3 ksi. For steam curing conditions, the average strength increased to 28.0 ksi and full-compressive strengths were achieved within 4 days of casting. Hernandez (2016) reported UHPC made with locally available materials were able to achieve compressive strengths over 15.0 ksi, after two weeks of standard curing and without the need for steam curing.

The tensile strength of UHPC is higher than that of conventional concrete. Moreover, UHPC presents sustained tensile strength (or toughness) after first cracking thanks to the bridging action of steel fibers. The typical uniaxial tensile stress-strain behavior of UHPC is illustrated in Figure 2.1. As shown, multiple tightlyspaced cracks will initially appear once the cracking strength of UHPC is reached (Phase II). Widening of these cracks will induce strain hardening of the material due to the action of the steel fibers (Phase III). The tensile resistance will start to decay when an individual crack reaches an excessive width resulting in the pull out of the fibers from the matrix (Phase IV). As a result of this behavior, the tensile strength of UHPC is commonly characterized by a tensile cracking strengths and a peak post-cracking strengths. Graybeal (2006a) reported tensile cracking strengths of 0.9 ksi and 1.3 ksi depending on the curing conditions.

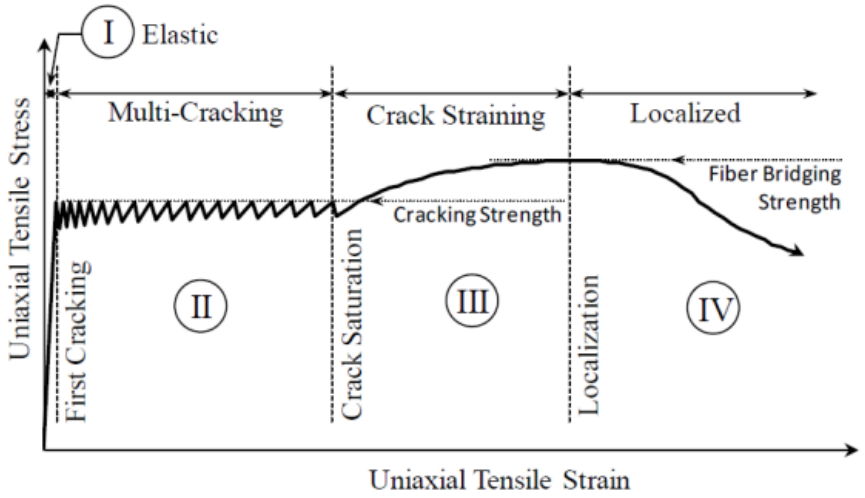

Figure 2.1 Uniaxial Tensile Stress-Strain Response of UHPC (Graybeal, 2013)

Currently, there is very limited data about the long-term tensile behavior (tensile creep and tensile fatigue) of UHPC (Yanni, 2009; Makira & Bruuhwiler, 2014; Bonetti, 2022). This is a key material property to assess the strength and deformation of structures in which reinforcement is eliminated and tensile stresses are resisted by UHPC solely, such as a girder web with no shear reinforcement. Yanni (2009) studied tensile creep for different fiber contents and thermal treatments, and found that tensile creep failure occurred at stress levels of 70% and 80% of the ultimate direct tensile strength. Based on these results, this study suggested a maximum design stress for bridge girders of 60% of the tensile strength. Makita and Bruuhwiler (2014) found that the fatigue limit of UHPC ranged between 45% and 70% of the cracking tensile strength depending on the initial condition (uncracked, cracked up to hardening phase, cracked up to the softening phase).

The tight, disconnected pore structure and reduced porosity of UHPC mitigates the intrusion and propagation of aggressive agents, such as chloride ions, into the matrix providing excellent durability properties. Moreover, the improved tensile properties of the material also contribute to restraining the formation and widening of large cracks. Tests conducted by Graybeal (2006a) showed that UHPC has negligible to very low chloride ion permeability, and it is very resistant to deterioration from freezing and thawing. Little data are available on long-term durability of UHPC. Significantly reduced chloride diffusion coefficients have been reported, owed to the reduced permeability and porosity of UHPC. There could be the potential for ASR in UHPC, if the correct materials and mixture proportions are not used. This is controllable but required knowledge of how local materials respond when used in UHPC. Most Texas river gravel and sand are reactive with regards to UHPC, and high cement contents increase internal alkali loading and increase the potential for ASR. The ASR mitigation will need to be achieved through the use of SCMs, typically silica fume. Hernandez (2016) showed the metakaolin was also effective in producing UHPC. If it is desired for a given UHPC mixture to be heat-cured to achieve high early release strengths, the potential for DEF would need to be evaluated. DEF can be controlled, even in steam-cured concrete, but once again, the potential for DEF is typically mitigated through the appropriate usage of SCMs. Silica fume is not effective as other SCMs, such as metakaolin, perhaps owing to its lack of alumina (compared to metakaolin, slags, or fly ash). Because of the general lack of long-term durability studies of UHPC, it is especially important to develop UHPCs that can be evaluated for long-term resistance to ASR and/or DEF.

2.3. UHPC as a Closure Pour Between Structural Elements

Upon reviewing literature regarding UHPC, it is clear that UHPC's structural properties in the field have seldom been studied. As a relatively new material, an extensive amount of work has been conducted to understand UHPC's material, durability, and structural properties in a lab setting. It is important to note that most UHPC research works were successfully completed by Benjamin Graybeal, the Lead Engineer for the FHWA's Bridge and Foundation Engineering Research team. Graybeal has conducted and completed extensive research on UHPC's material and structural properties in the last decade. Therefore, the high compressive and tensile strengths of UHPC as compared to conventional concrete are well documented and established in literature. The following literature review will provide an overview on UHPC as a structural joint material as well as summarize several case studies on the implementation of UHPC across the country.

2.3.1. Rebar Bond Behavior and Closure Joint Width

An initial literature review was conducted to find how deformed steel rebar interacts with UHPC and to understand why smaller lap lengths are required for deformed steel rebar when used in conjunction with UHPC as compared to traditional concrete for bridge construction. Refer to Figure 2.2 for a typical UHPC connection with non-contact lap splices. This UHPC closure joint connection will be the focus of this thesis as well as the large-scale structural testing portion of this research project.

In the study "Bond Behavior of Reinforcing Steel in UHPC" (Graybeal, 2014b), Graybeal evaluated the factors that affect bond strength between deformed reinforcing steel bars and UHPC. By using a direct tension test with A1035 No. 5 bars, Graybeal found that the bond behavior of deformed bars in UHPC is different than that found in traditional concrete in many aspects. Most importantly, it was found that non-contact lap splice specimens exhibit higher bond strength when compared to contact lap splice specimens. This phenomenon can most likely be attributed to the tight spacing of contact lap splice specimens, which decreases the contact area between the rebar and UHPC. Moreover, decreasing the contact area limits the ability of the fiber reinforcement from enhancing the mechanical resistance of UHPC (Graybeal, 2014b).

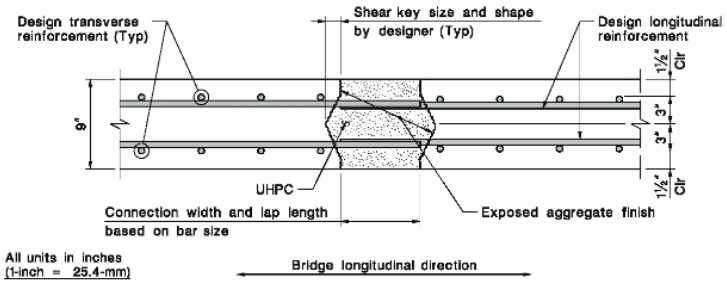

Figure 2.2 Example of a Typical UHPC Field Connection (Graybeal, 2019)

Graybeal also published the "Design and Construction of Field-Cast UHPC Connections" (Graybeal, 2019) to provide guidance on the design and deployment of field-cast UHPC connections. Unlike conventional concrete, Graybeal states that UHPC provides material-property benefits such as better internal distribution of stress, better confinement of embedded rebar, and reduced rebar development and splice lengths (Graybeal, 2019). In terms of rebar embedded in UHPC, the development length is usually a fraction of that required in conventional concrete which is, according to AASHTO, at least 24 times the nominal bar diameter. Therefore, empirical data has shown that shorter, straight lengths of rebar can be placed in less complicated configurations to connect PBESs with UHPC. Specifically, the rebar is placed to create non-contact lap splices where rebar from one structural deck panel overlaps the rebar from an adjacent panel, and the space between them is filled with UHPC. This configuration allows for the transfer of moment, shear, and tensile forces across the joint. According to Graybeal, many constructed UHPC closure joints on bridge decks have widths that vary between six and eight inches. In terms of design, Graybeal points out that "For lap splices of straight lengths of deformed steel reinforcement, the lap splice length, ls, shall be at less 0.75ld", where ld is the development length of the rebar. These design specifications, which are justified by empirical data, allude to the ability of UHPC to develop and embed reinforcing bars over relatively small distances, therefore creating a smaller joint width.

Focusing on experiments conducted regarding closure joint width, Lee and Lee (2015) performed a study to determine the behavior of non-contact lap splice connections and found that a 7db (db = bar diameter) splice length of uncoated rebar, along with an approximately 6" wide closure joint, was sufficient in allowing a transition from a tension splice failure mode to a compressive failure mode where the precast deck concrete fails first (Lee and Lee, 2015). Therefore, the researchers were able to conclude that straight bars were effective and efficient for lap-splice connections when using UHPC.

Recently, many research studies have been focusing on sourcing UHPC materials locally to drive down costs. According to Peruchini et al., UHPC costs on the order of 20-30 times more than conventional concrete (Peruchini et al., 2017). Most of Graybeal's UHPC research work has primarily been around the use of a commonly used commercially available proprietary UHPC similar to one of the mixtures studied in Chapter 3 and 4. For instance, in 2013, Graybeal and Florent Baby established the idealized tension stress-strain relationship for the commercially available proprietary UHPC as shown in Figure 2.3. This figure also highlights the effects of the steel fibers on post-cracking strength. In stage IV, it can be seen that failure only occurs until after the cracks have widened enough to cause the steel fibers to pull out from the cement paste. Many researchers are testing the material and structural properties of their own non-proprietary UHPC mixes to help push the future use of UHPC.

Mouhamed Alkaysi at the University of Michigan (Alkaysi, 2016) developed a low-cost UHPC material and performed structural level tests by connecting precast bridge deck elements with 4", 6", and 8" wide UHPC closure joints (Figure 2.4). The objective of this study was to probe the lower limits of the UHPC lap-splice connection joint sizes in order to gain a better understanding of the UHPC joint response. After performing four-point flexural bending tests and combined shear and moment offset three-point bending tests, Alkaysi found that panels with 4" wide joints failed to transfer load between the precast decks, which resulted in the splitting failure of the joint. In other words, the bond between the UHPC and deformed bars was insufficient. Conversely, the 6" and 8" joint widths were sufficient in achieving the required force transfer between the precast deck elements and therefore failed through steel yielding followed by concrete crushing, which is the desired failure mode.

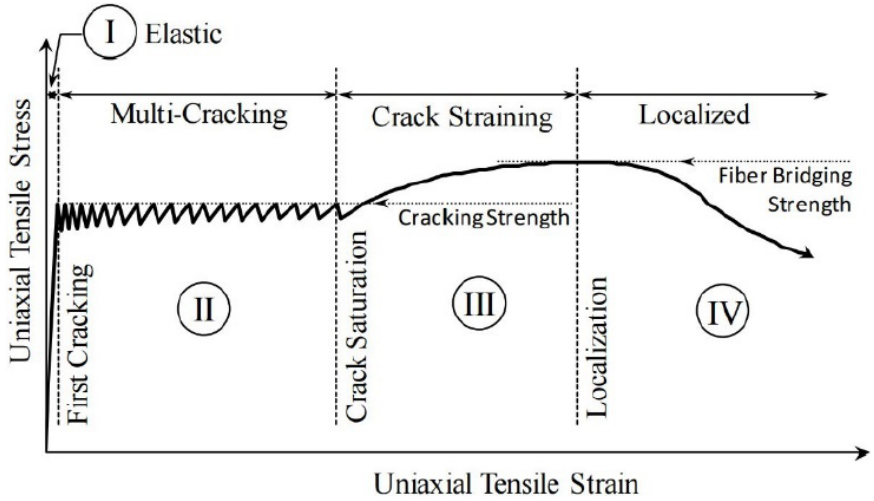

Figure 2.3 Idealized Uniaxial Tensile Response of UHPC (Graybeal & Baby, 2013)

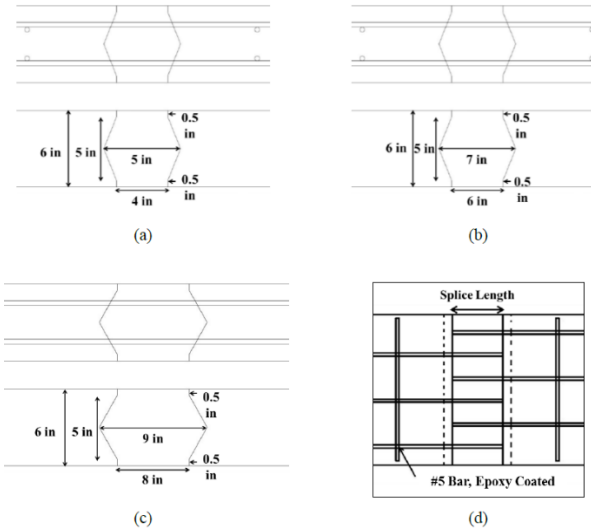

Figure 2.4 Joint Widths used in Alkaysi Testing Program (Alkaysi, 2016)

2.3.2. Structural Failure Behavior of UHPC

In the November 2010 study "Behavior of Field-Cast UHPC Bridge Deck Conditions Under Cyclic and Static Structural Loading" (Graybeal, 2010), Graybeal evaluated the structural response of field-cast UHPC connections linking precast concrete deck components. Graybeal accomplished the research project's objectives by fabricating bridge deck components with either longitudinal or transverse closure joints and testing them under both cyclic and static (monotonic) wheel loading. Specifically, the transverse joints were meant to imitate a connection between full-depth precast panels while the longitudinal joints were meant to emulate a connection between adjacent deck bulb tee girders, which are sections of deck that are precast monolithically with the girder.

Graybeal included four transverse specimens and two longitudinal specimens, where each specimen was identical except for their discrete reinforcing configuration (i.e., non-contact straight lapped bars, headed bars, intersecting hoop bars). Figure 2.5 presents one of the bridge deck components used for testing with a straight bar configuration. All connection details were developed by the New York State DOT (NYSDOT), who were motivated by their need to find a more efficient joint, both in terms of material and structural performance.

The testing program for the closure joints involved loading the simple span panel with cyclic loads first and then static loads until ultimate failure. This loading program was designed to allow for the assessment of the following three critical behaviors:

1. Cyclic loading below the specimen's cracking load allowed for the assessment of the field-cast UHPC's cracking performance and aided in evaluating the bonding performance of the UHPC to the precast concrete interface (Graybeal, 2010).

2. Cyclic loading that generated stresses above the cracking strength of the precast panel helped assess the cracking performance of the system, including understanding if there was any uncontrolled and progressive cracking or any debonding of the UHPC from the precast concrete interface (Graybeal, 2010). Wait 1 minute, then add remaining HRWA over 30 seconds

3. Static overload of the system allowed for the researcher to understand whether the system effectively emulated the performance anticipated from a monolithic concrete deck (Graybeal, 2010). Continue mixing until the mix turns from a dry powder to a thick paste (time may vary)

With these behaviors in mind, Graybeal was able to demonstrate that UHPCs can exhibit exceptional bond when cast against previously cast concrete. Looking at Figure 2.6, the cyclic loading data results show that the strain remained relatively constant through the closure joint section, which therefore acknowledges that the load distribution between the UHPC and the precast concrete remained intact.

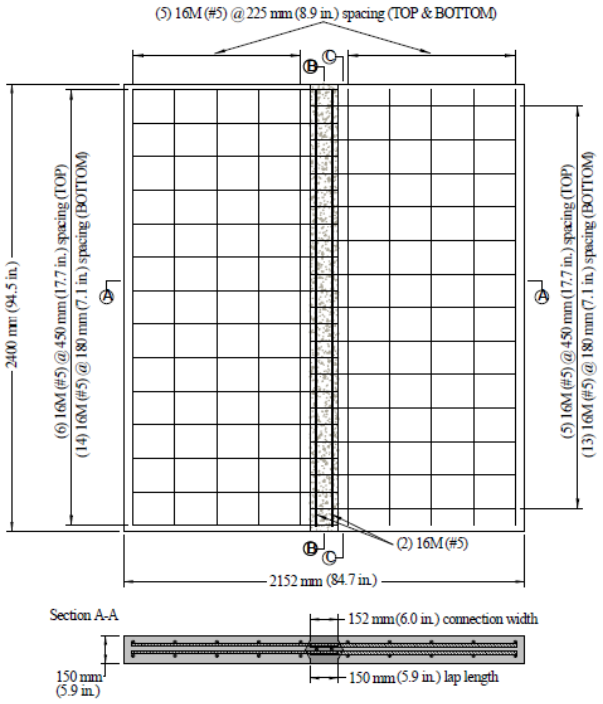

Figure 2.5 UHPC Longitudinal Joint Specimen with Straight Non-Contact Lap Splice Rebar Configuration (Graybeal, 2010)

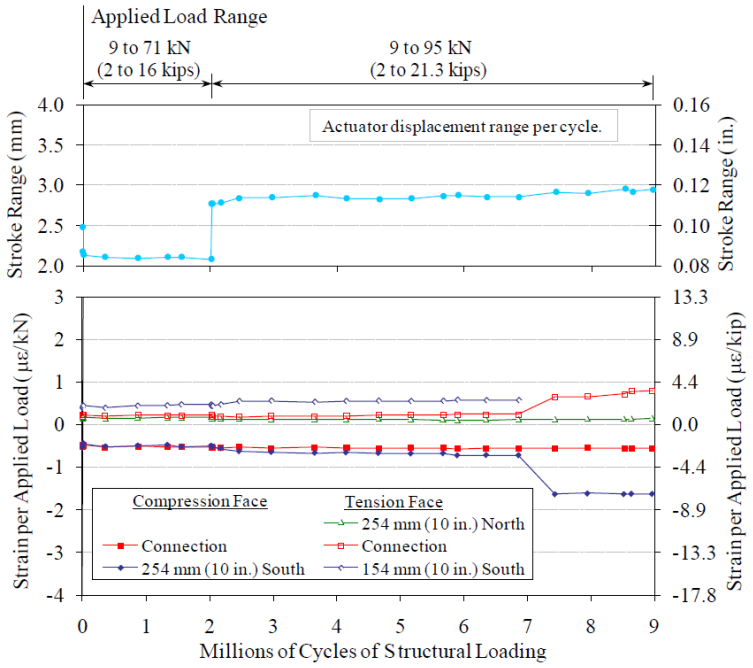

Figure 2.6 Cyclic Strain Data (Graybeal, 2010)

Overall, upon completion of structural testing, Graybeal found that the test specimens demonstrated no interface debonding between the UHPC and precast concrete, exactly as the data had shown. Specifically, the transverse panels demonstrated favorable cracking behavior with no interface debonding in the cyclic stage. Similarly, the large flexural stresses oriented perpendicular to the UHPC connection of the longitudinal panels did not result in interface debonding as well. Furthermore, static loading to the transverse panels resulted in global flexural failure of the simply supported panels. Specifically, the material behavior progressed through cracking, rebar yielding, and ultimately concrete crushing. Graybeal stated that the structural behavior of the transverse panels either matched or surpassed the behavior that would be anticipated from a monolithic concrete bridge deck (Graybeal, 2010). This data therefore supports the viability of UHPC as a closure joint material.

In 2016, Graybeal and Zachary Haber (Haber & Graybeal, 2016) evaluated the performance of five different commercially available UHPC class materials that could be used within closure joints to connect prefabricated bridge elements (Table 2.2). Each UHPC mix contained 2% steel fibers by volume, and each had a compressive strength between 20 and 25 kips per square inch (ksi) after 28 days. This was another research study that focused on how each UHPC material behaved in a closure joint when subjected to different loading regimes including cyclic and static loading. The behavior of each UHPC material was compared to each other as well as to non-shrink cementitious grout (NSG), which is currently widely used as

a connection material in prefabricated bridge systems around the country. The NSG for this project was portland cement based, non-metallic, and had a 28-day compressive strength of 8 ksi. Testing was conducted in two phases for this project: 1) the interface bond behavior between the precast concrete and the different UHPC materials was analyzed; and 2) the performance of the UHPC materials as a connection between adjacent prefabricated bridge deck elements was evaluated, which was conducted using large-scale precast deck panel specimens (Haber & Graybeal, 2016). The UHPC connections were 6" wide and employed straight bars with 5.5" non-contact lap splices while the NSG connection was 10" wide and employed U-bars with an 8.5" non-contact lap splice length, as shown in Figure 2.7.

Table 2.2 UHPC Mix Designs for Graybeal and Haber Study (Haber & Graybeal, 2016)

Designation	U-A	U-B	U-C	U-D	U-E
Mix Design	lb/yd^3 (kg/m^3)	lb/yd^3 (kg/m^3)	lb/yd^3 (kg/m^3)	lb/yd^3 (kg/m^3)	lb/yd^3 (kg/m^3)
Pre-blended dry powders	3503† (2078)†	3516 (2086)	3600 (2136)	3700 (2195)	3236 (1920)
Water	278 (165)	354 (210)	268 (159)	219 (130)	379 (225)
Chemical admixtures	23 (13.7)	48 (28.7)	preblended*	89†† (53)††	73 (44)
Steel fiber content	277 (126)	88 / 179 (52 / 106)	272 (123.6)	263 (156)	156 (156)
Steel Fiber Tensile strength, ksi (MPa)	160 (1100)‡	≥305 (2100) / ≥305 (2100)	348 (2400)	399 (3750)	399 (3750)
Length, in (mm)	1.18 (30)‡	0.5 (13) / 0.79 (20)	0.5 (13)	0.5 (13)	0.5 (13)
Diameter, in (mm)	0.022 (0.55)‡	0.012 (0.3) / 0.012 (0.3)	0.012 (0.3)	0.008 (0.2)	0.008 (0.2)

†: Not pre-blended but come in as separate ingredients, which include fine silica sand, finely ground quartz flour, portland cement, and amorphous micro-silica
*: The chemical admixtures were dry powders and pre-blended with other powder ingredients
††: It includes three chemicals, a modified phosphonate plasticizer, a modified polycarboxylate high-range water-reducing admixture, and a non-chloride accelerator
‡ : Fibers were straight with hooked ends and did not have a brass coating

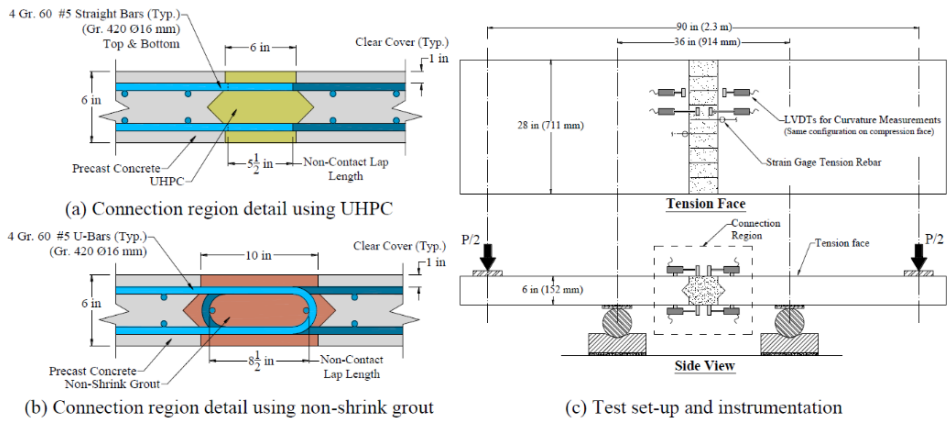

Figure 2.7 Specimen Geometry, Test Setup, and Instrumentation Plan for Graybeal and Haber Study (Haber & Graybeal, 2016)

In this study, Haber and Graybeal found that 83% of the specimens failed within the precast concrete, which indicates a relatively good bond between the UHPC materials and the precast concrete. In terms of the deck panel tests, the researchers found that in cyclic loading, UHPC exhibited higher initial flexural stiffnesses than the panel employing NSG, which can be seen in Figure 2.8. This can be explained by the fact that NSG exhibited significant shrinkage cracking prior to loading and the elastic modulus of the material is much lower than that of UHPC (Haber & Graybeal, 2016). In the fatigue cyclic stage (overload cycles), the researchers found new cracks formed within the precast concrete deck of the UHPC specimens (i.e., Specimen "U-C") while new cracks formed within the connection and precast concrete for the NSG specimen as can be seen in Figure 2.8 as well.

Finally, in the third loading protocol of the test (static loading), it was found that the NSG had lower initial stiffness, ultimate strength, and ultimate displacement when compared to the UHPC specimens (Figure 2.9). Moreover, the NSG failed due to non-contact lap splice failure while the UHPC specimens failed as a result of precast concrete crushing.

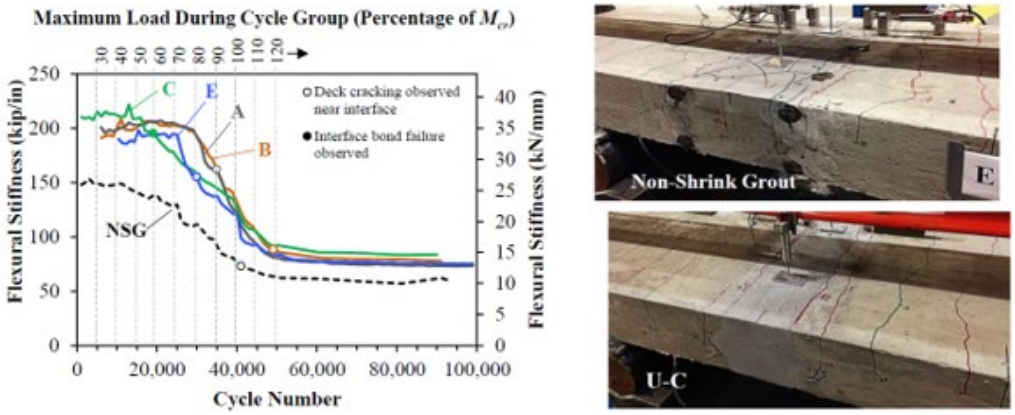

Figure 2.8 Degradation of Flexural Stiffness During Cyclic Load Testing (Left) (Haber & Graybeal, 2016); Cracking in Test Specimens due to Overload Cycles (Right) (Haber & Graybeal, 2016)

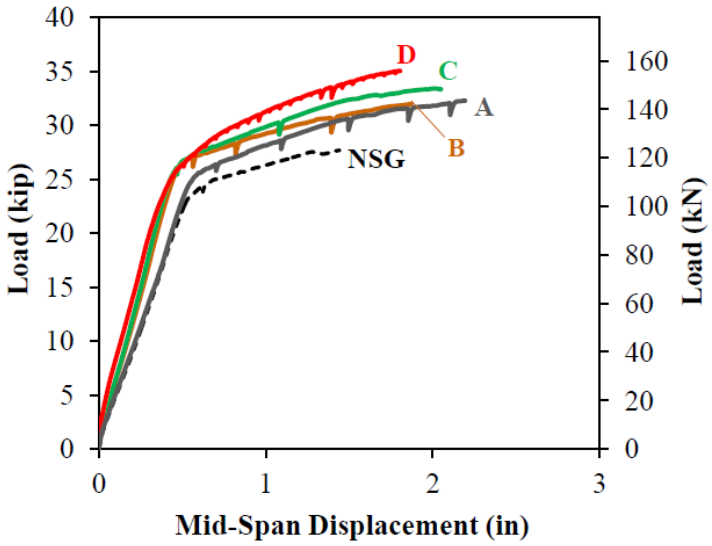

Figure 2.9 Force-Displacement Relationships for UHPC and NSG Specimens (Haber & Graybeal, 2016)

Ultimately, it can be seen from this study that prefabricated bridge systems utilizing UHPC typically have higher initial stiffness as well as better stiffness retention when compared to NSG materials. When used as a connection material, UHPC will also have good resistance to fatigue and post-fatigue ultimate loading, as was clearly shown in Graybeal's extensive studies. UHPC also exhibits ductile failure with good displacement ductility (Haber & Graybeal, 2016). Overall, this study by Graybeal and Haber illustrates that prefabricated bridge systems with UHPC-based closure joints perform better than bridge systems that employ the conventional NSG connection material.

It has been known that UHPC closure joint connections are relatively easy to fabricate given their relatively simple reinforcement configuration; however, the reinforcement detail, connection material, and geometry can have a significant impact on the long-term performance of the connection. In November 2018, Graybeal and Haber completed another research study (Haber & Graybeal, 2018) to advance the understanding of deck connections between prefabricated deck elements. Similar to other studies reviewed, this study assessed the structural performance of the closure joint with different types of materials and connection details. Apart from the fill material, Graybeal and Haber also looked closely at the reinforcement types (i.e., black, epoxy-coated, GFRP, headed), shear key surface preparation, shear key geometry, and transverse reinforcement.

The closure joint region was placed within a constant moment region between the center supports and was tested in four-point bending, as shown in Figure 2.10. The closure joints were also subjected to three different loading protocols including

crack cyclic loading, post-cracking fatigue loading, and monotonic ultimate loading, which were all applied in succession. Graybeal and Haber also ensured to observe each deck specimen for shrinkage cracking before testing. Shrinkage cracking in prefabricated deck panel closure joints can lead to durability issues and can become significant in the event of mechanical loading, resulting is damage and loss of stiffness. Shrinkage cracking was found in 6 of the 16 UHPC connection specimens as can be seen in Figure 2.11.

The researchers found that the UHPC specimens exhibited ultimate performance and were comparable to the monolithic baseline specimens that were tested. Specifically, the UHPC specimens developed the full flexural capacity of the deck panel prior to failure and exhibited good ductility. Moreover, Graybeal and Haber found that the test variables mentioned previously had varying influence on the behavior of the closure joint. For instance, the shear key geometry had little to no effect on the flexural performance of the closure joint; the precast concrete surface preparation and lap splice length affected certain aspects of the connection performance such as cracking behavior and fatigue/ultimate behavior; however, the most important aspect of the closure joint was the material used, which impacted all aspects of the closure joint performance (Haber & Graybeal, 2018). Ultimately, although UHPC has higher initial costs as mentioned previously, it could be beneficial in terms of constructability, long-term performance, and required maintenance.

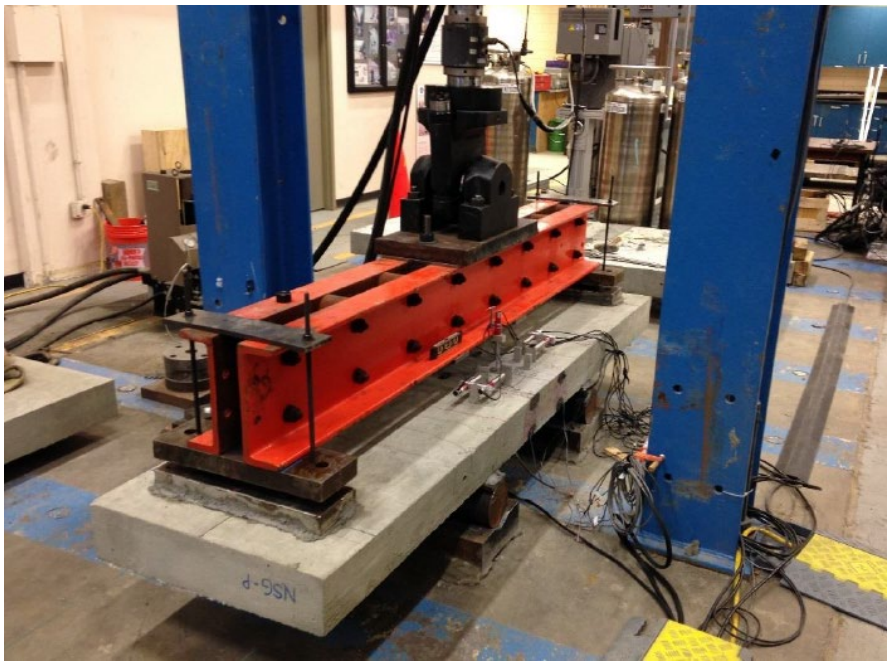

Figure 2.10 Deck Testing Layout – Four-Point Flexural Bending (Haber & Graybeal, 2018)

Figure 2.11 Shrinkage Cracking in UHPC Specimen (Haber & Graybeal, 2018)

Several research studies have been completed to investigate the behavior of UHPC as a closure joint material between precast bridge elements. Areas of focus include the bond of UHPC to precast concrete and the structural performance of UHPC connections for prefabricated bridge systems using large-scale structural testing. There are many more studies regarding UHPC that can be found within the literature. However, many of these research studies are relatively similar to those that were covered in this literature review and only help to support the data on the material properties and structural performance of UHPC.

2.4. Case Studies of UHPC Applications in Accelerated Bridge Construction (ABC)

UHPC is increasingly being used in infrastructure materials such as, overlay applications, bridge connections, impact resistance structures. For example, UHPC connects precast deck panels to other precast panels and girders. The enhanced properties of this material allow for simpler details and more durable connections as compared to conventional concrete and grout. The cost increment of materials is small because of the limited volume of UHPC required, and this is compensated by the faster on-site operations due to simpler connection details. UHPC connection details can be as simple as the lap-splicing of straight reinforcing bars. The higher compressive and tensile strengths of the material significantly reduce the required development and lap-splice lengths as compared to conventional concrete, and that allows for shorter lap-splice connections for precast panels. Research has demonstrated that an embedment length (l_d) of 8 times the bar diameter is sufficient for most common reinforcement configurations, and that for reinforcement embedded l_d into a connection a lap splice length of 0.75 l_d is sufficient to develop its full strength (Yuan and Graybeal, 2014).

2.4.1. Pulaksi Skyway Deck Replacement

There are numerous case studies related to the use of UHPC as a closure joint material on DOT projects across the United States. One such was on New Jersey's deteriorating Pulaski Skyway, which is a very narrow and heavily trafficked bridge. These conditions prevented the New Jersey DOT (NJDOT) from being able to fully close the bridge for deck replacement. The NJDOT also wanted to refrain from any major deck repairs for the next 75 years in order to avoid future disruptions. To meet NJDOT's criteria regarding minimizing traffic disruption and future deck maintenance, they went with using precast concrete deck panels connected with full-depth transverse UHPC closure joints as can be seen in Figure 2.12. This method was advantageous in that it accelerated the deck replacement and created a durable system that would meet NJDOT's desired design life of 75 years. According to the FHWA, "the choice of UHPC for the panel connections made the connections the strongest and most durable part of the deck, as opposed to the weak link typically associated with connections between precast concrete elements" (Leidos & WSP, 2018).

UHPC was chosen for this project because of its material properties, including its high strength, fast cure time, fluidity, and long-term durability, making it an ideal material to connect prefabricated concrete bridge elements. The use of UHPC also allowed for very short rebar extensions from the panels, which created narrow panel connections of 8 inches or less as shown in Figure 2.13 (Leidos & WSP, 2018). The Pulaski Skyway deck replacement represents the single largest use of UHPC in North America, using over 5,000 cubic yards. According to the FHWA, UHPC was successfully used to connect nearly one million square feet of deck panels and will help in minimizing deck maintenance for the next 75 years.

Figure 2.12 Transverse Closure Joints of Pulaski Skyway to be filled with UHPC (Leidos & WSP, 2018)

Figure 2.13 Close-Up of Pulaski Skyway Transverse Closure Joint Between Precast Full-Depth Concrete Panels Prior to UHPC Placement (Leidos & WSP, 2018)

2.4.2. NYSDOT Bridge Replacement

Another case study involving UHPC was conducted on bridges in Lyons and Oneonta, New York. Although these bridges had steel superstructures, precast deck panels were used in conjunction with UHPC closure joints. Notably, these bridges utilized non-contact lap splices between precast panels as shown in Figure 2.14. As evidenced by Graybeal's bond behavior study, non-contact lab splices exhibit higher bond strengths with UHPC than contact lap splices. Figure 2.15 shows the precast approach slabs and interior precast panels prior to UHPC placement while Figure 2.16 highlights the finalized bridge deck prior to being opened to traffic.

The testing program in "Behavior of Field-Cast UHPC Bridge Deck Conditions Under Cyclic and Static Structural Loading" actually demonstrated the viability of the field-cast UHPC system that NYSDOT deployed. NYSDOT has had a strong interest in deploying full-depth precast deck panels for use in construction and reconstruction of bridges. Through this collaboration, Graybeal demonstrated that both transverse and longitudinal UHPC closure joints are practical solutions for our nation's outdated highway infrastructure.

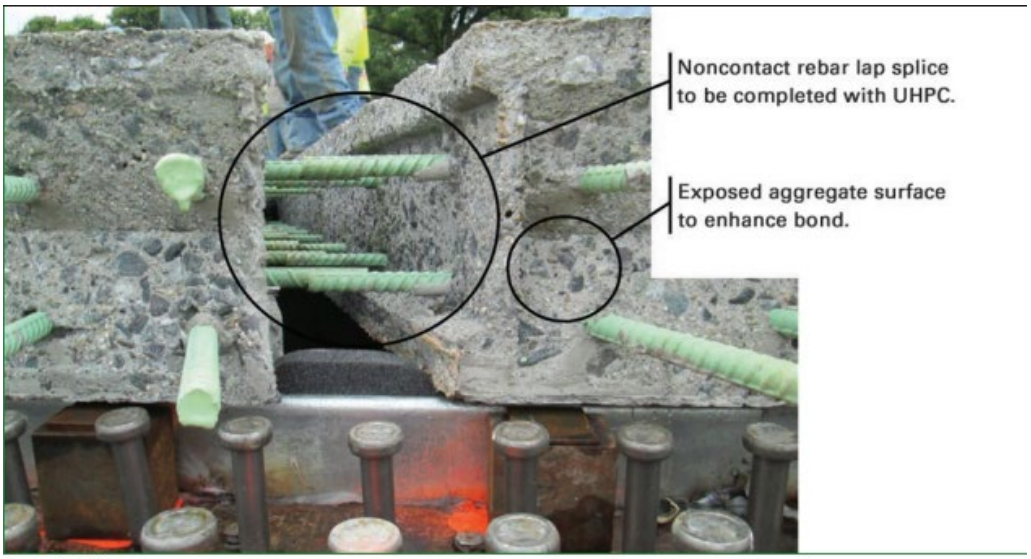

Source: FHWA.

Figure 2.14 Close-Up of Non-Contact Rebar Lap Splice in NYSDOT Project (Graybeal, 2019)

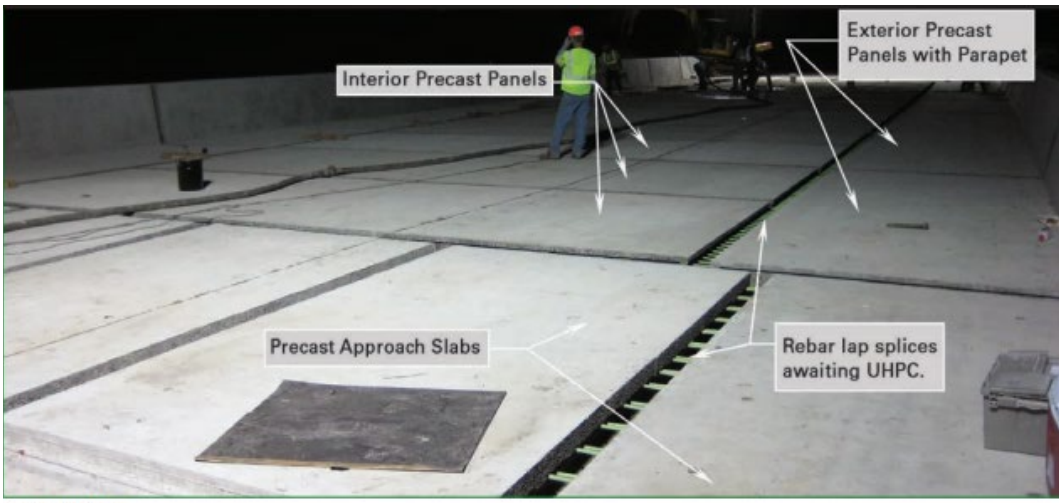

Source: FHWA.

Figure 2.15 Bridge Deck after Panel Installation and Before UHPC Placement (Graybeal, 2019)

Source: FHWA.

Figure 2.16 Finalized Bridge Deck after UHPC Grinding and Grooving (Graybeal, 2019)

2.5. Summary

The construction and reconstruction of highway bridges across the United States using prefabricated bridge elements and systems is an appealing concept. Unfortunately, the implementation of this system has been slowed by the cost of UHPC and the possible deterioration of field-cast connections. However, the advanced material properties of UHPC allow engineers to design and develop simple and sturdy connection systems for prefabricated elements. It has been thoroughly documented that UHPC as a closure joint material can allow for simplified reinforcement configurations, narrower joints, better interface bonding, and better long-term durability.

Chapter 3. Laboratory Evaluation of Proprietary and Non-Proprietary UHPC Mixes

This chapter presents the findings of a comprehensive laboratory investigation on prioprietary and non-proprietary ultra high performance concrete (UHPC) as well as mixes with rapid setting properties. The use of materials, mixture proportions, and mix procedures are outlined as well as the laboratory testing program and results for the fresh, hardened, and durability properties of mixes.

3.1. Overview

The goal of the comprehensive laboratory investigation is aimed at developing a suite of RSFRC and UHPC mixes, with a range of strength and durability charactersistics, that will most likely be considered for (and be readily available) for TxDOT closure pour applications in ABC superstructure systems. At the onset of this project, the target properties for UHPC evaluated in this project were in accordance with TxDOT Special Specification 4119 for Ultra-High Performance Concrete (UHPC), as summarized in Table 3.1.

Table 3.1 Requirements under TxDOT Special Specification 4119

Property	Test Method	Requirement
28 Day Compressive Strength, Min (psi)	ASTM C1858	21,000
4 Day Compressive Strength, Min (psi)	ASTM C1858	14.000
Flexutral Tensile Toughness (10 in span)	ASTM C1018	$I_{30} \geq 48$
28 Day Shrinkage, Microstrain	ASTM C157	≤ 800
Permeability, coulombs	ASTM C1202	≤ 250
Scaling Resistance	ASTM C672	$y < 3$
Freeze-Thaw Resistance, 300 cycles, % RDM	ASTM C666A	> 96
Alkali Silica Reactivity, % Max, 14 day expansion	ASTM C1260	< 0.1

A total of 16 mixes were developed and tested in the laboratory program consisting of 6 proprietary and 10 non-proprietary mixes as outlined in Table 3.2. The last three mixes included in Table 3.2 (UHPC-RS and UHPC-C1 mixes) are non-UHPC mixtures that are included in the table for convenience although they do not meet the specifications for UHPC. Testing of fresh, hardened, and durability properties of mixes was conducted as summarized in Table 3.3.

Table 3.2 Mixes Developed in Laboratory Testing Program

Mix	Proprietary/Non-Proprietary	UHPC	Rapid Setting
UHPC-P1-2	Proprietary	✓	
UHPC-P2-1	Proprietary	✓	✓
UHPC-P2-2	Proprietary	✓	✓
UHPC-P3-2	Proprietary	✓	
UHPC-N1-0	Non-Proprietary	✓	
UHPC-N1-2	Non-Proprietary	✓	
UHPC-N2-1	Non-Proprietary	✓	
UHPC-N2-2	Non-Proprietary	✓	
UHPC-N3-2	Non-Proprietary	✓	✓
UHPC-N4-1	Non-Proprietary	✓	
UHPC-N4-2	Non-Proprietary	✓	
UHPC-N5-1	Non-Proprietary	✓	
UHPC-N5-2	Non-Proprietary	✓	
UHPC-RS-0	Proprietary		✓
UHPC-RS-1	Proprietary		✓
UHPC-C1-1	Non-Proprietary		

Table 3.3 Fresh, Hardened, and Durability Testing

Fresh Properties	Hardened Properties	Durability Properties
• Slump • Unit Weight • Air Content • Setting Time • Temperature • Heat of Hydration	• Compressive Strength • Splitting Tensile Strength • Elastic Modulus • Flexural Strength • Flexural Toughness • Coefficient of Thermal Expansion • Drying Shrinkage • Pull-Out Testing	• Alkali-Silica Reaction • External Sulfate Attack • Delayed Ettringite Formation • Electrical Resistivity • Chloride Diffusion • Surface Sorptivity • Carbonation • Chloride-Induced Corrosion • Freezing and Thawing • Salt Scaling

3.2. Materials & Mix Proportions

As highlighted in Table 3.2, a total of 6 proprietary and 10 non-proprietary mixes were included in the testing program. To classify the various mixes, a nomenclature was developed: UHPC – (code for unique mix design) – (steel fiber percentage by volume). For example, a proprietary mix codified as P2 that contains 1% fibers has the nomenclature of UHPC-P2-1 while the same mix design with 2% fibers is labelled UHPC-P2-2.

3.2.1. Proprietary UHPC

A total of 6 proprietary UHPC mixes were tested as shown in Table 3.4; this primarily consisted of 4 different proprietary concrete products (P1, P2, P3, RS) with various combinations of steel fiber content. UHPC-P1 is a proprietary UHPC product while UHPC-P2 is a similar product with an additional accelerating admixture. The UHPC-P1 and UHPC-P2 mixes are the same as the commercially available proprietary UHPC that is prevalent in many of Graybeal's studies on UHPC. UHPC-P3 is a proprietary product from a different manufacturer than UHPC-P1 and UHPC-P2; this mix was used in the Amarillo field trial. UHPC-RS is a rapid-setting fiber-reinforced concrete (RSFRC) that contains a small volume of synthetic fibers to which 1% was added to the UHPC-RS-1 mix. A combination of bagged premix, high range water reducer (HRWR), cement accelerator, and steel fiber was provided by the manufacturers and proportioned based on manufacturer recommendation.

Table 3.4 Proprietary UHPC Mixes in the Laboratory Testing Program

Mix	Proprietary/Non-Proprietary	UHPC	Rapid Setting
UHPC-P1-2	Proprietary	✓	
UHPC-P2-1	Proprietary	✓	✓
UHPC-P2-2	Proprietary	✓	✓
UHPC-P3-2	Proprietary	✓	
UHPC-RS-0	Proprietary		✓
UHPC-RS-1	Proprietary		✓

3.2.2. Non-Proprietary UHPC

A total of 9 non-proprietary UHPC mixes were tested as shown in Table 3.5. In the testing program, particular emphasis was placed on a non-proprietary mix design developed through previous in-house research (Hernandez, 2016; Bonetti, 2022) that exhibited lower cost, reduction of health risks associated to the exposure of crystalline silica, and comparable hardened and durability properties to existing proprietary mixes. This mix design is represented in 5 non-proprietary mixes (UHPC-N1, UHPC-N2, UHPC-N3) with identical mix proportions but variations in the cement type and chemical admixtures used.

Table 3.5 Non-Proprietary UHPC Mixes in the Laboratory Testing Program

Mix	Proprietary/Non-Proprietary	UHPC	Rapid Setting
UHPC-N1-0	Non-Proprietary	✓	
UHPC-N1-2	Non-Proprietary	✓	
UHPC-N2-1	Non-Proprietary	✓	
UHPC-N2-2	Non-Proprietary	✓	
UHPC-N3-2	Non-Proprietary	✓	✓
UHPC-N4-1	Non-Proprietary	✓	

UHPC-N4-2	Non-Proprietary	✓	
UHPC-N5-1	Non-Proprietary	✓	
UHPC-N5-2	Non-Proprietary	✓	

The suite of non-proprietary mixes was developed using the materials listed in Table 3.6. Detailed mix proportions are outlined in Table 3.7. A high range water reducer was used in all mixtures to achieve adequate workability (dosages range from 12 - 70 oz/cwt). For mixture containing a set accelerator, a dosage of approximately 60 oz/cwt was used.

Table 3.6 Materials used in Non-Proprietary UHPC Mixes

Materials	Information on Sources/Types of Materials
Portland Cement	• ASTM C150 Type I/II • ASTM C150 Type V
Silica Fume	• ASTM C1240 (densified)
Metakaolin	• ASTM C618 (Class N)
Limestone Powder	• ASTM C1797
Fine Aggregate	• ASTM C33 (Concrete Sand) • ASTM C144 (Masonry Sand)
High Range Water Reducer	• ASTM C494 Type A/F (Polycarboxylate)
Set Accelerator	• ASTM C494 Type C (Non-chloride accelerator)
Fiber Reinforcement	• Steel fibers (ASTM A820)

Table 3.7 Mixture Proportions in Non-Proprietary UHPC Mixes

	Cement (lb/yd^3)		SCMs (lb/yd^3)		Aggregate (lb/yd^3)			Limestone (lb/yd^3)	Fiber (lb/yd^3)	Water (lb/yd^3)
Mix	II	V	Silica Fume	Metakaolin	Masonry Sand	Concrete Sand	Coarse			
UHPC-N1-0	-	1100	-	330	1540	-	-	580	-	357
UHPC-N1-2	-	1100	-	330	1540	-	-	580	264	357
UHPC-N2-1	1100	-	-	330	1540	-	-	580	132	357
UHPC-N2-2	1100	-	-	330	1540	-	-	580	264	357
UHPC-N3-2	1100	-	-	330	1540	-	-	580	264	357
UHPC-N4-1	1500	-	225	-	-	1600	-	-	132	500
UHPC-N4-2	1500	-	225	-	-	1600	-	-	264	500
UHPC-N5-1	1500	-	-	225	-	1600	-	-	132	500
UHPC-N5-2	1500	-	-	225	-	1600	-	-	264	500

3.2.3. Non-UHPC

A singular non-UHPC mix, known as UHPC-C1-1, is a normal strength concrete mix without the properties of UHPC or RSFRC but included steel fibers in the mix design. It was included in the testing program due to its application on the TxDOT ABC project constructed over the Navasota River on the TX-OSR state highway near Bryan, Texas. The materials used in this mix are listed in Table 3.8 and the detailed mix proportions are shown in Table 3.9. Details regarding the construction of this bridge will be discussed in Chapter 5.

Table 3.8 Materials Used in Non-UHPC Mix

Materials	Information on Sources/Types of Materials
Portland Cement	• ASTM C150 Type I/II
Coarse Aggregate	• ASTM C33 (Grade 57)
Fine Aggregate	• ASTM C33 (Concrete Sand)
Water Reducer	• ASTM C494 Type A/F (Polycarboxylate) • ASTM C494 Type A/D
Set Accelerator[1]	• ASTM C494 Type C (Non-chloride accelerator)
Fiber Reinforcement	• Steel fibers (ASTM A820)
Note: *[1] A set accelerator was added on site for the closure pour on the Navasota River ABC project but was not used for samples in the lab testing program*	

Table 3.9 Mixture Proportions in Non-UHPC Mix

	Cement (lb/yd^3)		SCMs (lb/yd^3)		Aggregate (lb/yd^3)			Limestone (lb/yd^3)	Fiber (lb/yd^3)	Water (lb/yd^3)
Mix	II	V	Silica Fume	Metakaolin	Masonry Sand	Concrete Sand	Coarse			
UHPC-C1-1	700	-	-	-	-	1238	1955	-	132	258

3.3. Laboratory Procedure

3.3.1. Mixing Procedure

The mixing, casting, and curing of UHPC followed ASTM C192 Standard Practice for Making and Curing Concrete Test Specimens in the Laboratory. For most mix designs apart from UHPC-C1 and UHPC-RS mixes, a 3 ft^3 vertical shaft mixer shown in Figure 3.1 was used to mix the materials. This was recommended by proprietary mix manufacturers to produce a workable and placeable UHPC product. The UHPC-C1 and UHPC-RS mixes were mixed using a tilting drum mixer as shown in Figure 3.2.

Figure 3.1 Vertical Shaft Mixer

Figure 3.2 Tilting Drum Mixer

The mixing of the proprietary mixes UHPC-P1 and UHPC-P2 followed the same procedure from the FHWA report by Graybeal (Graybeal, 2006) as shown below.

4. Weight all materials and add half HRWA to water
5. Place premix bags in pan and mix for 2 minutes
6. Add water (with half HRWA) to premix over 2 minutes
7. Wait 1 minute, then add remaining HRWA over 30 seconds
8. Wait 1 minute, then add accelerator over 1 minute
9. Continue mixing until the mix turns from a dry powder to a thick paste (time may vary)
10. Add fibers to mix over 2 minutes
11. Mix for an additional 1 minute to ensure dispersion of fibers

The mixing of the non-proprietary UHPC-N4 and UHPC-N5 mixes had a similar procedure with minor variations shown below.

1. Weigh all materials adding HRWR to half the water and keep the other half of water in a separate container
2. Add sand and half water without HRWR to mixer and mix for 1 minute
3. Stop mixer and add cement and supplementary cementitious material to pan and mix for 30 seconds
4. Add water with half HRWR over one minute
5. Mix materials until the UHPC is observed to self-level (reverse paddles if necessary to ensure mixing of the material). Time may vary

6. Add fibers to mix over 1 minute
7. Mix for an additional 1 minute to ensure dispersion of fibers

The mixing of the non-proprietary UHPC-N1, UHPC-N2, and UHPC-N3 mixes had the procedure shown below.

1. Add sand and limestone powder and mix for 90 seconds
2. Add all other dry materials and mix for 90 seconds
3. Combine 75% of the water and HRWR in a container, slowly incorporate into the mix over 30-45 seconds
4. Continue mixing for another 5 minutes, then add remaining 25% of the water (without superplasticizer)
5. Continue mixing until mix reached self-consolidating consistency. Then add steel fibers and continue mixing for two minutes to ensure dispersion of the fibers.

The non-proprietary UHPC-RS mixes had the procedure shown below.

1. Add water and 2/3 of the pre-bagged mix and mix for 60 seconds
2. Add remaining pre-bagged mix and mix for 60 seconds
3. Add steel fibers and mix for 60 seconds

The non-proprietary UHPC-C1 mixes had the procedure shown below.

1. Add rock, sand, and half of water to mixer and mix for 1 minute
2. Add cement and mix for 30 seconds
3. Pour second half of water with chemical admixtures to mix over 30 seconds
4. Mix for 2 minutes and allow concrete to rest for 3 minutes. Mix for additional 2 minutes
5. Add fibers and mix for 2 minutes to ensure dispersion of fibers

3.3.2. Fresh Properties

The testing program for fresh properties is outlined in Table 3.10. Each mix was conducted in an environmentally controlled room set at 73 ± 3 °F. As soon as mixing was complete, fresh property testing and the casting of specimens was conducted to avoid initial set of the mix.

Table 3.10 Testing Program for Fresh Properties

Fresh Property	Test Method	Methodology/Notes
Slump Flow	ASTM C143 (modified)	• Based on slump flow after lifting 3x6 cylinder
Unit Weight	ASTM C138	
Air Content	ASTM C231	
Setting Time	ASTM C403	
Temperature	ASTM C1064	
Heat of Hydration	Semi-adiabatic calorimetry	• "Q" drum testing

3.3.3. Hardened Properties

The testing program for hardened properties is outlined in Table 3.11. All test specimens were demoulded 24 hours after water was added to the cement. Specimens requiring wet curing were placed in an environmentally controlled fog room set at 73 ± 3 °F and 95-100% relative humidity until time of testing.

Table 3.11 Testing Program for Hardened Properties

Hardened Property	Test Method	Methodology/Notes
Compression Strength	ASTM C39	• Tested at 1, 3, 7, 28, 91 days
Splitting Tensile Strength	ASTM C496	• Tested at 28, 91 days
Flexural Strength and Toughness	ASTM C1609	• Tested at 28 days
Elastic Modulus	ASTM C469	• Tested at 28, 91 days
Coefficient of Thermal Expansion	TEX-428-A	
Drying Shrinkage	ASTM C157	
Pull-Out	ASTM E488 (modified)	• Field version of test with hand pump

3.3.4. Durability Properties

The testing program for durability properties is outlined in Table 3.12, this comprehensive evaluation covers the key factors that may adversely affect the long-term performance of closure pour connection in ABC applications.

Table 3.12 Testing Program for Durability Properties

Durability Property	Test Method	Methodology/Notes
Alkali Silica Reaction	Outdoor Exposure Block AASHTO T380	• ASR block • ASR mortar bars
Chloride Induced Corrosion	Marine Exposure Beams	• Exposure site at Gulf of Mexico
Electrical Resistivity	ASTM C1876	• Tested at 28, 91 days

Carbonation	Outdoor exposure beams	• Stored outdoors in Austin, TX
Freeze Thaw	ASTM C666	• 1 day moist curing before testing
Sorptivity	ASTM C1585	• Tested for water uptake after 28 days
Salt Scaling	ASTM C672	
External Sulfate Attack	ASTM C1012	• Specimens submerged in 5% sodium-sulphate solution
Delayed Ettringite Formation	Kelham Test	

3.4. Experimental Results and Discussion

3.4.1. Fresh Properties

For each concrete mixture, the slump, air content, unit weight, and fresh temperature were measured and provided in Table 3.13. Mixing and fresh concrete testing were performed at 73 °F. HRWR dosages adjusted to achieve self leveling property. However, UHPC-C1-1 exhibited poor workability as it is technically not a UHPC mixture but is meant to replicate the closure pour mix used at the Navasota River ABC project.

Table 3.13 Slump, Air Content, Unit Weight, and Temperature of Mixes

Mix	Slump Flow (in.)	Air Content (%)	Unit Weight (lbs/cu.ft)	Temperature (F)
UHPC-P1-2	11.00	3.4	145.6	73
UHPC-P2-1	11.50	2.0	142.8	74
UHPC-P2-2	11.50	2.4	151.6	72
UHPC-N1-0	13.00	4.0	143.2	86
UHPC-N1-2	-	1.2	148.4	79
UHPC-N2-1	15.75	2.8	144.4	78
UHPC-N2-2	16.00	-	147.2	81
UHPC-N4-1	16.50	1.7	144.0	73
UHPC-N4-2	13.25	3.0	143.2	74
UHPC-N5-1	18.50	2.0	140.4	73
UHPC-N5-2	13.00	1.5	140.0	74
UHPC-RS-0	10.00	3.4	-	74
UHPC-RS-1	8.00	3.8	150.4	73
UHPC-C1-1	0.00	4.4	157.8	78

The set time was evaluated, according to ASTM C403, for initial set at 500 psi and final set at 4000 psi. The initial and final set times are shown in Figure 3.3.

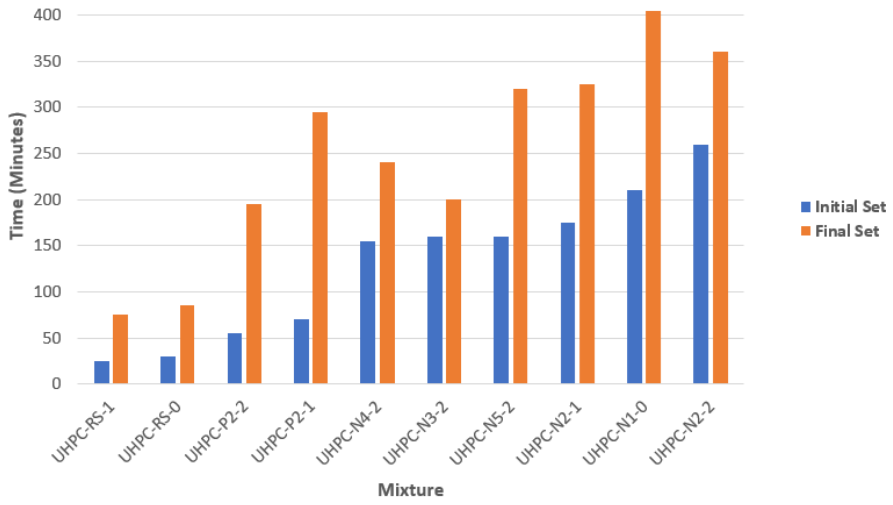

Figure 3.3 Set Time

The heat of hydration for concrete mixtures were measured, the following figures (3.4 – 3.11) below show the measured and calculated temperatures as well as the false and true adiabatic temperatures. Each graph presents the instantaneous and cumulative heat curves, as measured, as well as the the same curves adjusted for heat loss based on calibration parameters for the semi-adiabatic calorimeter used in this testing. As such the curve labelled as true adiabatic is meant to represent the cumulative heat generation of concrete in an adiabatic environment. For the graphs below, an apparent activation energy (E_a) of 40,000 J/mol was assumed, based on previous experience with UHPC.

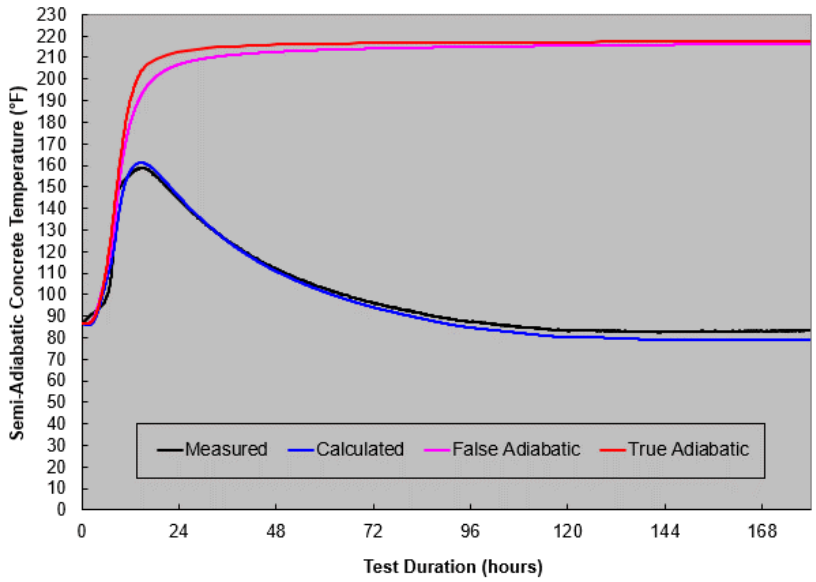

Figure 3.4 UHPC-P2-1 (Heat of Hydration)

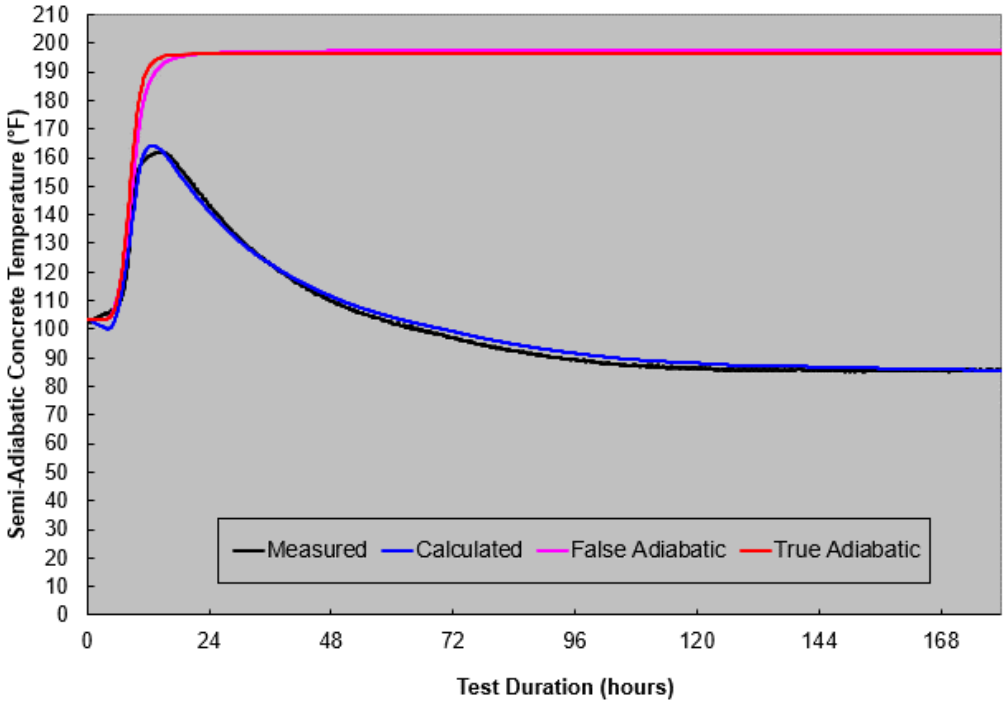

Figure 3.5 UHPC-P2-2 (Heat of Hydration)

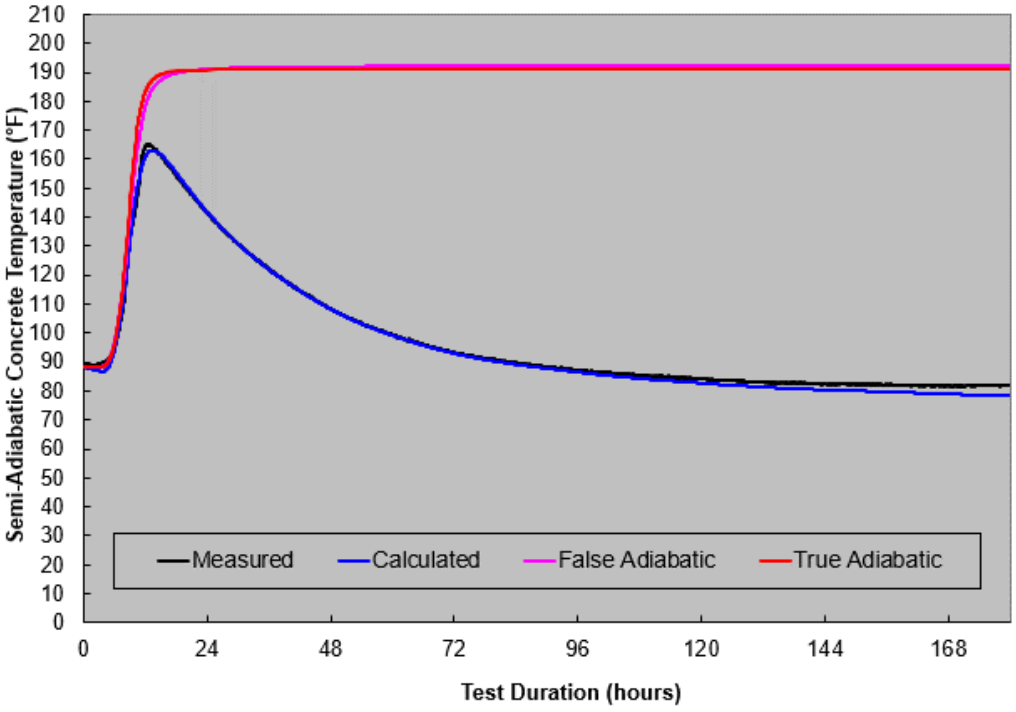

Figure 3.6 UHPC-N1-0 (Heat of Hydration)

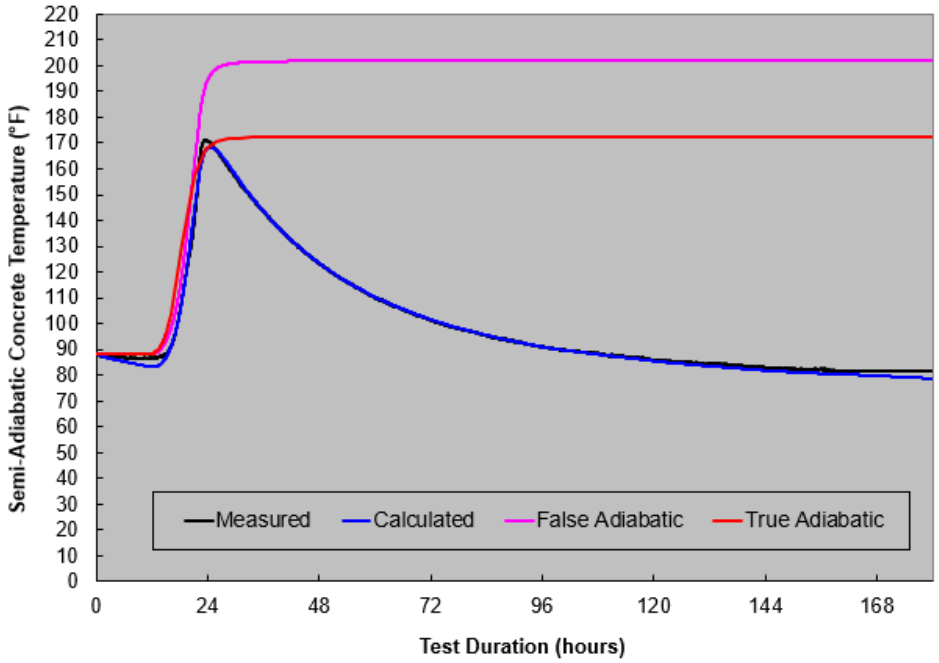

Figure 3.7 UHPC-N2-2 (Heat of Hydration)

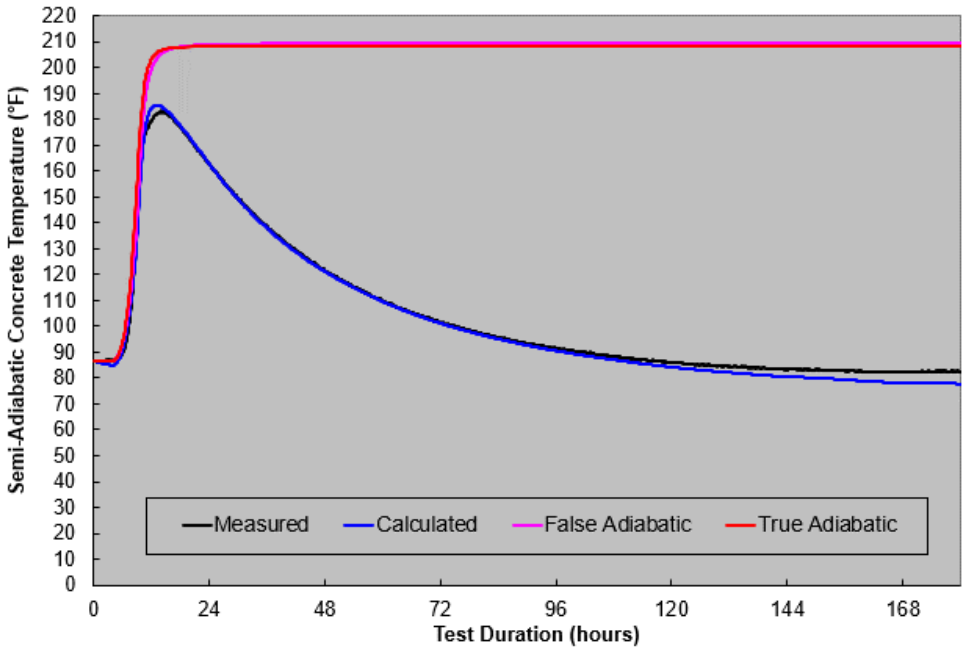

Figure 3.8 UHPC-N4-2 (Heat of Hydration)

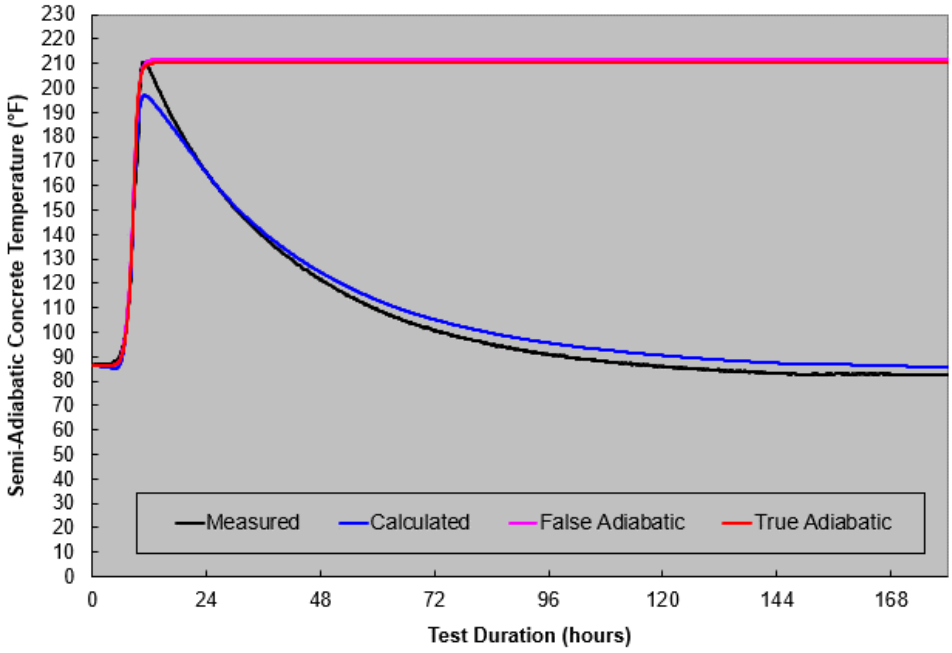

Figure 3.9 UHPC-N5-2 (Heat of Hydration)

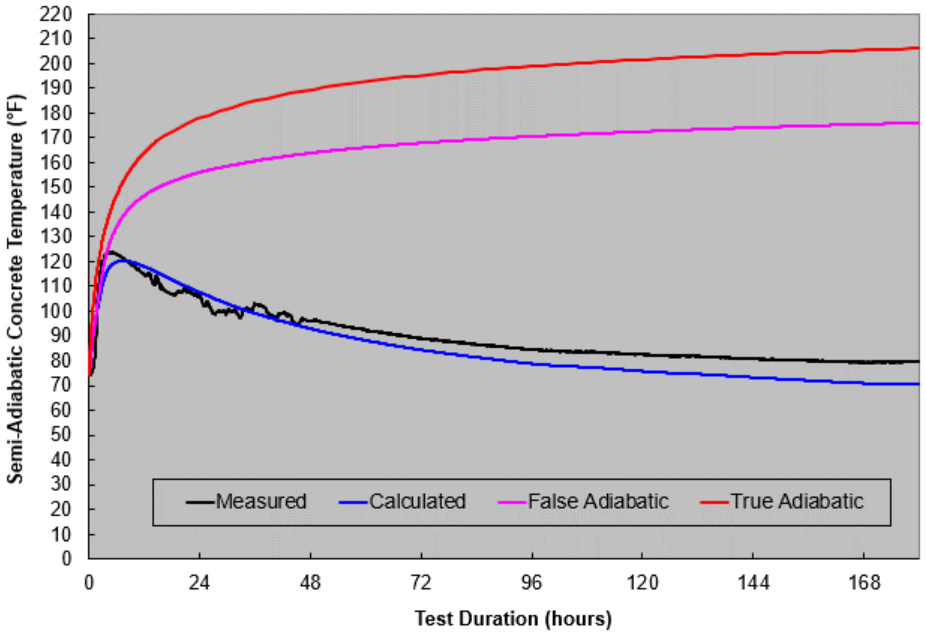

Figure 3.10 UHPC-RS-1 (Heat of Hydration)

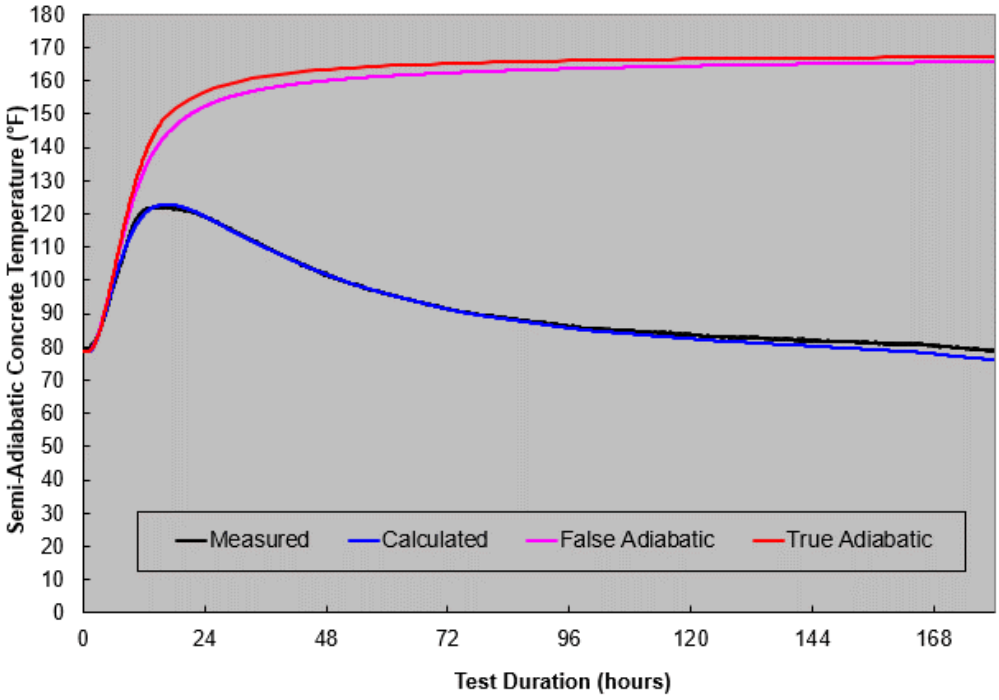

Figure 3.11 UHPC-C1-1 (Heat of Hydration)

3.4.2. Hardened Properties

The compressive strengths were evaluated at 1, 3, 7, 28, and 91 days. Results for the compressive testing program is shown in Table 3.14. Cube specimens (2 inch x 2 inch) were generally used for compressive testing. Mixes that incorporated cylinders (3 inch x 6 inch, 4 inch x 8 inch) into the compression testing are specifically highlighted in the footnote of the table. Since there is no firm criteria for minimum strength of UHPC, the goal of the project was to develop strengths above 20,000 PSI @ 28 days to encompass the requirements of a range of DOT requirements. For example, Florida DOT specifies a requirement of 17,000 PSI. Similar to published literature (Graybeal, 2013), the early age compressive strength of non-heat treated UHPC was relatively low but the strengths substantially increased after ages of 7 days. The addition of accelerators helped improve the early strength gain even in the absence of heat treatment.

Table 3.14 Compressive Strength of Mixes (PSI)

Mix	1 Day	3 Day	7 Day	28 Day	91 Day
UHPC-P1-2[a]	3260	8910	14210	18150	-
UHPC-P2-1	11030	12420	15450	16570	19670
UHPC-P2-2	11880	13460	16030	19630	21080
UHPC-P3-2[b]	-	17210	21240	26340	-
UHPC-N1-0[c]	7450	10030	10810	16970	17750
UHPC-N1-2[c]	-	12040	13540	17550	24410

UHPC-N2-1[c]	8080	9090	14510	17000	20160
UHPC-N2-2[c]	7300	11520	16510	17140	22200
UHPC-N3-2	7410	12440	16120	19000	-
UHPC-N4-1	4610	7320	8490	13370	15240
UHPC-N4-2	7710	9500	12060	14960	15190
UHPC-N5-1	7280	10810	12460	12570	13560
UHPC-N5-2	7840	9000	12690	13200	13670
UHPC-RS-0	6300	8450	8650	9180	11370
UHPC-RS-1	8420	10150	11280	12610	13940
UHPC-C1-1[d]	4620	9260	10100	10230	12550

Notes:
[a]Mix of cubes and 3x6 cylinders
[b]Only 3x6 cylinders
[c]Mix of cubes and 4x8 cylinders
[d]Only 4x8 cylinders

The splitting tensile strength was evaluated and results are shown in Table 3.15. Although it is recognized that the splitting tensile strength is not as accurate as direct tensile strength measurements, it was used as the standard method since it is the most common method of measuring tensile strength. A comparison between the tensile and compressive strengths for the mixes are shown in Figure 3.12. The ratio of tensile strength to compressive strength is presented as a percentage in Figure 3.13. The majority of mixes are in the range of 8-12% of compressive strength with some outliers. The omission of steel fibers in a mix contribute to lower ratios as shown by mix UHPC-N1-0 (7-8%) and UHPC-RS-0 (6%). The UHPC-N5 mixes exhibited stronger tensile strengths with a ratio of 11-19%.

Table 3.15 Splitting Tensile Strength of Mixes (PSI)

Mix	28 Day	91 Day
UHPC-P2-1	1855	2035
UHPC-P2-2	2230	2560
UHPC-P3-2	3080	-
UHPC-N1-0	1170	1430
UHPC-N2-1	1910	2065
UHPC-N2-2	1880	2260
UHPC-N4-1	1195	1385
UHPC-N4-2	1370	1440
UHPC-N5-1	1755	1554
UHPC-N5-2	2510	2630
UHPC-RS-0	555	670
UHPC-RS-1	880	1075
UHPC-C1-1	840	1050

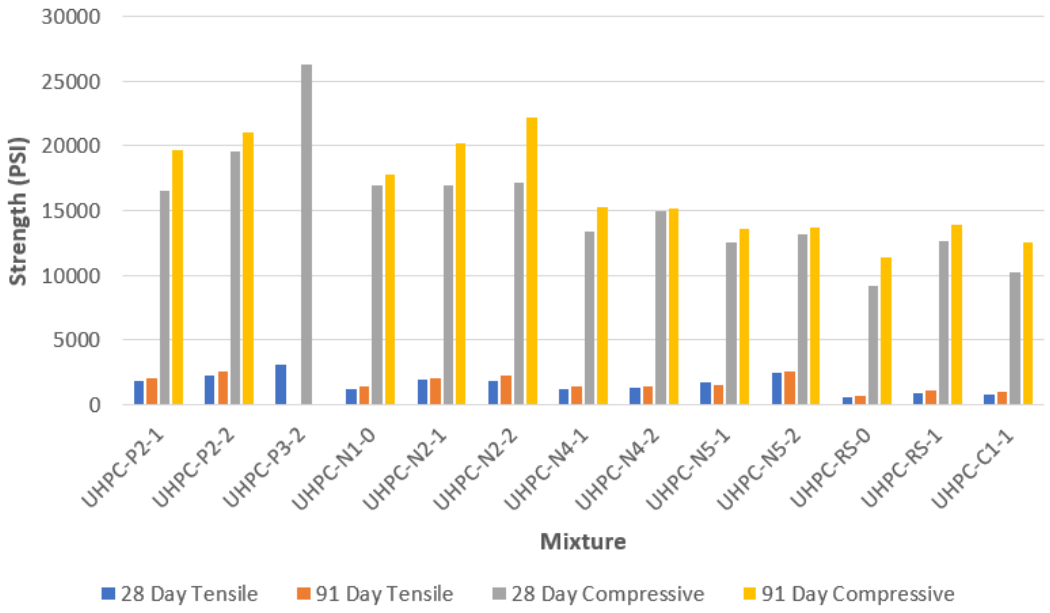

Figure 3.12 Comparison of Tensile and Compressive Strengths

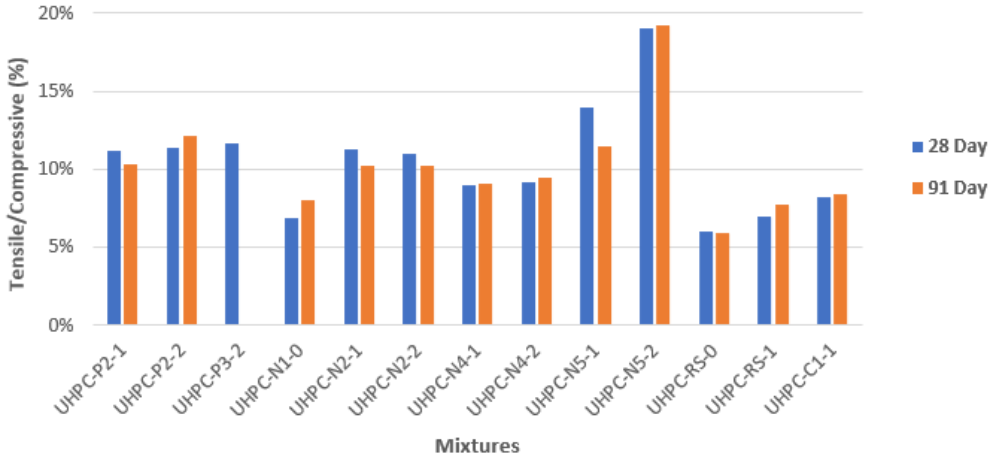

Figure 3.13 Tensile to Compressive Strength Ratio (%)

The modulus of elasticity was evaluated and results are shown in Table 3.16. As expected, the elastic modulus for the proprietary UHPC mixtures was the highest followed by the non-proprietary UHPC mixes.

Table 3.16 Modulus of Elasticity

Mix	28 Day (10^6 PSI)	91 Day (10^6 PSI)
UHPC-P2-1	9.37	8.59
UHPC-P2-2	8.82	9.05
UHPC-P3-2	8.10	-
UHPC-N1-2	6.50	6.67

UHPC-N2-1	6.44	6.87
UHPC-N2-2	7.05	6.85
UHPC-N4-1	5.16	4.53
UHPC-N4-2	5.11	5.69
UHPC-N5-1	4.58	5.77
UHPC-N5-2	4.87	6.24
UHPC-RS-0	4.09	4.53
UHPC-RS-1	4.09	4.96
UHPC-C1-1	7.60	8.01

The coefficient of thermal expansion was evaluated and results are shown in Table 3.17. The coefficient of thermal expansion of mixtures are consistent with pre-existing literature (Graybeal, 2013) mentions values within the range of 5.6-8.7 με/°F.

Table 3.17 Coefficient of Thermal Expansion of Mixes

Mix	Coefficient of Thermal Expansion (με/°F)
UHPC-P2-1	7.29
UHPC-P2-2	7.04
UHPC-P3-2	7.34
UHPC-N1-0	5.85
UHPC-N1-2	6.13
UHPC-N2-1	5.74
UHPC-RS-0	6.98
UHPC-RS-1	6.94

Drying shrinkage values were taken at 4, 7, 14, 28 days and 8, 16, 32 weeks in acoordance with ASTM C157. The results are shown in Table 3.18 and Figure 3.14. The typical range of shrinkages in published literature (Graybeal, 2013) was 0.05-0.08%. Most of mixes fell within this range, although some mixes such as UHPC-N5 and the UHPC-C1-1 mix exhibited higher shrinkages.

Table 3.18 Drying Shrinkage of Mixes

Mix	Day 4	Day 7	Day 14	Day 28	Day 56	Day 112	Day 224
UHPC-P2-1	-0.002%	0.000%	0.000%	-0.001%	-0.003%	-0.005%	-0.006%
UHPC-P2-2	0.003%	0.000%	-0.009%	-0.008%	-0.005%	-0.006%	-0.007%
UHPC-N1-0	0.000%	-0.002%	-0.003%	-0.006%	-0.006%	-0.009%	-0.015%
UHPC-N1-2	0.000%	-0.001%	-0.002%	-0.005%	-0.007%	-0.013%	-0.031%
UHPC-N2-1	-0.007%	-0.013%	-0.022%	-0.023%	-0.037%	-0.048%	-0.055%
UHPC-N2-2	-0.008%	-0.015%	-0.022%	-0.024%	-0.037%	-0.048%	-0.054%
UHPC-N4-1	0.000%	-0.001%	-0.004%	-0.005%	-0.017%	-0.017%	-0.063%
UHPC-N4-2	0.000%	-0.001%	-0.001%	-0.005%	-0.008%	-0.018%	-0.057%
UHPC-N5-1	-0.013%	-0.025%	-0.036%	-0.050%	-0.062%	-0.069%	-0.090%
UHPC-N5-2	-0.012%	-0.024%	-0.029%	-0.042%	-0.050%	-0.063%	-0.094%
UHPC-RS-0	-0.006%	-0.013%	-0.018%	-0.025%	-0.031%	-0.043%	-0.067%
UHPC-RS-1	-0.007%	-0.014%	-0.023%	-0.025%	-0.031%	-0.033%	-0.068%
UHPC-C1-1	-0.048%	-0.051%	-0.058%	-0.071%	-0.081%	-0.089%	-0.096%

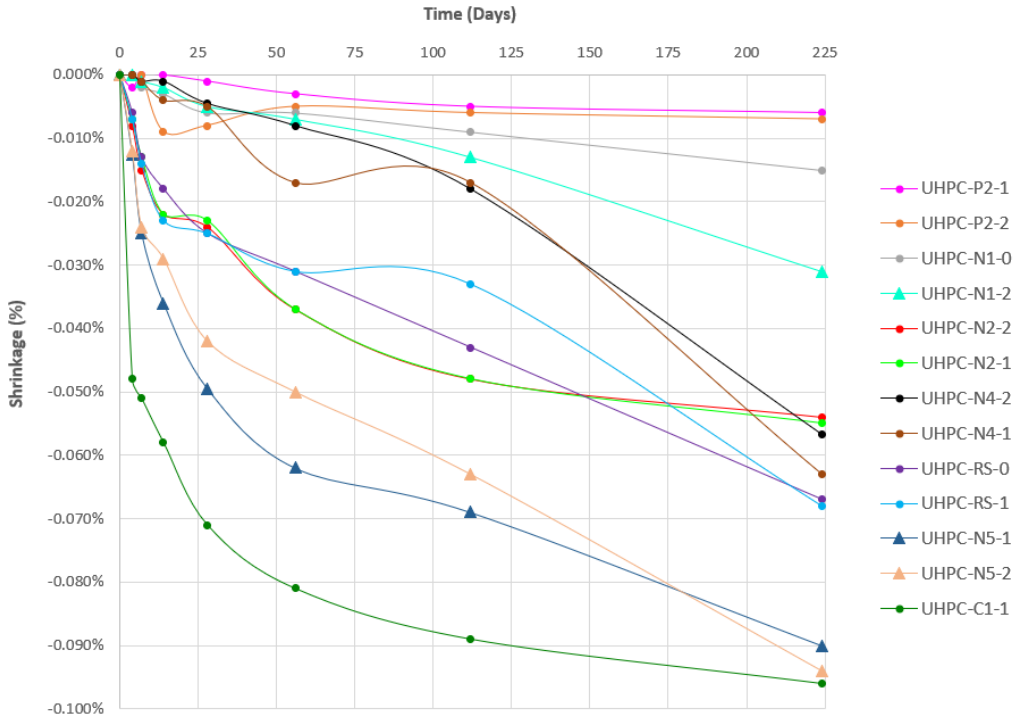

Figure 3.14 Drying Shrinkage Plot (Time vs % Shrinkage)

Pullout testing was conducted on mix specimens according to ASTM E488. Testing was conducted on 6x12 inch cylinders with #6 rebar cast in the center of the specimen. A minimum pullout strength requirement of 2650 PSI at 7 days was used per TxDOT requirememt. All mixes passed the requirements as shown in Table 3.19.

Table 3.19 Pull-Out Strength of Mixes

Mix	7 Day Strength (PSI)	Requirement Passed?
UHPC-P1-2	> 7000	✓
UHPC-P2-1	> 7000	✓
UHPC-P2-2	> 7000	✓
UHPC-P3-2	> 7000	✓
UHPC-N1-0	2750	✓
UHPC-N1-2	> 7000	✓
UHPC-N2-1	> 2650	✓
UHPC-N2-2	> 7000	✓
UHPC-N4-1	3300	✓
UHPC-N4-2	> 7000	✓
UHPC-N5-1	4000	✓
UHPC-N5-2	4800	✓
UHPC-RS-0	3250	✓
UHPC-RS-1	5600	✓
UHPC-C1-1	> 3000	✓

The specimens chosen for flexural testing according to ASTM C1609 were the two mixes used for large-scale testing, UHPC-P2-2 and UHPC-N3-2. A third mix, UHPC-P2-1, was also tested. The specimens used were 4 inch x 4 inch x 14 inch beams. The results of testing are shown in Table 3.20 below. The results of the UHPC-P2-1 and UHPC-P2-2 were comparatively higher than the non-proprietary mix, UHPC-N3-2. One reason for this difference in behaviour may be due to the observed segregation of UHPC-N3-2 which led to higher fiber contents on the bottom of the specimen as cast.

Table 3.20 Summary of ASTM 1609 Testing

Mix	Sample	Peak Load (lbf)	Peak Strength (PSI)	Peak Strain	F_{600}^{d} (PSI)	F_{150}^{d} (PSI)
UHPC-P2-1	A	12059	2247	0.003	1650	160
UHPC-P2-1	B	10839	2057	0.003	925	325
UHPC-P2-1	C	10445	1970	0.003	550	435
UHPC-P2-1	Average	11110	2090	0.003	1040	310
UHPC-P2-2	A	12020	2282	0.015	2245	1590
UHPC-P2-2	B	14373	2712	0.010	2510	1775
UHPC-P2-2	C	11693	2193	0.009	2148	1315
UHPC-P2-2	Average	12700	2400	0.011	2300	1560
UHPC-N3-2	A	7436	1457	0.0015	1296	744
UHPC-N3-2	B	4229	829	0.0035	766	497
UHPC-N3-2	C	7299	1412	0.0025	966	684
UHPC-N3-2	Average	6320	1230	0.003	1010	640

3.4.3. Durability Properties

The potential for alkali-silica reaction of mixtures was evaluated using the procedure outlined in AASHTO T380. The length change of specimens were measured at 3, 7, 10, 14, 21, 28, 42, 56, 70, and 84 days and the results are shown in Figure 3.15. Under AASHTO T380, all UHPC specimens were classified as non-reactive (expansions less than 0.04% at 56 days). The two UHPC-RS mixes exhibited the highest expansions. Large outdoor exposure blocks were also cast to see the effects of steel fibers in reducing ASR expansion. No expansion has been observed and the results are shown in Table 3.21.

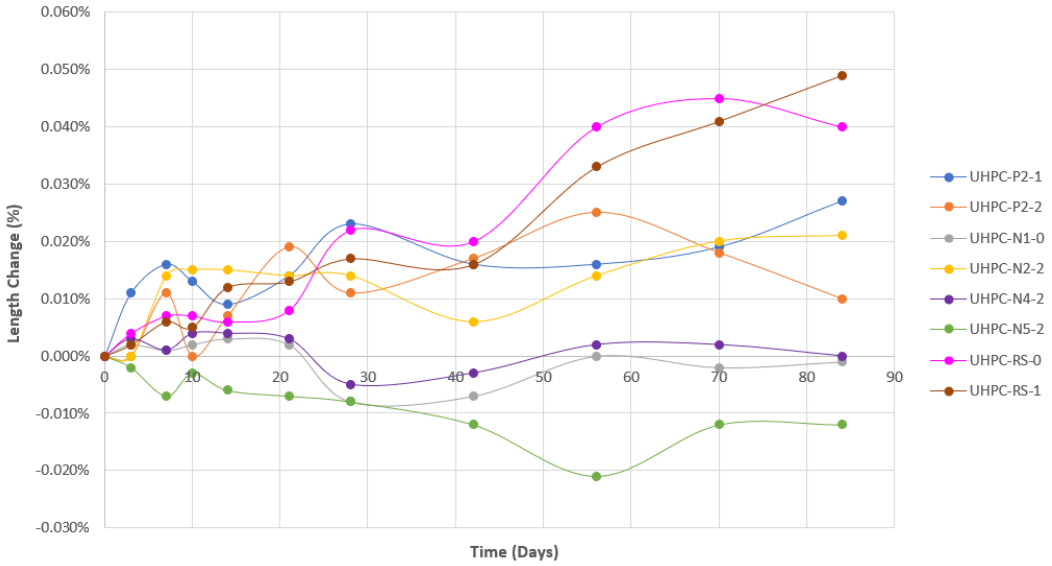

Figure 3.15 Alkali Silica Reaction Test Results per AASHTO T380

Table 3.21 ASR Block Expansion

Mix	Age (years)	Expansion (%)
UHPC-P1-2	2.5	0
UHPC-N2-2	1.5	0
UHPC-N4-2	2.8	0
UHPC-N5-2	2.8	0

Chloride induced corrosion testing was conducted on mixes using marine exposure beams placed at an exposure site on the Gulf of Mexico in Port Aransas, Texas. The samples are halfway submerged as shown in Figure 3.16, with two reinforcement bars placed at 1 and 2 inch cover for each sample. The Giatec iCOR, a connectionless corrosion rate measurement device for reinforced concrete structures, was used for measurements. Table 3.22 shows the corrosion measurements and Table 3.23 explains the colour coding that classifies performance. After 1 to 3 years of exposure, the blocks do not have any visual distress. The resistivity of all mixes are high with the exception of the UHPC-N4-2 mix that has moderate resistivity. The corrosion rates for all mixes were low to moderate. The corrosion potential of the UHPC-P1-2 and UHPC-P2-2 mixes showed high probability of corrosion activity but this may be due to fibers corroding on the exterior of the samples which may be tied to the reinforcement. The corrosion rate for these mixtures is still low.

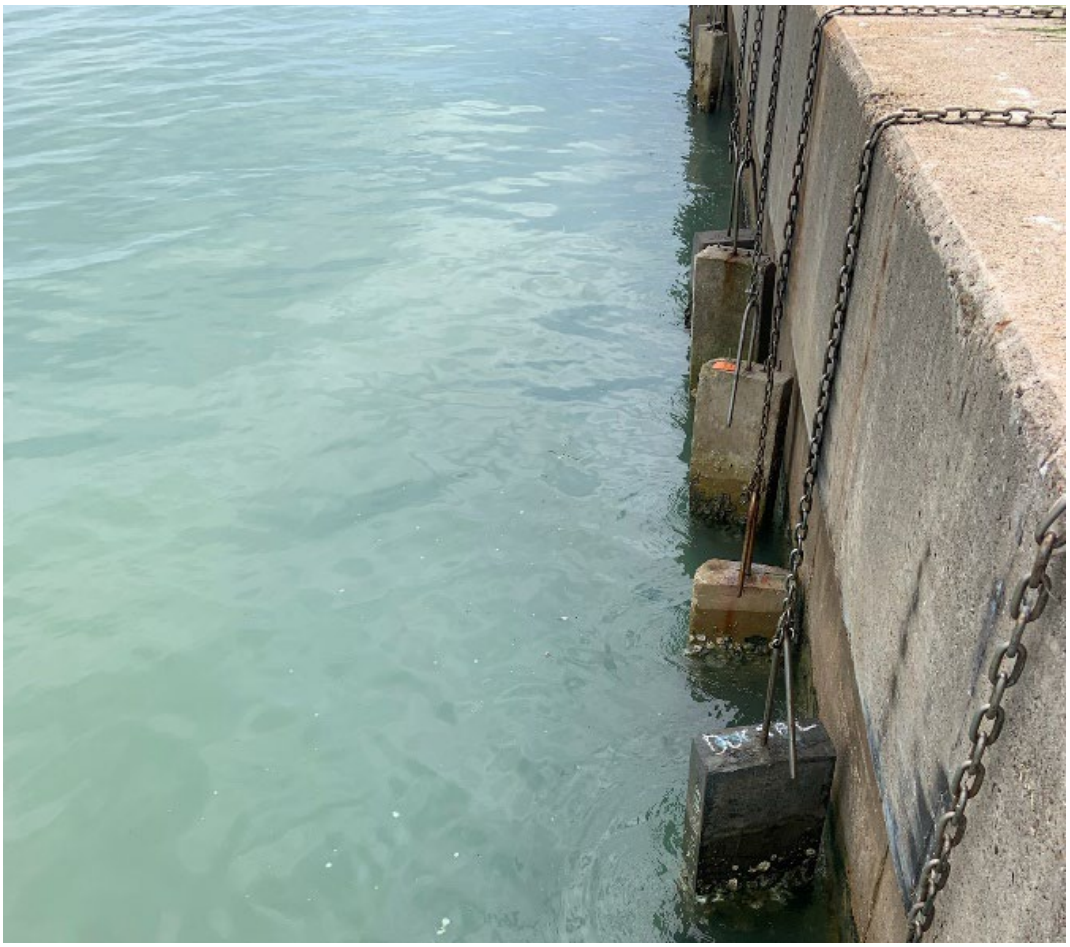

Figure 3.16 Marine Exposure Blocks for Chloride Induced Corrosion Testing

Table 3.22 Chloride Induced Corrosion Test Results

Mix	Corrosion Potential (mv)		Corrosion Rate ($\mu A/cm^2$)		Concrete Resistivity ($\Omega \cdot m$)	
	1"	2"	1"	2"	1"	2"
UHPC-P2-2	-298	-380	0.74	0.63	647	532
UHPC-P1-0[a]	-469	-463	1.08	1.04	520	501
UHPC-P1-2	-435	-499	0.89	0.5	445	327
UHPC-C1-2[b]	-183	-154	2.63	1.25	128	143
UHPC-P2-0[c]	-224	-192	2.81	1.05	512	378
WACO-NEXT[d]	-181	-145	1.31	0.67	259	456
UHPC-N4-2	-151	-118	0.54	0.91	145	94
UHPC-N5-2	-130	-210	0.15	0.44	523	140
UHPC-N1-2	-216	-196	0.68	1.18	523	395
UHPC-P3-2	-180	-325	0.74	1.17	515	289

Notes:
[a]Variation of UHPC-P1 mix with 0% fiber, specimen cast specifically for this test
[b]Variation of UHPC-C1 mix with 2% fiber added as per mix design on Navasota River ABC project
[c]Variation of UHPC-P2 mix with 0% fiber, specimen cast specifically for this test
[d]Mixture used on NEXT beams for the pre-cast panel sections in the Amarillo field trial

Table 3.23 Colour Codes for Chloride Induced Corrosion Performance

Resistivity		
Color Code	**Resistivity (Ω·m)**	**Classification**
Green	> 200	Very High
Yellow	100 – 200	High
Orange	50 – 100	Moderate
Red	< 50	Low
Corrosion Rate		
Color Code	**Corrosion Rate (μA/cm²)**	**Classification**
Green	< 1	Passive / Low
Yellow	1 – 3	Moderate
Orange	3 – 10	High
Red	> 10	Severe
Corrosion Potential		
Color Code	**Potential Value (mV)**	**Probability of Steel Corrosion Activity**
Green	> -200	Less than 10%
Yellow	-200 to -350	Uncertain
Red	< -350	More than 90%

The electrical resistivity of mixtures was measured at 28 and 91 days and the results are shown in Table 3.24. According to the AASHTO TP 95 classification for chloride ion penetrability, the UHPC-C1-1, UHPC-N4-2, UHPC-N2-2, and UHPC-RS-1 mixes have a high risk of penetration even after 91 days. Since resistivity measurements were taken on 4x8 inch cylinders with the presence of fibers dispersed throughout the sample, the presence of fibers may be conducting electricity leading to the lower resistivity values.

Table 3.24 Electrical Resisitivity of Mixes

Mix	7 Day Resistivity (Ω·m)	28 Day Resistivity (Ω·m)
UHPC-P2-1	498.7	1288.7
UHPC-P2-2	371.9	1919.1
UHPC-N1-0	654.3	1077.3
UHPC-N2-2	68.2	120.0
UHPC-N4-2	33.0	97.3
UHPC-N5-2	281.9	372.2
UHPC-RS-0	368.0	404.1
UHPC-RS-1	91.4	109.1
UHPC-C1-1	18.9	24.5

The depth of carbonation was measured at 3, 6, and 9 months and the results are shown in Table 3.25. Based on early age testing of carbonation, the carbonation depth is negligible for all mixes. Long term carbonation measurements will continue beyond the end of this project.

Table 3.25 Carbonation Depth of Mixes

Mix	3 Month Depth (inches)	6 Month Depth (inches)	9 Month Depth (inches)
UHPC-P1-2	0.00	0.00	0.00
UHPC-P3-2	0.00	0.00	0.00
UHPC-N1-0	0.00	0.00	0.00
UHPC-N1-2	0.00	0.00	0.00
UHPC-N4-1	0.00	0.00	-
UHPC-N4-2	0.00	0.00	-
UHPC-N5-1	0.00	0.00	-
UHPC-N5-2	0.00	0.00	-
UHPC-RS-0	0.00	0.00	0.00
UHPC-RS-1	0.00	0.00	0.00
UHPC-C1-1	0.00	0.00	0.00

Freeze thaw testing was conducted on 4x3x14 inch beams according to ASTM C666. Testing commenced after 1 day of moist curing and the specimens were subjected to a total of 308 cycles. All mixes passed the freeze thaw test criteria apart from the UHPC-C1-1 mix that was non-UHPC. This mix was terminated at 245 cycles as its dynamic modulus reached the early termination criteria of 60% of initial modulus. The results are shown in Table 3.26. The trend of increasing modulus values with the increasing number of freeze thaw cycles may be attributed to the hydration of cementious materials during the test. This is likely more pronounced with these specimens since the testing was started after only 1 day of curing to best reflect field curing conditions. Hence, the effects of continued hydration during the test disproportionally increased the dynamic modulus.

Table 3.26 Dynamic Modulus and Durability Factor ASTM C666

Mix	Cycles	Durability Factor
UHPC-N1-2	308	110
UHPC-N2-1	308	117
UHPC-RS-1	308	116
UHPC-C1-1	245	48
UHPC-RS-2	308	136

The surface sorptivity of mixes were measured after a 28 day curing period and tested according to ASTM C1585. The initial rate of water absorption was measured from 1 minute to 6 hours of submersion while the secondary rate of absorption was measured from 1 day to 7 days. The results are shown in Table 3.27. All the mixes tested exhibited very low values of initial and secondary rate of absorption.

Table 3.27 Surface Sorptivity of Mixes

Mix	Initial Rate of Absorption ($mm/s^{0.5}$)	Secondary Rate of Absorption ($mm/s^{0.5}$)
UHPC-P2-1	0.00107	0.00045
UHPC-P2-2	0.00092	0.00038
UHPC-N1-0	0.00013	0.00011
UHPC-N2-2	0.00102	0.00011
UHPC-N4-2	0.00146	0.00030
UHPC-N5-2	0.00109	0.00013
UHPC-RS-0	0.00110	0.00029
UHPC-RS-1	0.00132	0.00028
UHPC-C1-1	0.00188	0.00088

Salt scaling resistance was measured by exposing a horizontal concrete surface to freezing and thawing cycles in the presence of deicing chemicals. Visual inspection of samples were performed at 5-50 cycles at 5 cycle intervals and rated in accordance with ASTM C672 standards shown in Table 3.28. At every interval, all the mixes exhibited no scaling as shown in Table 3.29.

Table 3.28 Visual Rating of Concrete Surface per ASTM C672

Rating	Condition of Surface
0	No scaling
1	Very slight scaling (3mm [1/8in.] depth, max, no coarse)
2	Slight to moderate scaling
3	Moderate scaling (some coarse aggregate visible)
4	Moderate to severe scaling
5	Severe scaling (coarse aggregate visible over entire surface)

Table 3.29 Visual Rating of Mixes Subject to Salt Scaling per ASTM C672

Mix	Cycles									
	5	10	15	20	25	30	35	40	45	50
UHPC-N2-1	0	0	0	0	0	0	0	0	0	0
UHPC-N2-2	0	0	0	0	0	0	0	0	0	0
UHPC-RS-0	0	0	0	0	0	0	0	0	0	0
UHPC-RS-1	0	0	0	0	0	0	0	0	0	0
UHPC-C1-1	0	0	0	0	0	0	0	0	0	0

The sulfate resistance of mixes was assessed according to ASTM C1012. Mortar bars were immersed in a sulfate solution and the length change was measured at 1, 2, 3, 8, 13, 15 weeks and 4 months. The maximum threshold of 0.1% expansion was not exceeded for any mixes. The results are shown in Figure 3.17. Mixes will be retained beyond project completion and continue to be monitored through an exposure period of 18 months.

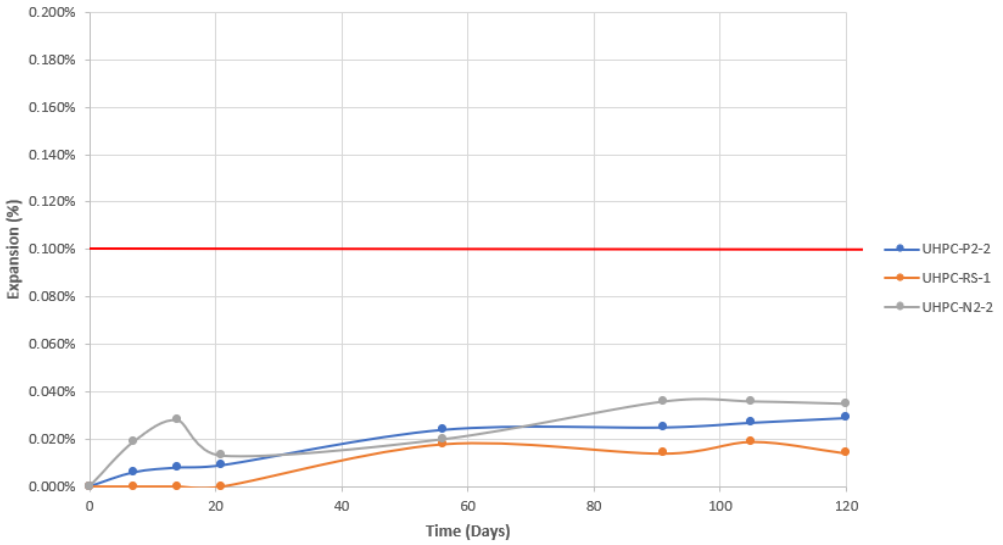

Figure 3.17 Sulfate Resistance Testing per ASTM C1012

The potential for delayed ettringite formation was tested using the Kelham Test method. Mortar bars were cast and placed in a 80 °C oven for 24 hours. The specimens were then submerged in lime water and measurements were taken at 1 day, every 7 days up until 28 days, and then every 28 days thereafter. The only mixtures that exhibited DEF induced expansion were the UHPC-RS-0 and UHPC-RS-1 mixes. The observed expansion of these mixes (Figure 3.18) was expected based on previous experience and the fact that these mixes are based on ettringite as the primary binder.

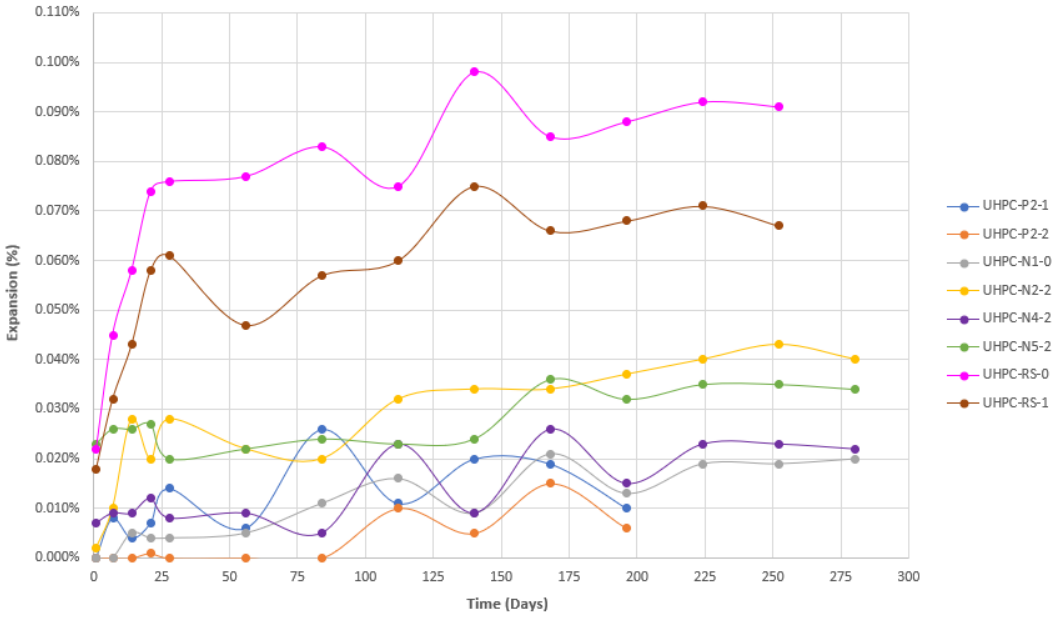

Figure 3.18 Kelham Test Results for Mixes

3.5. Recommendations and Conclusions

A comprehensive laboratory and exposure site testing was conducted, various UHPC mixtures (as well as some non-UHPC mixtures) were evaluated, and a range of fresh, hardened, and durability properties were assessed. Overall, it was found that proprietary UHPC mixtures, as well as some non-proprietary UHPC mixtures developed using locally available materials, exhibited satisfactory performance, with respect to closure pour applications in ABC applications. UHPC mixtures were found to exhibit adequate self-leveling capabilities, high compressive strength (> 18 ksi), and outstanding durability characteristics. Some of the UHPC mixtures developed or evaluated in the work described in this chapter were subsequently used in full-scale structural testing assessing the use of UHPC in closure pours in ABC bridge applications, as described in Chapter 4.

Chapter 4. Large Scale Testing of UHPC Closure Joint Decks

This chapter presents the findings of comprehensive laboratory testing that investigated the usage and performance of proprietary and nonproprietary ultra-high performance (UHPC) mixes as closure joint material for large-scale bridge decks. The specimen design and fabrication, testing matrix, testing frame, and results are all outlined within this chapter.

4.1. Overview

The primary objective of the large-scale testing program was to evaluate the structural performance of closure joints in accelerated bridge construction (ABC). Therefore, the research team prepared a testing program at the Ferguson Structural Engineering Laboratory. The experimental program consisted of two phases: flexural testing and shear testing. Each of the phases included two different UHPC mixtures being tested at two different timings. Test results were compared to the control specimen, which was monolithically cast, to evaluate the feasibility of the UHPC closure joints.

4.2. Development of Test Matrix

4.2.1. Types of Testing

The first step in creating the testing matrix was to determine the types of tests that were to be conducted. After an extensive literature review of related research, it was determined that the specimens would be subjected to flexural and shear loads in order to fully evaluate the performance of the closure joint.

The main objective of the flexural test was to investigate the performance of the closure joint when it is subjected to transverse bending across the deck. An essential performance goal was to ensure that the closure joint provides adequate continuity, and that moment transferred through the joint into the precast panels. Ideally, the controlling failure mode in the flexure series for these closure joint decks was a flexural failure within the precast section of the deck. In other words, the design goal was for the UHPC closure joint to have at least the same or superior flexural capacity. However, additional criteria, including ultimate capacity, were used when evaluating the overall performance of the closure joint decks.

Additionally, the shear testing sequence was conducted to primarily evaluate the deformation of the deck and closure joint area when it is subjected to shear. This

was included in the testing matrix in order to account for uneven distributions of live loads along decks. The shear test is designed to be the worst-case scenario, and the performance was evaluated considering several criteria, including failure mode and cracking size. Ideally, a shear failure beyond the anticipated shear force will occur. However, if another failure mode occurs past this failure load, it will also be successful as the capacity exceeds the anticipated.

4.2.2. Types of Specimens

One of the main goals of accelerated bridge construction is to optimize construction time. This is often achieved through utilizing precast panels as is with the project which is the topic of this report. The alternative to using precast panels is cast-in-place standard bridge decks. Therefore, it was important to include these standard bridge decks as the control against which the UHPC closure joint specimens would be evaluated.

As previously stated, accelerating the construction time is an essential objective for this research project. This essential goal was the ultimate factor that shaped the testing matrix. After an extensive literature review, it was decided that the UHPC closure joint specimens would be tested in the short term and long term. The time at which short-term was defined was 24 hours after the time at which the joint was cast. Less time could not be achieved due to the material properties of the UHPC at such an early stage. The long-term specimens were defined at any time past the time at which the UHPC closure joint reached 28 days.

4.2.3. Types of UHPC

Following the extensive testing on numerous UHPC mixes conducted by the research team, two mixes were chosen for the large-scale testing program. Numerous factors, including strength and durability, were considered in the Materials Laboratory Testing Program. Once this testing program was completed, it was decided to use one proprietary mix and one non-proprietary mix for the large-scale testing program.

The proprietary mix UHPC-P2-2 was selected due to its overall performance as well as it is one of the most commonly used proprietary mixes. UHPC-N3-2 was selected because it was a high-performing, non-proprietary mix that used locally available materials that were easily accessible.

4.2.4. Testing Matrix

The comprehensive testing program developed by the research team included a total of ten large-scale structural tests as shown in Figure 4.1; five test specimens were

to be loaded in flexure, and five test specimens were to be loaded in shear. There were three specimen types: the monolithic control specimen, the proprietary UHPC joint with straight bars, and the non-proprietary UHPC with straight bars. Each UHPC joint detail was to be tested in the short-term (approximately 24 hours) and long-term (past 28 days).

Loading Type	Test ID	Joint Detail		
		Control (Monolithic)	Proprietary UHPC	Non-Proprietary UHPC
	Design Basis	Standard Bridge Deck Detail	Straight Bar w/ Shear Key	Straight Bar w/ Shear Key
Flexure	F1			
	F2-S			
	F2-L			
	F3-S			
	F3-L			
Shear	S1			
	S2-S			
	S2-L			
	S3-S			
	S3-L			

Figure 4.1 Large-Scale Testing Matrix

A nomenclature was developed to define the short-term and long-term specimens. These are denoted by the -S or -L in the testing ID (see Figure 4.1).

4.3. Specimen Preparation

4.3.1. Specimen Design

The design of the closure joint was based on the joint detail that was used in the Farwell Creek Bridge in the Amarillo District as shown in Figure 4.2 (Texas Department of Transportation, 2020). The development of this detail was inspired by the numerous papers published by Dr. Benjamin Graybeal at the Federal Highway Administration and specific design characteristics follow findings and recommendations from said papers. The non-contact straight bar lap splice design consideration stems from the findings published by Graybeal in the paper titled "Bond Behavior of Reinforcing Steel in UHPC" (Graybeal, 2014b). This paper found that a non-contact lap splice demonstrated greater bond behavior with UHPC, likely due to the greater amount of surface area. A greater side cover, increased embedment length, clear bar spacing, and higher UHPC compressive strength are all factors that increase the bond strength of the UHPC to the reinforcement. The bond strength ultimately defines the performance and failure of the panels;

therefore, the research team considered the recommendations of the paper during the design of the closure joint as well as during the development of the test matrix.

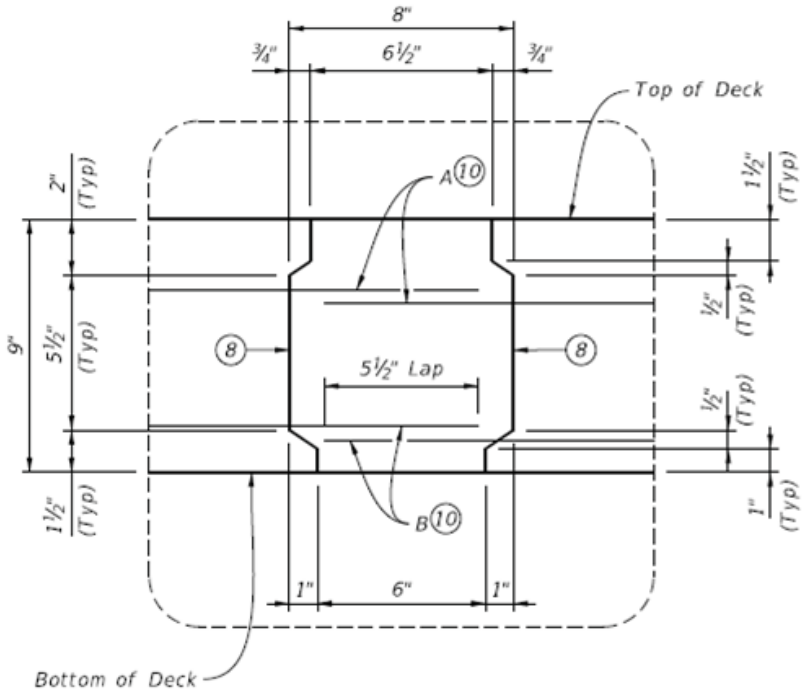

Figure 4.2 Straight Bar Closure Joint Detail from Farwell Creek Bridge

The 5 ¾ inch embedment length and 6-inch joint area design choices derive from the Technical Notes published by Dr. Graybeal titled "Design and Construction of Field-Cast UHPC Connections" (Greybeal, 2019). The design embedment length exceeds the recommended eight times the bar diameter which for #5 reinforcement requires 5-inches. A 6-inch minimum joint area was implemented in several projects highlighted within the technical report and as the basis of the 6-inch joint design choice for the closure joint specimens. This design consideration would allow for simplified reinforcement details, as well as minimize costs associated with a greater volume of UHPC.

Finally, the shear key geometry and surface preparation design considerations stemmed from two main sources. Firstly, the report titled "Performance of Grouted Connections for Prefabricated Bridge Deck Elements" by Dr. Graybeal and Dr. Zachery Haber yielded further information on improving the UHPC-Precast deck bonding (Haber & Greybeal, 2018). Following the findings that the surface preparation was essential for optimized performance; the detail included a note that called for exposed aggregate or a surface preparation of at least $1/8^{th}$ inch indentation. This paper also stated that the geometry of the shear key did not significantly change the resulting capacity. Thus, it was decided to follow the

geometry of the Farwell Creek Bridge in the Amarillo District (Texas Department of Transportation, 2020). Figure 4.3 shows the shear key detail that was evaluated in Task 4, and Figure 4.4 shows the precast panel design, which mirrors a standard deck design. The panel had a width of 3 feet and a length of 8.5 feet, being reinforced with number four longitudinal reinforcement spaced at 9 inches. In the transverse direction, the deck was reinforced with number 5 reinforcement, also spaced at 9 inches. Figure 4.5 illustrates the monolithic control specimen detail, which is a standard 9-inch-deep deck panel with 9-inch rebar spacing.

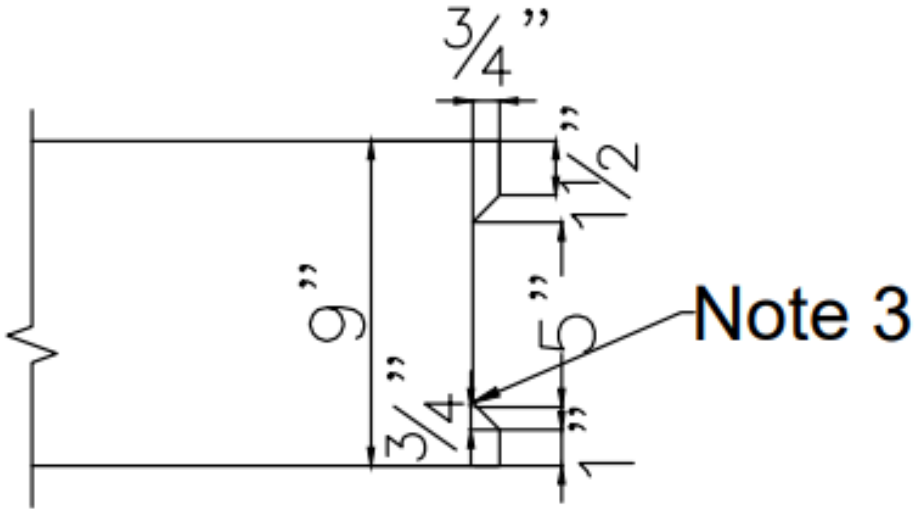

Figure 4.3 Shear Key Detail

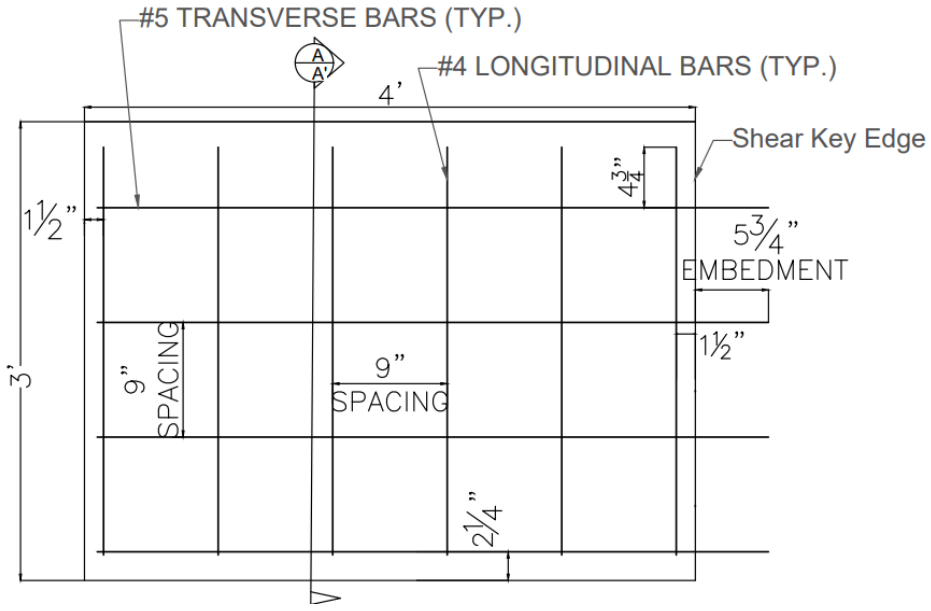

Figure 4.4 Precast Panel Detail for Closure Joint Specimens

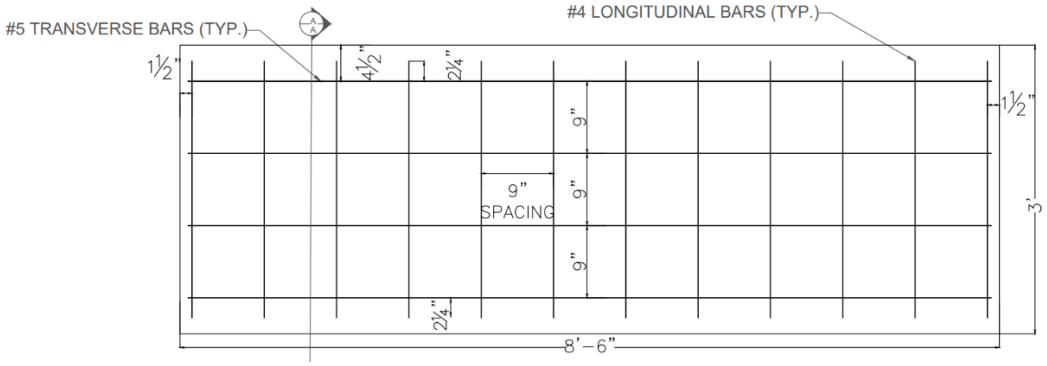

Figure 4.5 Monolithic Control Specimen Detail

The concrete cover for all the specimens and bar spacing were the same at a 3-inch top cover and a 1 ¼ inch cover for the bottom. This control specimen had an anticipated negative moment capacity of 690 kip-inch and a 1070 kip-inch positive moment capacity.

4.3.2. Precast Panel Fabrication

For the fabrication of the monolithic control specimen and the precast deck portions, the research tasked a pre-caster to ensure the specimens were comparable to those typically placed in the field. Site visits to inspect the formwork and rebar placement were conducted to confirm the joint detail was properly constructed. Figures 4.6 & 4.7 show some of the panels cast during the first site visit. The precasters constructed the formwork using plywood and wooden members, the shear key indentation was fashioned using a foam inset that was cut at the angles needed to satisfy the detail provided by the research team.

Figure 4.6 Closure Joint Deck Specimens Prior to Cast

Figure 4.7 Closure Joint and Control Specimens Post Cast

Cylinders were also cast alongside each pour to verify the compressive strength of concrete per ASTM C39 on test days. These tests found that the compressive strength of the precast sections was approximately 11 ksi.

L/D	Local	Stress
1.984	124,365	9,886
1.97	147,255	11,789
1.955	142,465	11,382

Figure 4.8 Average Strength of Concrete per ASTM C39

Rebar coupons were also collected, the tensile strength per ASTM A370 showed that the rebar tensile strength is approximately 66 ksi, which is typically the case.

4.3.3. UHPC Joint Preparation and Casting

At the time of specimen delivery, the surface preparation (see Figure 4.9) was inspected and the research team determined the surface roughness to be inadequate in order to ensure the preferred surface bonding. To remediate this, it was decided

to achieve a surface profile of 7-9 according to the ICRI Surface Profile Standards. This was achieved through the usage of a Rotary Hammer and Bush Bit, which was determined to be the typical surface roughening method used by contractors. Figure 4.10 shows the surface roughness following this method, and Figure 4.11 shows the ICRI Surface Profiles (ICRI Standard 310.2) that were referenced when evaluating the roughness.

Figure 4.9 & Figure 4.10 Shear Key Surface Profiles Before (Left) and After (Right) Surface Roughening

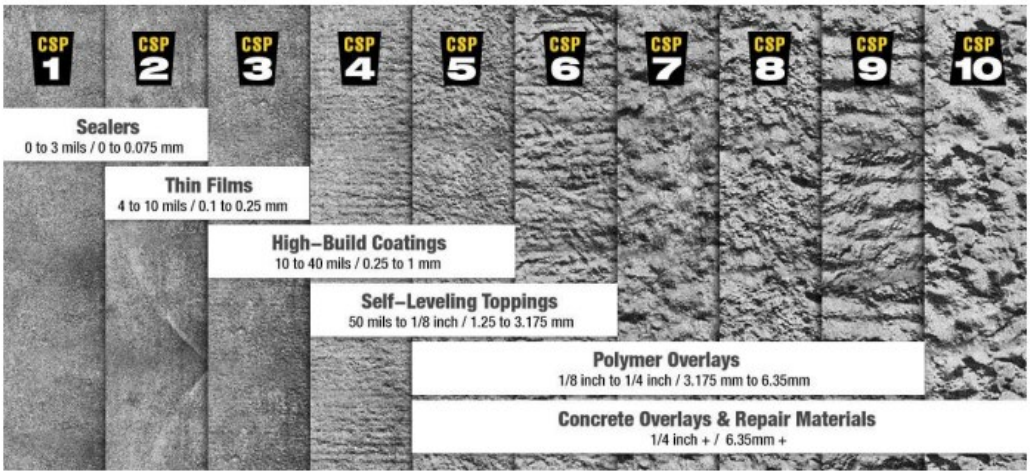

Figure 4.11 ICRI Surface Profiles

The fabrication of the UHPC joint area differed based on the time designation of the specimen. Short-term specimens were cast in place in order to optimize the testing process. Long-term specimens were cast in locations where the specimens could be undisturbed for a long period of time. The mixing process for all specimens involved mixing the UHPC in a tilting drum mixer then transferring the mix into buckets for easy transfer to the joint area. Figure 4.12 shows the closure joint cast for a long-term specimen with a nonproprietary mix.

Figure 4.12 UHPC Closure Joint Cast

Figures 4.13 and 4.14 show the joint area before and after UHPC was cast. This particular case was for the non-proprietary mix to be tested at 24 hours. The precast joint interface was prepared to saturated-surface-dry or SSD as it aids in the bonding between the UHPC and Precast sections. Pipe clamps were used to hold the formwork in place and allowed for the formwork to be removed promptly to optimize the test preparation. To ensure that formwork was removed at the earliest time, a maturity sensor was embedded within the joint. This maturity sensor is the white cable seen in the joint area prior to the cast and provided compressive strength of the UHPC at updates of 15-minute intervals. Formwork was removed once a minimum compressive strength of 4,000 psi was achieved, which allowed for adequate time to instrument the specimens prior to the start of the test at 24 hours.

Figure 4.13 & 4.14 UHPC Closure Joint Before (left) and After Cast (right)

4.4. Test Setup and Instrumentation

4.4.1. Test Frame

4.4.1.1. Flexure Test Setup

The flexure testing involves a four-point bending test frame designed to maximize the moment through the UHPC joint area. The 6-inch closure joint (shaded dark gray) is placed at the midspan between load points and within a constant moment region in order to achieve no shear within the closure joint area. The test frame consisted of a portal frame and a ram with a capacity of 100 kips was attached to the cross beam through a metal plate and rod system and was used to apply load transferring through a spreader beam to both edges of the specimen. Load points were 30 inches from the supports making a moment arm of 30 inches; therefore delivering a constant moment of 30 times the applied load.

Figure 4.15 shows the closure joint as a rectangle, this does not reflect the joint detail and is only to illustrate the location. The closure joint specimens are to be tested in a negative moment to allow for better joint interface crack monitoring. The pedestal-type testing system allows the closure joint to be cast in place, which simulates in-field conditions. The flexure testing frame optimizes the

instrumentation process, which benefits the short-term testing schedule. Figure 4.16 shows specimens placed within the test frame prior to the UHPC cast.

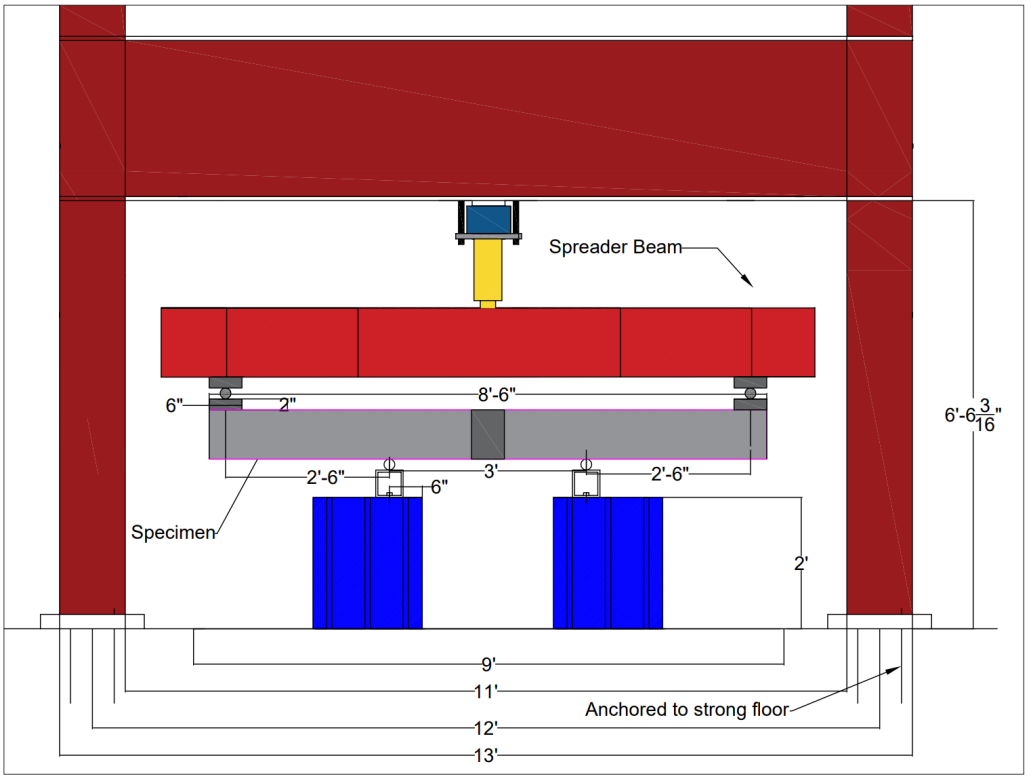

Figure 4.15 Flexure Test Setup

Figure 4.16 Monolithic Control Specimen in Flexure Test Setup

4.4.1.2. Shear Test Setup

The shear testing frame was designed in order to optimize the testing procedure and instrumentation process. As mentioned earlier in this chapter, the shear tests are to be conducted to primarily evaluate the deformation of the deck and closure joint area when it is subjected to shear. Once again the pedestal-type testing system was used in order to optimize the short-term casting as well as simplify the instrumentation. The shear test is designed with the shear area of interest is 22 inches in order to achieve the worst-case scenario and maximize the shear force within the UHPC closure joint. Figure 4.17 shows the shear testing setup. Figure 4.18 shows a UHPC joint specimen within the shear loading frame prior to loading.

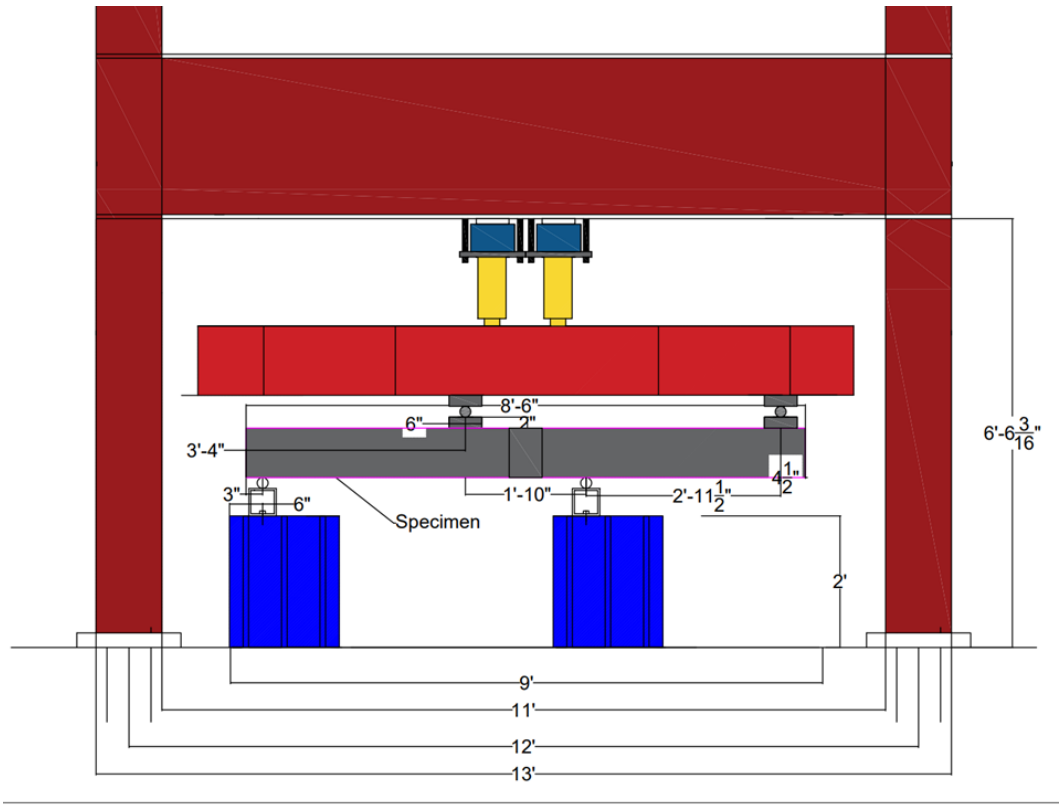

Figure 4.17 Shear Test Setup

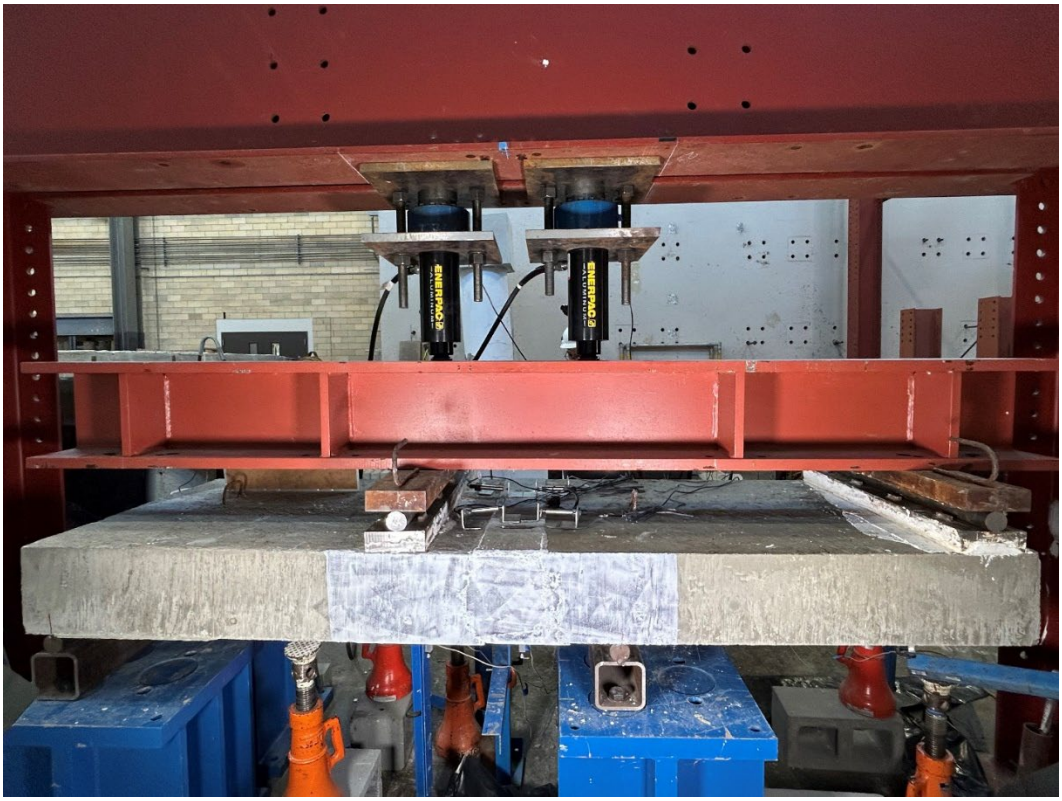

Figure 4.18 UHPC Closure Joint Specimen in Shear Test Setup

4.4.2. Instrumentation

4.4.2.1. Flexure Testing Instrumentation

The flexure series focused on evaluating the performance of the closure joint under a constant moment region. Concrete surface gauges, embedded steel reinforcement gauges, maturity sensors, linear variable differential transformers (LVDTs), and linear potentiometers (LPOTs) were being used to monitor joint interface opening, reinforcement yielding, deck deflections, and concrete strength. The embedded steel reinforcement gauges are located on the center rebar on both precast panels. Surface gauges are attached directly along the center line as well as 9 inches off the center on the precast panels. These surface gauges are located on both the top and bottom of the specimen. The LVDTs were placed over the joint interface opening to monitor the opening of the interface with great accuracy. The LPOTs were placed directly below the load points as well as along the center of the panel in the joint area. The locations of all of these sensors are shown in Figures 4.19 and 4.20 below. A load cell located at the hydraulic ram monitored the applied load so that the applied moment could be calculated at any time during the test.

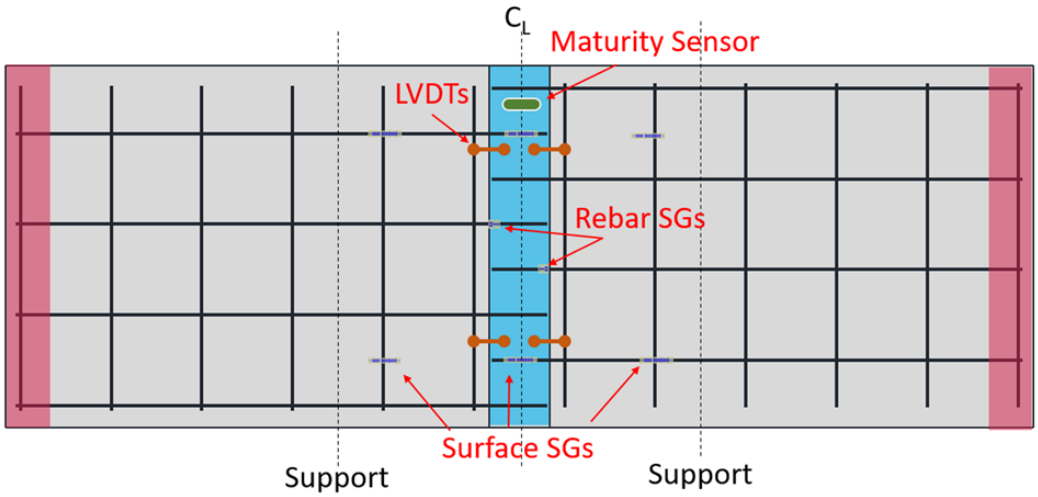

Figure 4.19 Flexure Series Instrumentation

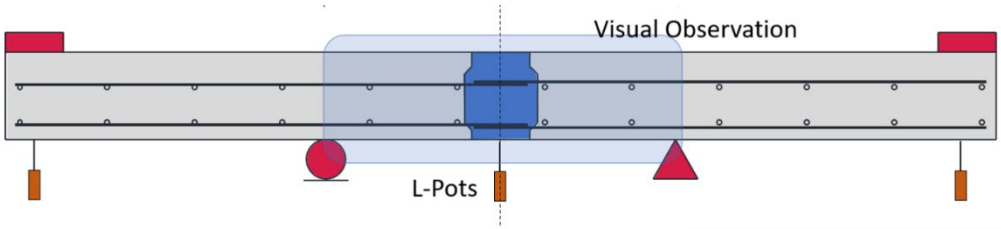

Figure 4.20 Linear Potentiometer Placement for Flexure Series

4.4.2.2. Shear Testing Instrumentation

The shear series focused on evaluating the performance of the closure joint under a high shear force. Concrete surface gauges, embedded steel reinforcement gauges, maturity sensors, linear variable differential transformers, and linear potentiometers are being used to monitor joint interface opening, reinforcement yielding, deck deflections, and concrete strength. The embedded steel reinforcement gauges are located on the center rebar on both precast panels. Surface gauges are attached directly along the center line of the closure. These surface gauges are located on both the top and bottom of the specimen. Linear variable differential transformer sensors are placed over the joint interface opening to monitor the opening of the interface with great accuracy. The linear potentiometers are placed directly below the load points as well as along the center of the panel in the joint area. The locations of all of these sensors are shown in Figures 4.21 and 4.22 below. A load cell located at the hydraulic ram monitors the applied load so that the applied shear and moment forces can be calculated at any time during the test.

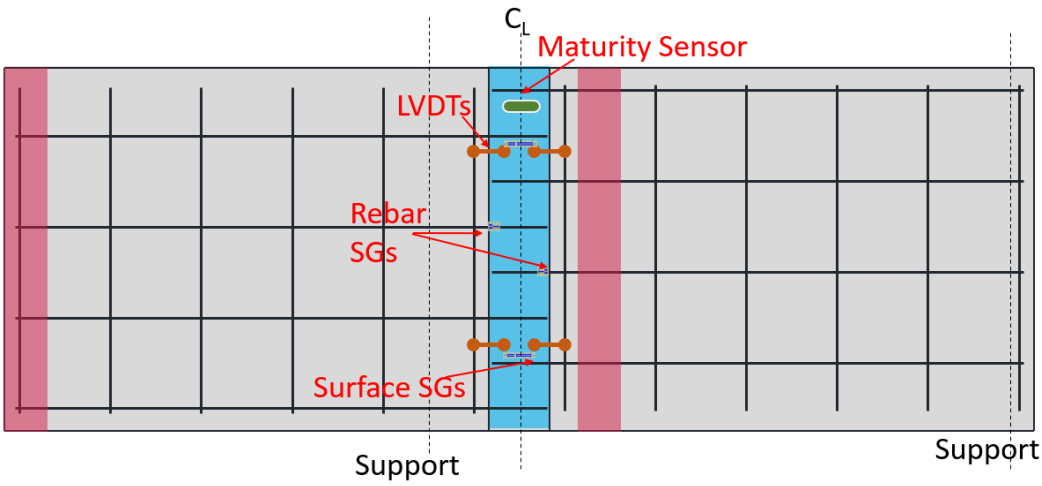

Figure 4.21 Shear Series Instrumentation

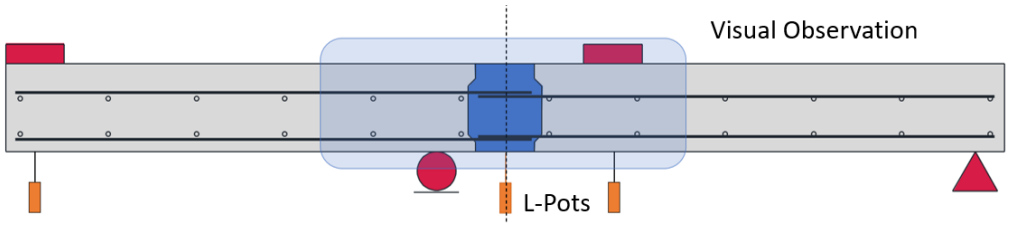

Figure 4.22 Linear Potentiometer Placement for Shear Series

4.5. Test Results

4.5.1. Flexure Series

4.5.1.1. Monolithic Control Specimen

The flexure series began with the testing of the monolithic control specimen. This control specimen had an anticipated negative moment capacity of 690 kip-inch or a 46-kip total center load. The central load was applied in 10 increments of 6-7 kips. Figure 4.23 shows the monolithic control specimen at an applied load of 0 kips, but a total load of 2 kips, including the spreader beam and metal loading plates. When approaching an applied load of 28 kips the specimen displayed a sudden flexure crack opening near a support and a load drop of approximately 8 kips. When approaching an applied load of 26 for a second time, this behavior was repeated with the crack forming by the other support. At formation, these cracks were 0.008-0.016 inch. Figure 4.24 shows the cracks at an applied load of 29.44 kips, which was after a third attempt to achieve a 30 kip applied load.

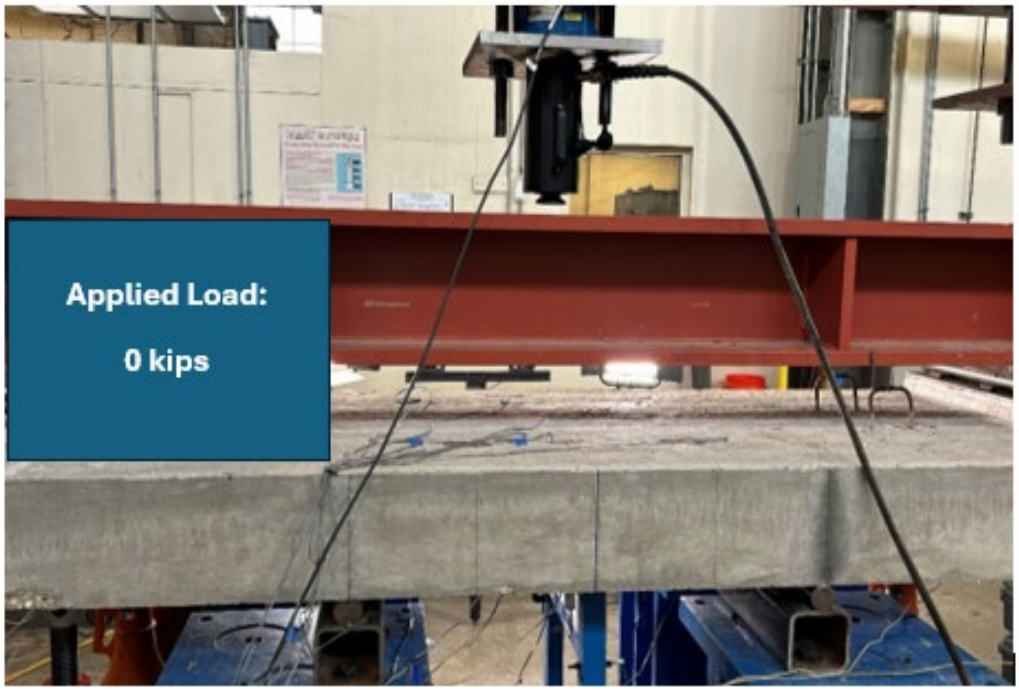

Figure 4.23 Control Specimen at 0 kips Applied Load

Figure 4.24 Control Specimen at 29.44 kips Applied Load

During each of these crack formations, the deflections measured at the edge load points jumped by approximately 0.08 inch at the side where the crack formed; by the second crack formation, the deflections became essentially identical. The ultimate capacity of the monolithic control specimen was at an applied load of 44 kips or an actual moment of 690 kip-in. The failure type for the control specimen was flexural or concrete crushing at the support. Figures 4.25 and 4.26 show the specimen at failure as well as the concrete crushing.

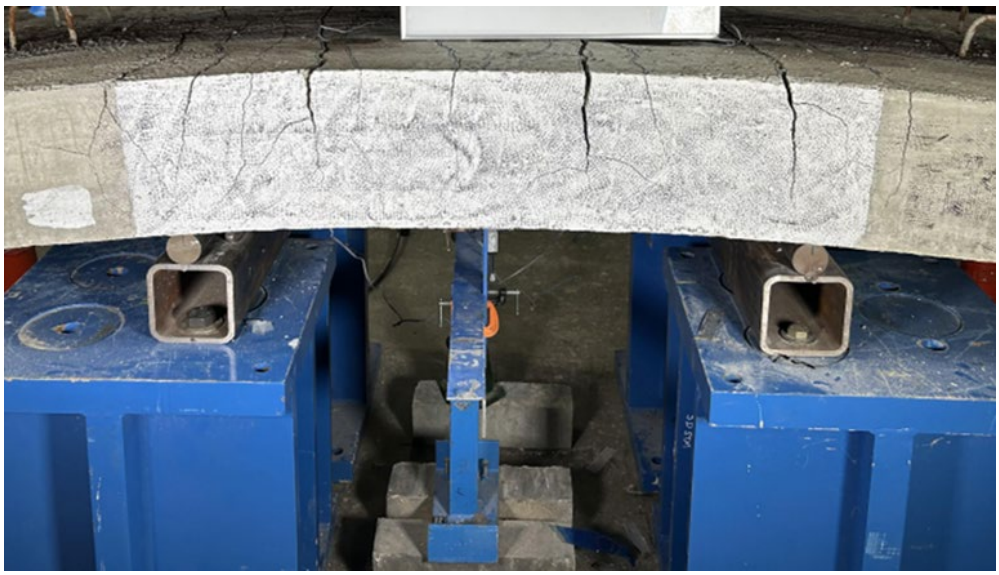

Figure 4.25 Control Specimen at Failure

Figure 4.26 Control Specimen Crushing

4.5.1.2. Short-Term Specimens

The short-term specimens were tested 24 hours after the cast of the UHPC closure joint. At 24 hours, the proprietary mix had a compressive strength of 12 ksi, and the non-proprietary mix had a compressive strength of 8 ksi. Both specimens were loaded in the same loading increments as the monolithic control specimen. At an applied load of approximately 20 kips for the proprietary mix and 23 kips for the nonproprietary deck, the same crack formation pattern occurred at the support, and then a load drop was recorded. The proprietary mix applied load dropped 3 kips in both instances, and the non-proprietary mix applied load dropped approximately 4 kips. The largest cracks, however, were located at the joint interface as it was opening more at each load step. The proprietary mix achieved a maximum applied load of 39 kips with an ultimate moment capacity of 615 kip-inches. Figures 4.27 and 4.28 show the joint section of both mixes at their associated failure points.

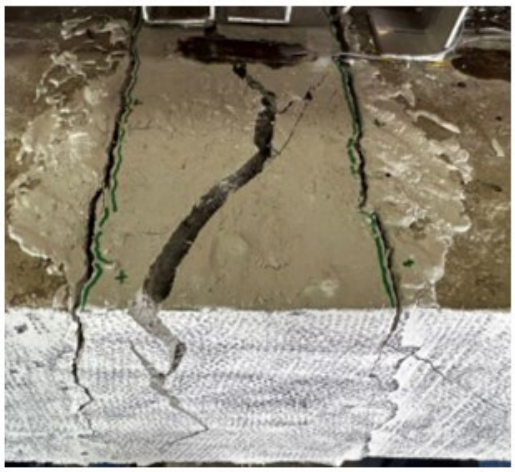

Figure 4.27 & 4.28 Proprietary mix closure joint at failure (left) & non-proprietary closure joint at failure (right)

4.5.1.3. Long-Term Specimens

The long-term specimens were tested at more than 28 days post the cast of the UHPC joint. At the time of the test, the compressive strength of the UHPC proprietary mix was 22.5 ksi, and the compressive strength of the non-proprietary mix was 18 ksi. As in the monolithic control specimen as well as the short-term specimens, the same cracking pattern occurring over the supports occurred. This pattern occurred at an applied load of 22 kips for the proprietary mix and at an applied load of 26 kips for the non-proprietary mix. The largest cracks were once again at the interface. The proprietary mix achieved a maximum applied load of 41 kips with an ultimate moment capacity of 645 kip-inches. This is approximately 93% of what the monolithic control specimen achieved. The non-proprietary mix

failed at an applied load of 40 kips with an ultimate capacity of 630 kip-inches. This failure was approximately 91% of the monolithic control specimen. The proprietary mix exhibited a flexural crushing failure within the precast panel. However, the non-proprietary mix exhibited an interesting failure of both pullout and flexure-crushing at the same time. Figures 4.29, 4.30, and 4.31 show the failure types.

Figure 4.29 Proprietary Mix Crushing

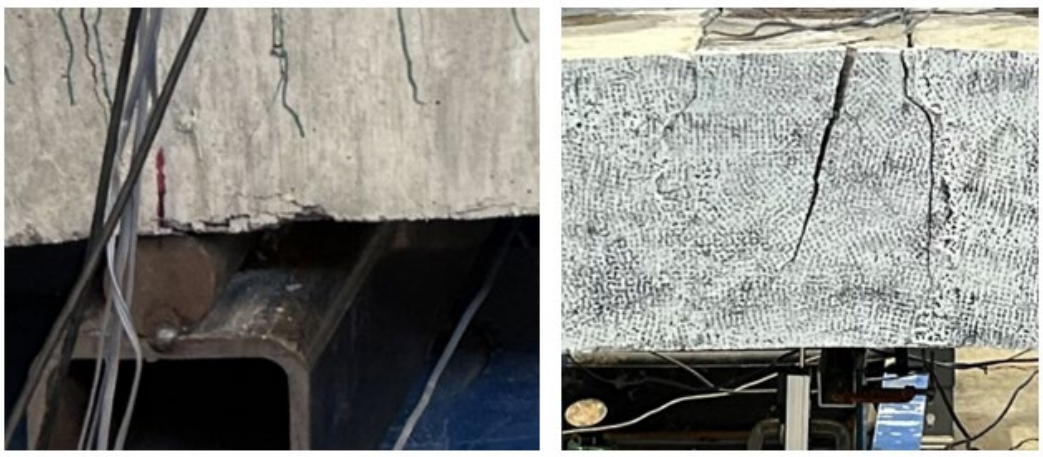

Figure 4.30 & 4.31 Non-Proprietary mix closure joint at failure (left) & (right)

4.5.2. Shear Series

4.5.2.1. Monolithic Control Specimen

The shear series began with the testing of the monolithic control specimen. This control specimen had an anticipated shear failure when the area of interest achieved a shear force of 62 kips according to ACI 318-19 Table 22.5.5.1 and AASHTO Bridge Design Manuel 9th ed. Section 5.7.3.3. The anticipated shear failure was calculated using 11 ksi for the concrete compressive strength and 66 ksi for the steel tensile strength. The load was applied in 10 increments of approximately 10 kip. During the loading stages closer to the theoretical shear failure, the load was applied slower and stalled halfway to check for significant cracking and continued if no major changes were detected. As in the flexure series, the true load was 2 kips greater than the recorded due to the self-weight of the spreader beam and metal loading plates. No cracking was observed until the 5th load step of where 55 kips were applied and the shear force through the area of interest was 33.6 kips. The first crack formed at the support on the edge of the shear area and was 0.002-0.025 inch in size. Figure 4.32 shows the crack formation at this loading step.

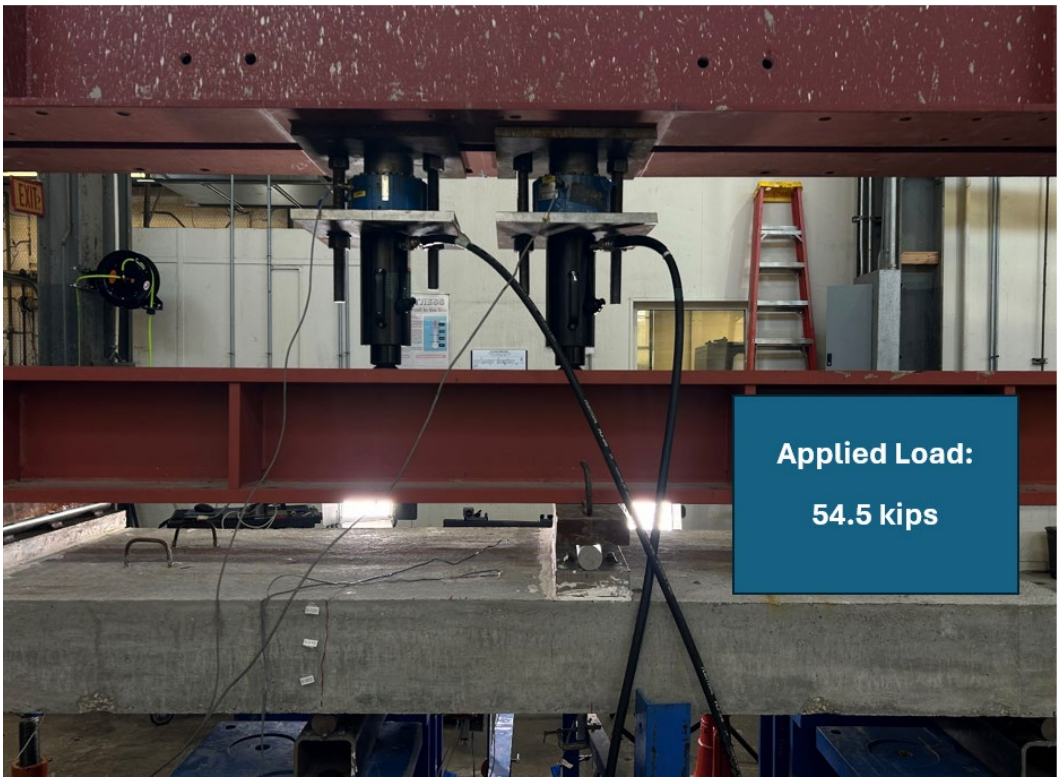

Figure 4.32 Control Specimen at 54.5 kips Applied Load

At the time of this crack formation, the deflection below the edge load point was 0.15 inches. The ultimate capacity of the monolithic control specimen was at an

applied load of 101.3 kips when the shear force was 62 kips within the shear interest area and the moment was 689.9 kip-inches outside this region when the loading system self weight was included. The failure type for the control specimen was flexural or concrete crushing at the support occurring outside the region of interest. Figures 4.33 and 4.34 show the specimen at failure as well as the concrete crushing.

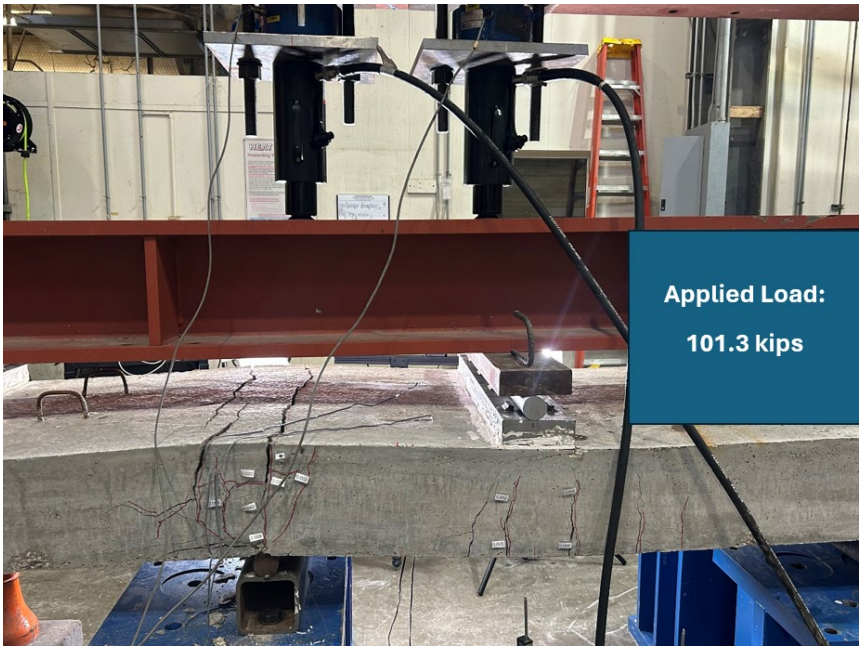

Figure 4.33 Control Specimen at Failure

Figure 4.34 Control Specimen Crushing

4.5.2.2. Short-Term Specimens

As in the flexural series, the short-term specimens were tested 24 hours after the cast of the UHPC closure joint. At 24 hours, the proprietary mix had a compressive strength of 12 ksi, and the non-proprietary mix had a compressive strength of 8 ksi. Both specimens were loaded in the same loading increments as the monolithic control specimen. At an applied load of approximately 40 kips for the proprietary mix and 50 kips for the nonproprietary deck, the same crack formation occurred at the support as in the monolithic control specimen with crack sizes matching that of what the monolithic specimen experienced.

The ultimate capacity of the proprietary specimen was at an applied load of 105.4 kips when the shear force was 62 kips within the shear interest area, and the moment was 714.7 kip-inches outside this region when the loading system self-weight was included. The failure type for the proprietary specimen was flexural or concrete crushing at the support occurring outside the region of interest. Figures 4.35 and 4.36 show the specimen at failure.

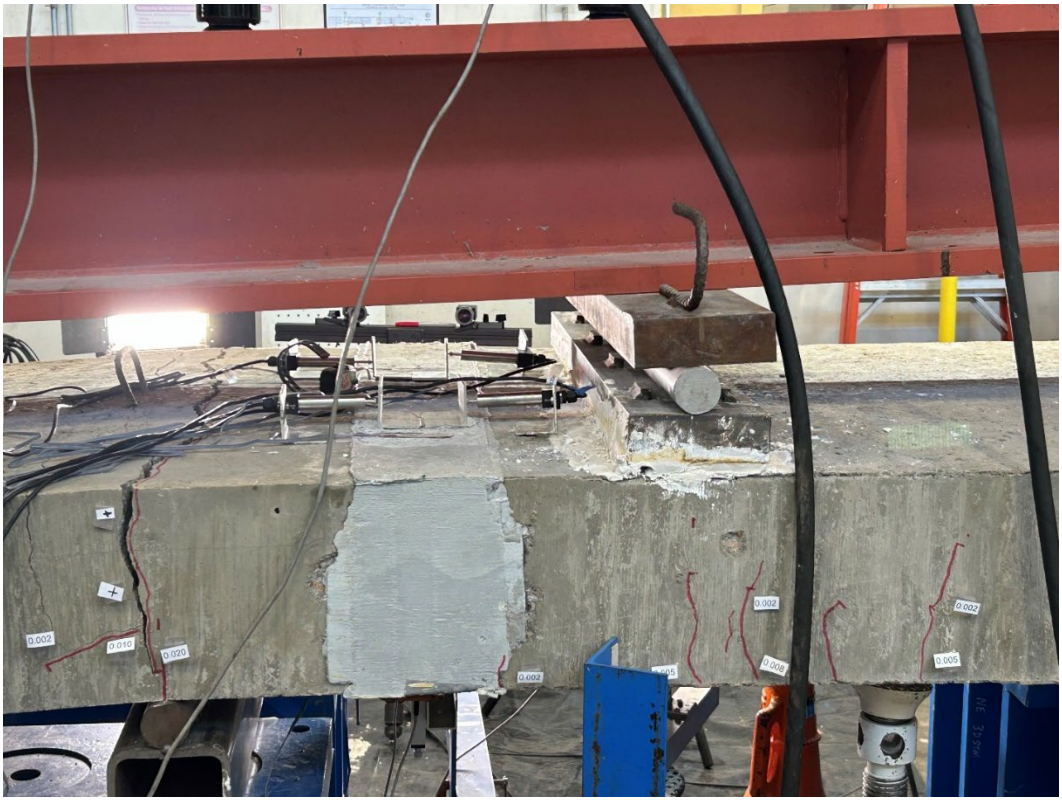

Figure 4.35 Proprietary Specimen at Failure

Figure 4.36 Proprietary Specimen at Failure

The ultimate capacity of the non-proprietary specimen was at an applied load of 85.3 kips when the shear force was 54.6 kips within the shear interest area, and the moment was 587.1 kip-inches outside this region when the loading system self-weight was included. The failure type for the non-proprietary specimen was a shear failure within the region of interest. Figures 4.37, 4.38, and 4.39 show the specimen at failure.

Figure 4.37 Nonproprietary Specimen at Failure

Figure 4.38 Support of Nonproprietary Specimen at Failure

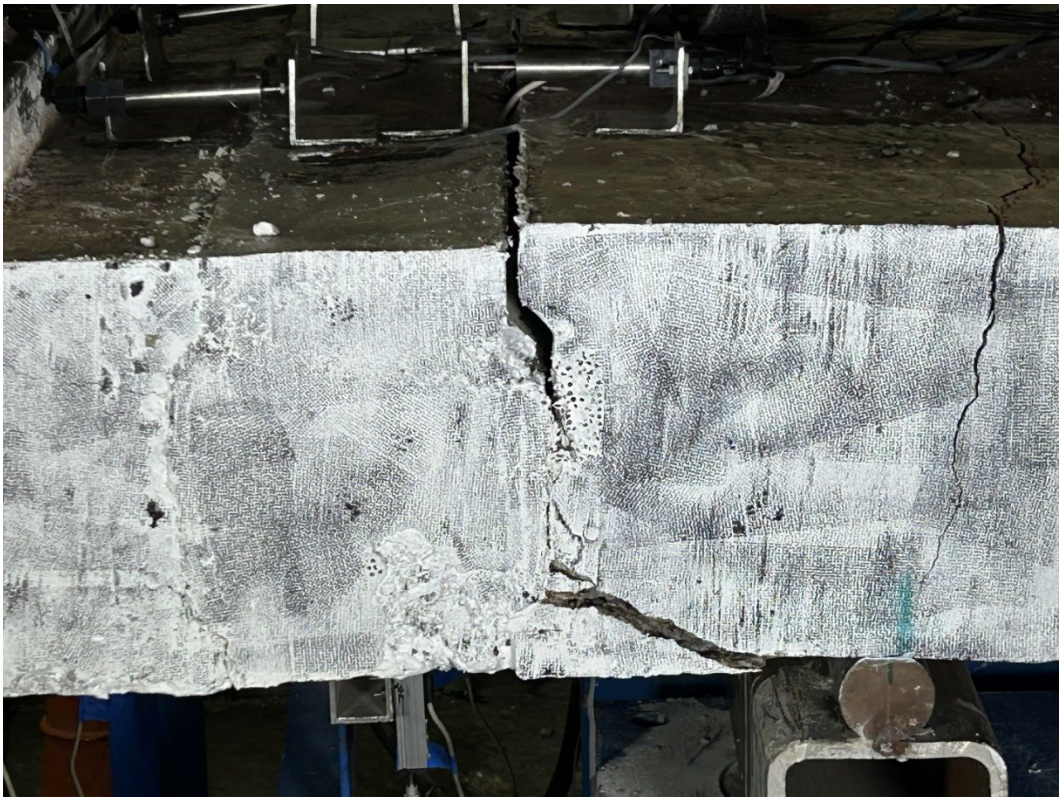

Figure 4.39 Nonproprietary Specimen at Failure

4.5.2.3. Long-Term Specimens

The long-term specimens were tested at more than 28 days post the cast of the UHPC joint. At the time of the test, the compressive strength of the UHPC proprietary mix was 24.8 ksi, and the compressive strength of the non-proprietary mix was 19 ksi. As in the monolithic control specimen as well as the short-term specimens, the same cracking pattern occurring several load steps into the test occurred. This initial crack occurred at an applied load of 41 kips for the proprietary mix and at an applied load of 40 kips for the non-proprietary mix.

The ultimate capacity of the proprietary specimen was at an applied load of 120.4 kips when the shear force was 75.6 kips within the shear interest area, and the moment was 809.4 kip-inches outside this region when the loading system self-weight was included. The failure type for the proprietary specimen was flexural or concrete crushing at the support occurring outside the region of interest. Figures 4.40 and 4.41 show the specimen at failure.

Figure 4.40 Proprietary Specimen at Failure

Figure 4.41 Proprietary Specimen Crushing

The ultimate capacity of the non-proprietary specimen was at an applied load of 101.4 kips when the shear force was 62 kips within the shear interest area, and the moment was 690 kip-inches outside this region when the loading system self-weight was included. The failure type for the non-proprietary specimen was a shear failure within the region of interest as well as a flexure crushing at the support on the opposite side of the panel. Figures 4.42 and 4.43 show the specimen at failure.

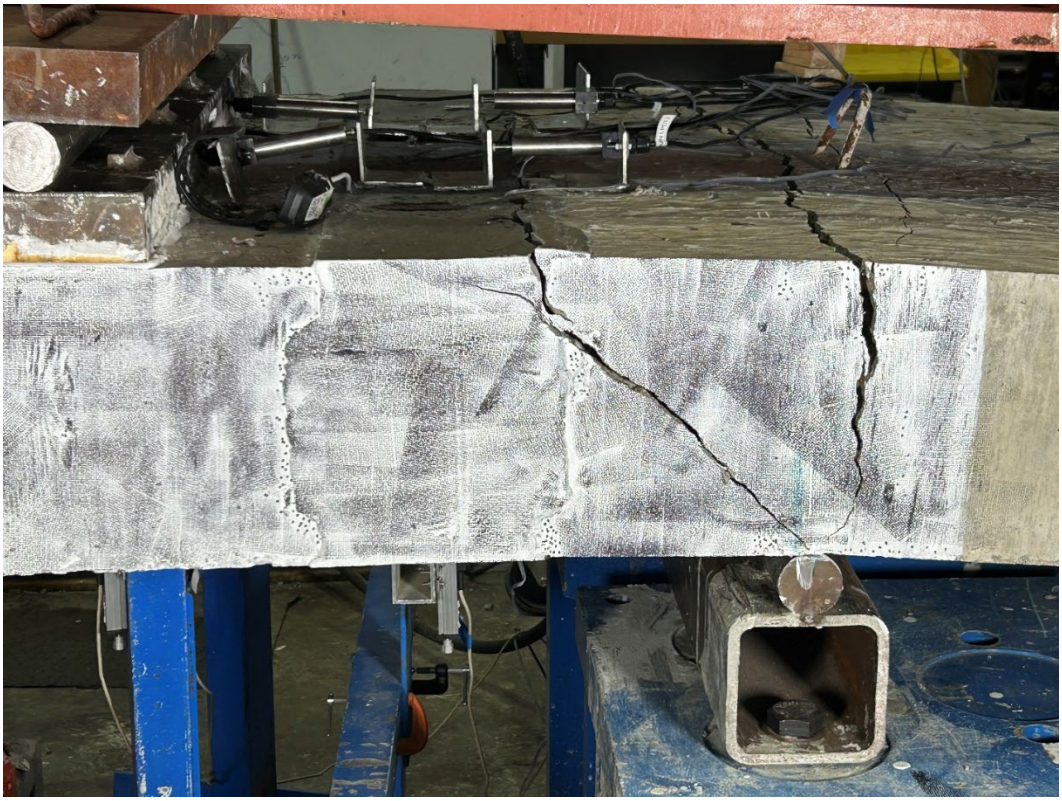

Figure 4.42 Non-proprietary Specimen at Failure

Figure 4.43 Non-proprietary Specimen Crushing

4.6. Data Analysis

4.6.1. Flexural Series Results

Figure 4.44 shows the load vs edge displacement for all the flexure series. The curves were cut off at approximately 2 inches when the LPOTs were removed for safety, and the test was resumed until the specimen failed. In the figure, it can be seen that all specimens behave in similar deflection patterns. Both 24-hour specimens achieve similar deflections at slightly lower applied loads; however, the behavior is essentially the same when compared to the other tests. Deflections at the time of the cracking behavior pattern that repeatedly occurred throughout all tests were roughly the same, and the point at which a 2-inch deflection was reached is also approximately the same. The only premature failure was that of the non-proprietary mix at 24 hours. This is also the only case in which the UHPC compressive strength was less than that of the precast section. Both short-term specimens exhibited pull-out failure due to the age of the closure joint section. Table 4.1 summarizes the compressive strength of the precast sections and UHPC at the time of the test. Figure 4.44 shows the load vs edge displacement for all the flexure series.

Table 4.1 Compressive Strength on the Test Day

Mix	Compressive Strength (KSI)
Control & Precast	11
Mix A-24	12
Mix A-28	22.5
Mix B-24	8
Mix B-28	18

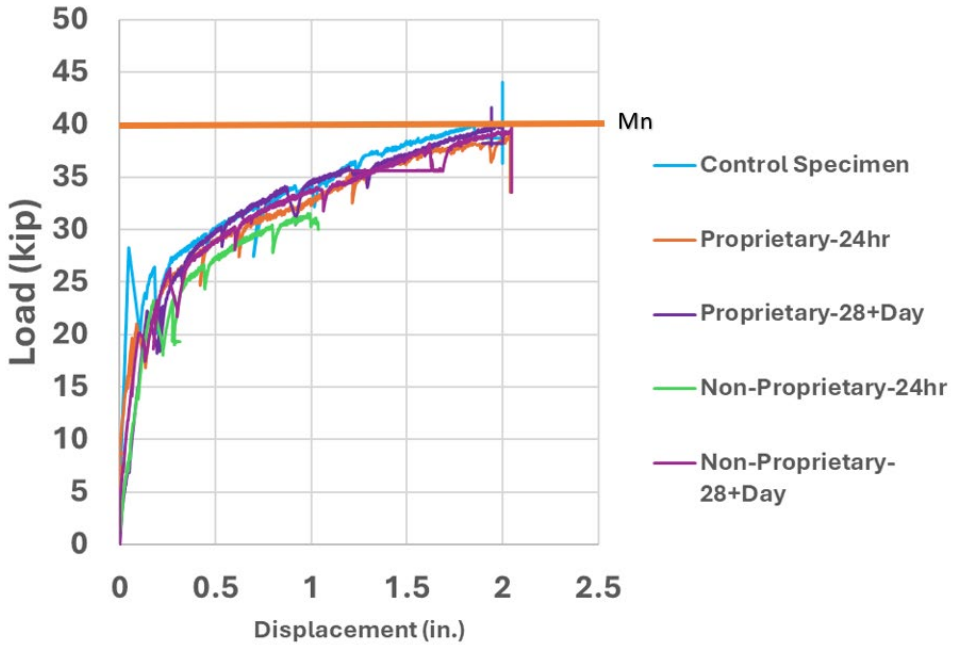

Figure 4.44 Load vs Edge Displacement

The nominal moment or Mn, as seen in Figures 4.44 and 4.45, was calculated using the material properties from testing listed prior and was calculated according to ACI 318-19 sections 10.2 and 10.3. A concrete compressive strength of 11 ksi was used and a steel yield strength of 66 ksi. This calculation accounted for the monolithic control specimen capacity and was the value the closure joint specimens were verified to. The nominal moment was 600 kip-inches. The ultimate capacity of the specimens is summarized in Figure 4.45 below. Overall, the proprietary mix achieved nearly 90% of the monolithic control specimen in both cases, and the non-proprietary mix achieved 91% in the long term, but the short-term only achieved 72%. The horizontal line in Figures 4.44 and 4.45 represents the nominal capacity of the monolithic control specimen as as seen by all of the closure joint specimens except for the premature failure case, where the nominal capacity was exceeded.

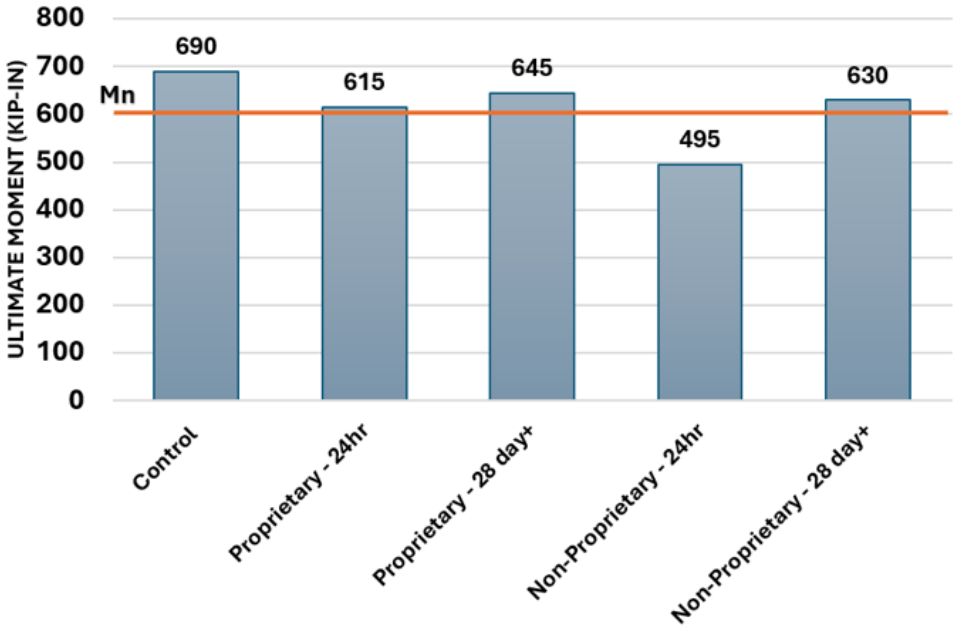

Figure 4.45 Ultimate Moment Capacity (Kip-in)

Figure 4.46 shows the crack sizes and locations for the monolithic control specimen at the time of failure. Full sequence crack mapping is located in Appendix B.

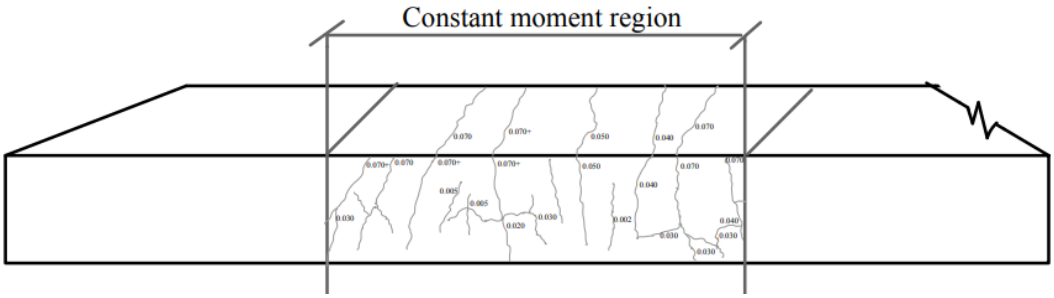

Figure 4.46 Crack Mapping for Monolithic Control Specimen at Failure

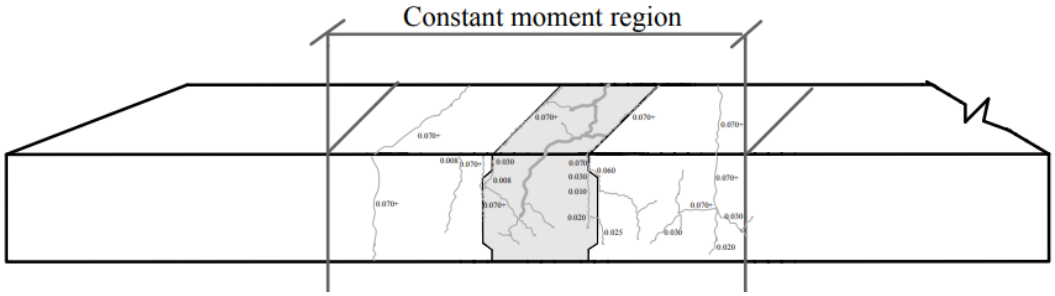

Figure 4.47 Crack Mapping for Proprietary Short-Term Specimen at Failure

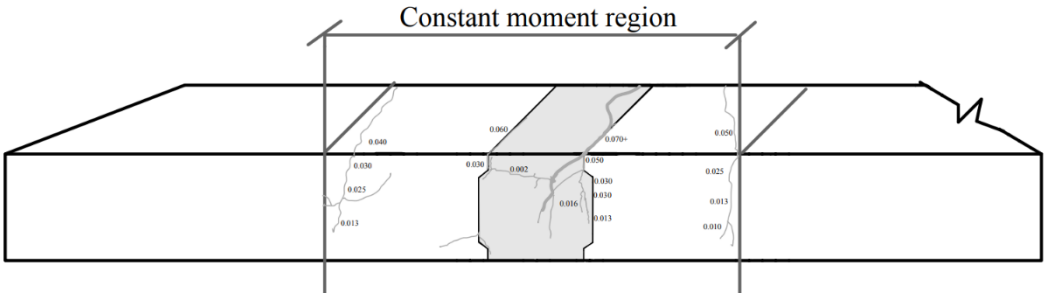

Figure 4.48 Crack Mapping for Non-Proprietary Short-Term Specimen at Failure

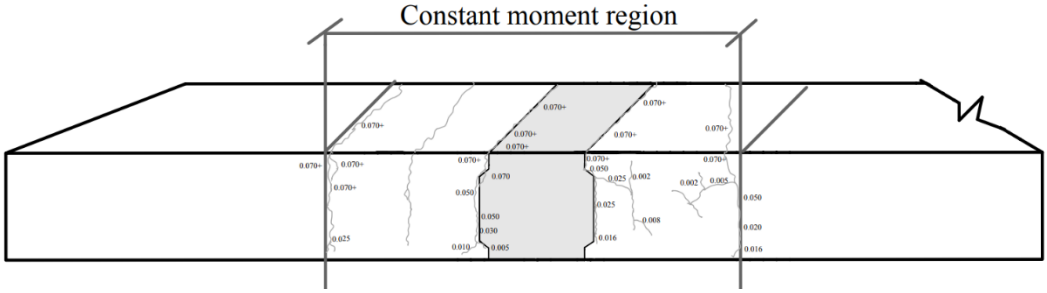

Figure 4.49 Crack Mapping for Proprietary Long-Term Specimen at Failure

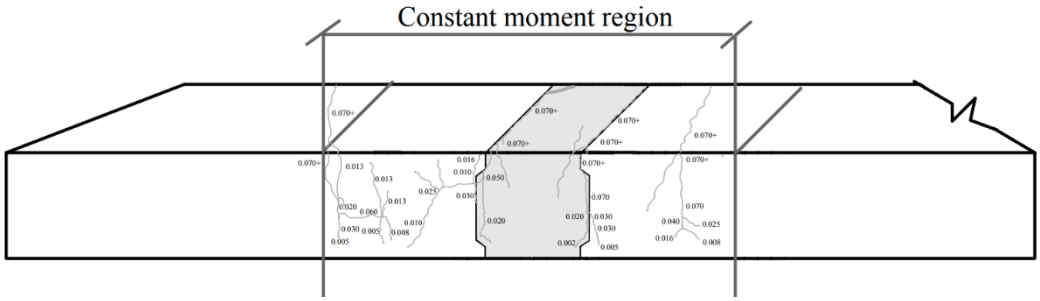

Figure 4.50 Crack Mapping for Non-Proprietary Long-Term Specimen at Failure

The final cracking patterns, as well as the cracking formation patterns for all of the specimens, were essentially the same. The premature failure specimen, as shown in Figure 4.48, however, has smaller crack widths due to this early failure. However, what is seen is that the specimens exhibit the same behavior as the monolithic panel, which shows that continuity is achieved. The interface opening, however, is the main difference between the monolithic control specimen and the closure joint specimens. The monolithic control specimen exhibited cracks greater than 0.070 inches in 3 locations within the constant moment region. However, the closure joint specimens experienced the interface opening of greater than 0.070 inches plus two other locations in all cases except one, which was the premature failure case.

4.6.2. Shear Series Results

The applied load versus displacement data shows that all specimens behave in similar deflection patterns. Both 24-hour specimens achieve similar deflections at slightly lower applied loads; however, the behavior is essentially the same when compared to the other tests The only premature failure was once again that of the non-proprietary mix at 24 hours. This is also the only case in which the UHPC compressive strength was less than that of the precast section. Table 4.2 summarizes the compressive strength of the precast sections and UHPC at the time of the test. Figure 4.51 shows the load vs edge displacement for all the shear series.

Table 4.2 Compressive Strength on the Test Day

Mix	Compressive Strength (KSI)
Control & Precast	11
Mix A-24	12
Mix A-28	24.8
Mix B-24	8
Mix B-28	19

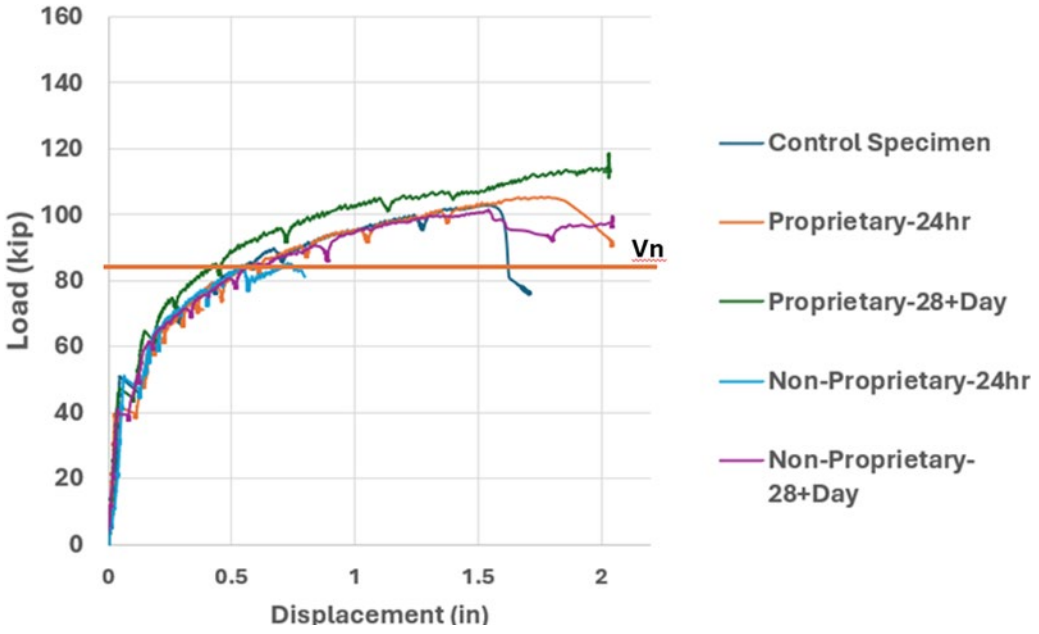

Figure 4.51 Load vs Edge Displacement

The maximum shear force is summarized in Figure 4.52. The nominal shear capacity for the monolithic control specimen was calculated using the material properties from testing shown in chapter 3 and was calculated according to ACI 318-19 table 22.5.5.1 and AASHTO Bridge Design Manuel 9th ed. Section 5.7.3.3. Overall, the proprietary mix exceeded the monolithic control specimen in both cases, and the non-proprietary mix had the same moment capacity during the long-

term shear testing as the monolithic control specimen and exceeded the nominal shear capacity of the control specimen in the short-term test. Shear failure did not occur in the long-term cases due to the moment capacity being reached prior, thus showing that the shear strength exceeded that of what was reached.

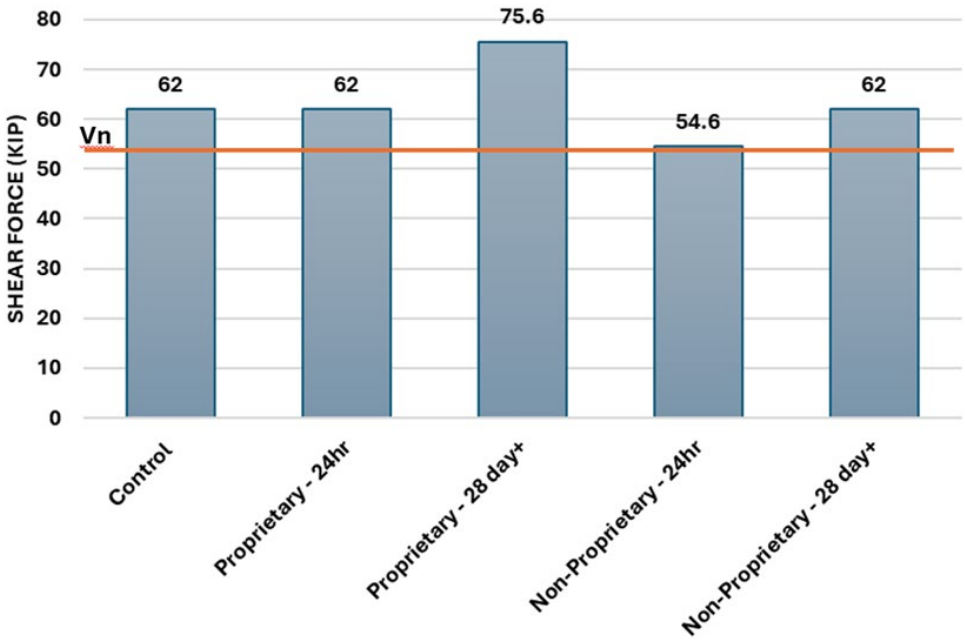

Figure 4.52 Maximum Shear Force (Kip) at Time of Failure

Figure 4.53 shows the crack sizes and locations for the monolithic control specimen at the time of failure. The failure mode for this test was a flexure failure. Full sequence crack mapping is located in Appendix C.

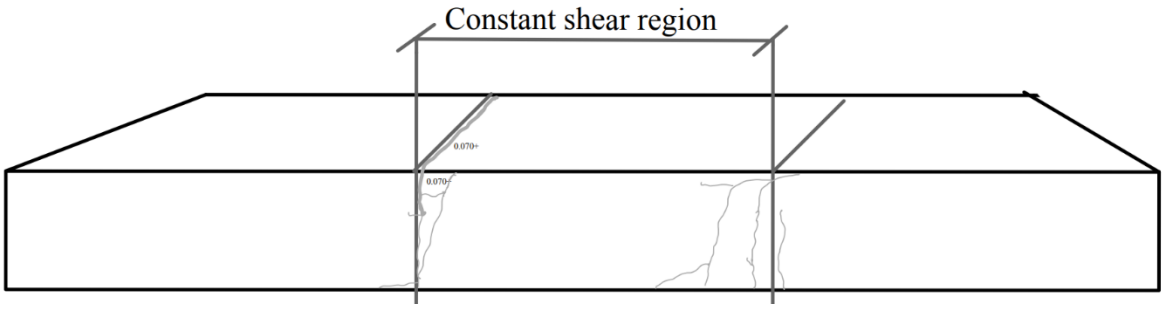

Figure 4.53 Crack Mapping for Monolithic Control Specimen at Failure

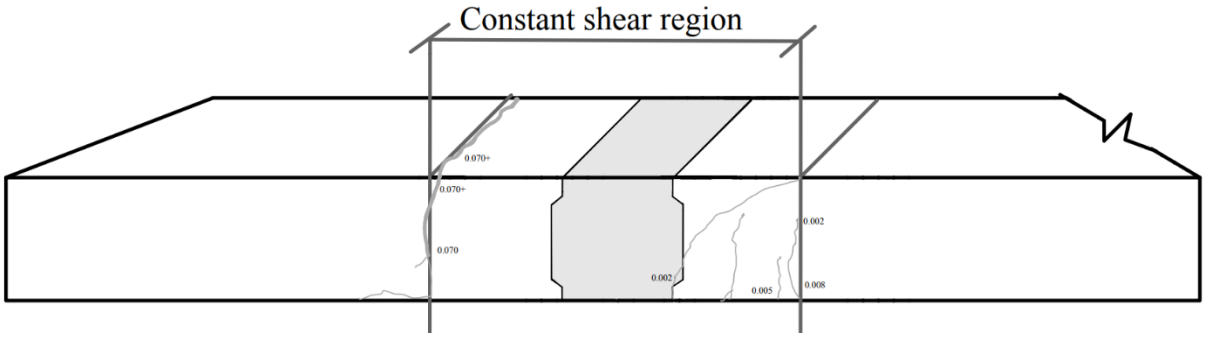

Figure 4.54 Crack Mapping for Proprietary Short-Term Specimen at Failure

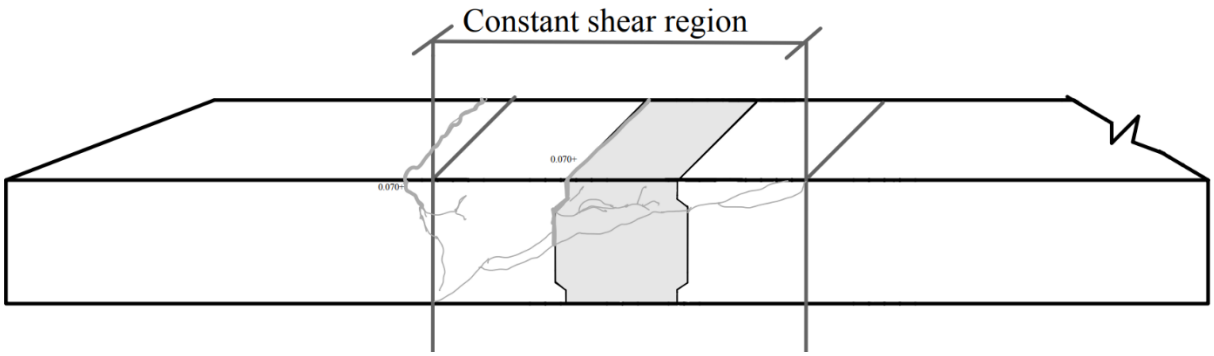

Figure 4.55 Crack Mapping for Non-Proprietary Short-Term Specimen at Failure

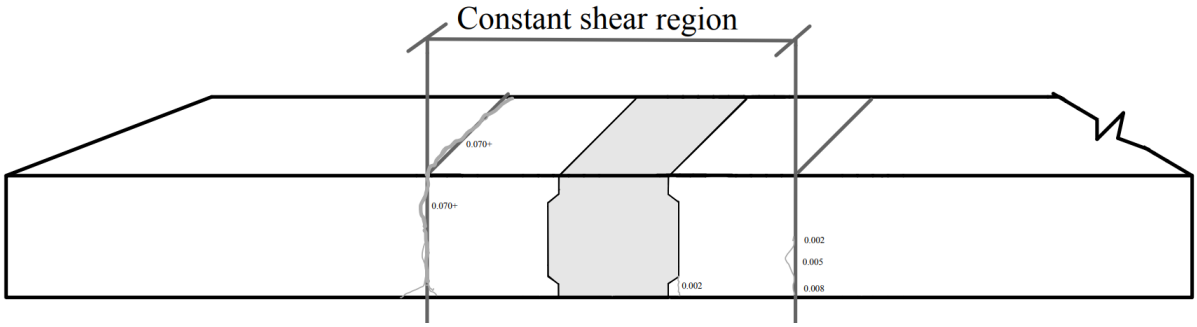

Figure 4.56 Crack Mapping for Proprietary Long-Term Specimen at Failure

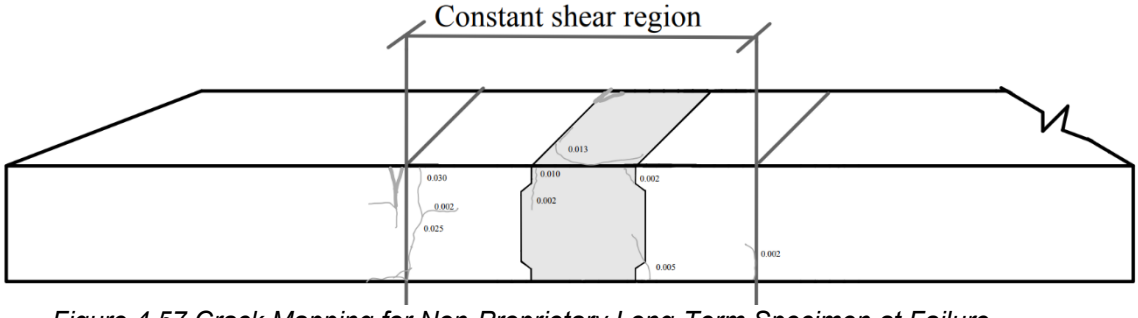

Figure 4.57 Crack Mapping for Non-Proprietary Long-Term Specimen at Failure

For all of the shear tests, the cracking within the shear region was minimal until nearing failure. For the non-proprietary mix, the formation of shear cracks was not seen until right before the time of failure. The cracking behavior that was visible for all specimens was the formation of negative moment flexure cracks, then positive moment cracks at the edges of the constant shear region. These cracks are where the crushing behavior occurred.

4.7. Summary and Recommendations

Throughout this chapter, the research team evaluated the structural performance of closure joints in ABC bridges using large-scale testing. The primary objective was to evaluate the closure joint connections at an early age and determine if it would still provide adequate continuity between the precast elements at 24 hours. The testing sequence included both a flexural series as well as a shear series in order to investigate the performance of the closure joints when they were subjected to transverse bending across the deck as well as when the joint area was subjected to shear.

This chapter discusses the development and comprehensive laboratory evaluation of two different UHPC mixes used as closure joints. Overall, the flexure series results show that the 24-hour specimens with the UHPC closure joint exhibit comparable moment strength to the control specimen. Premature failure occurs when the UHPC compressive strength is less than that of the precast section. Early age changes the failure mode; however, the ultimate capacity at 24 hours was still comparable to the nominal moment capacity. All but one specimen exceeded the nominal moment capacity.

- Proprietary UHPC Mix at 24 hours achieved 89 % of the Control Ultimate Capacity when tested in flexure
- Proprietary UHPC Mix at 24 hours exceeded the Nominal Moment Capacity of Control when tested in flexure
- Non-Proprietary UHPC Mix at 24 hours achieved 72% of the Control Ultimate Capacity when tested in flexure
- Both 24 hour specimens experienced pullout failure
- Proprietary UHPC Mix at 28+ days achieved 92% of the Control Ultimate Capacity when tested in flexure
- Non-Proprietary UHPC Mix at 28+ days achieved 91% of the Control Ultimate Capacity when tested in flexure

The shear series results show that flexure failure prior to shear failure is more likely to occur when the UHPC is at a younger age when the full strength and bonding are still developing. The nominal shear capacity was exceeded by all specimens.

- Proprietary UHPC Mix at 24 hours achieved 104% of the Control Ultimate Capacity when tested in shear
- Proprietary UHPC Mix at 24 hours exceeded the Nominal Shear Capacity of Control
- Non-Proprietary UHPC Mix at 24 hours achieved 84% of the Control Ultimate Capacity when tested in shear
- Both proprietary specimens experienced flexure failure
- Proprietary UHPC Mix at 28+ days achieved 118% of the Control Ultimate Capacity when tested in shear
- Non-Proprietary UHPC Mix at 28+ days achieved 100.1% of the Control Ultimate Capacity when tested in shear

In conclusion, this testing series investigated the performance of UHPC closure joints in two different loading cases: flexure and shear. Each loading case included testing two UHPC mixtures at both 24 hours and post-28 days. The following design notes and recommendations are a result of the large-scale testing series:

- Shear Key geometry is subject to the designer and project goals impact design
- Rebar embedment length should exceed what is required to have the minimum recommended bar development length
- Minimum bar development length is satisfied with eight times the bar diameter
- Non-contact lap splices increase surface area to which the UHPC can bond to
- Shear key surface roughness is essential, recommended ICRI profile of 7-9 or 1/8 or 1/4 inch
- Opening to traffic is dependent on UHPC maturity
- UHPC compressive strength is recommended to be at least that of the precast panel when opening

Through this project and study, the research team evaluated the performance of UHPC as a closure joint material in both short-term and long-term applications to alleviate any safety or performance concerns. It is believed that it was determined that the UHPC performed sufficiently in the short term since the worst-case scenario was tested, and even then, 70% of the standard deck specimen was achieved. This is especially useful in opening to construction or partial traffic if such is the intent of the project team. It is recommended that UHPC mixes be at or greater compressive strength of the precast section in order to prevent a pullout failure. Maturity monitoring is a very helpful tool that can allow for this condition to be satisfied.

Chapter 5. Field Trials

5.1. Monitoring and Instrumentation of Closure Joints

Due to COVID-19 and project timeline shifts, the researchers performed the field monitoring task of this study before conducting the large-scale structural testing task. In January 2021, CBEI was notified that there was an opportunity to instrument a new TxDOT ABC bridge. Therefore, with only one more phase left in this TxDOT bridge replacement project, the researchers immediately began to prepare for instrumentation. Field instrumentation programs were employed at two locations: the Navasota River Bridge in the Bryan District and the Farwell Creek Bridge in the Amarillo District. Instrumentation was also installed in some precast elements for both projects prior to delivery to the bridge site from the precast yard. The instrumentation of these TxDOT ABC bridges was intended to provide an indication of how close the strain values of the closure joints were to the design assumptions. This section will provide an overview of the field instrumentation program by outlining the process of designing and installing the instrumentation as well as by explaining the equipment that was used. Bridge concrete properties and mix designs will also be discussed herein.

5.1.1. Instrumentation Sensor Choice

The primary objective of the instrumentation program was to capture the change in strain in both the longitudinal and transverse directions within the closure joint connections directly after they were poured (denoted as “time zero”) and through the first year or so of use in service. Specifically, the concrete strains would allow the research team to evaluate the closure joint’s response to stresses and time-dependent strain changes. Temperature values were also of interest as they would be used to correct the strain values for any potential thermal effects.

Therefore, the instrumentation of choice for this project was the vibrating wire gauge (VWG) due to its ability to collect concrete strain and temperature values simultaneously in a single scan interval. VWGs also have a history of being accurate, precise, durable, and easy to install as evidenced by previous studies at the University of Texas at Austin (Yousefpour et al., 2014). The researchers decided to select the Geokon Model 4200 Series VWG, as shown in Figure 5.1, due to its concrete embedment capabilities and intended design for long-term strain collection.

A VWG works by the “plucking” of a steel wire that is tensioned between two end blocks within the VWG. The “plucking” is initiated by an electrical current that is sent through the plucking coil from the lead wire. Since the steel wire can freely

vibrate at its natural frequency, any relative displacement of the concrete around the VWG will change the tension within the steel wire, which will consequently change the natural frequency of the steel wire. This measure of natural frequency is then processed by the VWG, and the concrete strain can then be calculated. In terms of temperature collection, the VWG contains a thermistor that provides accurate and precise temperature readings at the location of the gauge. expansions.

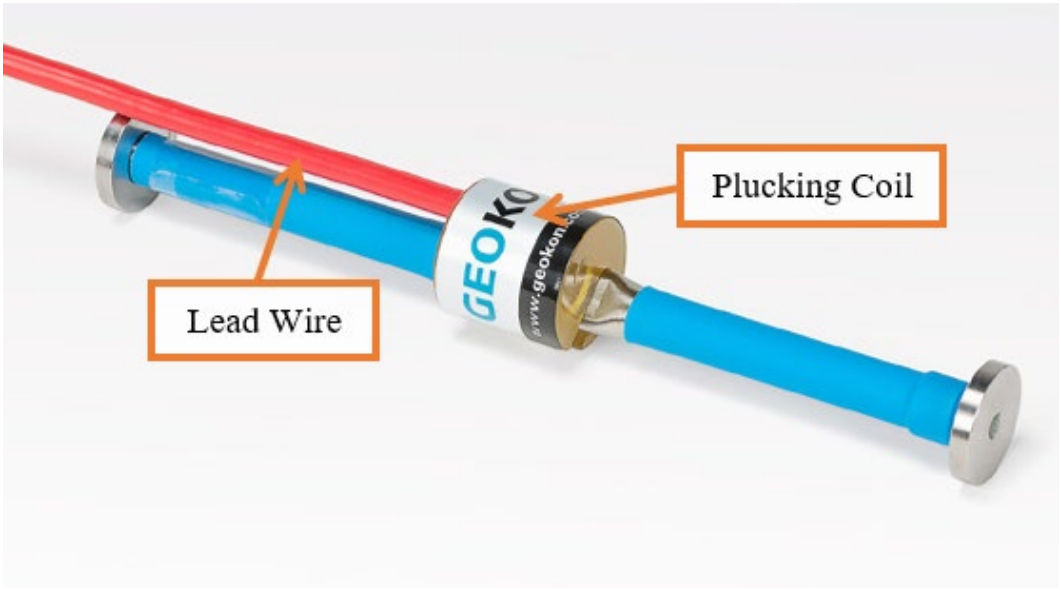

Figure 5.1 Geokon Model 4200 Series VWG with Plucking Coil and Lead Wire

5.1.2. Navasota River Bridge

5.1.2.1. Location and Bridge Specifications

The first bridge that was instrumented in this project was the Navasota River Bridge in the TxDOT Bryan District. Located along Old San Antonio Road (OSR) near Franklin, Texas, the Navasota River Bridge was part of a TxDOT bridge replacement project on OSR in Brazos County to replace seven bridges and reconstruct 25 miles of roadway. These bridges were functionally obsolete and did not meet current safety standards. Figures 5.2 and 5.3 show the exact location of the Navasota River Bridge using Google Maps screenshots.

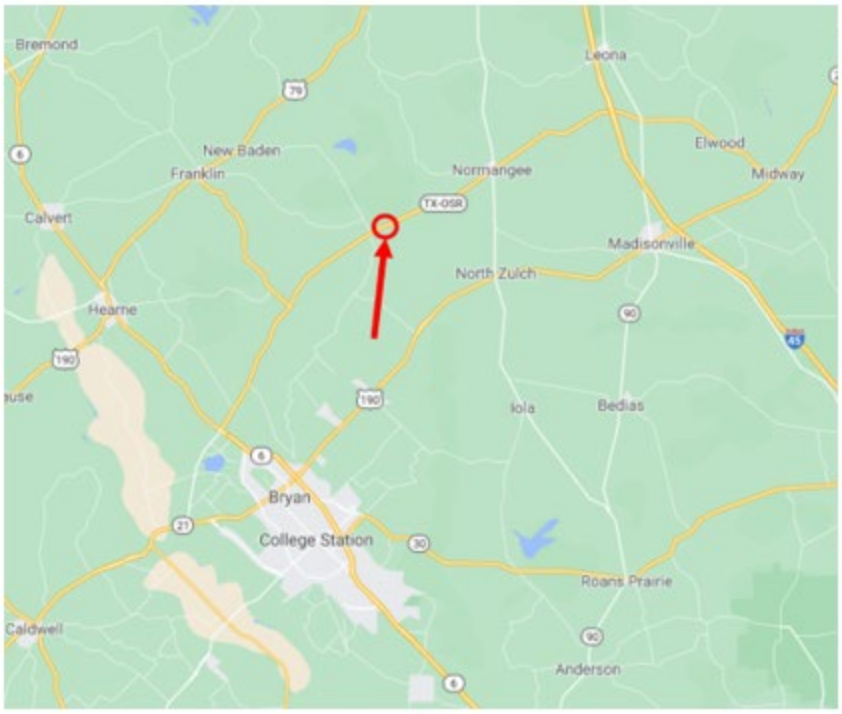

(a)

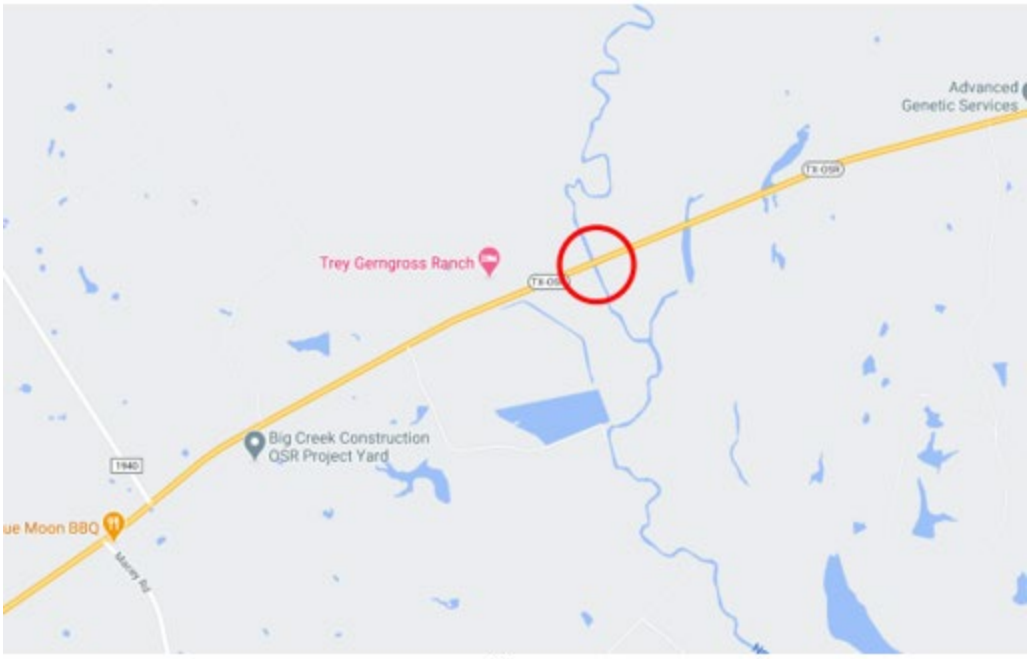

(b)

Figure 5.2 Location of Navasota River Bridge. (a) Google Maps Aerial View of Approximate Location along OSR; (b) Closer Aerial View of Location

Figure 5.3 Closer View of Navasota River Bridge Location. (a) Zoom-In Map Aerial View; (b) Zoom-In Satellite Aerial View

The Navasota River Bridge consists of simple span prestressed concrete girder assemblies that are integrated with a concrete bridge deck that is prefabricated together as an individual unit as shown in Figure 5.4. The prefabricated deck elements are approximately nine inches in depth and are constructed with Class S Concrete, which has a compressive strength of 4,000 pounds per square inch (psi). No. 5 reinforcement bars run transversely through the bridge deck and lap adjacent deck panel rebar to create non-contact lap splices within the closure joints. On the other hand, no. 4 bars run longitudinally or, in other words, into the page when looking at a bridge section, as shown in Figure 5.6. Figure 5.6 also shows that the bridge has a total of six girders and each closure joint runs along the length of one of the four interior girders.

While UHPC is the recommended material to be placed into the closure joints by designer Johnson, Mirmiran & Thompson (JMT) and TxDOT in this project, the contractor, Big Creek Construction, Ltd, opted to use rapid setting fiber reinforced keyway concrete (RSFRC) which is clearly defined in TxDOT's special specification 4144. Under the laboratory testing program in chapter 3, this mixture is referred to as UHPC-C1. A typical RSFRC connection between Unit 3 and Unit 1/Unit 2 can be found in Figure 5.5. Unit 3 differed from the other two units in that the deck panel was not integrated with the girders due to its slenderness. The prefabricated deck panels for Unit 3, which were broken up into two pieces with a transverse closure joint between them, were placed atop the girders at the bridge site.

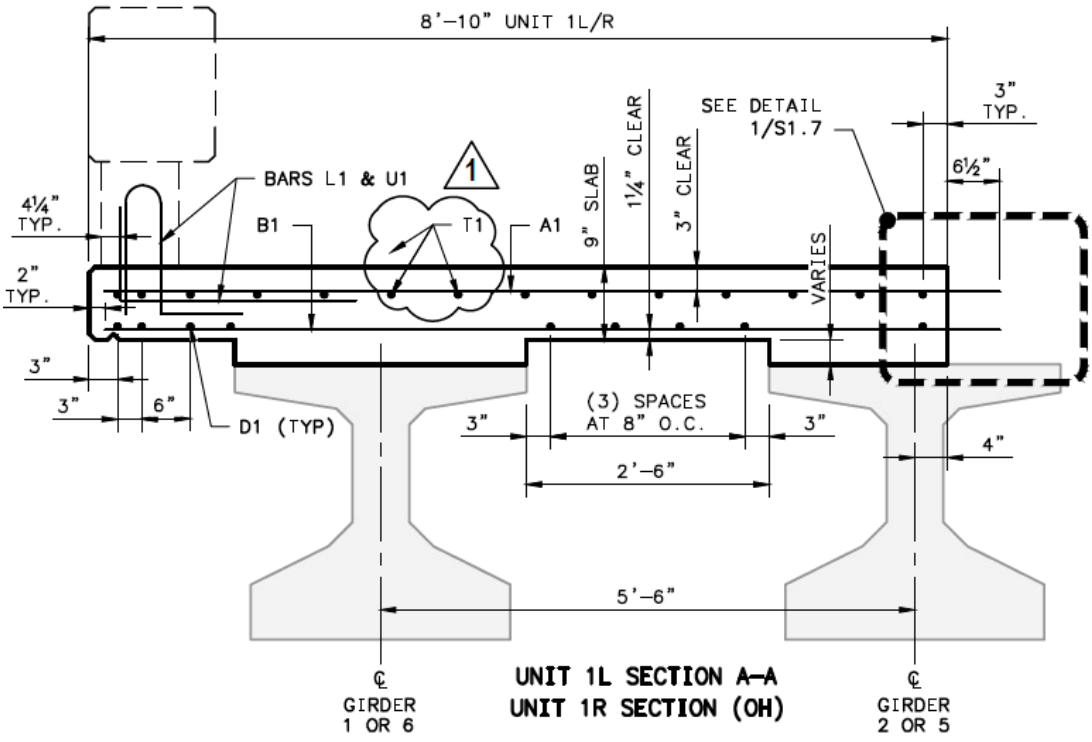

Figure 5.4 Prefabricated Concrete Decked Girder Assembly

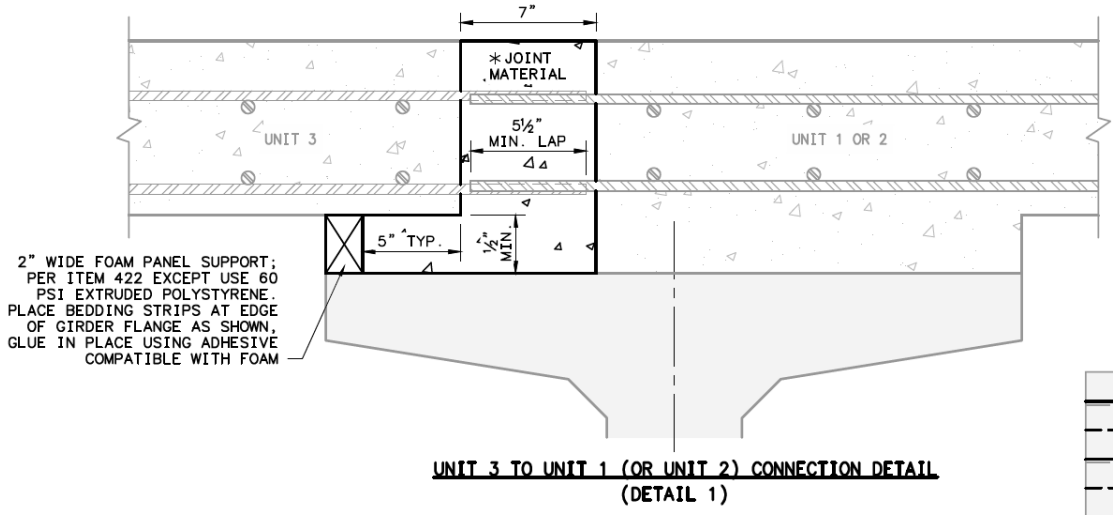

Figure 5.5 Closure Joint Detail Between Unit 3 and Unit 1/Unit 2

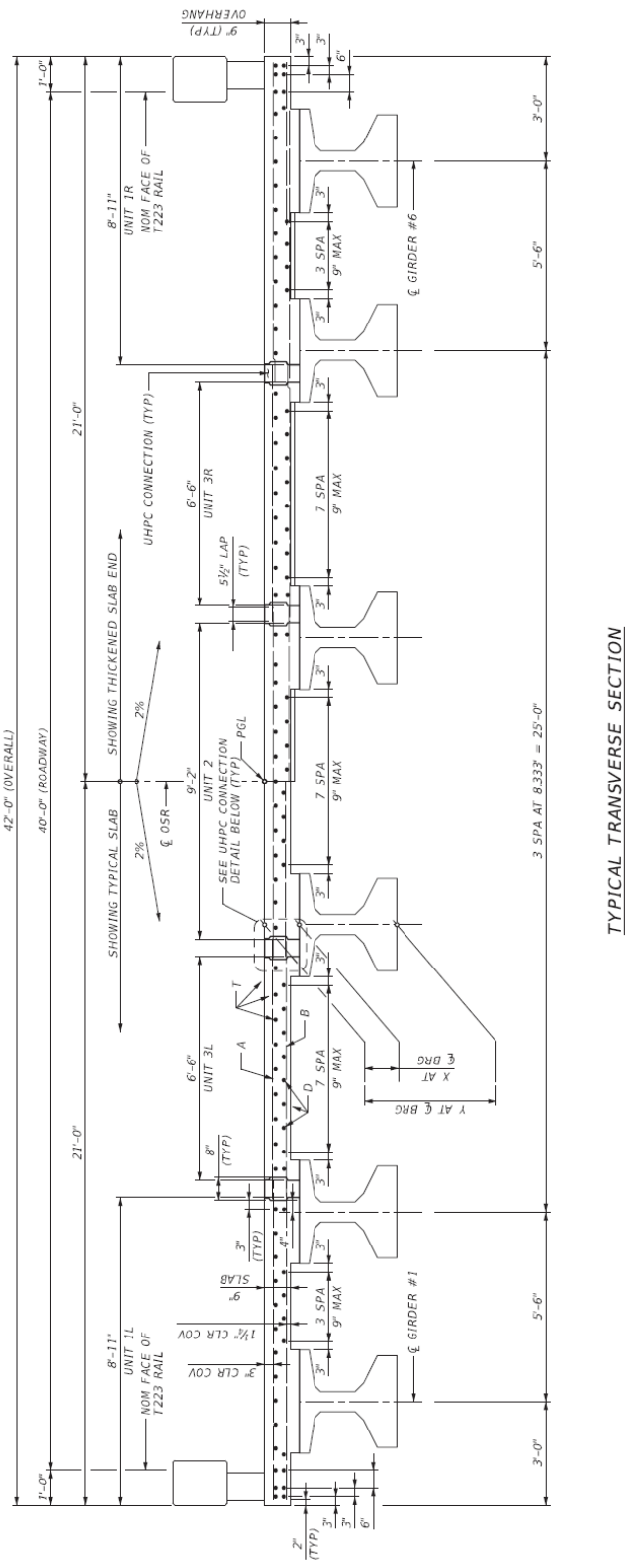

Figure 5.6 Navasota River Bridge Transverse Section

5.1.2.2. Mixture Proportions and Testing Data for Navasota River Bridge Closure Joint

Table 5.1 below shows the mixture proportions used in the Navasota River Bridge closure joints, as per the contractor's submittal. As mentioned in the previous section, the contractor opted to use RSFRC with 2% steel fiber and the mixture met the pull-out strength requirement.

Table 5.1 Mixture Proportions for the Navasota River Bridge Closure Joint Material

Material	Mass (lbs/cu.yd)
Portland Cement (Type I/II)	700
Water	258
Fine Aggregate (ASTM C33)	1238
Coarse Aggregate (ASTM C33, #57)	1955
Water Reducer (ASTM C494, Type A/D)	6 oz/cwt
High-Range Water Reducer (ASTM C494, Type A/F)	6 oz/cwt
Set Accelerator (ASTM C494 Type C)	Not Disclosed
Steel Fibers (ASTM A820)	264

Table 5.2 shows the results of the field and laboratory data obtained from the closure joint mixture used in the Navasota River Bridge. Pull-out tests were performed on site 24 hours after the closure joint placement. All other concrete specimens were cast on site on the day of the closure joint placement, cured on site for 24 hours, and then transported to a curing room (73˚F, 100% Relative Humidity (RH)) at the Laboratory for Infrastructure Materials Engineering at the University of Texas at Austin, where the specimens remained until the age of testing.

Table 5.2 Laboratory and Field Test Results for the Navasota River Bridge Closure Joint

Mixture	Compressive Strength (PSI)				Elastic Modulus (PSI)	Splitting Tensile Strength (PSI)	Rebar Pull-Out Strength (PSI)
	1 Day	7 Day	28 Day	91 Day	28 Day	28 Day	1 Day
Navasota River Closure Joint	3340	7230	8990	10150	7.38×10^6	770	3200

5.1.2.3. Instrumentation Plan

The first step in creating the instrumentation plan was reviewing all the bridge drawings provided by TxDOT in order to determine the ideal locations for monitoring. Factors affecting the instrumentation locations included accessibility,

closure joint cross-section, and distance from potential structural anomalies in the bridge. In order to understand how the prefabricated deck panels acted on the closure joints, gauges in the deck and closure joints were placed in line with each other as shown in Figure 5.7. Furthermore, it was decided that the gauges would be placed at both the top and bottom of the closure joint in order to develop a strain profile along its depth. Gauges denoted "TX-T" or "LX-T" represented transverse or longitudinal gauges, respectively, at the top of the closure joint ("T"), while gauges denoted "TX-B" or "LX-B" represented transverse or longitudinal gauges, respectively, at the bottom ("B"). The "X" term is defined as the VWG number for planning and data acquisition purposes. Some longitudinal gauges were placed in the middle of the closure joint and these VWGs were referred to as "LX-S", where "S" stands for singular.

Prior to finalizing the instrumentation plan, the researchers conducted a site visit to one of the other bridges being replaced along OSR with similar bridge specifications on January 25th, 2021. Visiting the site before instrumentation helped with addressing any potential issues on site that were not made clear in the drawings. Due to restrictions created by the VWG cables, which were 100 feet in length, it was decided that span 5 would be instrumented as shown in Figure 5.8. This would also allow the researchers to place the data acquisition (DAQ) system near the abutment of the bridge between two girders. It was decided that a total of 20 VWGs would be installed on this bridge to understand the structural behavior of the closure joints. 12 gauges would be installed transversely while 8 would be installed longitudinally as shown in Figure 5.7. It is important to note that transverse means perpendicular to the direction of the bridge and longitudinal is parallel to the direction of the bridge in terms of traffic flow.

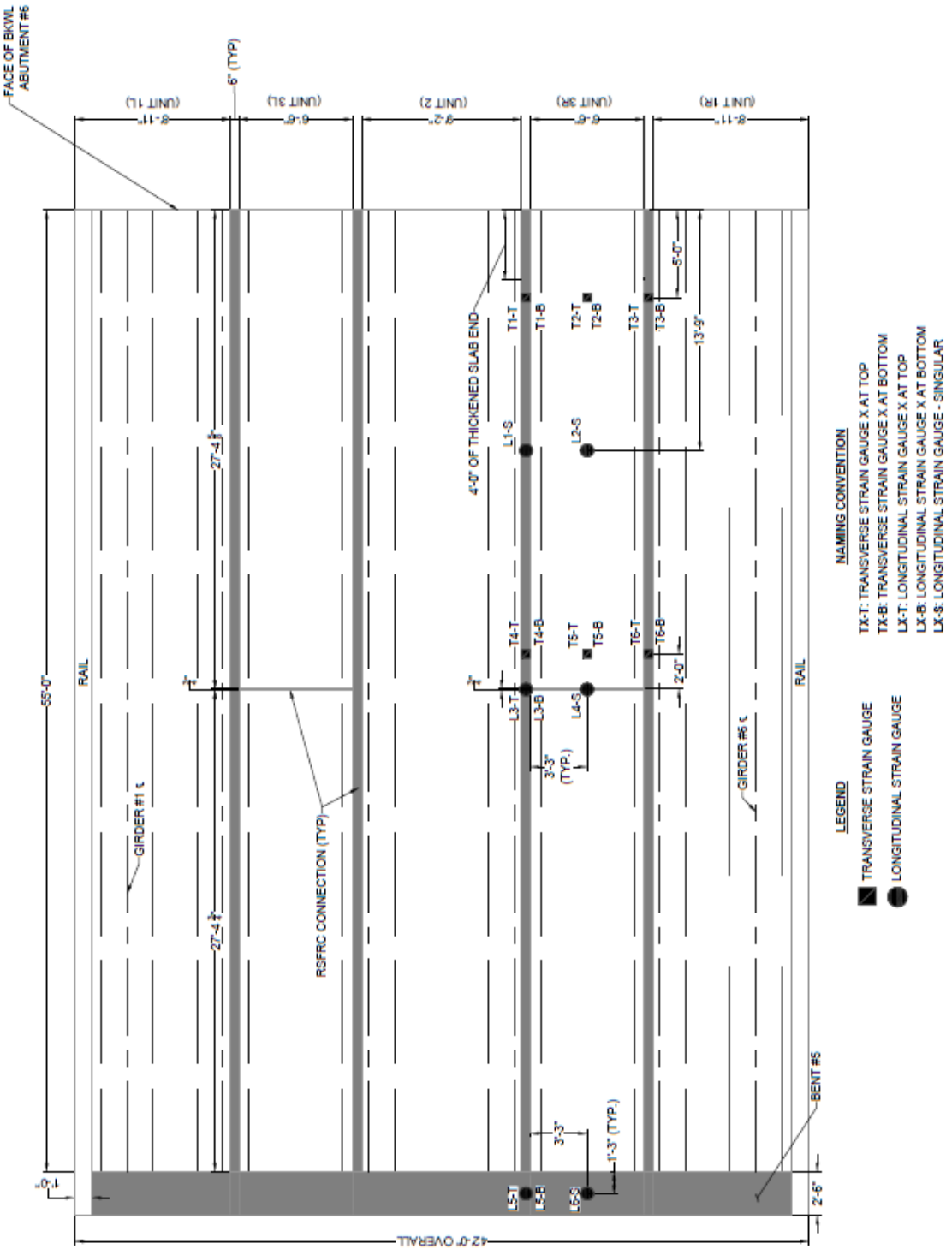

Figure 5.7 Navasota River Bridge Span 5 Instrumentation Plan

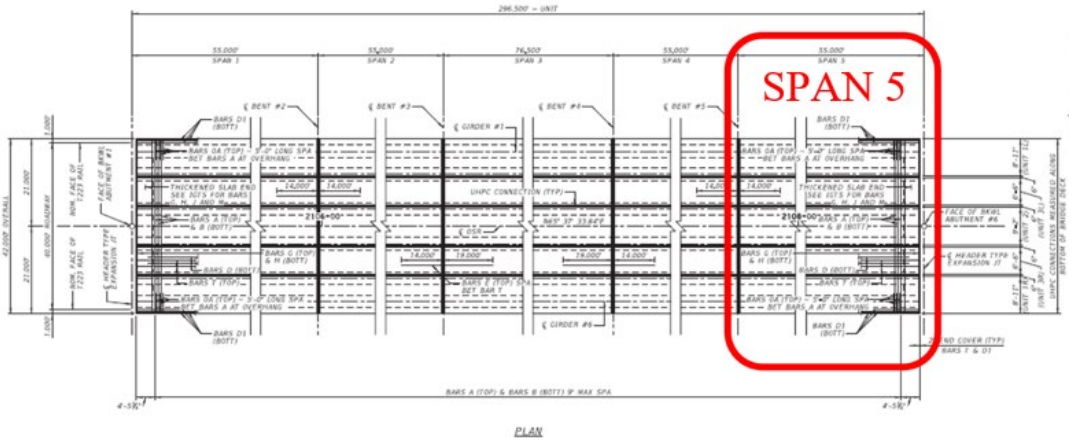

Figure 5.8 Plan View of Span 5 Location in relation to the Navasota River Bridge

5.1.2.4. Prefabricated Drop-In Panel Instrumentation

On February 24th, 2021, the researchers were notified that the precast deck panel for Unit 3 of span 5 of the bridge would be poured on February 26th, 2021. Therefore, to get the five VWGs into the drop-in panel, the researchers went to the OSR Project Yard on February 25th, 2021, where all the precast bridge elements were cast and stored. It was located west of the OSR bridge projects and was officially referred to as the "Big Creek Construction OSR Project Yard" as shown in Figure 5.2b. Refer to Figure 5.9 to see how the transverse and longitudinal gauges were installed, which will be explained in more detail in the "Standardized VWG Installation Process" section of this chapter (Section 5.1.4).

Because the VWGs were not going to be connected to a DAQ system until the drop-in panel was installed at the bridge site, the wires needed to be protected. Therefore, once all the VWGs were installed within the deck panel, the wires were run along the length of the rebar, as shown in Figure 5.10a, and pulled out from the formwork at the end of the drop-in panel. The wires, which are the most vulnerable portion of the gauge, were then neatly placed in a sturdy bag and taped to ensure they did not get loose or get cut during transportation from the project yard to the Navasota River Bridge site as shown in Figure 5.10b.

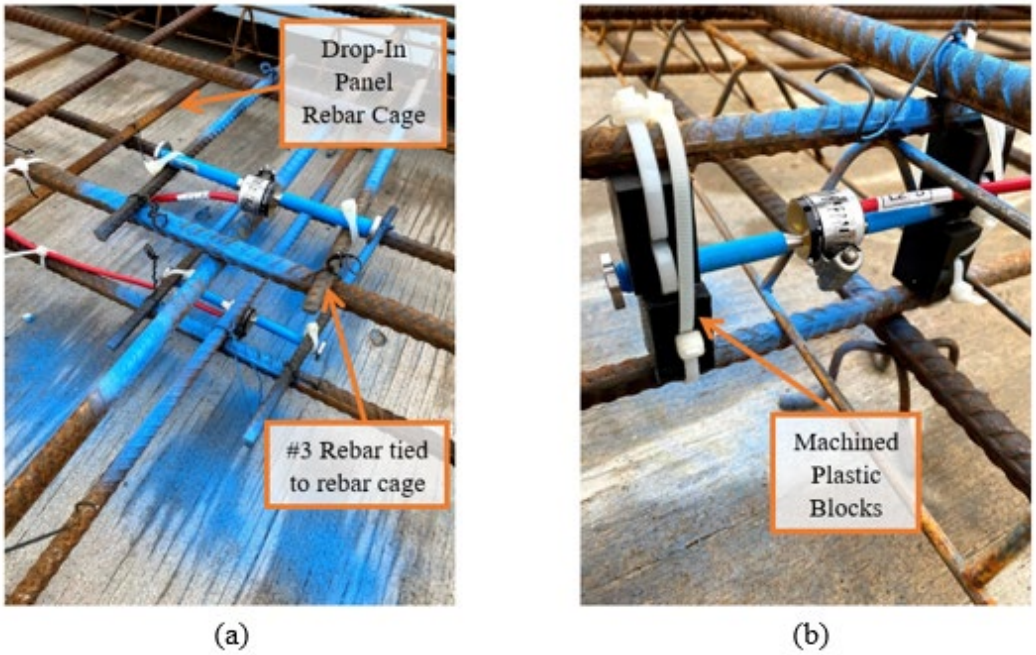

Figure 5.9 Drop-In Panel VWG Installation. (a) Installation of Transverse Gauges; (b) Installation of Longitudinal Gauges

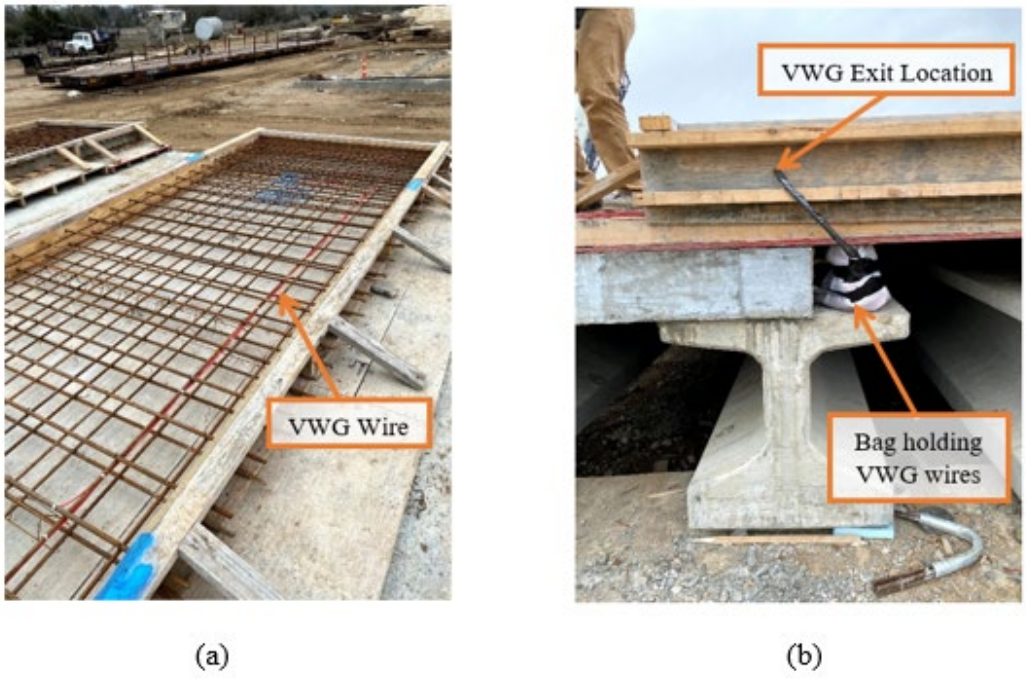

Figure 5.10 Drop-In Panel Wire Management. (a) VWG Wires Running Along Length of Rebar; (b) Storage of Wires

5.1.3. Farwell Creek Bridge

5.1.3.1. Location and Bridge Specifications

The second bridge that was instrumented in this project was the Farwell Creek Bridge in the TxDOT Amarillo District. Located along State Highway 15 (SH15) near Gruver, Texas, the Farwell Creek Bridge was part of the TxDOT US83 and SH15 bridge replacement project which aimed at removing and replacing the last five timber pile bridges in the Amarillo District. Since it was built in the 1930s, the Farwell Creek Bridge also had exceeded its intended design life. Figures 5.11 through 13 show the exact location of the bridge.

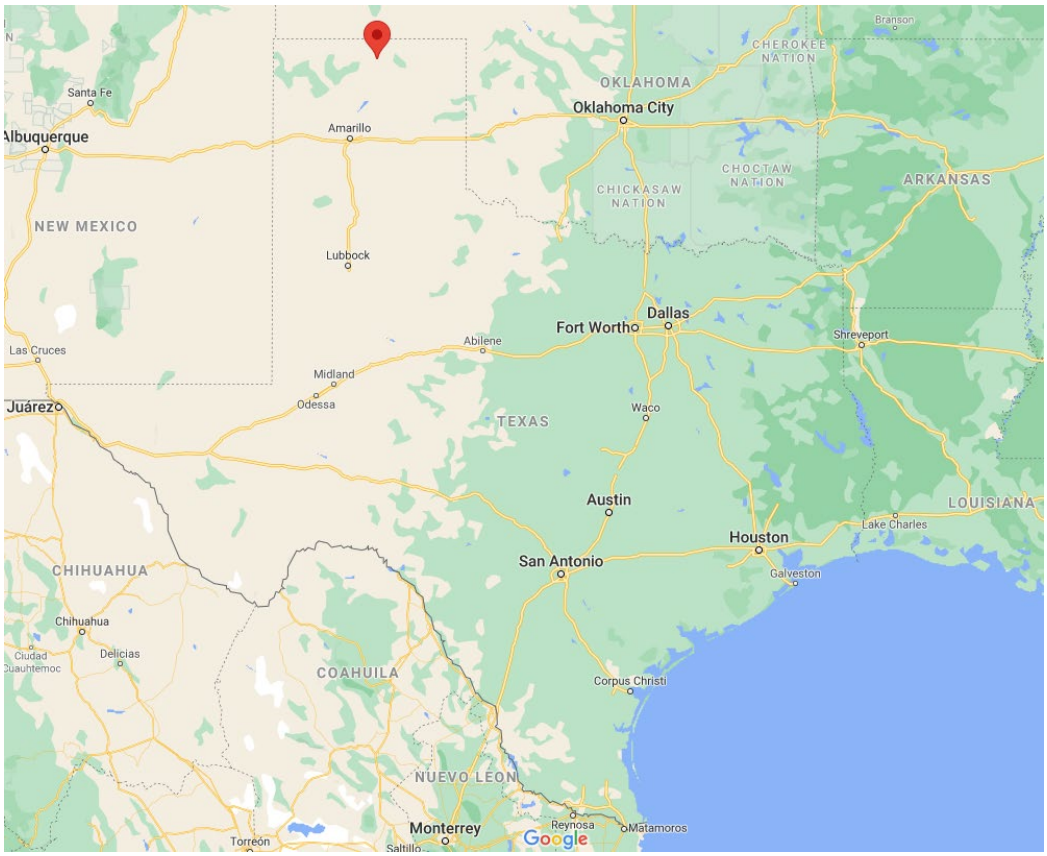

Figure 5.11 Location of Farwell Creek Bridge in relation to the State of Texas

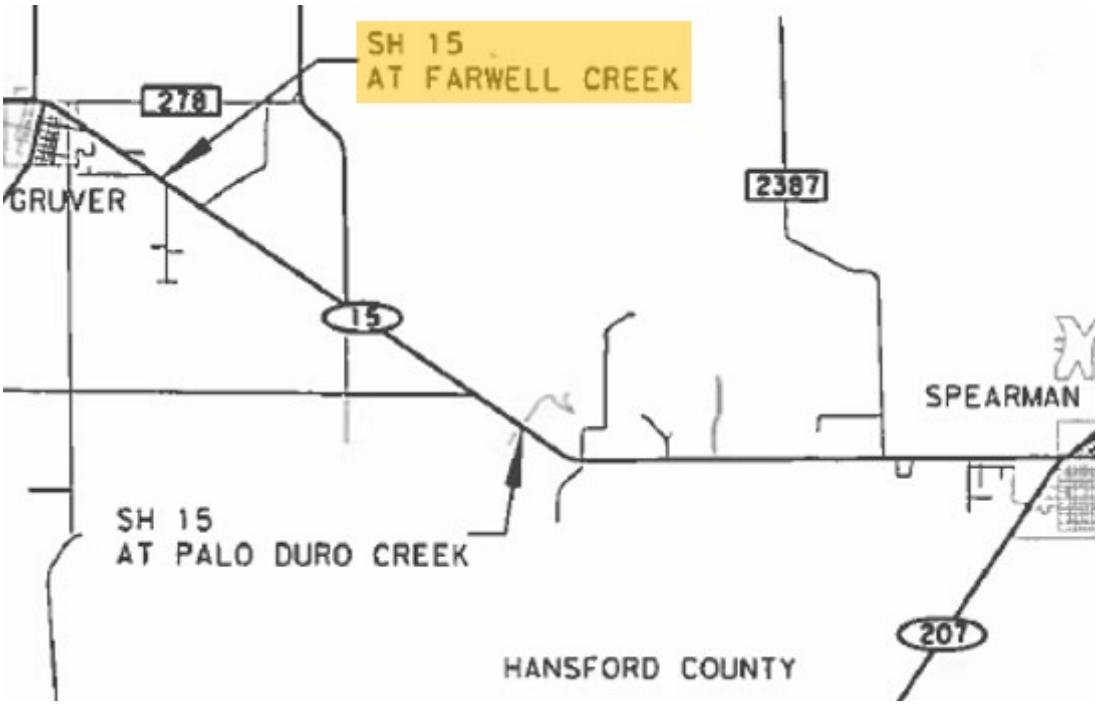

Figure 5.12 Location of Farwell Creek Bridge from Plan Set

Figure 5.13 Street View of Original Farwell Creek Bridge

The Farwell Creek Bridge has two spans that each have four 70-foot long Northeast Extreme Tee (NEXT) beams connected via transverse and longitudinal UHPC closure joints, as shown in Figures 5.14 and 5.15. Under the laboratory testing program in Chapter 3, the mixture for this beam is referred to as WACO-NEXT. NEXT beams will be defined in more detail in the "Mixture Proportions and Testing Data for NEXT Beams" and "NEXT Beam Instrumentation" sections (section 5.1.3.3 and 5.1.3.5, respectively). Each NEXT beam had two girders integrated with a driving deck that was approximately nine inches in depth. Similar to the Navasota River Bridge, the Farwell Creek Bridge has no. 5 reinforcement bars running

transversely through the bridge that lap with adjacent prefabricated elements to create non-contact lap splices within the closure joint.

Due to longer than normal detour lengths and the reliance of small town locals on the limited routes in the North Texas area, TxDOT wanted to significantly reduce the amount of time US83 and SH15 were closed. Therefore, along with the use of NEXT beams, TxDOT decided to use a proprietary UHPC product which was imported from France. Under the laboratory testing program in Chapter 3, the mixture for this beam is referred to as UHPC-P3-2.

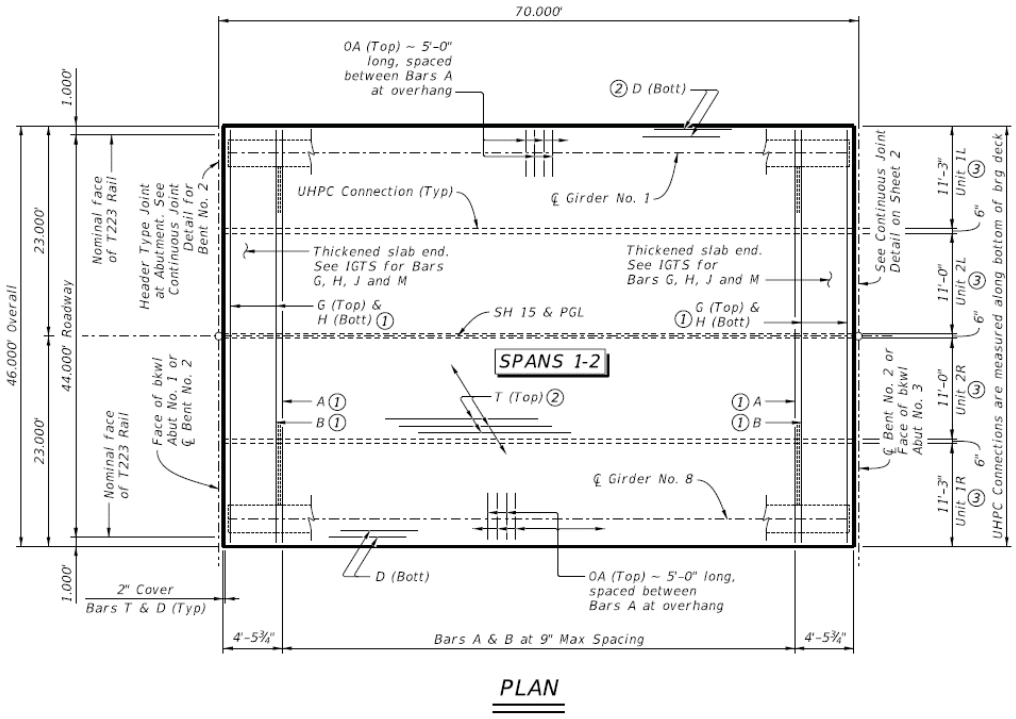

PLAN

Figure 5.14 Plan View of Farwell Creek Bridge Span

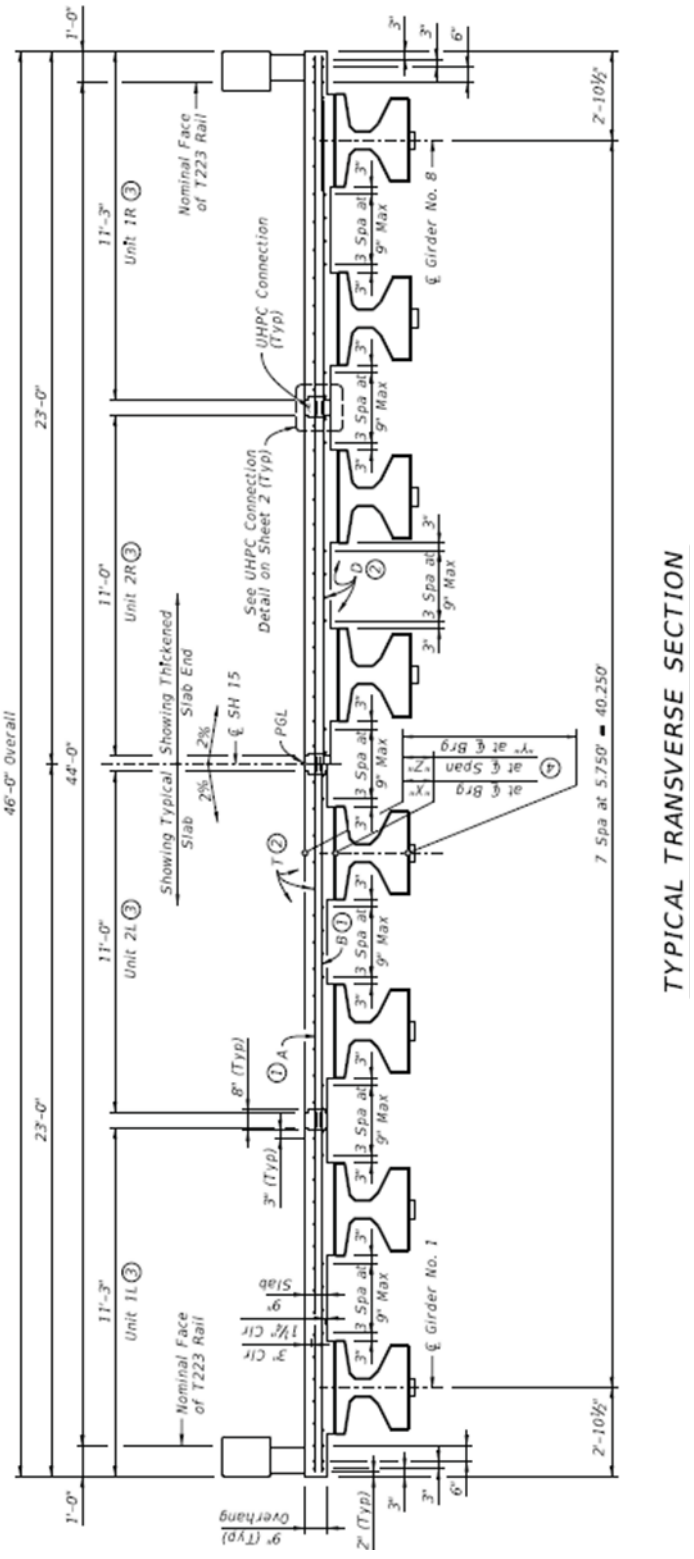

Figure 5.15 Farwell Creek Bridge Transverse Section

5.1.3.2. Mixture Proportions and Testing Data for Farwell Creek Bridge Closure Joints

The UHPC mixture used in the Farwell Creek Bridge closure joints was a proprietary mixture from France and was produced onsite by a specialty contractor with significant experience with UHPC in North America. Under the laboratory testing program in chapter 3, this mixture is referred to as UHPC-P3-2. Due to the proprietary nature of the UHPC, no information is available regarding the materials or mixture proportions.

Test cylinders were cast and cured on site for 24 hours and then transported to the moist-curing room (73˚F, 100% RH) at the Laboratory for Infrastructure Materials Engineering at the University of Texas at Austin, where the specimens remained until the age of testing. Table 5.3 shows the results of the laboratory tests performed on the UHPC test cylinders.

Table 5.3 Laboratory Test Results for UHPC used in the Farwell Creek Bridge Closure Joint

Mixture	Compressive Strength (PSI)	Elastic Modulus (PSI)	Splitting Tensile Strength (PSI)	Coefficient of Thermal Expansion (με/°F)
	28 Day	28 Day	28 Day	240 Day
Farewell Creek Bridge UHPC Closure Joint	26340	8.10×10^6	3080	7.77

5.1.3.3. Mixture Proportions and Testing Data for NEXT Beams

Table 5.4 below shows the mixture proportions used in the NEXT beams for the Farwell Creek Bridge, as per the mix design submittal. These precast beams were cast in Elm Mott, TX and test cylinders were cast on site. After 24 hours, the cylinders were transported to the moist-curing room (73˚F, 100% RH) at the Laboratory for Infrastructure Materials Engineering at the University of Texas at Austin, where the specimens remained until the age of testing. Table 5.5 shows the results of laboratory tests performed on the NEXT beam test cylinders.

Table 5.4 Mixture Proportions for NEXT Beams

Material	Mass (lbs/cu.yd)
Portland Cement (Type III)	600
Fly Ash (Class F)	150
Water	259
Fine Aggregate (ASTM C33)	1425
Coarse Aggregate (ASTM C33, #57)	1535
Air-Entraining Admixture	0.2 oz/cwt
High-Range Water Reducer (ASTM C494, Type A/D)	8 oz/cwt
Calcium Nitrite (30%) Corrosion Inhibitor	51 oz/cwt

Viscosity-Modifying Admixture	1 oz/cwt
Set-Retarding Admixture	2 oz/cwt
Synthetic Microfibers	1 lb/yd^3
Synthetic Macrofibers	5 lb/yd^3

Table 5.5 Laboratory Test Results for NEXT Beams

Mix	Compressive Strength (PSI)	Elastic Modulus (PSI)	Splitting Tensile Strength (PSI)	Coefficient of Thermal Expansion (με/°F)
	28 Day	28 Day	28 Day	270 Day
NEXT Beam	11360	6.40 x 10^6	620	4.97

5.1.3.4. Instrumentation Plan

The process in finalizing the Farwell Creek Bridge instrumentation plan was the same as that of the Navasota River Bridge. However, due to the rigorous travel required to get to the Farwell Creek Bridge site from FSEL, the researchers could not conduct a site visit and had to rely on maintaining effective communication with the TxDOT Amarillo District representatives and the site contractor. The researchers still thoroughly reviewed all drawings provided by TxDOT to get a better understanding of potential instrumentation locations.

The factors affecting the instrumentation locations included accessibility, closure joint cross-section, and locations where instrumentation was going to be embedded in the NEXT beams. Specifically, to discern how the NEXT beams affected the closure joints, gauges in the NEXT beams and closure joints were placed in line with each other as shown in Figure 5.16. Again, most gauges were placed at the top and bottom of the closure joint to develop a strain profile along the depth.

Also, due to the limiting number of spans at the Farwell Creek Bridge, the researchers decided to instrument span two for safety reasons. Span two was located closer to the site entrance where the researchers would enter from, and it allowed for a safer material unloading experience on the construction site. The DAQ system was to be placed near the abutment wall below span two of the bridge.

All VWG naming conventions remain the same as those established in the Navasota River Bridge Instrumentation Plan section (Section 5.1.2.3). Once finalized, it was decided that a total of 26 VWGs would be installed: 16 in the NEXT beam and 10 in the closure joints.

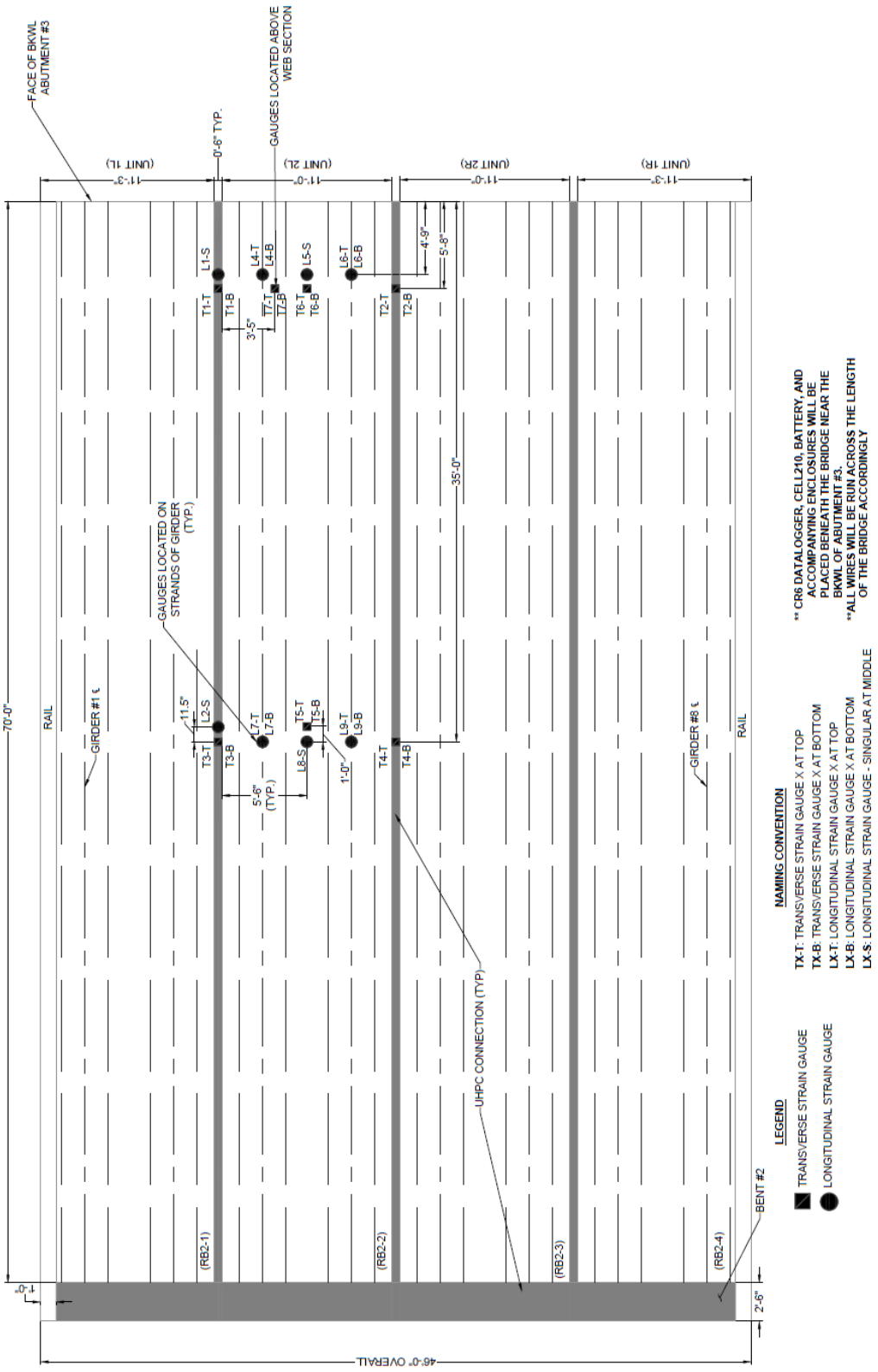

Figure 5.16 Farwell Creek Bridge Span 2 Instrumentation Plan

5.1.3.5. NEXT Beam Instrumentation

The NEXT beam was developed in 2008 by the Precast/Prestressed Concrete Institute (PCI) Northeast Bridge Technical Committee. As an integral part of ABC, NEXT beams, depicted in Figure 5.17, are sections that resemble standard double-tee beams but have wider stems in order to handle the moment and shear demands of bridge loads (Culmo & Seraderian, 2010). In the case of the Farwell Creek Bridge, the NEXT beams were fully precast *and* prestressed, and integrated a full-depth structural deck slab intended to be the bridge's driving surface, which allowed TxDOT to reduce construction time. Figure 5.18 provides a cross-section view of one of the Farwell Creek Bridge's NEXT beams.

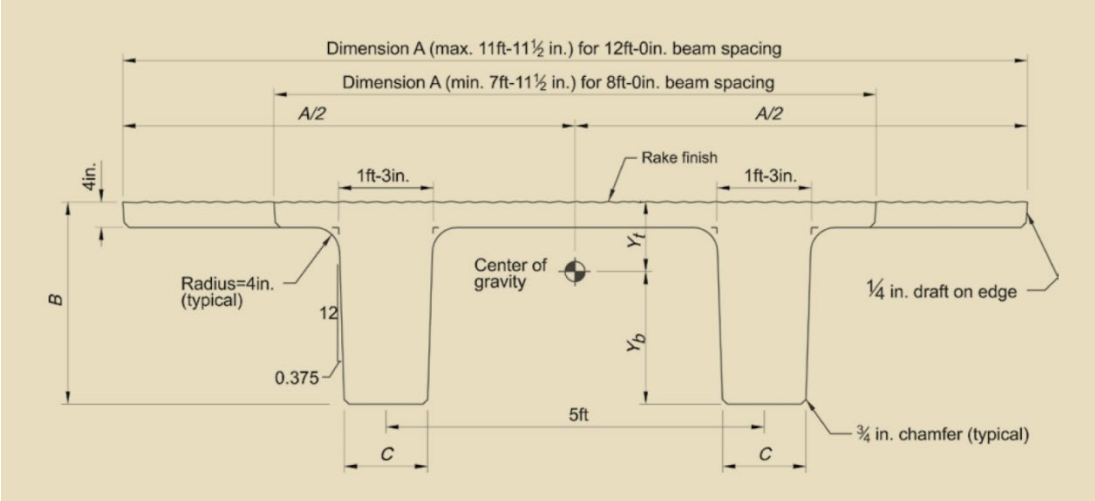

Figure 3. This drawing illustrates the final beam dimensions. Note: A = beam width; B = beam depth; C = stem base width; Y_b = distance from bottom of beam to center of gravity; Y_t = distance from top of beam to center of gravity. 1 in. = 25.4 mm; 1 ft = 0.305 m.

Figure 5.17 Schematic of Typical NEXT Beam (Culmo & Seraderian, 2010)

The NEXT beams for this project were precast and transported to the bridge site from Texas Concrete Partners in Elm Mott, Texas, which is approximately 500 miles from the Farwell Creek Bridge. The researchers determined that instrumenting the NEXT beams would be useful and conducted an initial site visit on June 10th, 2021, to ensure instrumentation of the beams was feasible and to discuss any possible instrumentation issues or complexities with personnel available on site.

Figure 5.18 NEXT Beam Section RB2-2 for Farwell Creek Bridge

After the site visit, the researchers found that instrumenting NEXT Beam RB2-2 (Figures 5.18 and 19) would work for both the research team's and precast plant's schedule. It was ultimately decided to focus on the interior of the NEXT beam since the setup was different from that of the Navasota River Bridge. The researchers wanted to investigate the demand required at the transverse closure joints. As shown in Figure 5.20, VWGs were placed in the deck section, web, and on the pretensioned strands of the NEXT beam. The placement of one gauge at the top of the web and another at the bottom would allow the researchers to calculate the tendency of the section to shrink or enlarge at the center of gravity of the cross section.

On July 7th, 2021, the researchers arrived at Texas Concrete Partners to instrument NEXT beam section RB2-2. It is important to note that when installing the VWGs, hot-dipped galvanized rebar was used to match what was used within the NEXT beam to avoid any adverse chemical reactions between the rebar metals. Refer to Figures 5.21 to 5.23 for an overview of the instrumentation efforts. This instrumentation was different from that of the Navasota River Bridge panel instrumentation in that data was going to be collected from the start of the NEXT beam cast until it needed to be transported to the Farwell Creek Bridge site. Therefore, a DAQ system needed to be setup at the precast plant to collect the necessary data as shown in Figure 5.24

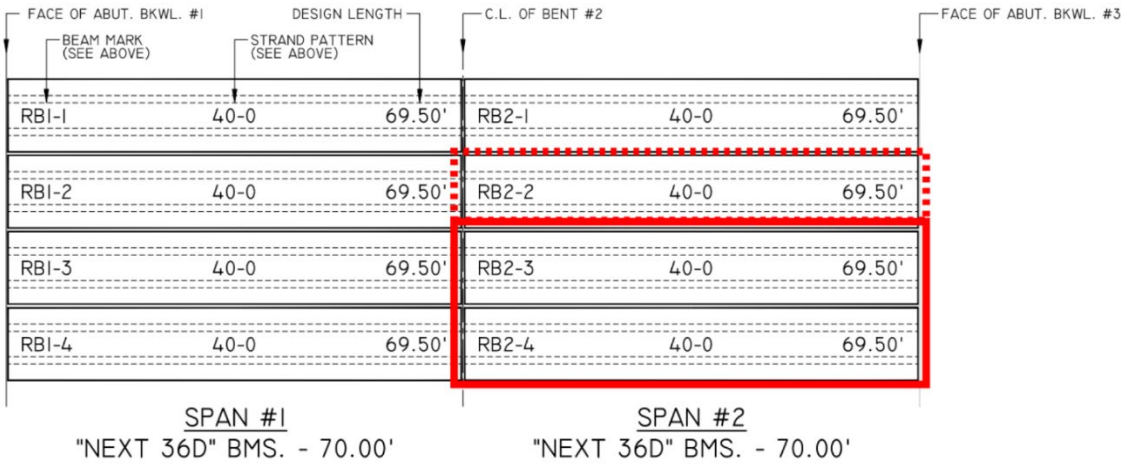

Figure 5.19 Plan View of NEXT Beam Section RB2-2

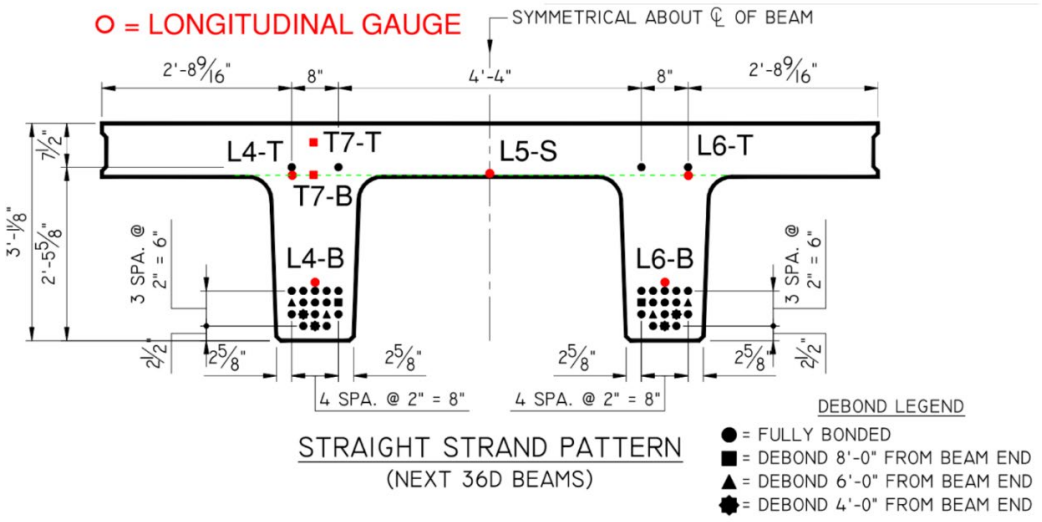

Figure 5.20 NEXT Beam Section RB2-2 Instrumentation Plan

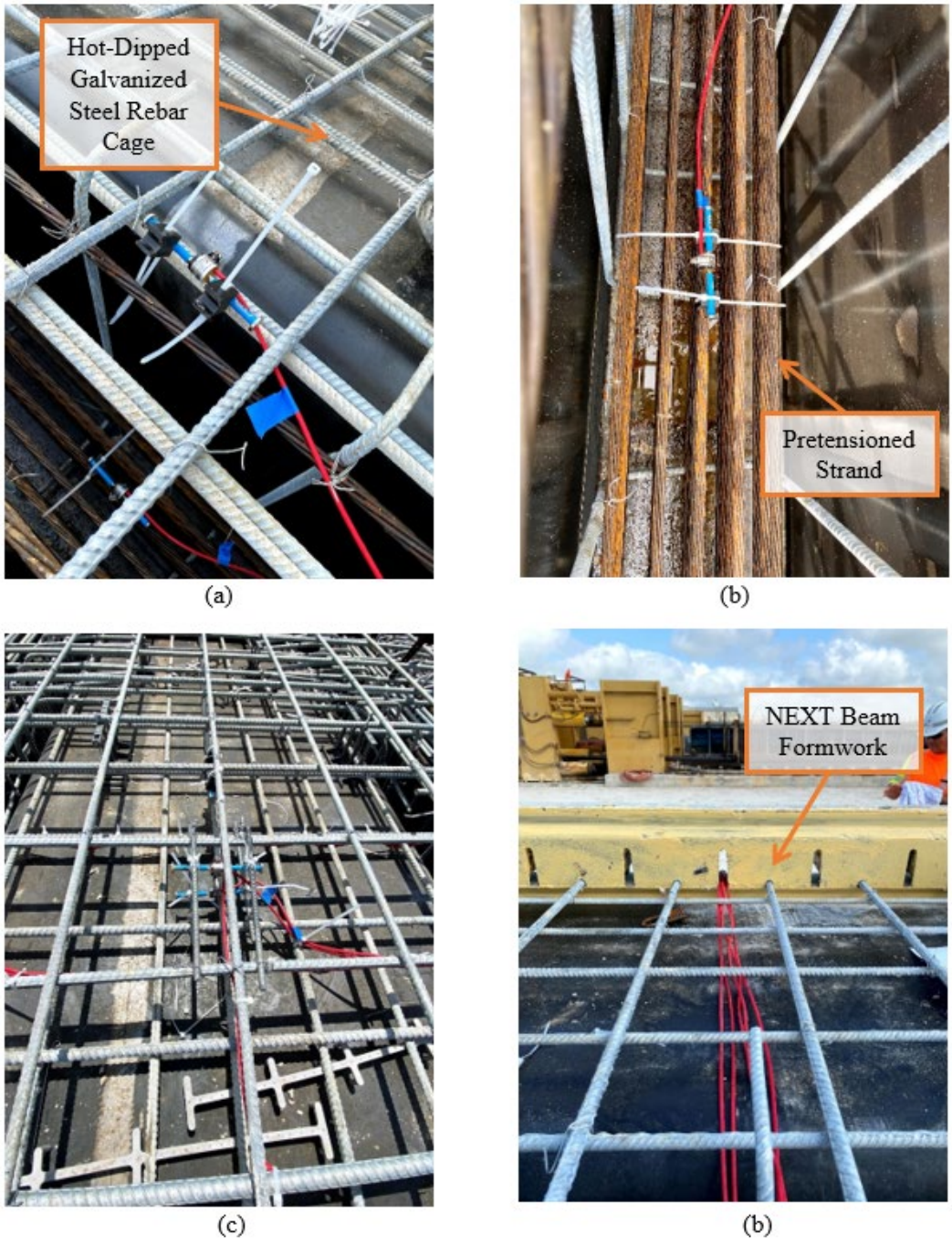

Figure 5.21 NEXT Beam VWG Installation. (a) Installation of longitudinal VWG using machined plastic blocks; (b) Installation of VWG on pretensioned strand; (c) Installation of transverse gauges; (d) VWG Wires exiting side formwork to be connected to DAQ.

Figure 5.22 Overview of NEXT Beam Section RB2-2 Prior to Casting and After Instrumentation Installed

Figure 5.23 NEXT Beam Section RB2-2 After Casting with VWG Wires Exiting Side of Beam and Running along Rebar Located within Future Closure Joint

Figure 5.24 DAQ System Equipped with Solar Power Setup at Precast Plant

Two days after the beam was casted, it was planned to be moved to the precast plant's curing area. With the gauges installed and the DAQ collecting data, the researchers needed to head back to site to prepare the instrumentation for the move and avoid any possible data loss due to damaged VWG wires. To avoid having to disconnect all the VWG wires, the DAQ and accompanying enclosure and solar panel were placed on top of the casted NEXT beam during transport. Once lifted and placed in the curing area, the beam was covered, and the enclosure and solar panel were placed adjacent to the beam to continue collecting data as shown in Figure 5.24. The researchers were present during the entire transport process to ensure the VWG wires were not damaged and to check that the DAQ was still collecting data. Refer to Figure 5.25 to see how the NEXT beam was transported.

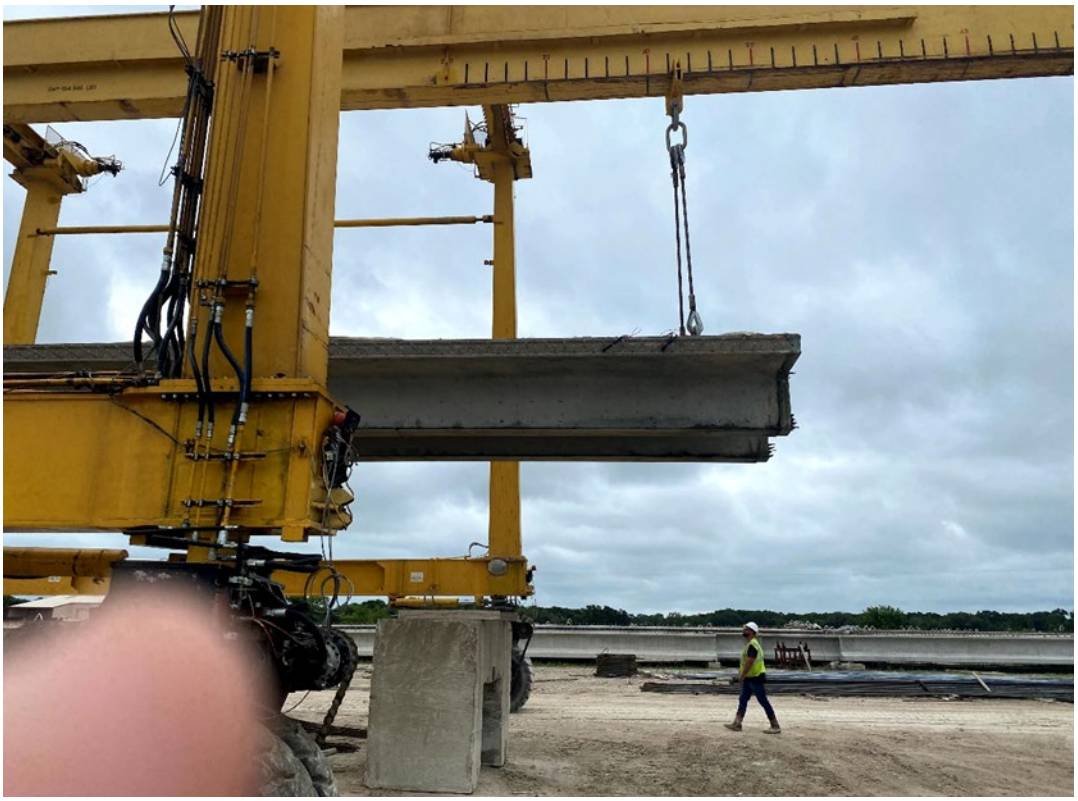

Figure 5.25 NEXT Beam RB2-2 Being Transported to Curing Area

Finally, once the NEXT beam was ready to be transported to the Farwell Creek Bridge site, the researchers returned to the precast plant on July 19th, 2021, to prepare the VWG wires and disconnect the DAQ to bring back to FSEL. All VWG wires were disconnected from the DAQ and safely placed within a weather-proof enclosure and taped at all openings to prevent any potential damage from water intrusion (Figure 5.26). Moreover, since the enclosure needed to be secured to the NEXT beam during transport, a ratchet strap was used. The ratchet strap went from the closure joint rebar on one end of the beam, up and over the enclosure, to the rebar on the other end for a tight fit (Figure 5.27a). Also, to avoid any possible tearing to the straps, plastic protectors were placed below the straps at edge locations of the beam (Figure 5.27b). Figure 5.28 provides an overview of the researcher's instrumentation shipping system.

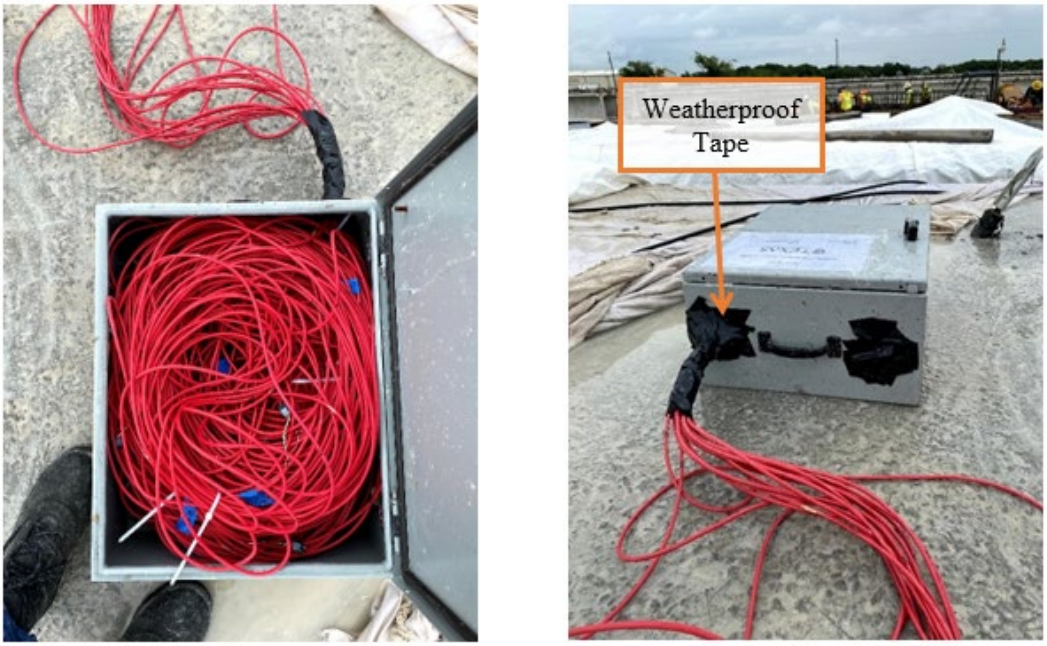

Figure 5.26 Shipping Enclosure Box Setup. (a) VWG wires placed within enclosure; (b) Weatherproof tape applied to openings of enclosure to prevent water intrusion.

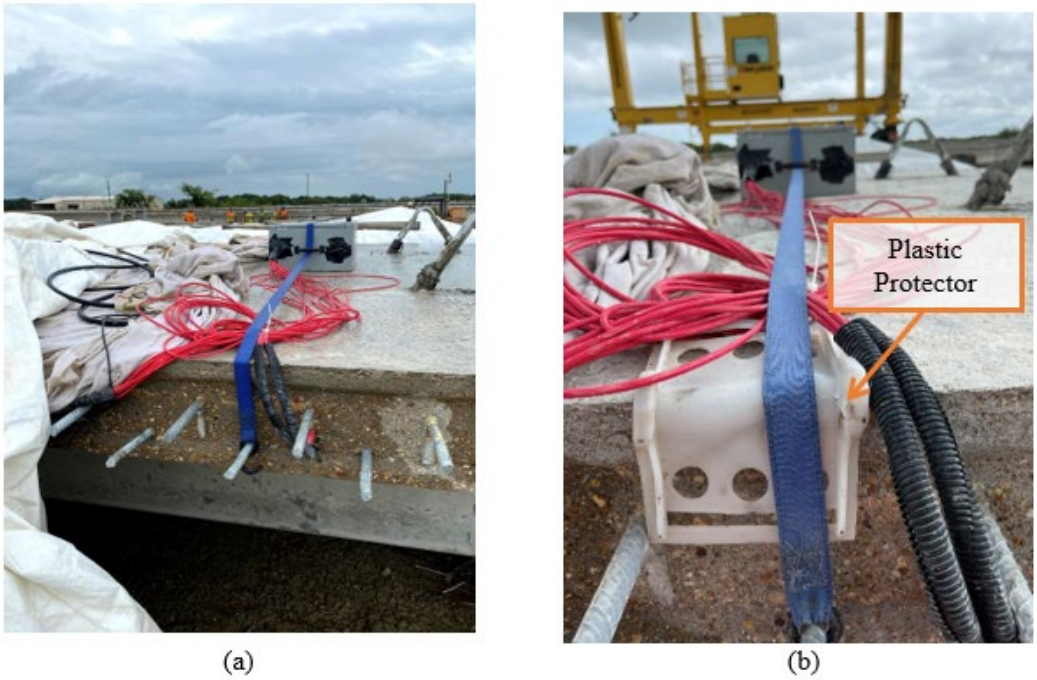

Figure 5.27 NEXT Beam Ratchet Strap Installation. (a) Ratchet strap used to keep enclosure in place atop NEXT beam; (b) Plastic protector placed at edge of NEXT beam to prevent damage to ratchet strap.

Figure 5.28 Overview of Instrumentation Shipping System

5.1.4. Standardized VWG Installation Process

Instrumentation of the closure joints began after all the prefabricated elements were placed on the bridge. This usually indicated that the closure joint would be poured within one or two days. Therefore, the Navasota River Bridge's closure joints were instrumented on March 17th, 2021, while those of the Farwell Creek Bridge were instrumented on August 15th, 2021. The instrumentation process was relatively similar for both bridges. Therefore, a standardized process will be explained below.

To avoid delays in the field and to keep the equipment organized, the DAQ was assembled at FSEL. The DAQ consisted of an enclosure box to protect the DAQ equipment from the natural environment; a Campbell Scientific (CS) Model CR6 Series datalogger to initiate and collect/store data; a CS AM16/32B multiplexer to increase the number of channels available for data collection; a CS Cell210 4G LTE CAT1 Cellular Module for remote connection capabilities; and a 12V sealed lead acid (SLA) rechargeable battery to power the system. The entire setup can be seen in Figure 5.29. Moreover, to make it easier for the researchers, identification markers were placed at both ends of the VWG wires to keep track of which gauge was associated with each multiplexer channel. Furthermore, outside of the enclosure box, a cellular antenna was connected to increase the range of the cellular module. A solar panel was also attached to the side of the bridge to allow for a continuous cycle of power for the long-term monitoring aspect of this project. All exposed wiring was wrapped in weatherproof tape. Figure 5.30 provides an overview of the cellular antenna and solar panel locations at both bridges.

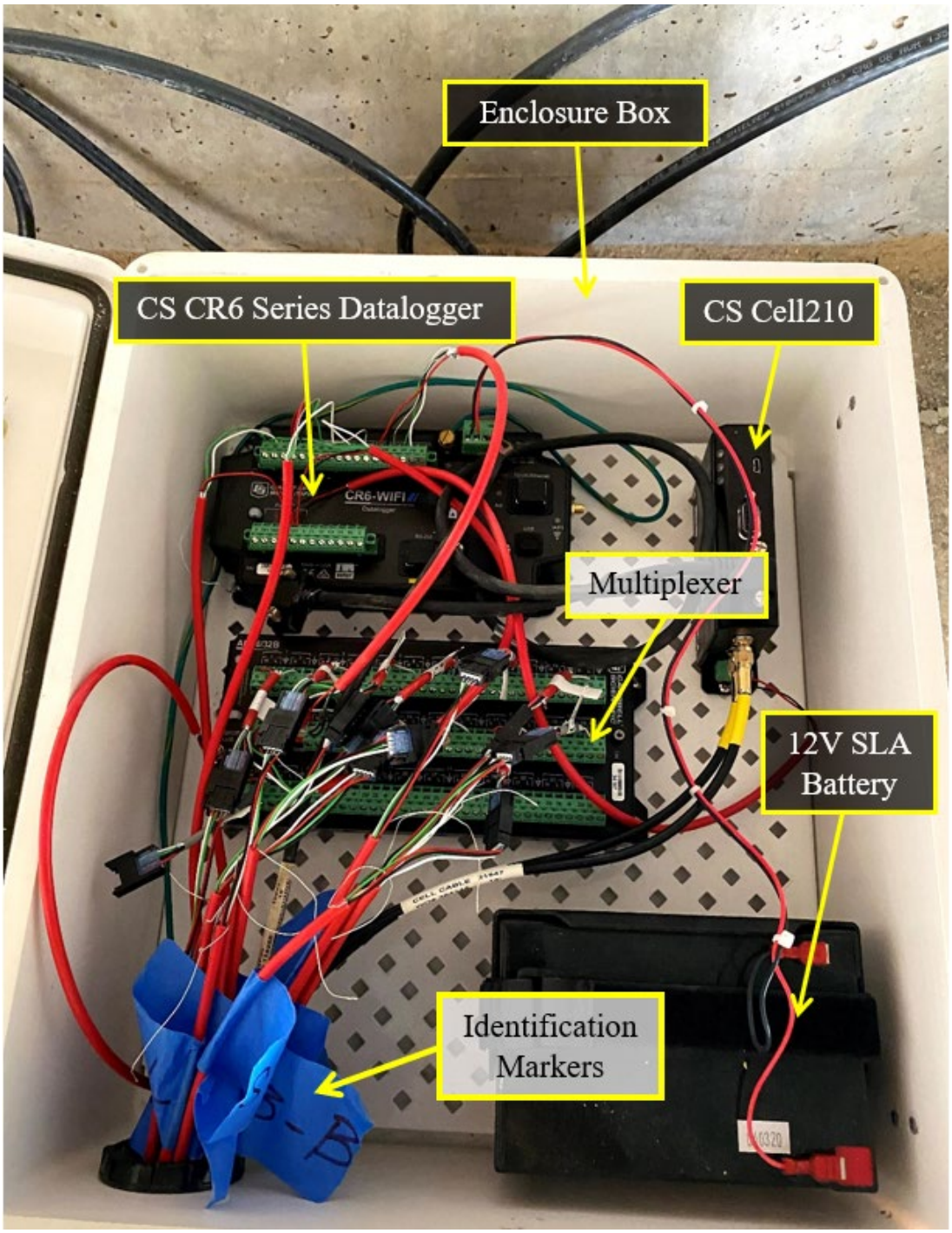

Figure 5.29 Overview of DAQ System

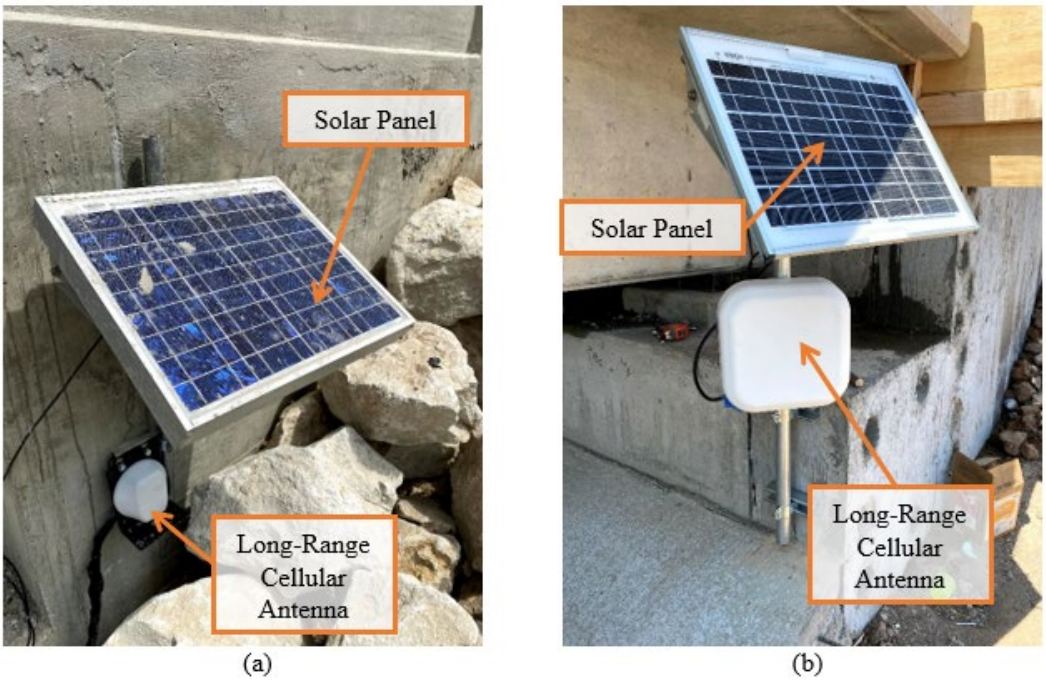

Figure 5.30 Solar Panel and Cellular Antenna Setup. (a) Navasota River Bridge; (b) Farwell Creek Bridge

Field installation was typically completed in one-day by the researchers at both bridge sites. The instrumentation installation procedure was as follows:

1. Provide markings at all VWG locations based on the instrumentation plan (Figure 5.31b).

2. Install VWGs using one-foot no. 3 rebars and plastic zip-ties. In terms of transverse gauges, two rebars were placed perpendicular to the closure joint rebar and tied down using metal ties (Figures 5.31c and 5.33c). Longitudinal gauges also used two rebars placed perpendicular to the closure joint rebar; however, to ensure the gauge was in the middle, machined plastic blocks were used as shown in Figure 5.32b. The plucker, thermistor, and lead wire were attached to the VWG and secured using a hose clamp (Figure 5.31c).

3. Using a Geokon Model GK-404 Vibrating Wire Readout machine (Figure 5.31d), calibrate the gauges to approximately 2500 με and note down the value.

4. Run VWG wires down the closure joint, snip excess wire, attach end connector dock (Figure 5.32a), and connect gauge wires to multiplexer. Place desiccant packs to minimize the impact of humidity and moisture collection that might cause damage to the DAQ.

5. Place DAQ enclosure in secure location (Figures 5.32c and 34c).

6. Record the time each joint with installed VWGs is poured to ensure a "time zero" value is available for data processing purposes.

Refer to Figures 5.31 to 34 below for an overview of the instrumentation installation steps from both bridges. Also, since the configured DAQ system was capable of wireless communication, no trips were needed to collect data. Data was readily available 24 hours a day and could easily be accessed through CS's LoggerNet program. Data was collected and stored in a backed-up Microsoft Excel spreadsheet regularly.

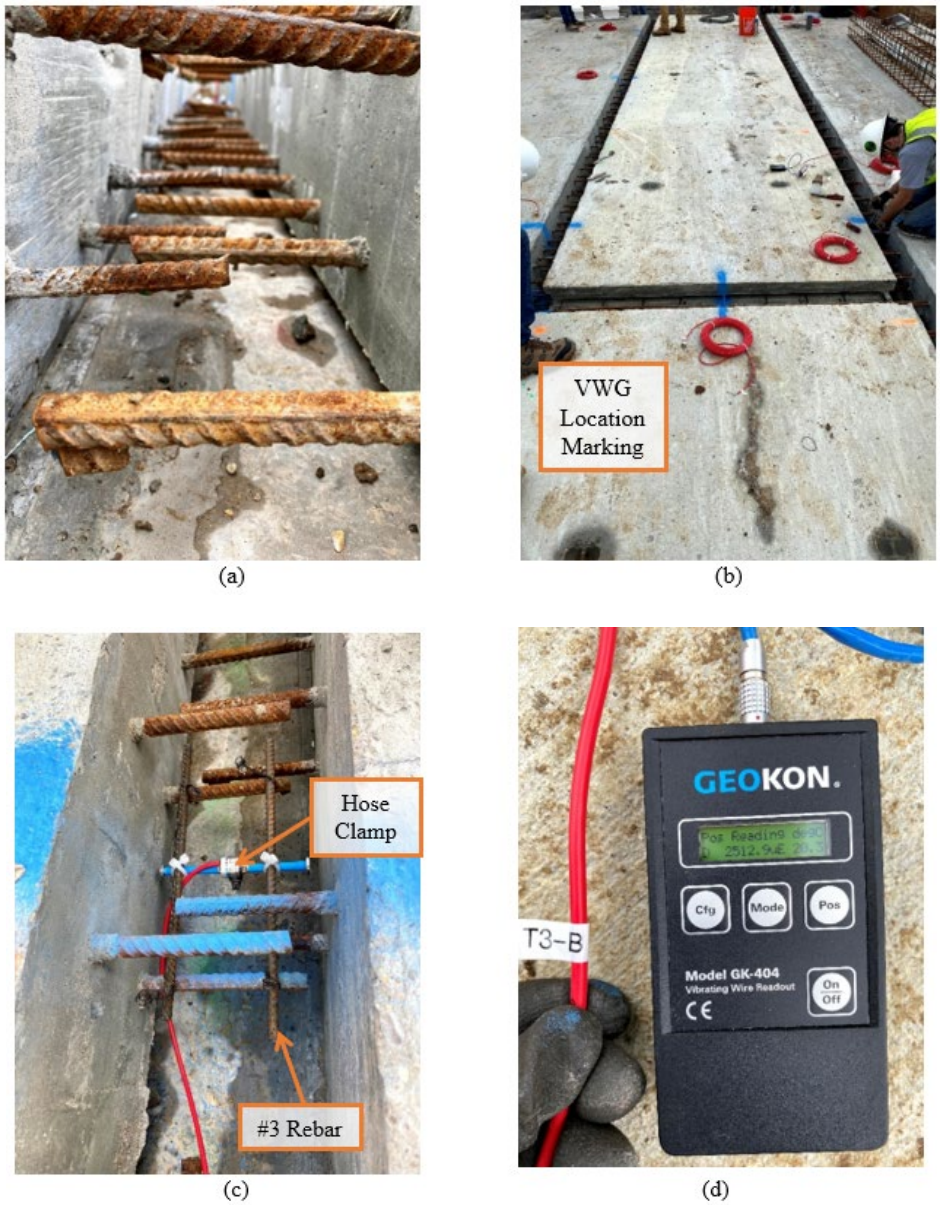

Figure 5.31 Navasota River Bridge Instrumentation. (a) Non-Contact Lap Splices; (b) Markings at VWG locations; (c) Installation of transverse VWG; (d) GK-404 to calibrate VWGs.

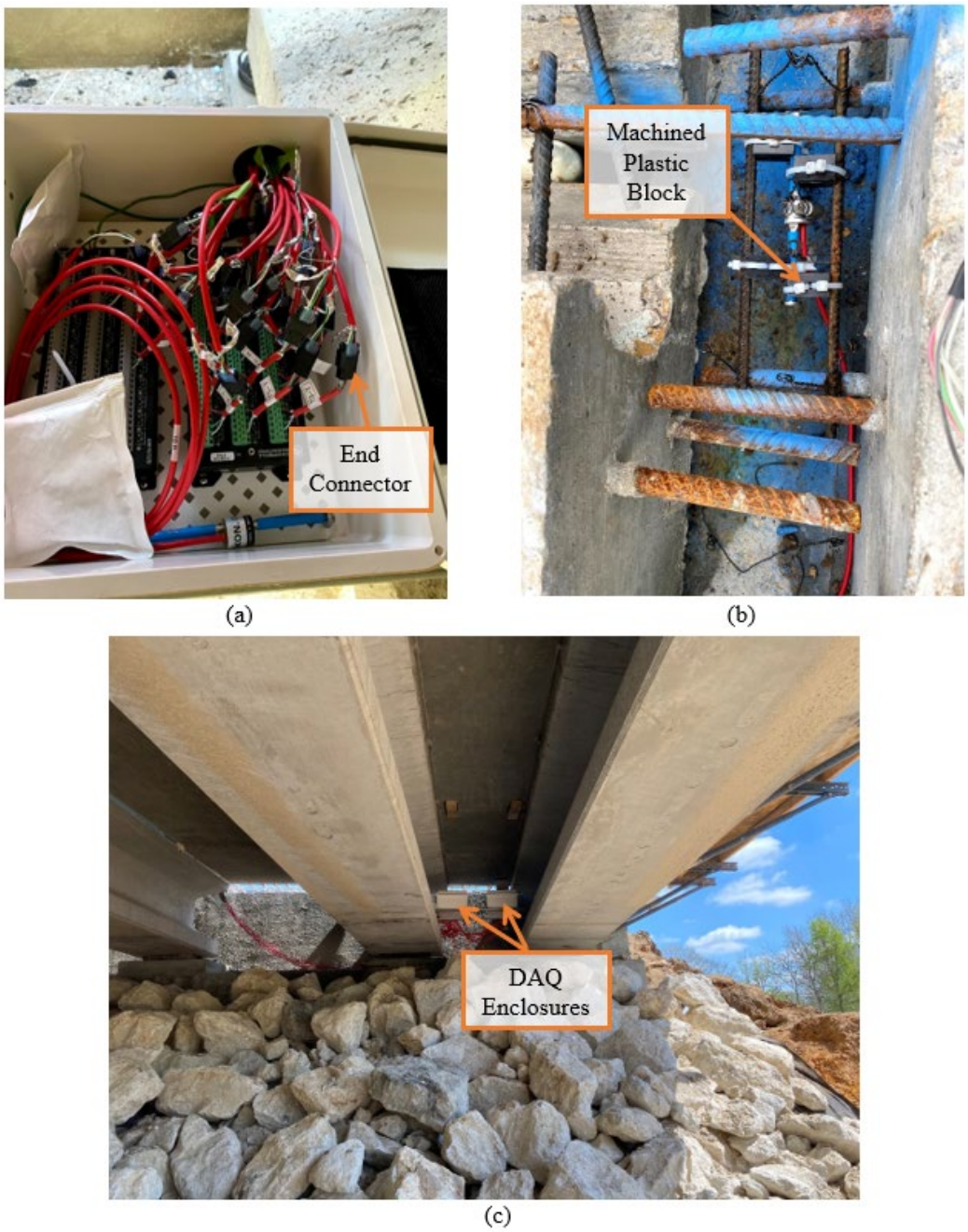

Figure 5.32 Navasota River Bridge Instrumentation (continued). (a) Connecting VWG wires to multiplexer using end connector; (b) Installation of longitudinal VWG using plastic machined blocks; (c) DAQ enclosures placed between girders near abutment wall.

Figure 5.33 Farwell Creek Bridge Instrumentation. (a) Holes created in formwork to direct VWG wires to DAQ; (b) Organization of VWG wires on bridge deck; (c) Installation of transverse VWGs; (d) Wire holes plugged with foam.

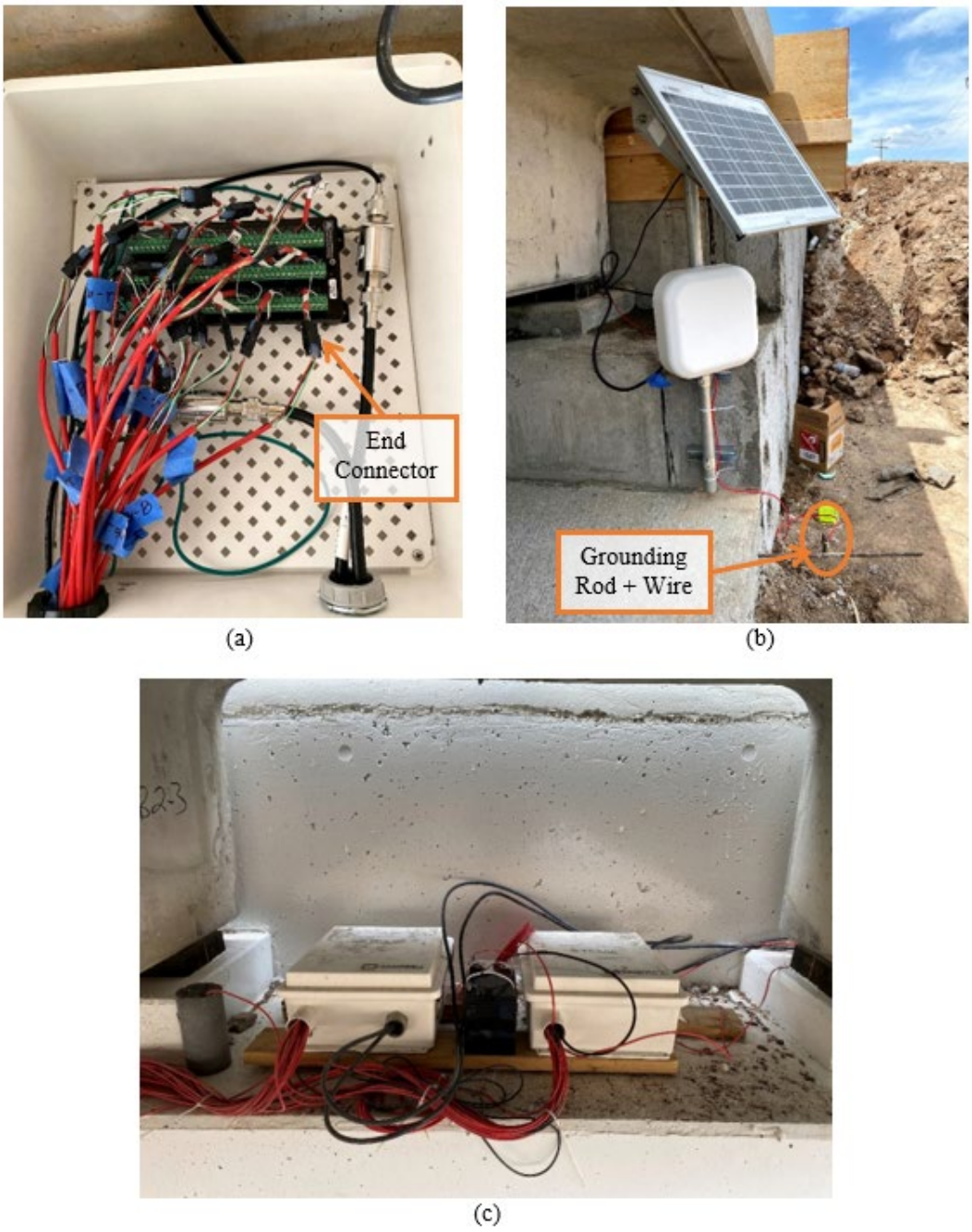

Figure 5.34 Farwell Creek Bridge Instrumentation (continued). (a) VWG wires connected to multiplexer via end connector; (b) Cellular antenna and solar power setup along with grounding rod and wire; (c) Setup of DAQ enclosures near abutment wall.

5.1.5. Problems Encountered During and After VWG Installation

Although the instrumentation installation and monitoring program were a success, there were some isolated issues that needed to be taken care of in a timely manner. For example, at the Navasota River Bridge, the researchers noticed data values not being collected by the VWGs embedded within the drop-in deck panel as of April 2nd, 2021, at 1:30 PM. During a site visit on April 19th, the researchers noticed a new expansion joint installed at the interface between the bridge and the approach slab. After reviewing the detail for this expansion joint, the researchers concluded that the VWG wires were most likely cut unintentionally during installation by the contractor. Figure 5.35a shows the VWG wires exiting the end of the panel near the future location of the expansion joint. Figure 5.35b shows the expansion joint installed between span 5 of the bridge and the approach slab.

Figure 5.35 Navasota River Bridge Drop-In Deck Panel Lost Gauges. (a) Gauge wires shown exiting front-end of panel near future location of expansion joint; (b) Installed expansion joint.

Furthermore, after installing the instrumentation at the Navasota River Bridge on March 17th, 2021, the researchers were having a lot of difficulty connecting remotely to the datalogger. The researchers realized that there was an issue with the type of cellular antenna used. Initially, a short-range dipole antenna was used; however, after conducting research on the cellular service in the area, the researchers realized the nearest cellular tower was more than five miles away near the town of North Zulch, Texas. Therefore, the antenna was replaced with a long-range antenna and remote capabilities were achieved on April 19th, 2021. Refer to Figure 5.30a for the antenna setup. The exposed antenna wire was wrapped in

weatherproof tape to ensure integrity of the system during the monitoring phase of the project.

At the Farwell Creek Bridge, the researchers had to deal with power issues related to the datalogger. On September 22, 2021, skipped data collection times were noticed. Then, on October 6th, the datalogger completely shut off. Battery values were shown to be falling steadily until the datalogger reached values lower than 8 volts. The researchers deduced that the issue was associated with the location of the solar panel since data was being collected during the day and not at night. Therefore, the researchers purchased a new battery and relocated the solar panel to the wingwall of the bridge to avoid any shadows and get the full range of sunlight. Therefore, there is a data collection gap for the Farwell Creek Bridge from October 6th, 2021 to November 13th, 2021, when the datalogger was powered back on after the repair. Refer to Figure 5.36 to see the relocation of the solar panel.

Figure 5.36 Farwell Creek Bridge Solar Panel Relocation. (a) View from bridge; (b) Relocation to wingwall – view from below deck

5.1.6. Overall Instrumentation Timeline

Figure 5.37 below outlines important events that occurred during the full instrumentation program and provides a general summary of the process.

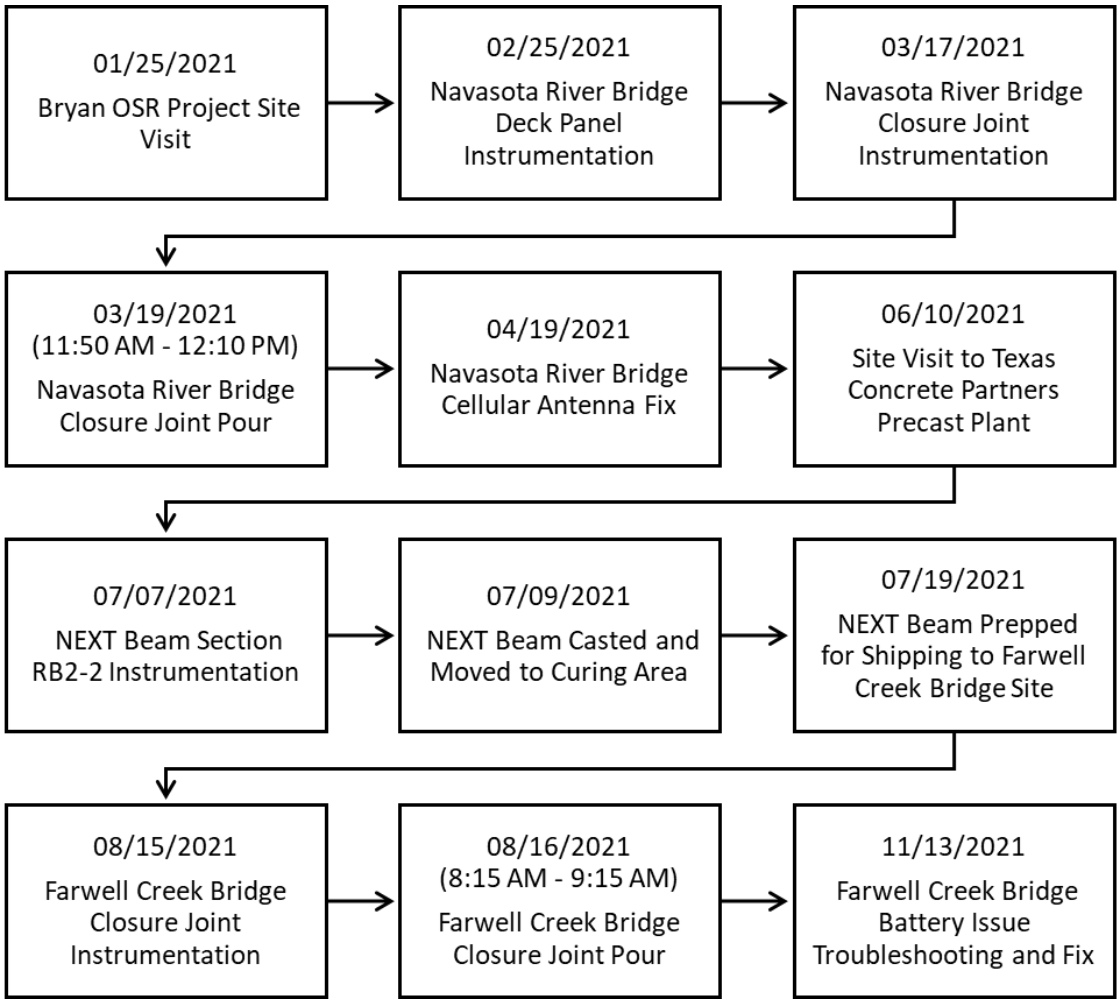

Figure 5.37 Instrumentation Timeline

5.2. Data Interpretation, Results, and Discussion

5.2.1. Introduction

During the time of analysis of data collected from our field instrumentation equipment, the Navasota River Bridge was monitored for approximately one year (March 19th, 2021 to March 14th, 2022) while the Farwell Creek Bridge was monitored for approximately seven months (August 15th, 2021 to March 14th, 2022). This monitoring timeframe will allow the researchers to provide an assessment of the short-term and long-term material and time-dependent behaviors of the RSFRC in the Navasota River Bridge (NRB) and the proprietary UHPC used in the Farwell Creek Bridge (FCB).

The raw data collected from the bridges included the strains in the VWGs as well as the temperatures at the locations of the gauges. These measurements were then

converted to the structural behavior parameter of engineering strain. Engineering strain, in this context, means that the researchers are assuming the length, and in some cases the width, of the concrete in which the VWG is placed remains constant throughout the monitoring period. In mathematical terms, this means that strain is computed as the change in length, or width, divided by the original length, or width, of the concrete section.

A summary of the concrete material properties can be found in Table 5.6 below.

Table 5.6 Instrumented Bridges' Concrete Properties

Concrete Properties					
Concrete	**28 Day Compressive Strength (PSI)**	**28 Day Modulus (PSI)**	**28 Day Splitting Tensile Strength (PSI)**	**Coefficient of Thermal Expansion (με/°F)**	**Tensile Cracking Strain (με)**
NRB Drop-In Panel (TxDOT Class S)	4000	3.83×10^6	425	5.50×10^6	111.00
NRB Closure Joint (UHPC-C1-2)	8990	7.38×10^6	770	7.00×10^6	105.00
NEXT Beam Mix (WACO-NEXT)	11360	6.40×10^6	620	5.00×10^6	97.00
FCB Closure Joint (UHPC-P3-2)	26340	8.10×10^6	3080	7.80×10^6	380.00
Notes: NRB = Navasota River Bridge FCB = Farwell Creek Bridge					

It is important to note that the Navasota River Bridge drop-in deck panel concrete properties were assumed given the specifications from the TxDOT plan sets. Testing was not conducted on this specific concrete mix. Also, the coefficient of thermal expansion value for the RSFRC mixture was estimated based on typical empirical data since testing could not be conducted on the cylinders collected from the bridge site.

Moreover, a general theme the researchers found in the strain data of the closure joints is that of concrete volume shrinkage. According to Xiaomeng Ge et al. in their study "Designing for Deck Stress Over Precast Panels in Negative Moment Regions", one of the major causes of cracking in bridge decks is concrete volume shrinkage, which primarily consists of plastic shrinkage, autogenous shrinkage, and drying shrinkage (Ge et al., 2021).

Plastic shrinkage occurs when moisture evaporates from the fresh concrete surface during the hardening process. This is why it is important to cover finished concrete immediately with moisture-proof mats to provide a humid environment during the curing process. Similarly, autogenous shrinkage also occurs during the hardening

process, and is caused by the hydration of cement. According to Ge et al., autogenous shrinkage is more significant in concrete mixtures with a low water-to-cement ratio (Ge et al., 2021). Therefore, it would be expected that higher strength concrete, which is the case in this study, would have more autogenous shrinkage than normal-strength concrete. Finally, drying shrinkage, which is the most dominant form of concrete volume shrinkage, occurs due to the loss of moisture from the cement paste since it is not kept underwater or in air with 100% relative humidity. Overall, the amount of concrete volume shrinkage is dependent on the size of concrete, environmental humidity, and length of time the concrete is kept exposed to dry air (Ge et al., 2021). These components of shrinkage will be broadly explored when deciphering the strain data.

5.2.2. Strain Change Calculations

The post-processing of the strain and thermal data collected from the VWGs was heavily influenced by Hossein Yousefpour's "Structural Monitoring of the World's First Precast Network Arch Bridge during Construction" (Yousefpour et al., 2014). According to Yousefpour, calculations related to strain change must account for thermal deformations in both the concrete *and the* VWG. In actuality, because the end blocks of the VWGs move together with the concrete, only the deformation of the surrounding concrete is recorded. The thermal expansion of the VWG is also not included in the strain measurement. The coefficient of thermal expansion of the VWG (α_{VWG}) is generally also different from that of concrete (α_C), albeit very miniscule. Therefore, in order to calculate the real total strain change within the VWG, the equation derived by Yousefpour in Figure 5.38 was used to analyze the collected bridge data.

$$\Delta\varepsilon_{Total}^{(i)}(t,t_0) = [\varepsilon_{VWG}^{(i)}(t) - \varepsilon_{VWG}^{(i)}(t_0)] + \alpha_{VWG} \times [T^{(i)}(t) - T^{(i)}(t_0)] \quad (5.3)$$

In which,

$\Delta\varepsilon_{Total}^{(i)}(t,t_0)$	= Total strain change at the location of VWG i, between time t and time t_0, including unrestrained thermal deformation
$\varepsilon_{VWG}^{(i)}(t)$	= Strain in VWG i at time t, as obtained from DAQ
$\varepsilon_{VWG}^{(i)}(t_0)$	= Strain in VWG i at time t_0, as obtained from DAQ
$T^{(i)}(t)$	=Temperature in VWG i at time t
$T^{(i)}(t_0)$	=Temperature in VWG i at time t_0
α_{VWG}	$=6.78 \times 10^{-6} \frac{1}{^\circ F}$, Coefficient of thermal expansion of the VWG

Figure 5.38 Total Strain Change Equation Derived by Yousefpour (Yousefpour et al., 2014)

Furthermore, to get the non-thermal part of the concrete strain change ($\Delta\varepsilon_{nth}$), the unrestrained thermal deformation of the concrete was subtracted from the $\Delta\varepsilon_{nth}$ term using the equations as shown in Figure 5.39. Note that negative strain values

correspond to compression of the section, while positive values correspond to tension.

$$\Delta\varepsilon_{nth}^{(i)}(t,t_0) = [\varepsilon_{VWG}^{(i)}(t) - \varepsilon_{VWG}^{(i)}(t_0)] + (\alpha_{VWG} - \alpha_C) \times [T^{(i)}(t) - T^{(i)}(t_0)] \quad (5.4)$$

In which,

$\Delta\varepsilon_{nth}^{(i)}(t,t_0)$ = Total strain change in the concrete at the location of VWG i, between time t and time t_0,excluding unrestrained thermal deformations

α_C = Coefficient of thermal expansion of the VWG, determined in Section 5.5

Figure 5.39 Non-Thermal Total Strain Change Equation Derived by Yousefpour (Yousefpour et al., 2014)

With the derived equations above, the researchers were able to analyze the strain data and determine patterns and conclusions, as will be discussed in the upcoming sections.

5.2.3. Navasota River Bridge VWG Strains – Interpetation and Discussion

5.2.3.1. Transverse VWGs

All the transverse gauges within the Navasota River Bridge closure joints had the same short-term strain patterns, with the only difference being in the actual strain values. For this reason, the researchers will only present one set of short-term transverse strain gauge data to provide a visual of the general strain trend, with the rest of the short-term transverse strain gauge data attached in Appendix A.1 of this paper for review.

Figure 5.40 below shows the short-term transverse strain gauge data for gauges T1-B and T1-T. By evaluating the transverse closure joint strain trends, early-age volume change (plastic, autogenous, and drying shrinkage) of RSFRC was quantified. It is important to note that during the site visit to the Navasota River Bridge site on 3/19/2021, the researchers observed that no wet curing was performed following the closure joint pour. Instead, the contractor opted to apply water via a brush, which left the closure joints exposed to the natural environment. Therefore, the researchers believe the initial steep drop in strain within the first day was due to a combination of plastic and autogenous shrinkage. The researchers are unable to quantify the exact amount of each type of shrinkage. Further materials testing at the bridge site and within the lab are needed to provide such an answer. As mentioned previously, this pattern was present in the short-term behavior of all transverse gauges within the closure joint – a steep strain drop followed by the strain value leveling out. In all cases, the bottom gauge (i.e., T1-B) had more

negative strain values than the top gauge (i.e., T1-T). These gauges never displayed tensile, or positive, strain values.

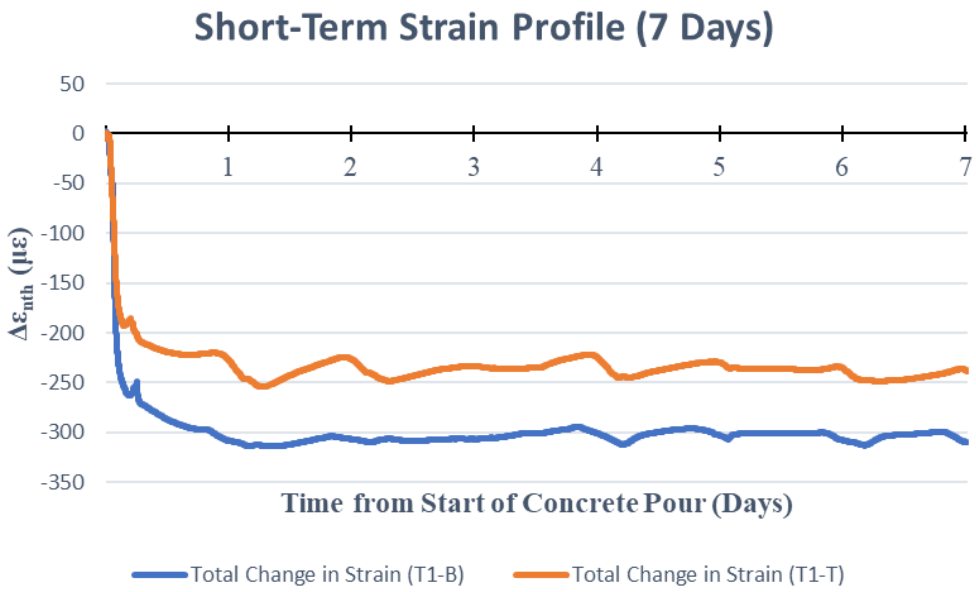

Figure 5.40 Short-Term Strain Profile for Navasota River Bridge Gauges T1-B and T1-T

When the gauges were first installed, the researchers decided to collect data every minute to better understand the behavior of the RSFRC immediately after being poured. On March 26th, 2021, the researchers changed the scan interval from one minute to thirty minutes since in-depth data was no longer required after one week of constant monitoring. The thirty minute scans would provide the researchers with a long-term visual of the RSFRC in the closure joints. Unlike the short-term strain data, the long-term transverse data varied.

Gauge sets T1 and T4 had similar trends (Figures 5.41 and 42). After the strain values of both the top and bottom gauges of each set leveled off around late March 2021, warmer months led to more negative strain values for the top gauge from the month of April to October. Once the weather started to cool off at the end of October 2021, the researchers noticed the top gauge strain data returned to levels similar to those seen in late March 2021. Therefore, it is safe to assume the top gauge is influenced more by environmental factors including direct sunlight and ambient temperature and moisture conditions than the bottom gauge. On the other hand, the bottom gauges seem to become less negative in a "linear" fashion until the strain of both the top and bottom gauges match around the beginning of January 2022. No distinct patterns were seen with the bottom gauges in terms of long-term behavior. Neither the top nor bottom strain gauge ever recorded tensile strain values.

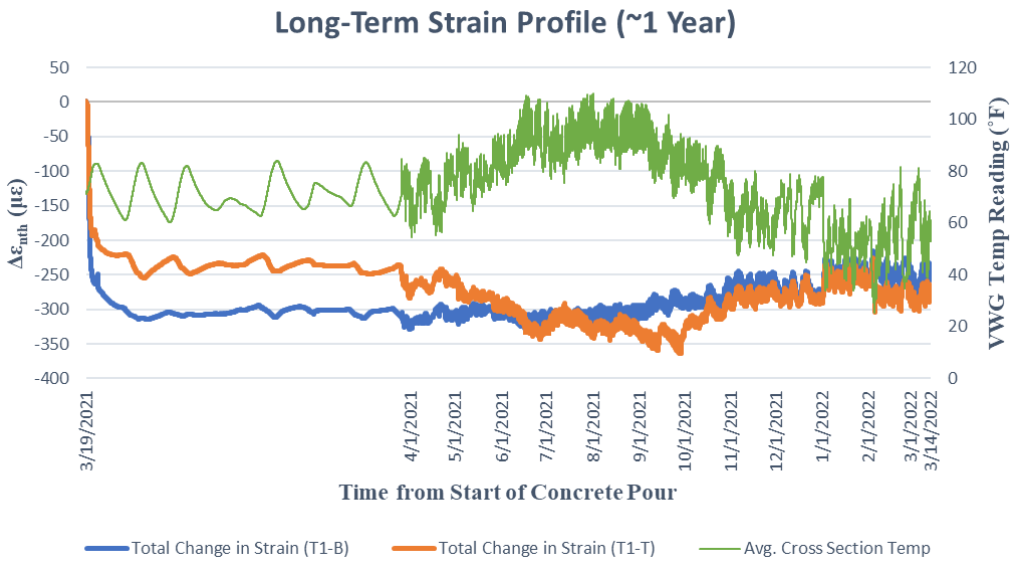

Figure 5.41 Long-Term Strain Profile for Navasota River Bridge Gauges T1-B and T1-T

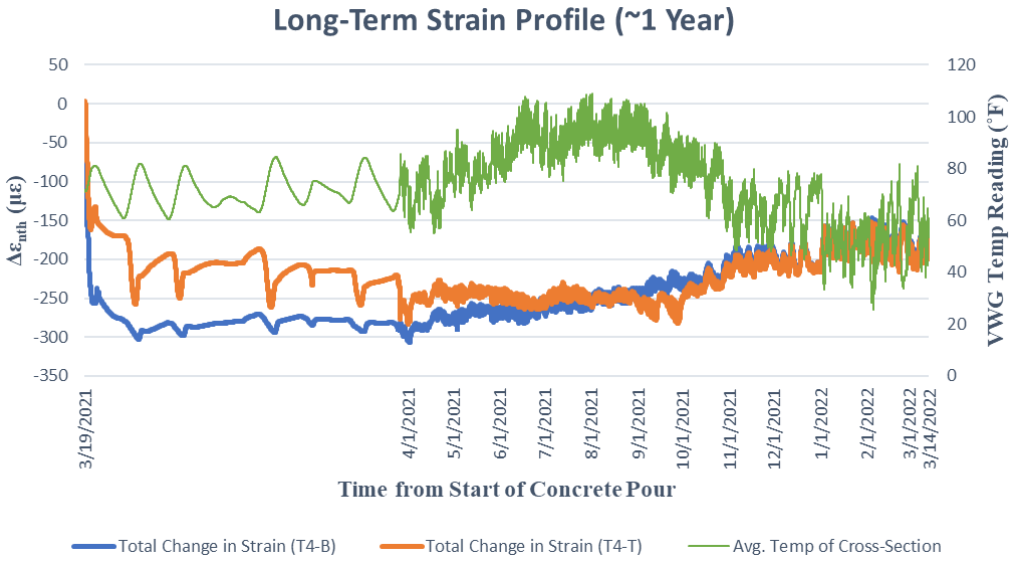

Figure 5.42 Long-Term Strain Profile for Navasota River Bridge Gauges T4-B and T4-T

Figures 5.43 and 44 below show that gauge sets T3 and T6 show different trends, respectively. However, the researchers believe there was a malfunction with gauge T3-B because strain and temperature values started to drop off after August 2021 and subsequently stopped being collected at this location after 10/10/2021. Therefore, the researchers focused on gauge T3-T at this location. Although gauge T3-T wasn't placed into significant compression, it still became less negative over time and oscillated around a strain value of -50 με. There were no temperature related patterns discerned from gauge T3-T.

Gauge set T6 showed a pattern that differed from what was expected. Instead of T6-T becoming less negative, it became more negative after August 2021 and did not have any clear patterns with temperature. The researchers are not sure about the origins of this anomaly. However, the bottom gauge T6-B followed the general trend of "linearly" becoming less negative and normalizing at a strain value.

Overall, after reviewing both the short-term and long-term transverse strain gauge data, the researchers believe that after three or four days, the RSFRC was no longer under autogenous shrinkage and was dominated by drying shrinkage after seven days. Because the strain values showed that the concrete section was in compression from the day of the pour, the researchers do not believe the strain values recorded are excessive or of significant concern. These seem to be typical strain values in bridges that were most likely assumed by the designers of the bridge.

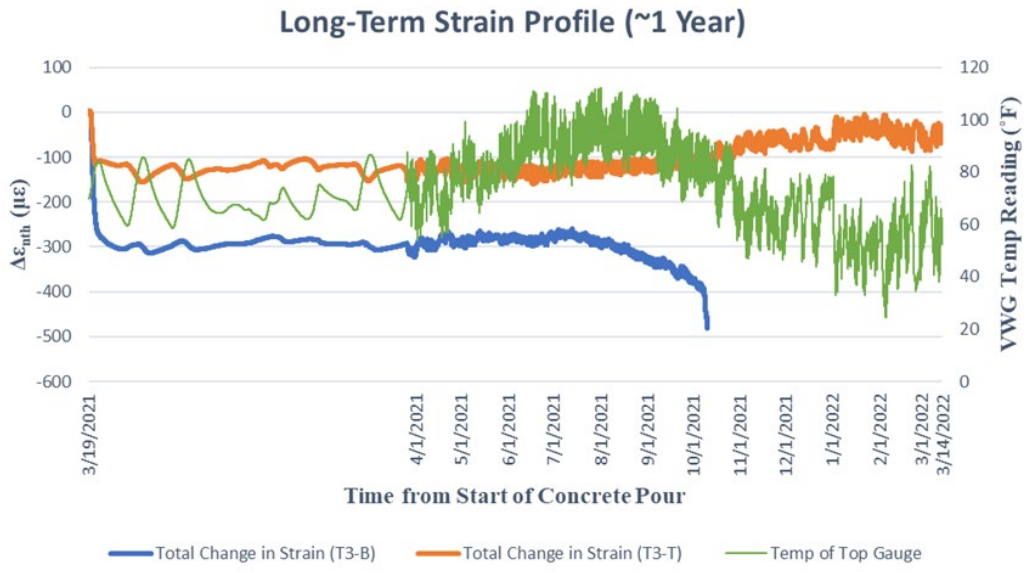

Figure 5.43 Long-Term Strain Profile for Navasota River Bridge Gauges T3-B and T3-T

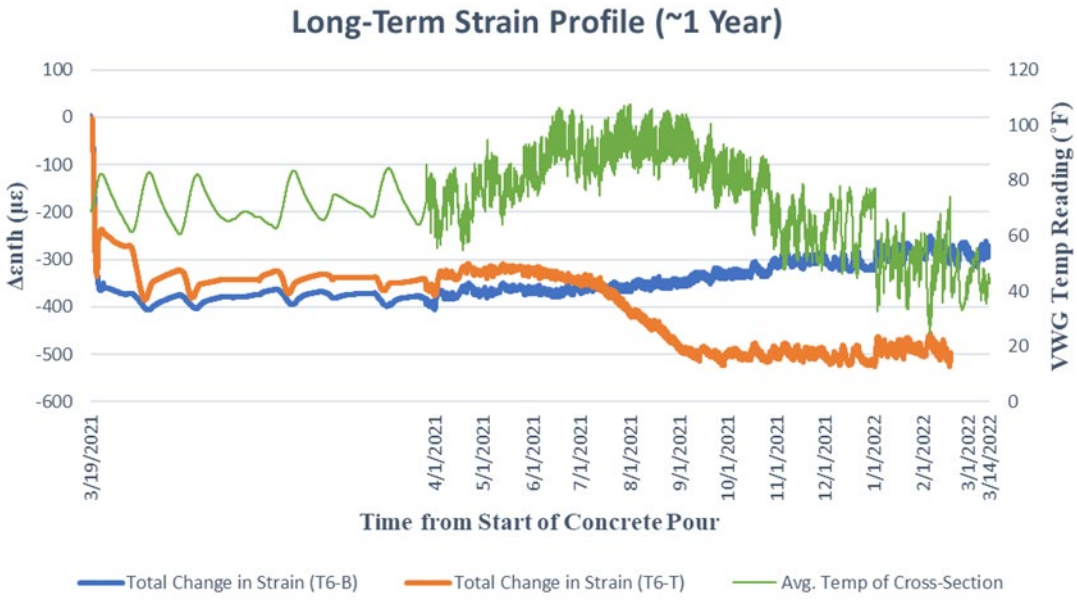

Figure 5.44 Long-Term Strain Profile for Navasota River Bridge Gauges T6-B and T6-T

5.2.3.2. Longitudinal VWGs

Longitudinal strain gauges were located within the longitudinal closure joints, the transverse joint between the Unit 3 drop-in deck panels, and the transverse closure joint between Span 4 and Span 5 of the bridge. The ensuing discussion will focus on each of these locations separately to provide an organized review.

The longitudinal gauges located within the longitudinal closure joints (i.e., L1-S, L3-B, and L3-T) had similar short-term and long-term behaviors. Figure 5.45 displays the short-term strain data for gauge L1-S while Figure 5.46 displays the short-term strain data for gauges L3-B and L3-T. The researchers observed in both cases, the gauges went immediately into tension following the closure joint pour. As shown in Table 5.6, the tensile cracking strain of RSFRC is 105 με, which is exceeded by the concrete in both strain gauge locations. Figures 5.45 and 5.46 also highlight the times the tensile cracking strain was exceeded. While the strain values are not significantly higher than the tensile cracking strain, there was cracking present within the longitudinal closure joints after the first day of the pour as shown in Figure 5.47 below. The cracks, which are extremely small, occur at the corner where the longitudinal closure joint meets the transverse closure joint between spans, typical of early-age shrinkage cracking.

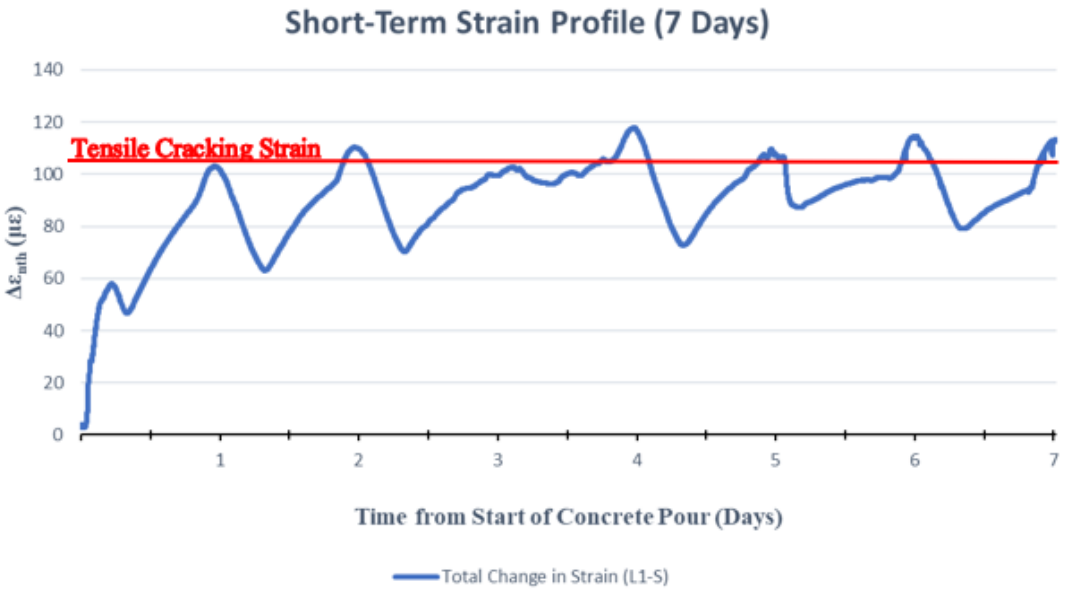

Figure 5.45 Short-Term Strain Profile for Navasota River Bridge Gauge L1-S

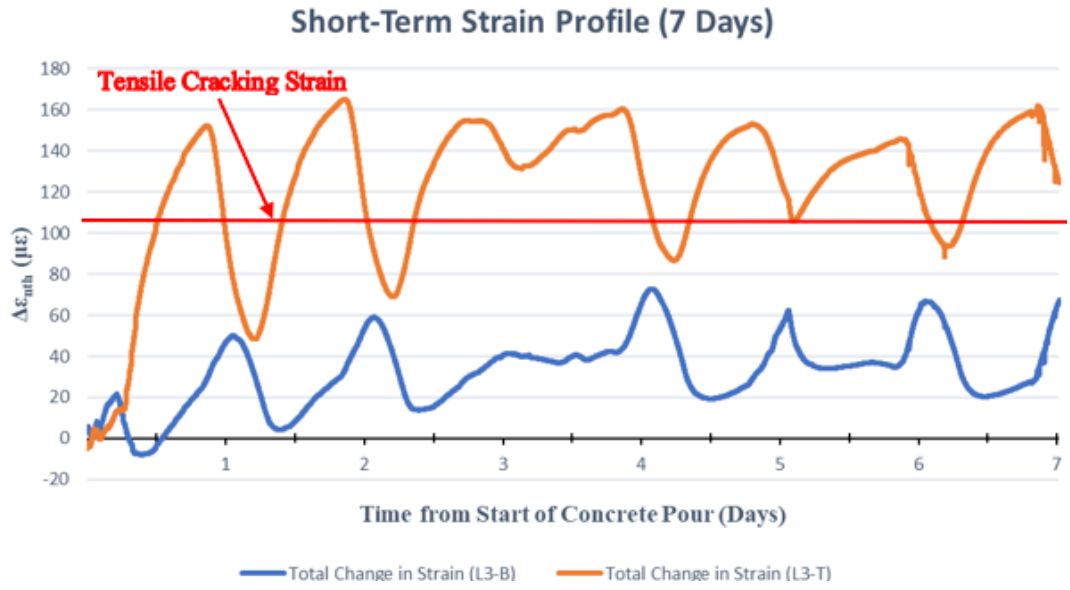

Figure 5.46 Short-Term Strain Profile for Navasota River Bridge Gauges L3-B and L3-T

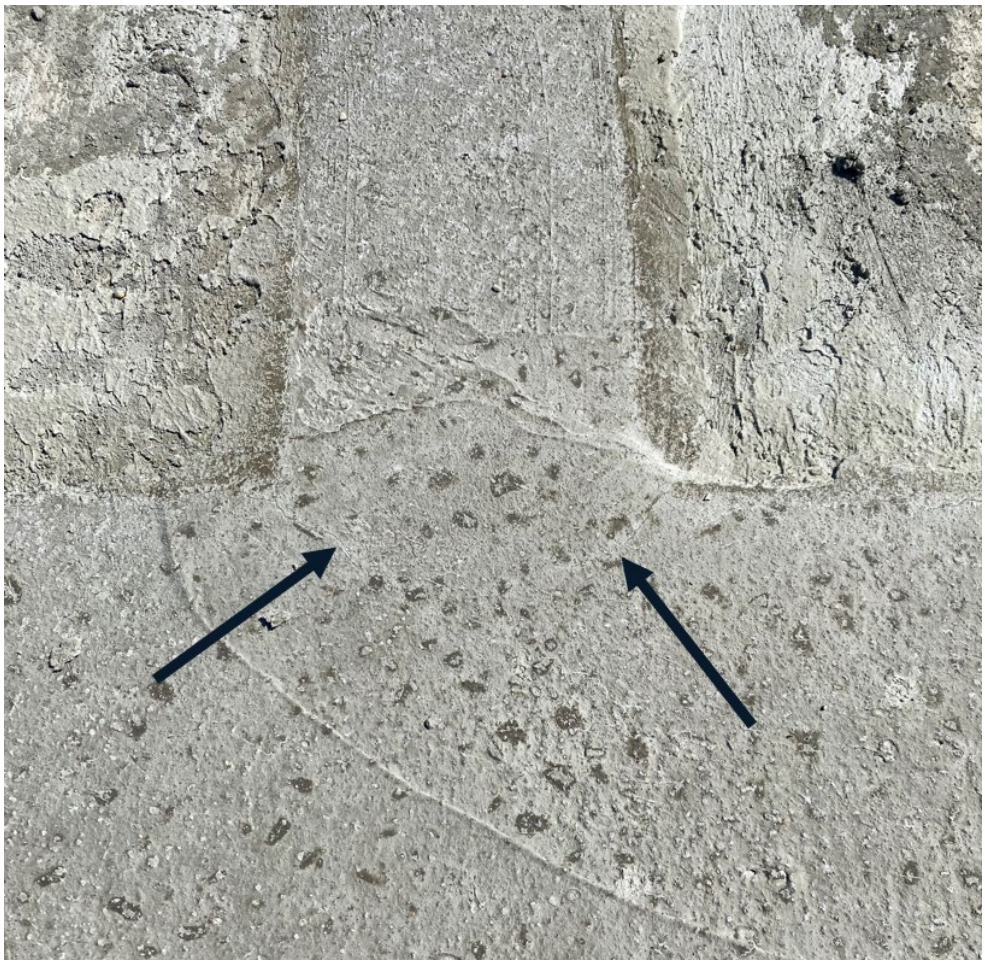

Figure 5.47 Cracking found in Navasota River Bridge Closure Joint

In terms of long-term behavior, which can be seen in Figures 5.48 and 49, the strain values continue to exceed the tensile cracking strain. No site visits have been conducted since April 19th, 2021, so the researchers are not certain if any further cracking has developed within the longitudinal closure joints. Furthermore, the strain values were observed to follow a pattern with the recorded temperature. For instance, as the temperature increased from April 2021 to September 2021, the strain recorded by the gauges decreased and the joint was under lower tensile stresses, which is beneficial for the joint as cracking is less likely to occur. Subsequently, as the recorded temperature started to cool, the strain values started to increase, placing the joint into higher tensile stresses, with the highest being in February 2022. Gauge L3-T was at significantly higher strain values when compared to L1-S, making the RSFRC in that location more susceptible to cracking.

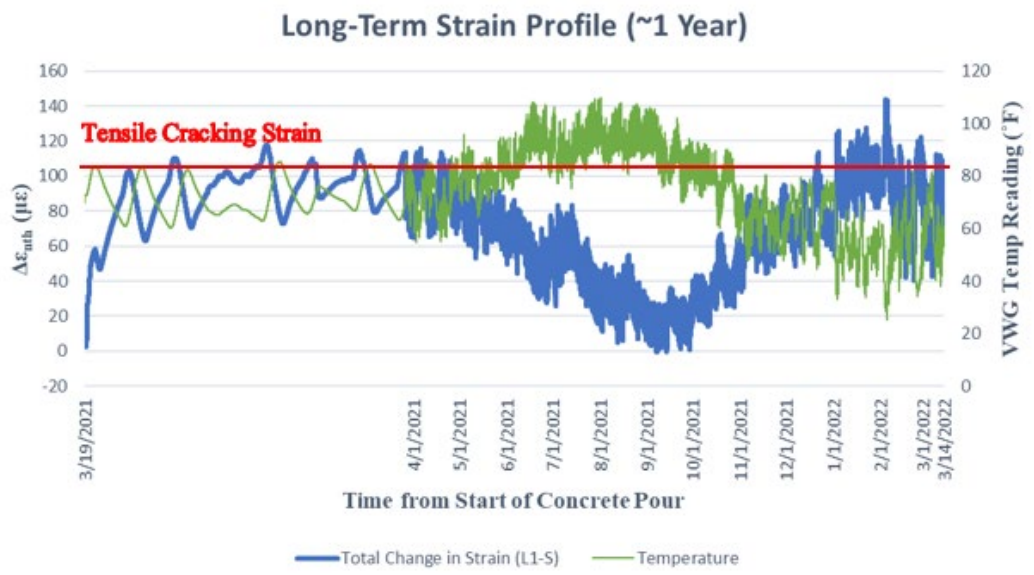

Figure 5.48 Long-Term Strain Profile for Navasota River Bridge Gauge L1-S

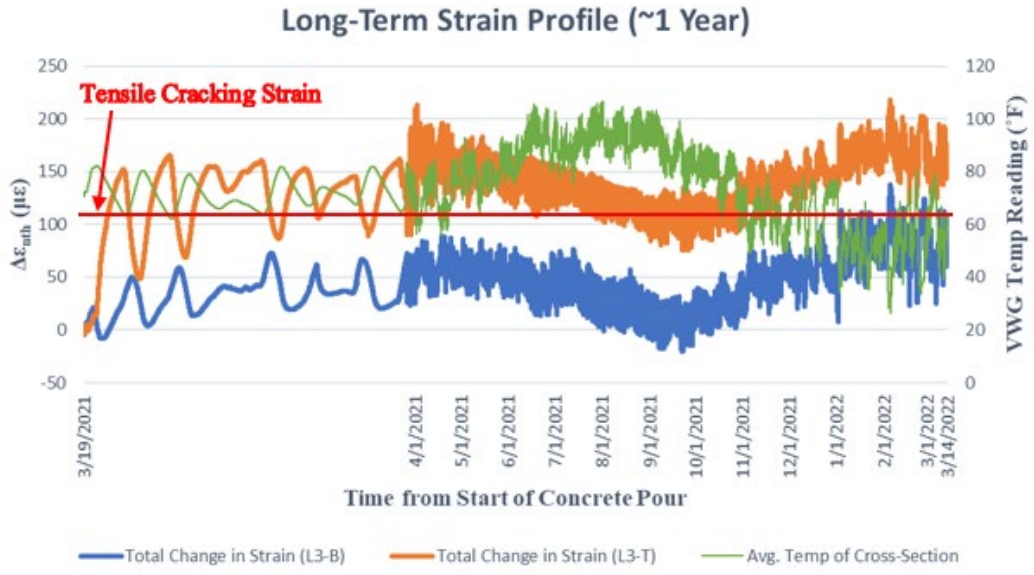

Figure 5.49 Long-Term Strain Profile for Navasota River Bridge Gauges L3-B and L3-T

For the gauges located within the transverse closure joint between Span 4 and Span 5 of the bridge (i.e., L5-B and L6-S), the short-term behavior shows the strains oscillating between tension and compression; however, never exceeding the tensile cracking strain as shown in Figures 5.50 and 51.

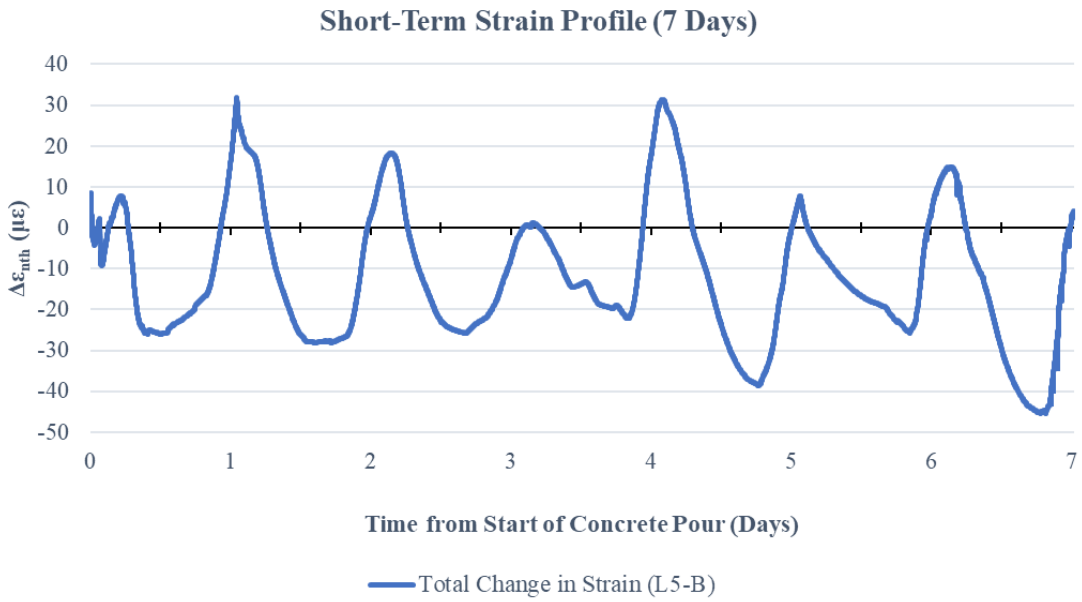

Figure 5.50 Short-Term Strain Profile for Navasota River Bridge Gauge L5-B

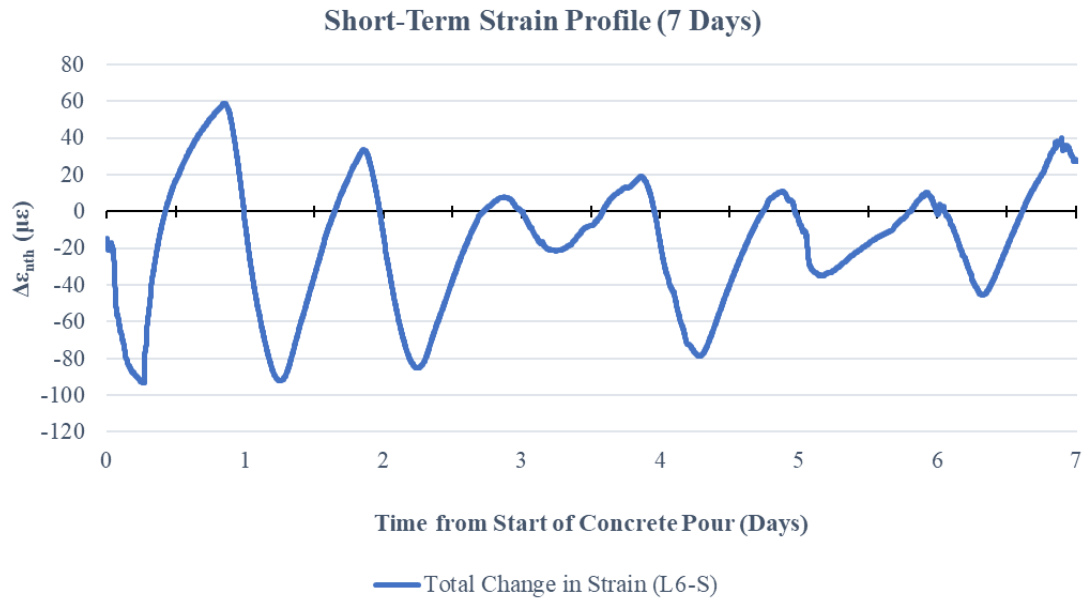

Figure 5.51 Short-Term Strain Profile for Navasota River Bridge Gauge L6-S

On the other hand, the long-term strain behavior of these two longitudinal gauges provides a different perspective. As shown in Figure 5.52, gauge L5-B's strain values cycle with the temperature; however, it does not surpass the tensile cracking strain. Gauge L6-S does not cycle with the temperature and remains in tension at approximately 450 με after April 1st, 2021, as shown in Figure 5.53. This strain value is significantly higher than those recorded by other longitudinal gauges, which shows that the location of L6-S is experiencing tensile strains approximately

four times that of the tensile cracking strain value. While this was only recorded by one gauge, further visual investigation of the region is required to confirm whether cracking has occurred.

Lastly, longitudinal gauge L4-S is located in the transverse joint between the Unit 3 drop-in deck panels. As seen in Figure 5.54 below, the gauge remains in compression like the transverse strain gauges. This makes sense because while L4-S is placed longitudinally in terms of the bridge orientation, it is actually placed transversely in terms of the joint. Long-term behavior of the gauge, as depicted in Figure 5.55, shows the concrete strain becoming less negative and approaching 0 με. Similar to the transverse gauges discussed in the previous section, this means the concrete in the location of L4-S is undergoing less compressive stress over time. No temperature patterns were observed.

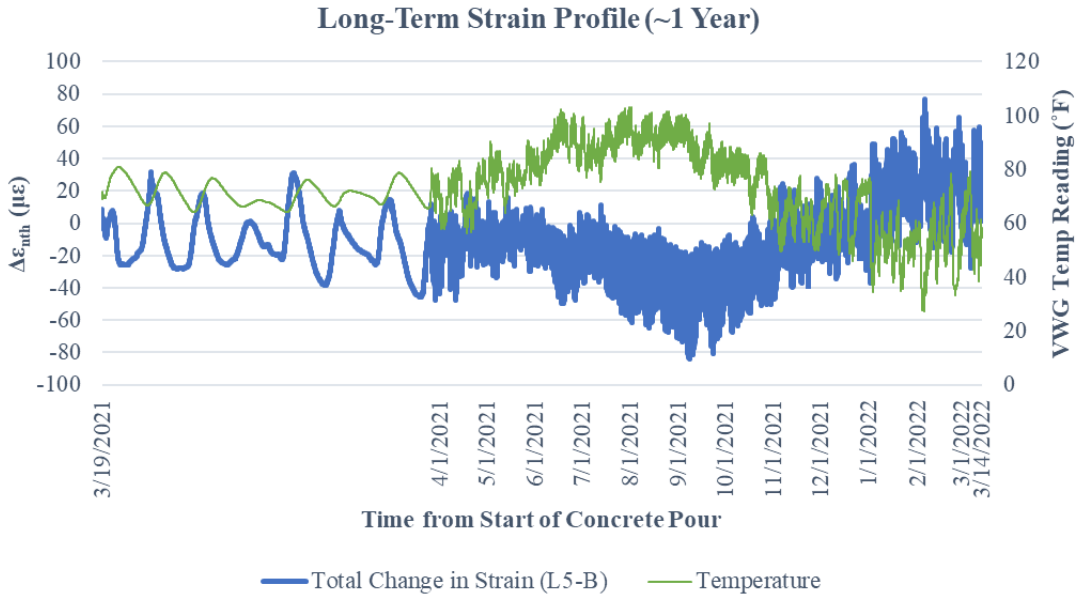

Figure 5.52 Long-Term Strain Profile for Navasota River Bridge Gauge L5-B

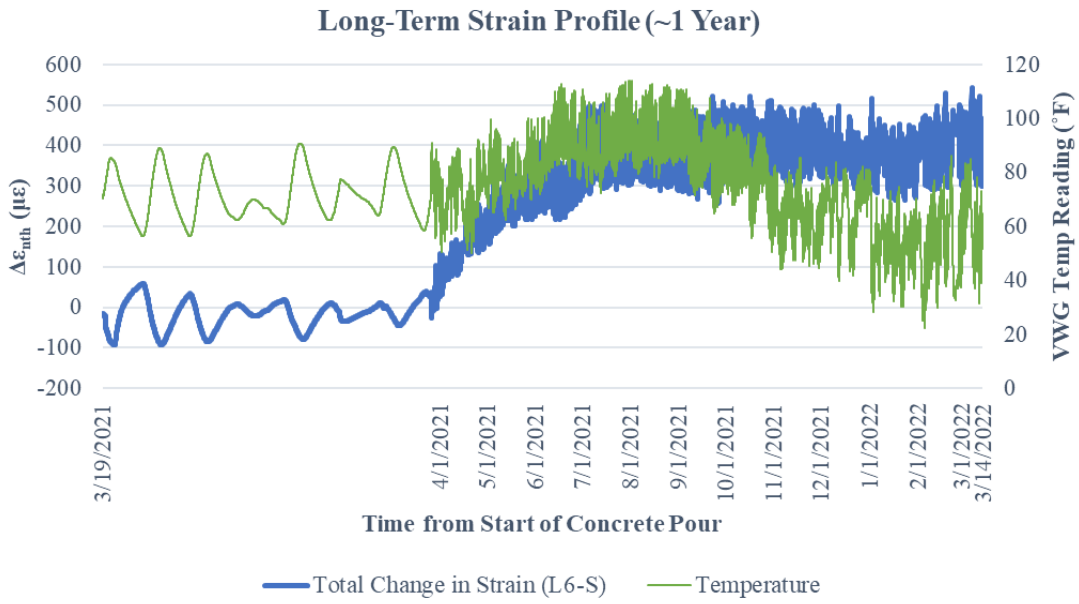

Figure 5.53 Long-Term Strain Profile for Navasota River Bridge Gauge L6-S

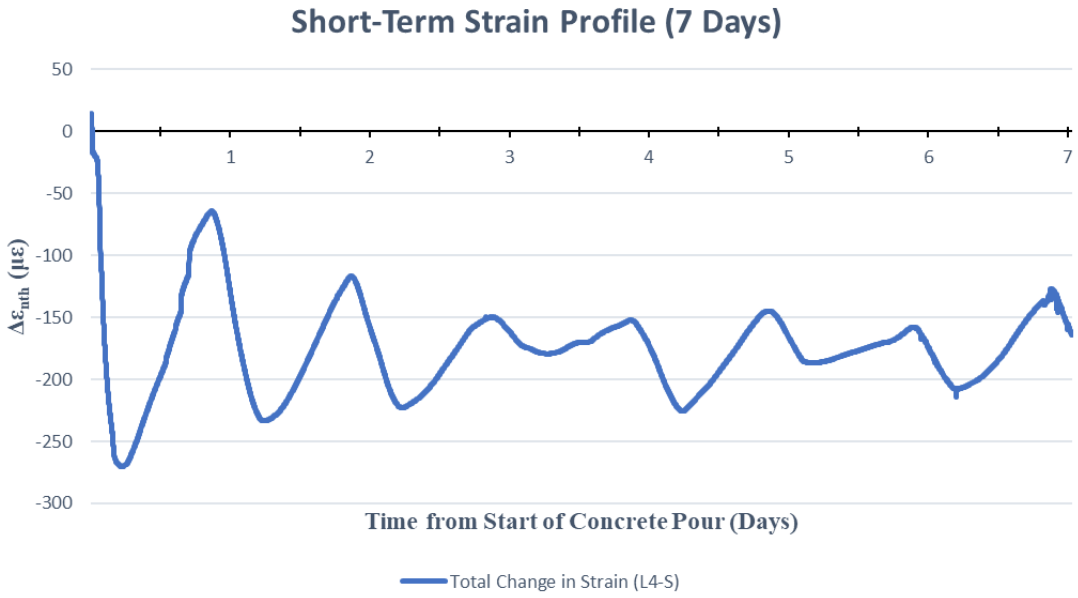

Figure 5.54 Short-Term Strain Profile for Navasota River Bridge Gauge L4-S

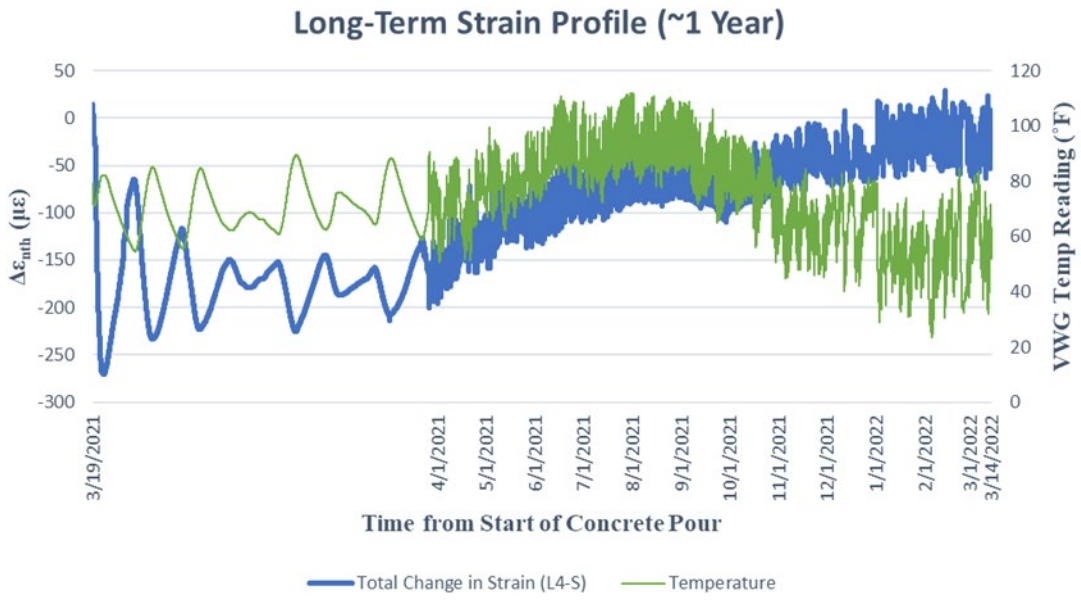

Figure 5.55 Long-Term Strain Profile for Navasota River Bridge Gauge L4-S

Overall, the researchers are only reporting what was seen from the field data up through the time of this thesis submittal. No objective conclusions can be provided regarding this data since there are multiple factors within the bridge interacting with each other. Further monitoring and research are required to understand some of the strain gauge trends.

5.2.3.3. Drop-In Panel VWGs

As mentioned previously, the wires for the drop-in deck panel strain gauges were cut and therefore the researchers only have approximately 14 days of recorded data. Unfortunately, due to minimal strain changes at this location, no patterns or conclusions could be made regarding this data. These strain gauge plots have been attached in Appendix A.2 for review.

5.2.4. Farwell Creek Bridge – Interpretation and Discussion

5.2.4.1. Transverse VWGs

Since both the short-term and long-term strain behavior was approximately the same for all transverse gauges located in the longitudinal closure joints of the Farwell Creek Bridge, the researchers will only present one set of transverse strain gauge data. Consult Appendix A.3 for the remaining transverse short- and long-term strain data. Furthermore, unlike the Navasota River Bridge, the collection interval for the Farwell Creek Bridge was set at thirty minutes due to DAQ limitations.

Figures 5.56 and 57 below show the short-term and long-term transverse strain gauge data, respectively, for gauges T1-B and T1-T. After analyzing the data, the researchers found that all of the transverse gauges initially started in tension and then quickly went into compression after the pour. It should be noted that unlike the Navasota River Bridge curing process, the use of UHPC at the Farwell Creek Bridge required the use of wet curing. Therefore, the researchers believe the initial drop in strain is associated with autogenous shrinkage, while drying shrinkage became dominant after approximately seven days. Again, the researchers are unable to explicitly quantify the exact amount of each type of shrinkage. Further materials testing is required.

In terms of the long-term behavior, the transverse gauges typically leveled off at a strain value between -500 με and -700 με as can be seen in Figure 5.57. Although the value at which the gauges leveled off at is two times larger than those found in the Navasota River Bridge transverse gauges, the proprietary UHPC used in Amarillo is significantly stronger in compression (and tension) than RSFRC. Furthermore, no patterns related to temperature were observed with the long-term strain data. The researchers believe these are typical strain values that were most likely assumed by the designers of the bridge.

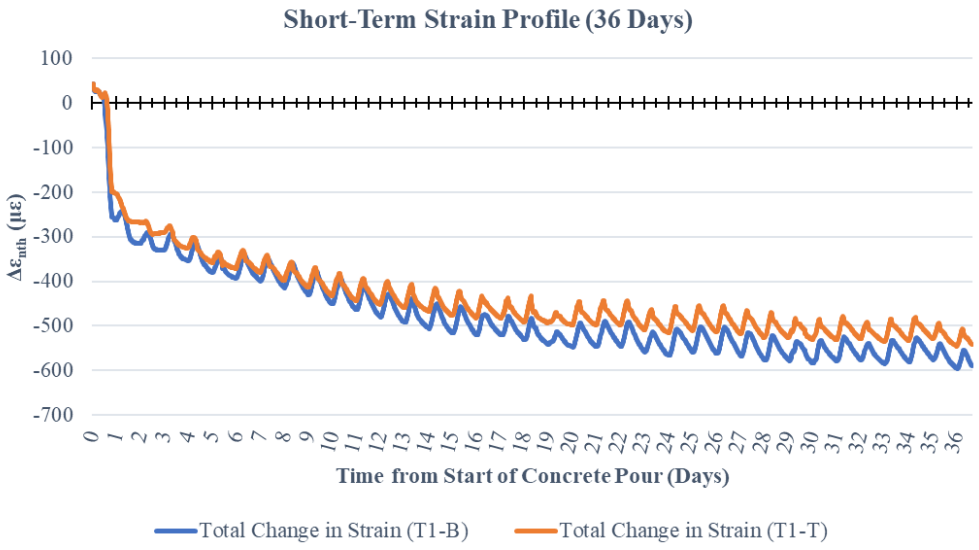

Figure 5.56 Short-Term Strain Profile for Farwell Creek Bridge Gauge Set T1

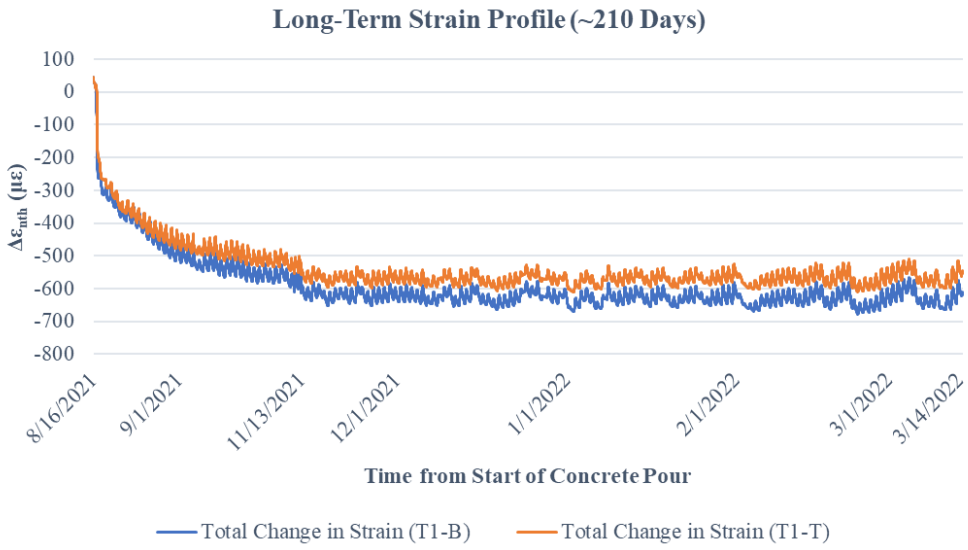

Figure 5.57 Long-Term Strain Profile for Farwell Creek Bridge Gauge Set T1

5.2.4.2. Longitudinal VWGs

Two longitudinal strain gauges (L1-S and L2-S) were located at separate locations along the length of the closure joint between Unit 1L and Unit 2L. Unlike the Navasota River Bridge longitudinal gauges, L1-S and L2-S had different short-term and long-term strain behaviors. Figures 5.58 and 59 show the short-term behavior while Figures 5.60 and 61 show the long-term behavior of the two longitudinal gauges.

Gauge L1-S initially started in tension in the short-term, but slowly decreased and entered compression around day 20. In the long-term, L1-S was observed to oscillate in tension and compression around 0 με. On the other hand, gauge L2-S went into compression for a short period of time before increasing steadily into tension in the short-term. After November 2021, L2-S was observed to oscillate around 225 με and remain in tension. No discernible temperature correlations were observed by the researchers.

It was found in Table 5.6 that a strain of 380 με would lead to cracking within the UHPC section. The researchers did not observe any values to exceed this tensile cracking strain value of the proprietary UHPC imported from France and therefore would not expect to see any tension cracking within the closure joints. However, there are multiple factors interacting with each other in the bridge which limits the researchers from providing objective conclusions. Since the Farwell Creek Bridge was not monitored as long as the Navasota River Bridge, it is possible that the researchers will find aberrations when inspecting future strain data.

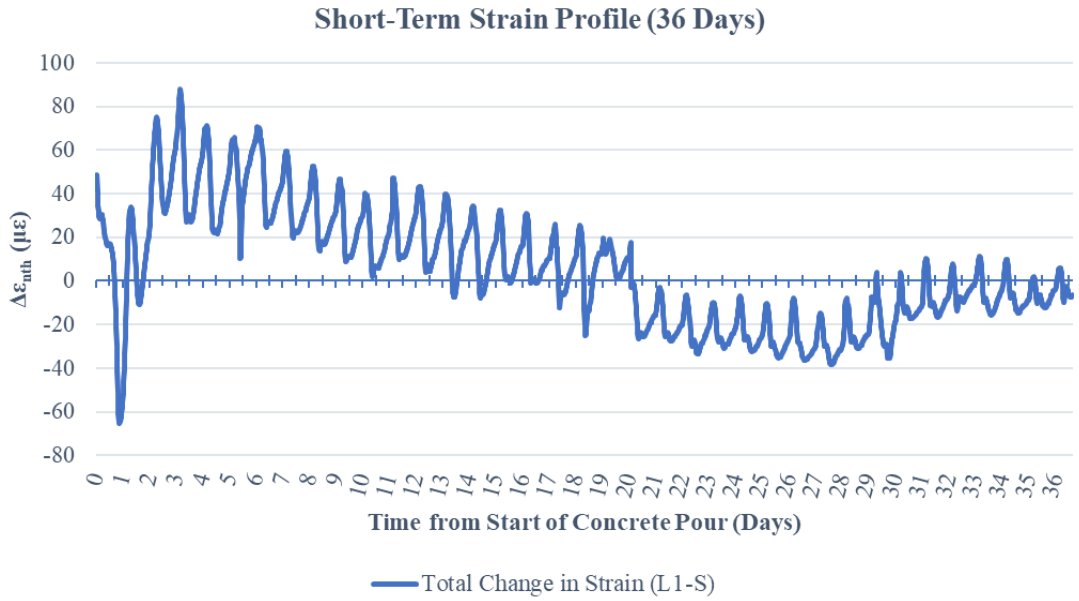

Figure 5.58 Short-Term Strain Profile for Farwell Creek Bridge Gauge L1-S

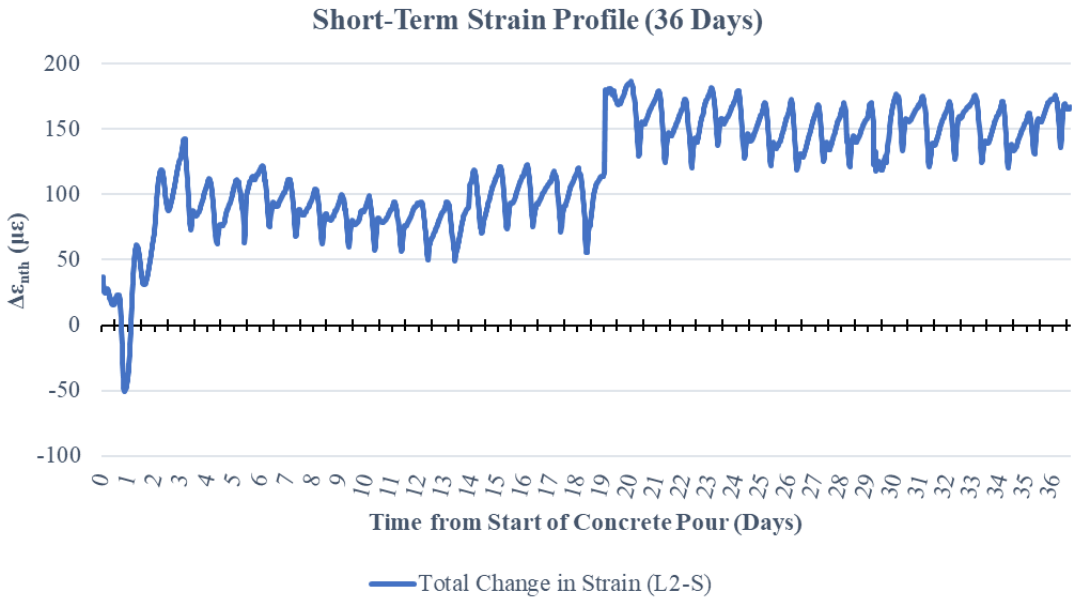

Figure 5.59 Short-Term Strain Profile for Farwell Creek Bridge Gauge L2-S

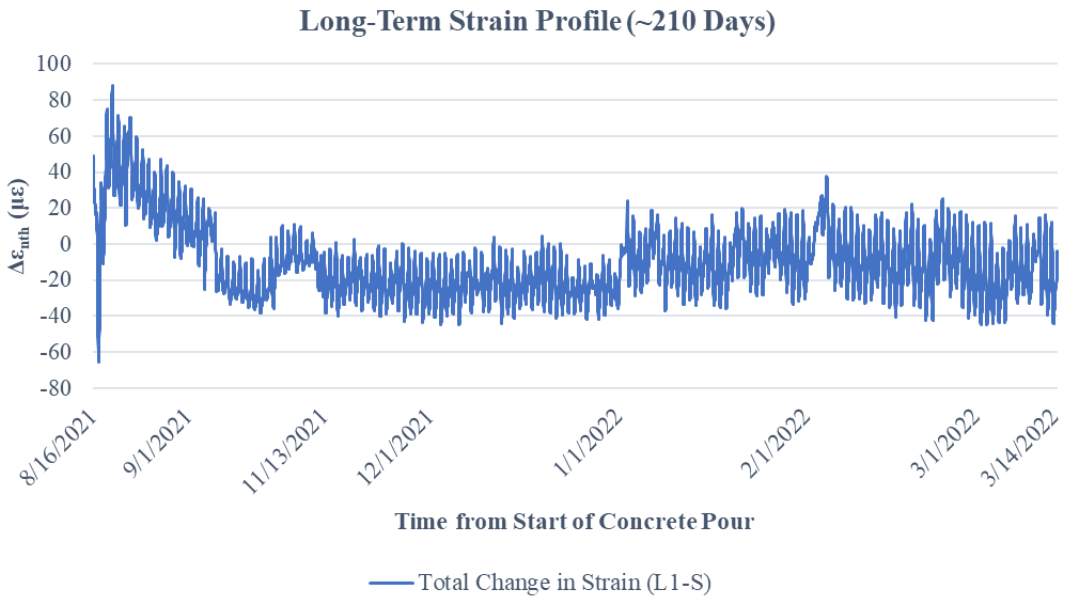

Figure 5.60 Long-Term Strain Profile for Farwell Creek Bridge Gauge L1-S

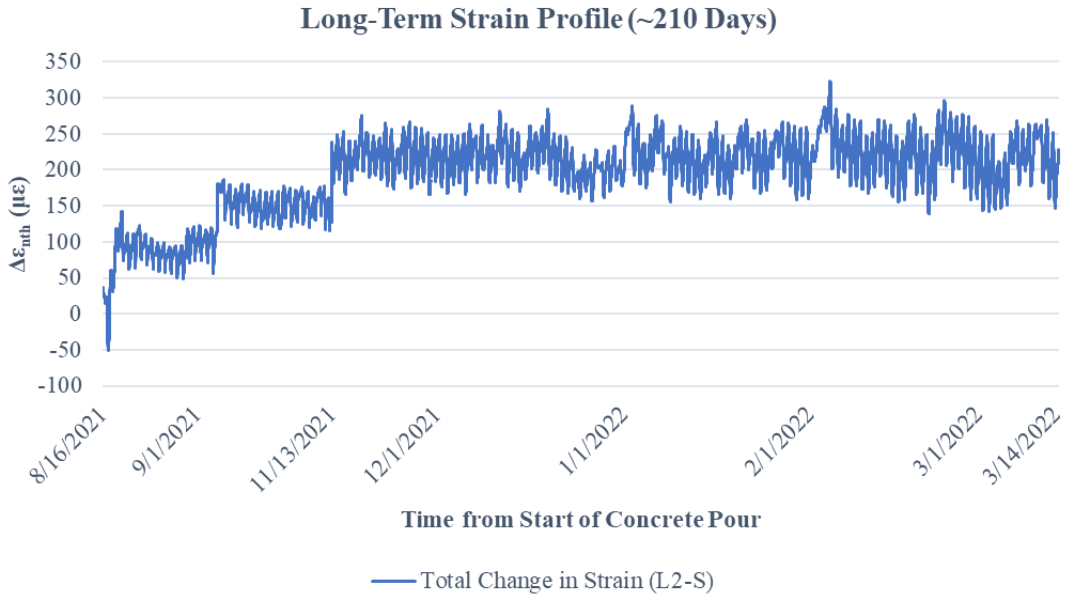

Figure 5.61 Long-Term Strain Profile for Farwell Creek Bridge Gauge L2-S

Since the instrumented NEXT beam was cast earlier on July 8th, 2021, the researchers expect that the autogenous shrinkage has already ceased, and the strain data will be dominated by drying shrinkage. Moreover, upon review of the data, the researchers found that the gauges embedded on the prestressed strands and within the deck itself have approximately the same behavior. Therefore, for the sake of brevity, only one set of data will be discussed, and the rest of the NEXT beam strain gauge data will be attached in Appendix A.4 for review.

In terms of the short-term behavior, the researchers did not notice any significant patterns or trends. Refer to Figure 5.62 for the short-term behavior of gauge L4-B and L4-T, which are both located on a prestressed strand. In terms of long-term behavior, the researchers noticed a trend between the top gauge strain data and the recorded temperature for all longitudinally installed gauges as shown in Figure 5.63. Similarly, a correlation between both top and bottom gauges and the recorded temperature was found with transversally installed gauges. Specifically, with higher temperatures, the recorded strain value would decrease (i.e., become more negative), while with lower temperatures, the gauge would record increasing strain values. In some instances, the gauge transitioned from compression to tension with decreasing temperatures. However, the strain values recorded by the gauges within the NEXT beam were relatively lower when compared to the data recorded by the gauges embedded within the longitudinal closure joint. Lastly, the researchers did not observe any significant tensile strains (i.e., greater than 97 με) that would lead to cracking of the beam.

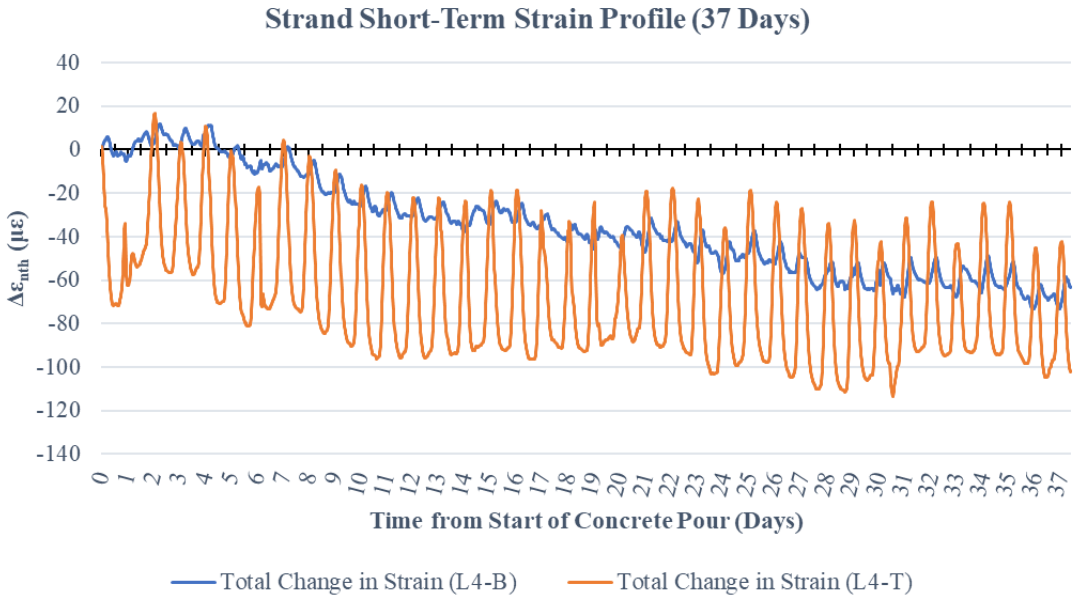

Figure 5.62 Short-Term Strain Profile for Farwell Creek Bridge Gauge Set L4

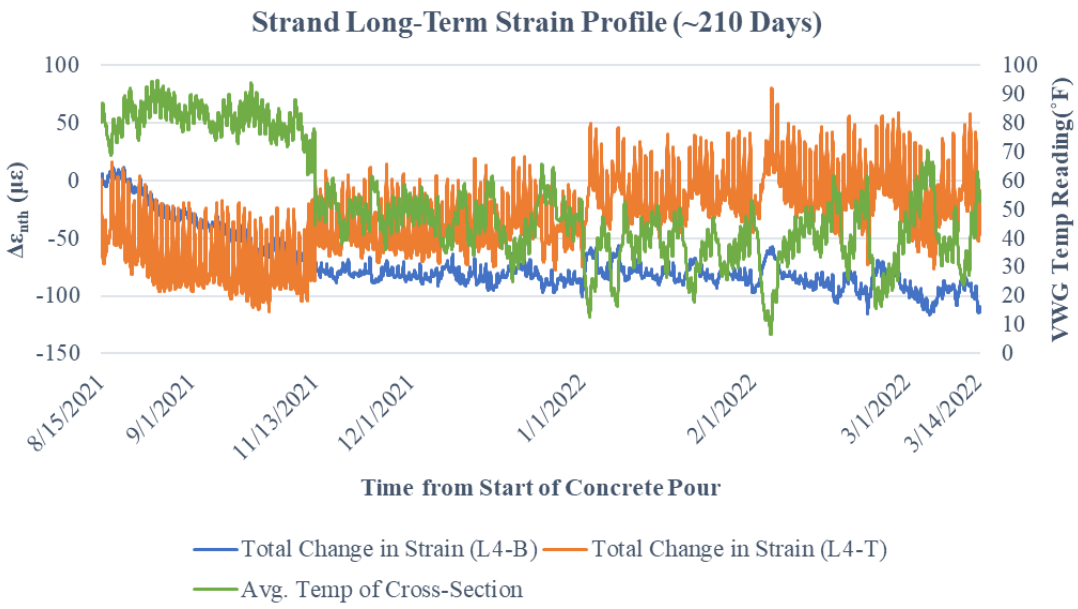

Figure 5.63 Long-Term Strain Profile for Farwell Creek Bridge Gauge Set L4

5.2.5. Summary and Material Comparison

The Navasota River Bridge, which has 20 strain gauges installed, was monitored for approximately one year while the Farwell Creek Bridge, which has 26 total gauges installed, was monitored for approximately seven months. Raw strains and temperatures were collected from various locations of the bridges and then converted to the structural behavior parameter of engineering strain. It should be noted that Hossein Yousefpour heavily influenced the calculations required to obtain accurate engineering strain values for data analysis purposes. Extensive work was completed to carry out the post-processing of the strain field data in order to present it in a meaningful and coherent manner.

The transverse gauges of the Navasota River Bridge had, on average, lower compressive strain values than those recorded by the transverse gauges of the Farwell Creek Bridge. However, as indicated previously, the proprietary UHPC imported from France used at the Farwell Creek Bridge is significantly stronger in compression than that of the RSFRC used at the Navasota River Bridge. The researchers believe the transverse strain values observed at both bridges was not significant to the point of concern. Furthermore, both bridges showed trends that led the researchers to believe that autogenous shrinkage dominated for the first three or four days. The researchers also deduced that drying shrinkage for both bridges became dominant after seven days. The main difference found with the transverse strain gauge data for both bridges is that most of the top transverse gauges at the Navasota River Bridge had some correlation with the recorded

temperature. The transverse gauges at the Farwell Creek Bridge had no observed trend with temperature. In other words, this could mean that UHPC is not as influenced by ambient temperature as RSFRC.

In terms of the longitudinal strain gauges located within the closure joints, the main concern of the researchers was the tensile strain values the concrete material would experience. For both bridges, the closure joints went immediately into tension during the pour. While the Navasota River Bridge closure joints exceeded the tensile cracking strain for RSFRC, the closure joints at the Farwell Creek Bridge did not experience excessive tensile strains which could lead to cracking. Although cracking was found at the Navasota River Bridge, the researchers cannot conclude that this came directly from the excessive tensile strains the RSFRC was experiencing. Ultimately, the researchers are only reporting what was observed from the field data. No objective conclusions can be provided regarding the data since there are multiple factors within the bridge interacting with each other. Further research is required to fully understand the trends seen in the field.

Overall, the researchers believe both materials are appropriate for closure joints. Although the tensile strain values of the RSFRC exceeded the tensile cracking strain at the Navasota River Bridge, the researchers believe the strain values were not significant enough to cause major cracking within the closure joints. The researchers also observed that UHPC does not cycle with ambient temperature like RSFRC does. Overall, the researchers believe UHPC is superior to RSFRC and should be the closure joint material of choice in projects under a time-constraint as well as in projects in areas with volatile ambient temperatures. It should be noted that the closure joint details used in both bridges were based on typical results from Graybeal's UHPC testing program; it will be of interest to compare how RSFRC performs in the Navasota River Bridge as there may not be other available data of its kind. It should also be noted that the NEXT beam and drop-in deck panel instrumentations were ancillary and not the major focus of this research project. Further monitoring, data analysis, and field tests are required to provide conclusions on how these precast elements truly affect closure joints.

5.3. Visual Surveys

After placement of the Navasota River and Farwell Creek bridges, the research team conducted additional field visits to inspect the bridges. Both quantitative and qualitative observations were made on the condition of the closure pours and the bridge decks.

5.3.1. Navasota River Bridge

5.3.1.1. Placement of Closure Pour

The closure pour was placed on March 19, 2021. A ready mix truck was brought on-site and the closure pour material was poured directly onto the joints, immediately after the addition of a set accelerator.

5.3.1.2. Field Survey Observations

On July 12, 2022 the research team conducted a field survey of the 5-span OSR bridge over the Navasota River near Bryan, TX. The field survey focused on the closure pours. A water truck (Figure 5.64) was provided to spray water onto the entire bridge pavement to locate cracks within the closure pours. The pavement was allowed to dry for a few minutes which led to visible cracks that held water as shown in Figure 5.65. The field survey found cracking throughout all the closure pours in each of the 5 spans. Figure 5.66 details the cracking in each closure pour section. The number within each closure pour in the longitudinal direction provides the number of cracks in that section. The middle span has the most cracks within the closure pours and the spans nearest the bridge abutments had the least cracks. The crack widths were measured throughout all of the closure pours. Table 5.7 provides an information on some of the larger cracks found. In section C-3, a 0.06” crack width was identified. Several other 0.04” cracks were identified throughout the closure pours. Figure 5.67 shows an image of one of the cracks. Most of the cracks in the longitudinal direction were visually similar to this crack. The transverse larger closure pours showed irregular crack pattern as shown in Figure 5.68. In addition to the cracks in each of the sections, several fiber clumps were visible in the closure pours. Figure 5.69 shows an image of the fiber clumps.

Figure 5.64 Water Truck Spraying the Pavement

Figure 5.65 Visible Cracks After Pavement Drying

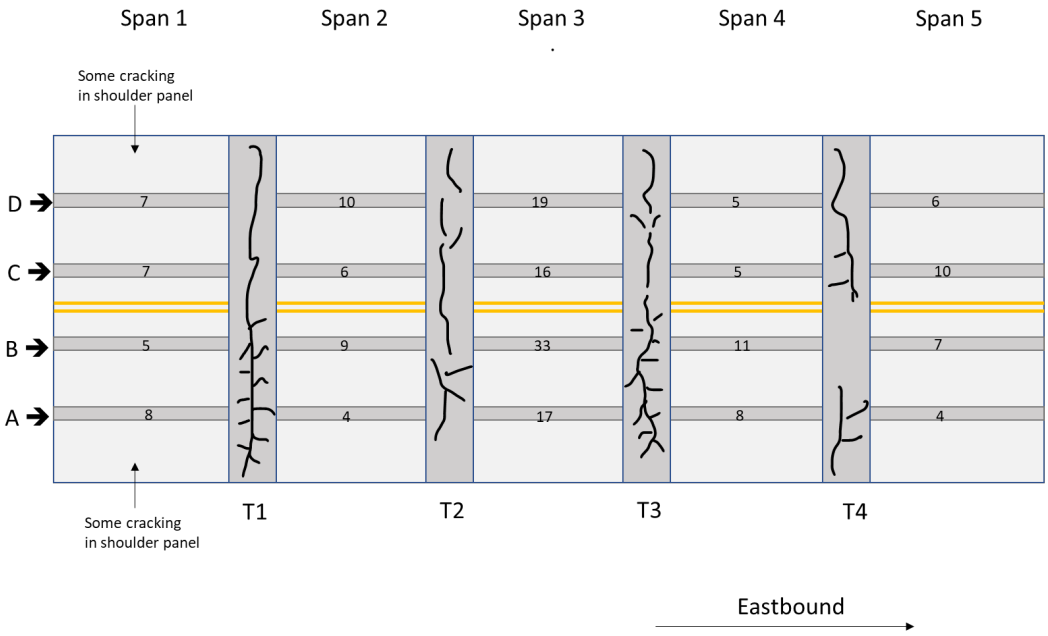

Figure 5.66 Survey of OSR over the Navasota River Bridge

Figure 5.67 Common Crack Found in the Longitudinal Closure Pour

Figure 5.68 Typical Cracking in Transverse Closure Pour

Figure 5.69 Fiber Clumping on Surface of Closure Pours

Table 5.7 Average Crack Widths Throughout Different Closure Pours

Closure Pour Location	Average Crack Width (in)
A-3	0.035
A-4	0.030
A-5	0.004
B-2	0.010
B-3	0.030
B-3 (max)	0.060
B-4	0.035
B-5	0.016
C-2	0.013
C-3	0.040
C-5	0.020
C-5 (max)	0.040
T-1	0.010

A second visual survey was conducted on March 24, 2023 and followed the same procedures of the first survey as highlighted above. Visible cracking was observed within the closure pour sections as well as the interface between the closure pour and the pre-cast sections as illustrated in Figures 5.70 to 5.75.

Figure 5.70 Cracking of Transverse Closure Pour

Figure 5.71 Cracking of Longitudinal Closure Pour

Figure 5.72 Cracking at Interface of Transverse Joint and Bridge Deck

Figure 5.73 Cracking of Bridge Deck

Figure 5.74 Debonding Between Closure Pour and Bridge Decks

Figure 5.75 Common Crack Found in the Longitudinal Closure Pour

5.3.2. Farwell Creek Bridge

The data previously presented for the Farwell Creek bridge was part of a chain of five bridges (Figure 5.76) in the Amarillo district. Although instrumentation and monitoring was only conducted on the Farwell Creek bridge, visual inspection was conducted on the entire chain.

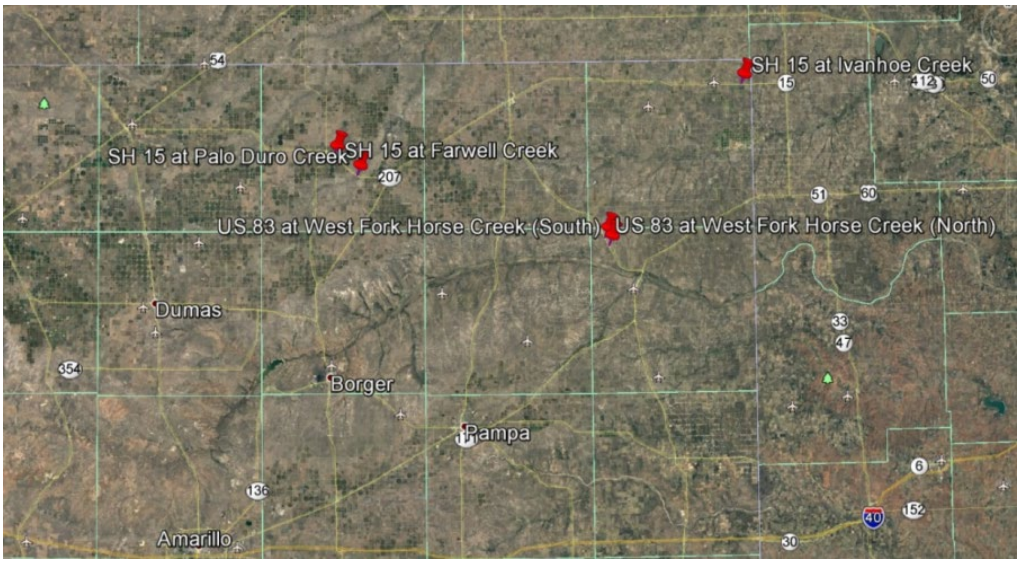

Figure 5.76 ABC Bridges in the Amarillo District

5.3.2.1. Placement of Closure Pour

A proprietary UHPC mobile mixer supplied by a specialty contractor was used to prepare the closure joint material as shown in Figure 5.77. The placement procedure on the closure joint is illustrated in Figure 5.78. Due to the self consolidating properties of UHPC, the majority of the mixture was placed at a singular location at each joint and the mixture flowed across the entire joint. Wooden strips were then placed above the joint and holes were created at intermediate points where workers manually added the remaining mixture to ensure the joint was fully topped-off. The wooden strips were kept in place for approximately 24 hours following completion of placement, after which they were removed by the contractor as shown in Figure 5.79.

Figure 5.77 Proprietary UHPC Mixer

Figure 5.78 Procedure for Placement of Closure Joint

Figure 5.79 Bridge After Placement of Closure Pour

5.3.2.2. Field Survey Observations

A field observation trip was taken on June 19, 2023 to monitor the chain of five bridges. Crack mapping was conducted and the results are shown in Figures 5.80 to 5.84 below.

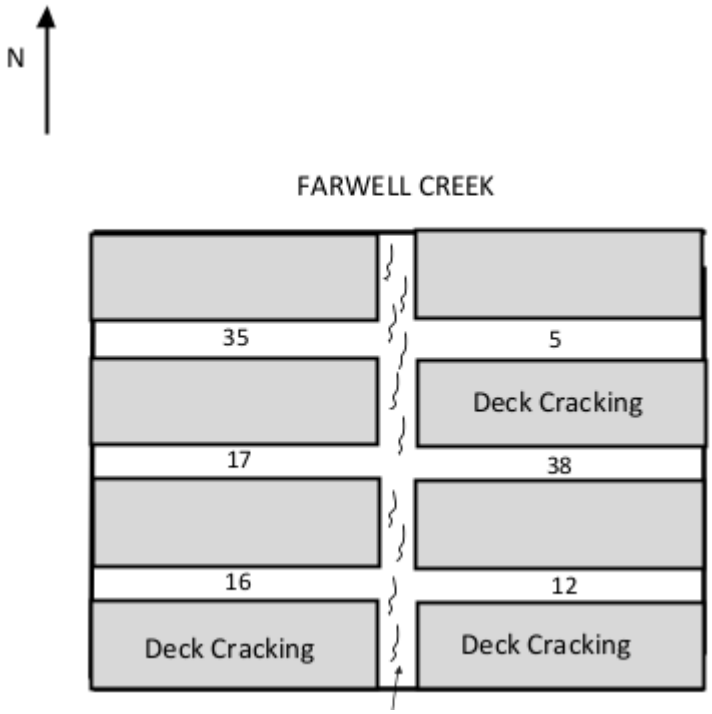

Figure 5.80 Cracking at Farwell Creek

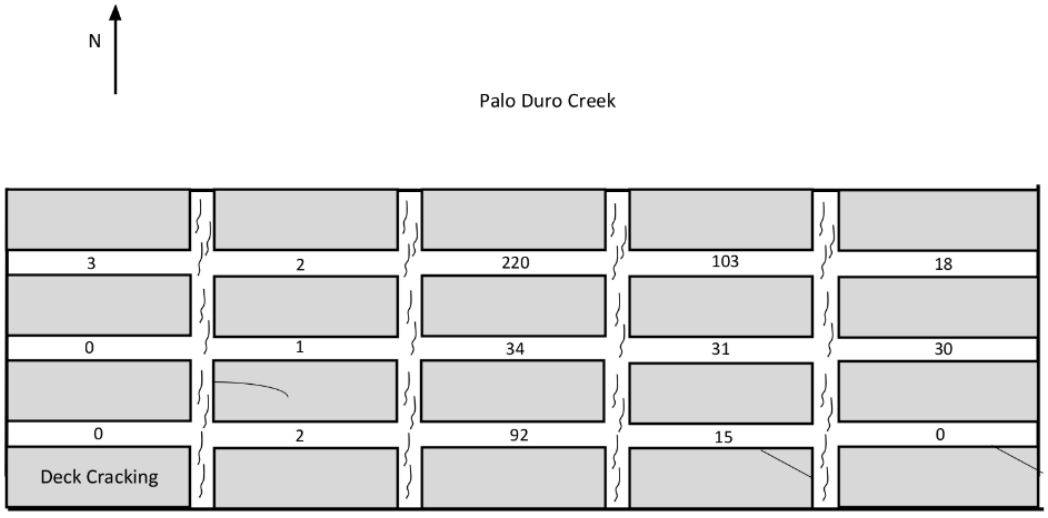

Figure 5.81 Cracking at Palo Duro Creek

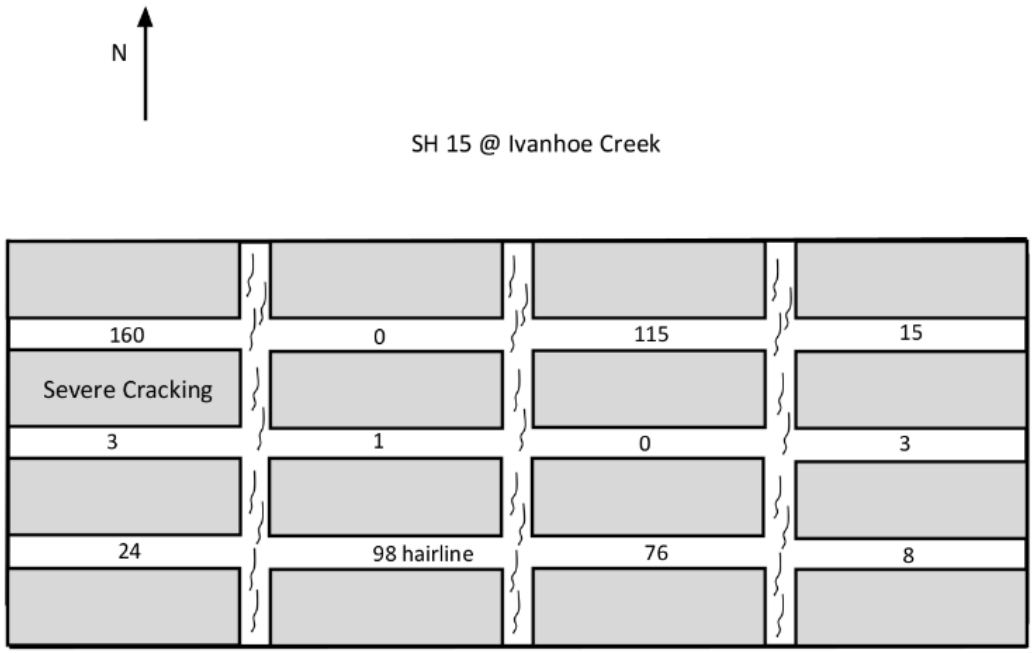

Figure 5.82 Cracking at Ivanhoe Creek

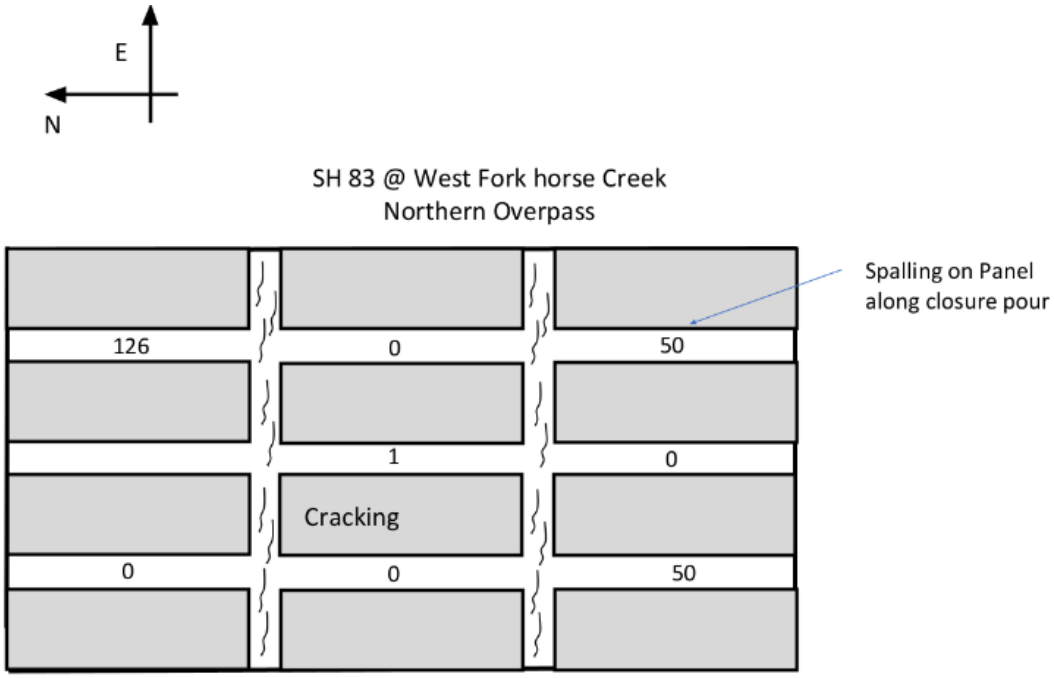

Figure 5.83 Cracking at West Fork Horse Creek (North)

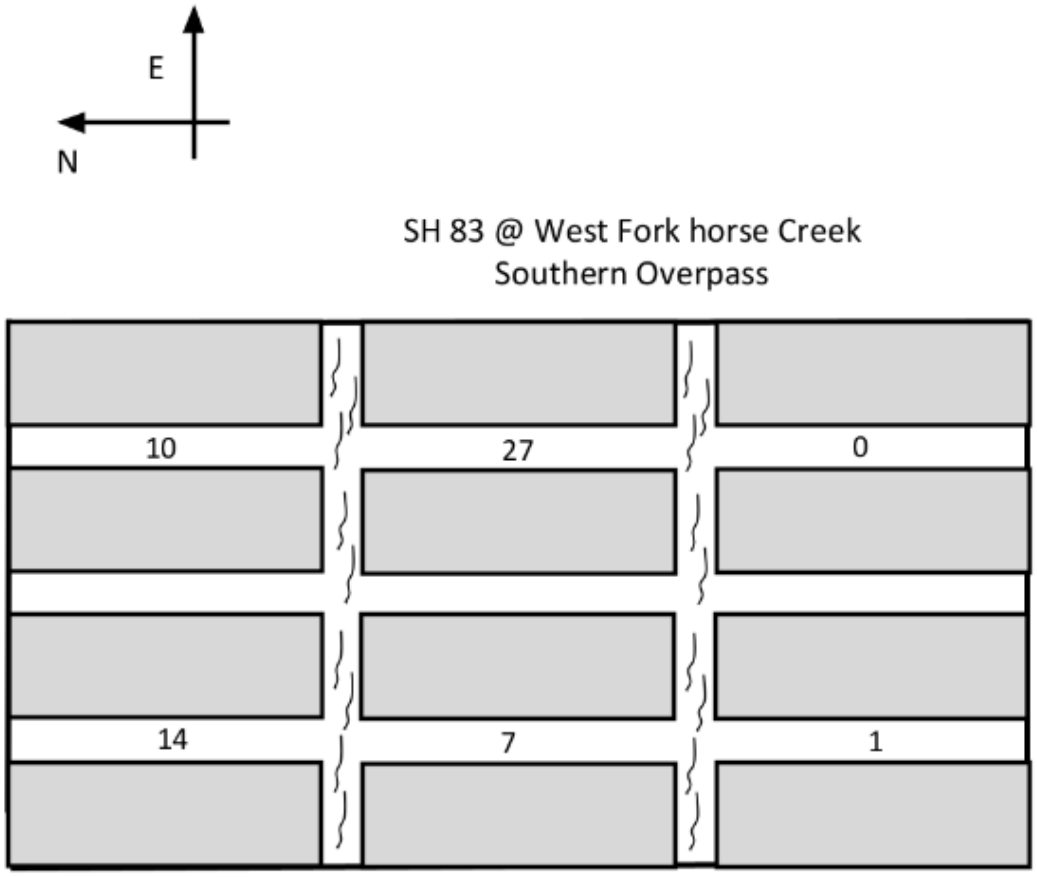

Figure 5.84 Cracking at West Fork Horse Creek (South)

Figures 5.85 to 5.88 show photographs taking during this visual survey. In general, only minimal cracking was observed in the closure pours and the crack widths were very tight. Some visible gaps were observed at the interface between the closure pour and pre-cast sections; most likely due to differential volume changes between the two materials. However, these gaps were considerably smaller than those observed in the Navasota River bridge. One interesting observation, shown in Figure 5.85, shows some surface irregularities which were most likely due to the accumulation of entrapped air at the top surface of the closure pours that was directly in contact with the wood strips. This effect may have been exacerbated by the physical removal of the wooden strips the day after the pour due to the adhesion of the UHPC with the wooden strips. However, this appears to be a near surface aesthetic impact and is not expected to influence long term behaviour.

Figure 5.85 Bubbling Effect

Figure 5.86 Cracking at Transverse Joints

Figure 5.87 Debonding at Longitudinal Joint

Figure 5.88 Debonding Between Closure Pour and Bridge Deck

5.4. Conclusions and Recommendations

Two bridges, one in Bryan district and the other in Amarillo district, were instrumented and monitored, and the UHPC and RSFRC mixtures used in these closure pours were sampled and tested in the laboratory and outdoor exposure site testing. Instrumentation was also installed in some precast elements for both projects prior to delivery to the bridge site from the precast yard. Overall, the closure pours evaluated in Bryan and Amarillo have performed well during the monitoring period of the project. The UHPC mixture used in the Amarillo district performed exceptionally well and compressive strengths were close to 30 ksi. Very little cracking, other than small interfacial gaps with the precast sections, were observed. The Bryan district bridge did not use UHPC, but rather RSFRC for the closure pour. This bridge has also performed satisfactorily to date, but there is significantly more cracking than the Amarillo bridge, and there was a more significant interfacial gap between the precast superstructure sections.

Chapter 6. Conclusions and Recommendations

Based on the findings of this comprehensive research project, significant knowledge and insight has been gained into the use of innovative materials, such as UHPC and RSFRC, in closure pour applications. Various UHPC and non-UHPC mixtures were evaluated in the laboratory, on outdoor exposure sites, in full-scale structural testing, and most importantly, in real-world applications in ABC bridge projects in Amarillo and Bryan districts. The data generated in the comprehensive laboratory and structural tests should provide a wealth of information that can be used to increase and improve the use of UHPC in accelerated bridge construction applications.

Like any emerging topic, more research is needed to better understand this unique material and its potential applications in accelerated bridge construction, as well as other applications where the unique properties of UHPC can be applied. Perhaps the most useful information can be derived from the continuous monitoring of the ABC bridges in Amarillo and Bryan districts to confirm and document the long-term performance. The research team will continue to evaluate and monitor outdoor exposure site specimens into the future, and knowledge gained and data generated in future monitoring will be communicated to TxDOT.

References

ACI Committee 318-19 (2019) Building Code Requirements for Reinforced Concrete (ACI 318-19) and Commentary (318R-19), American Concrete Institute, Farmington Hills, MI.

Alkaysi, M. (2016). Strength and Durability of Ultra-High Performance Concrete Materials and Structures (dissertation). ProQuest Dissertations & Theses, Ann Arbor.

ASHTO LRFD (2020) Bridge Design Specifications, 9th Edition, 2020, American Association of State Highway and Transportation Officials, Washington, D.C.

Bonetti, R. (2022), Development of Non-Proprietary Ultra-High Performance Concrete (UHPC) and Determination of Its Key Mechanical Properties, PHD Dissertation, University of Texas at Austin

Culmo, Michael P., & Rita L. Seraderian (2010), "Development of the Northeast Extreme Tee (NEXT) Beam for Accelerated Bridge Construction." PCI Journal, vol. 55, no. 3, 2010, pp. 86–101., https://doi.org/10.15554/pcij.06012010.86.101.

Ge, Xiaomeng, et al. (2021), University of Texas at Austin: Center for Transportation Research, Austin, TX, 2021, Designing for Deck Stress over Precast Panels in Negative Moment Regions.

Graybeal, B. (2006). Material Property Characterization of Ultra-High Performance Concrete. Virginia: Turner-Fairbank Highway Research Center

Graybeal, B. (2010). Behavior of Field-Cast Ultra-High Performance Concrete Bridge Deck Connections Under Cyclic and Static Structural Loading (FHWA Publication No. FHWA-HRT-11-023). McLean, Virginia: Office of Infrastructure Research & Development, Federal Highway Administration.

Graybeal, B. A., & Baby, F. (2013). Development of Direct Tension Test Method for Ultra-High-Performance Fiber-Reinforced Concrete. ACI Materials Journal.

Graybeal, B. (2013), Ultra-High Performance Concrete: A State-of-the-Art Report for the Bridge Community, Report No. FHWA-HRT-13-060, Federal Highway Administration, McLean, VA.

Graybeal, B. (2014a), Construction of Field-Cast Ultra-High Performance Concrete Connections, TechNote No. FHWAHRT-14-084, Federal Highway Administration, McLean, VA.

Graybeal, B. (2014b). Bond Behavior of Reinforcing Steel in Ultra-High Performance Concrete (FHWA Publication No.: FHWA-HRT-14-089).

McLean, Virginia: Turner-Fairbank Highway Research Center, Federal Highway Administration.

Graybeal, B. (2019). Design and Construction of Field-Cast UHPC Connections (FHWA Publication No: FHWA-HRT-19-011). McLean, Virginia: Turner-Fairbank Highway Research Center, Federal Highway Administration.

Haber, Z. B., & Graybeal, B. A. (2016). Performance of Multiple UHPC-Class Materials in Prefabricated Bridge Deck Connections. First International Symposium on UHPC.

Haber, Z. B., & Graybeal, B. A. (2018). Performance of Grouted Connections for Prefabricated Bridge Deck Elements. McLean, VA: U.S. Department of Transportation Federal Highway Administration.

Hernandez, J.A. (2016), Development and Laboratory Testing of Ultra High Performance, MS Thesis, University of Texas at Austin.

ICRI Standard 310.2 Selecting and Specifying Concrete Surface Preparation for Sealers, Coatings, Polymer Overlays, and Concrete Repair with CSP Chips.

Lee, J. K., & Lee, S. H. (2015). Flexural Behavior of Ultra-High-Performance Fiber-Reinforced Concrete Moment Connection for Precast Concrete Decks. ACI Structural Journal.

Leidos Incorporated & WSP USA. (2018). Project Case Study: Rehabilitation of the Pulaski Skyway - Ultra-High Performance Concrete Connections (Tech.). McLean, Virginia: Federal Highway Administration.

Li, V.C. (1993). From Micromechanics to Structural Engineering – the design of cementitious composites for Civil Engineering applications. JSCE J. of Struc. Mechanics and Earthquake Engineering 10(2):37-48

Makita, T. Bruuhwiler, E. (2014), Tensile fatigue behaviour of ultra-high performance fibre reinforced concrete (UHPFRC), Materials and Structures, Vol. 47, No. 3, pp 475–491.

Peruchini, T. J., Stanton, J., & Calvi, P. (2017). Investigation of Ultra-High Performance Concrete for Longitudinal Joints in Deck Bulb Tee Bridge Girders. Seattle, WA: Washington State Department of Transportation.

Texas Department of Transportation (2020). Plans of Proposed State Highway Improvement-SH 15 at Farwell Creek (UHPC Connection Detail). TXDOT

Wille, K., Boisvert-Cotulio, C. (2013) Development of Non-Proprietary Ultra-High Performance Concrete for Use in the Highway Bridge Sector, Report No. FHWA-HRT-13-100, McLean, VA.

Yanni, V. Y. G. (2009), Multi-scale investigation of the tensile creep of ultra-high performance concrete for bridge applications. Ph.D thesis, Georgia Institute of Technology.

Yousefpour, Hossein, et al. Center for Transportation Research, Austin, TX, (2014), Structural Monitoring of the World's First Precast Network Arch Bridge during Construction.

Yuan, J. and Graybeal, B. (2014), Bond Behavior of Reinforcing Steel in Ultra-High Performance Concrete, FHWA-HRT-14-090

Appendix A. Additional Strain Data Figures

A.1 Navasota River Bridge Short-Term VWG Strain Data

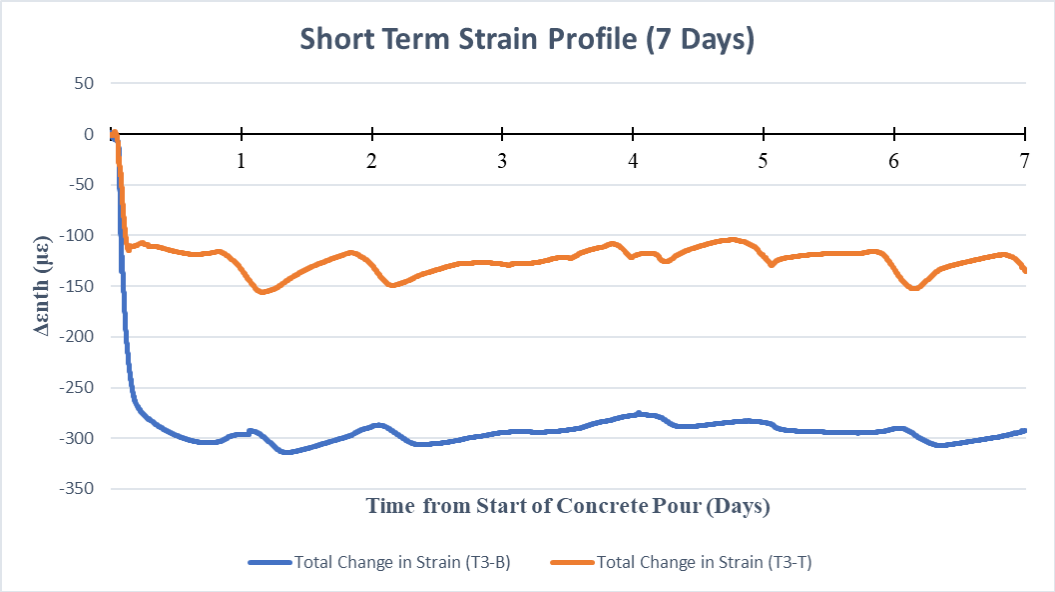

Figure A.1: Short-Term Strain Profile for Navasota River Bridge Gauges T3-B and T3-T

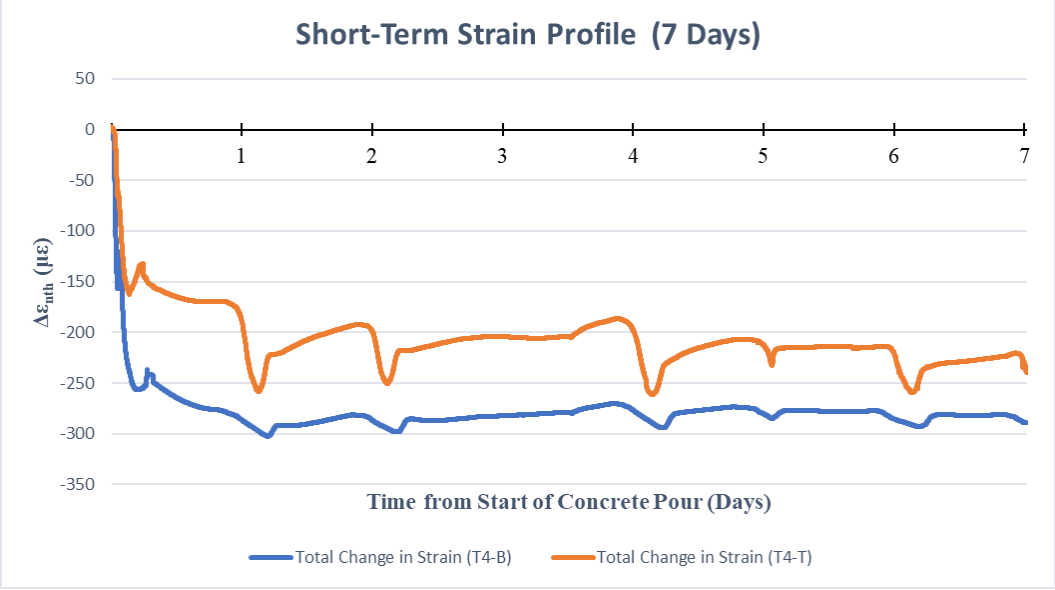

Figure A.2: Short-Term Strain Profile for Navasota River Bridge Gauges T4-B and T4-T

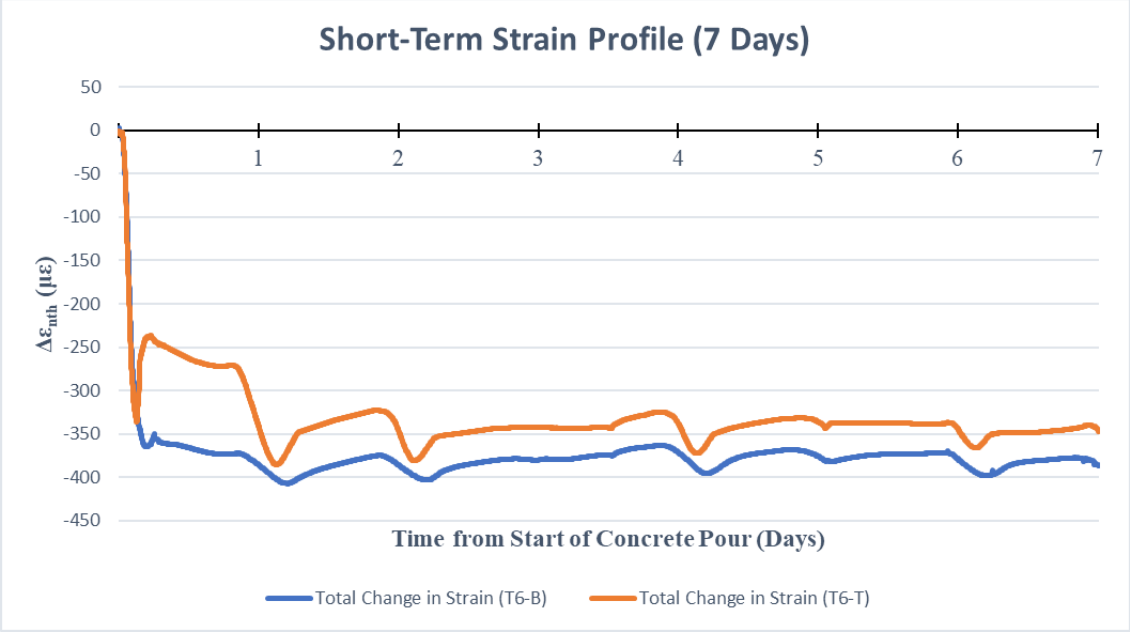

Figure A.3: Short-Term Strain Profile for Navasota River Bridge Gauges T6-B and T6-T

A.2 Navasota River Bridge Drop-In Panel Strain Data

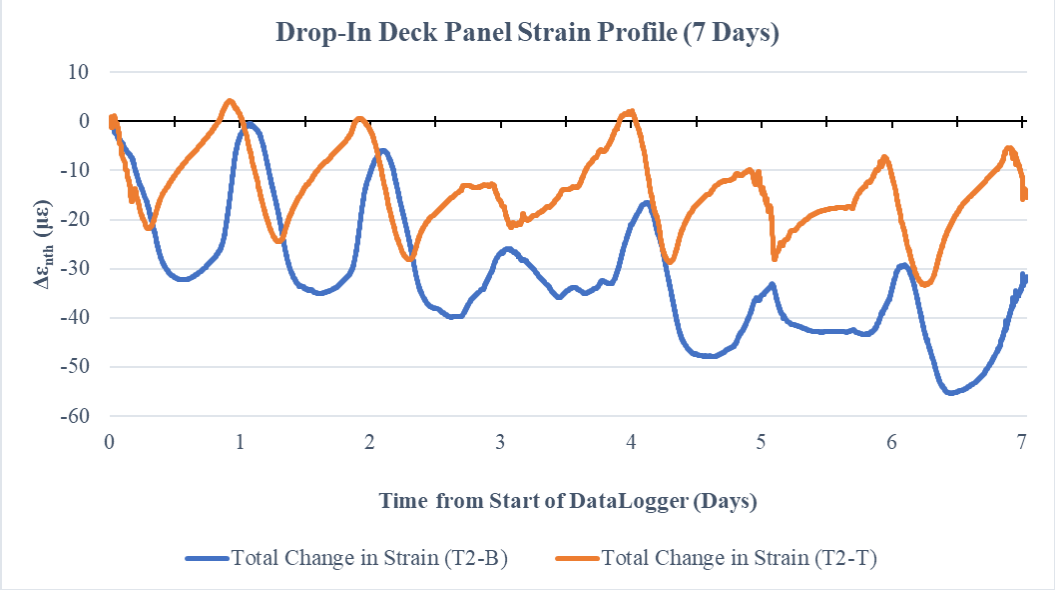

Figure A.4: Navasota River Bridge Drop-In Deck Panel Strain Profile for Gauges T2-B and T2-T

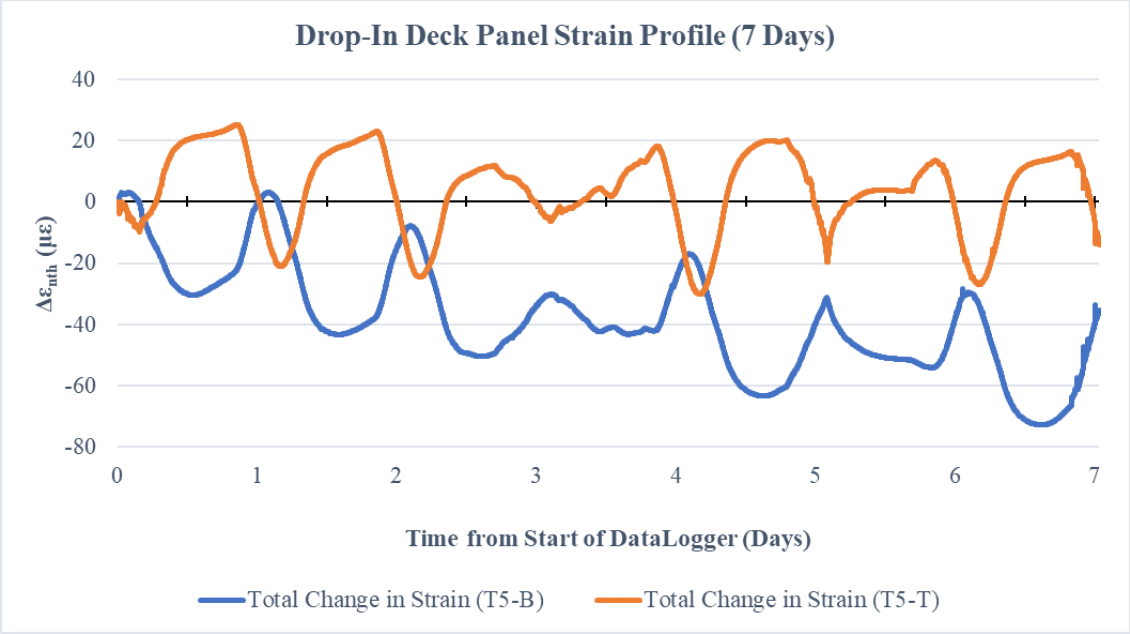

Figure A.5: Navasota River Bridge Drop-In Deck Panel Strain Profile for Gauges T5-B and T5-T

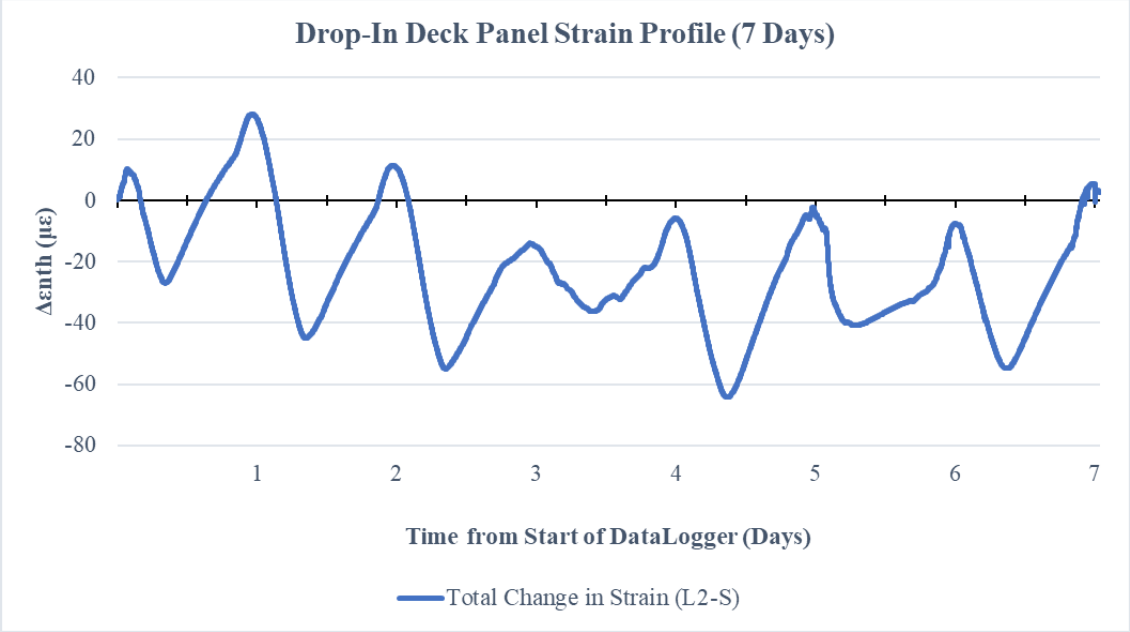

Figure A.6: Navasota River Bridge Drop-In Deck Panel Strain Profile for Gauge L2-S

A.3 Farwell Creek Bridge Short-Term and Long-Term Transverse VWG Strain Data

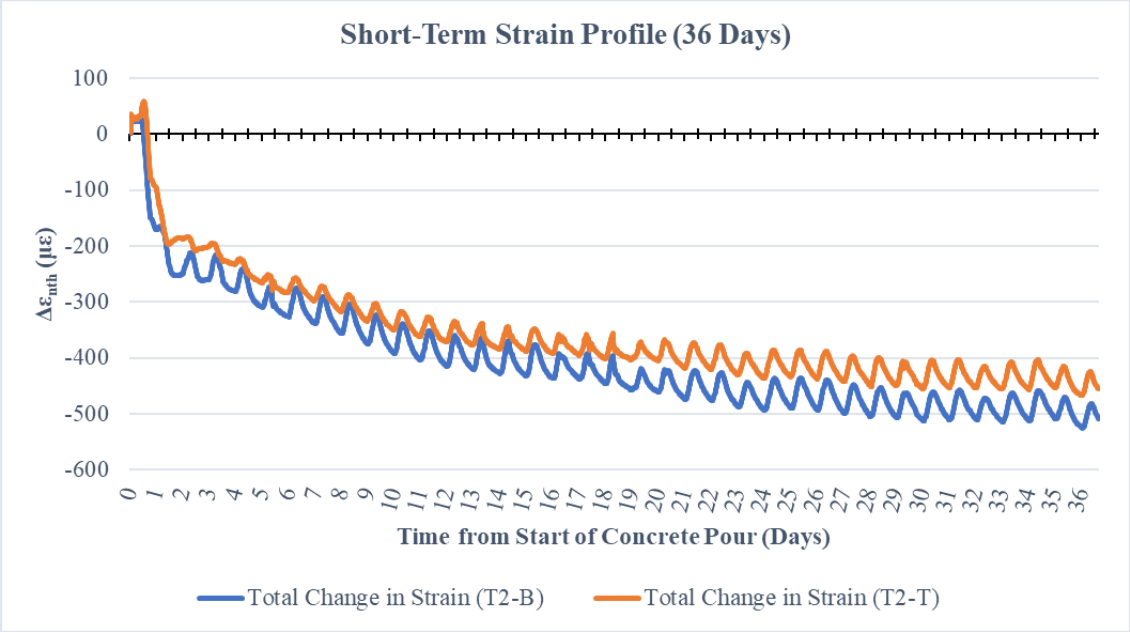

Figure A.7: Short-Term Strain Profile for Farwell Creek Bridge Gauges T2-B and T2-T

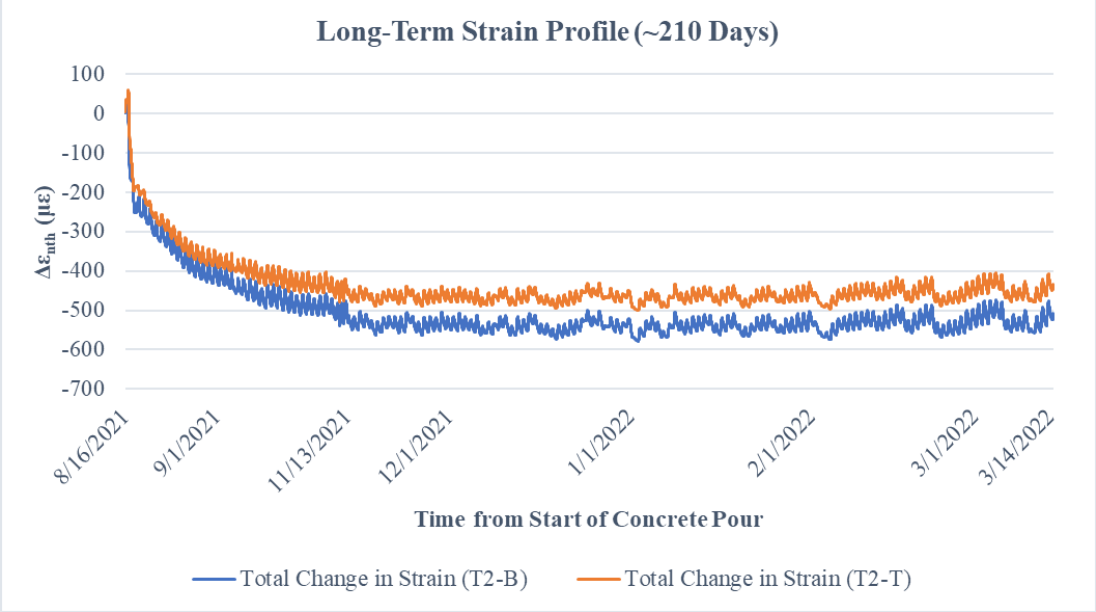

Figure A.8: Long-Term Strain Profile for Farwell Creek Bridge Gauges T2-B and T2-T

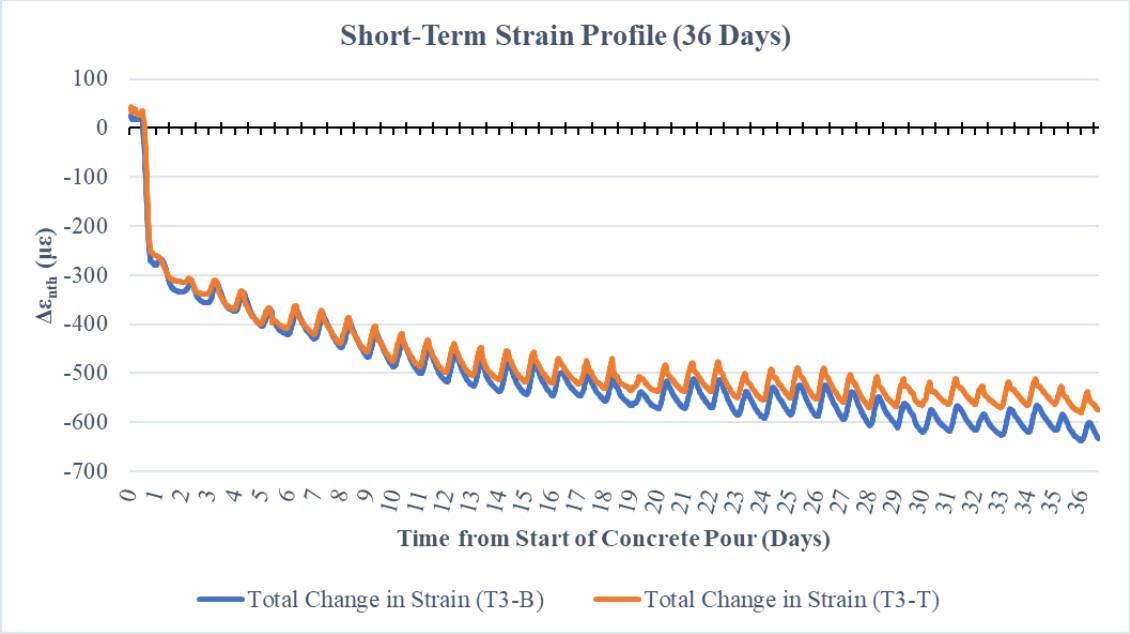

Figure A.9: Short-Term Strain Profile for Farwell Creek Bridge Gauges T3-B and T3-T

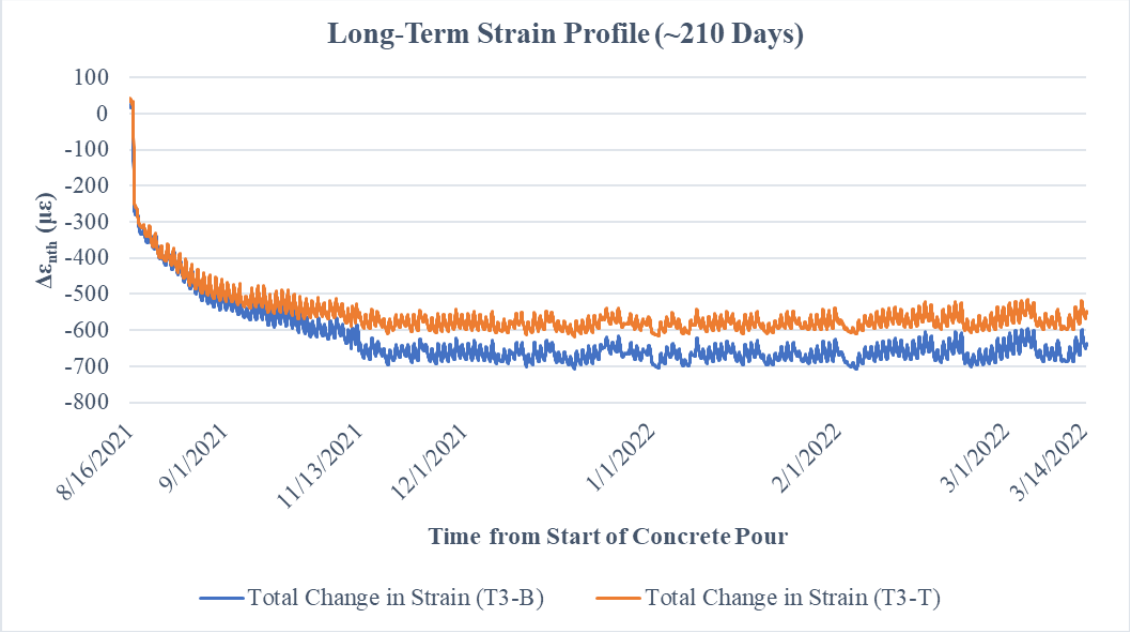

Figure A.10: Long-Term Strain Profile for Farwell Creek Bridge Gauges T3-B and T3-T

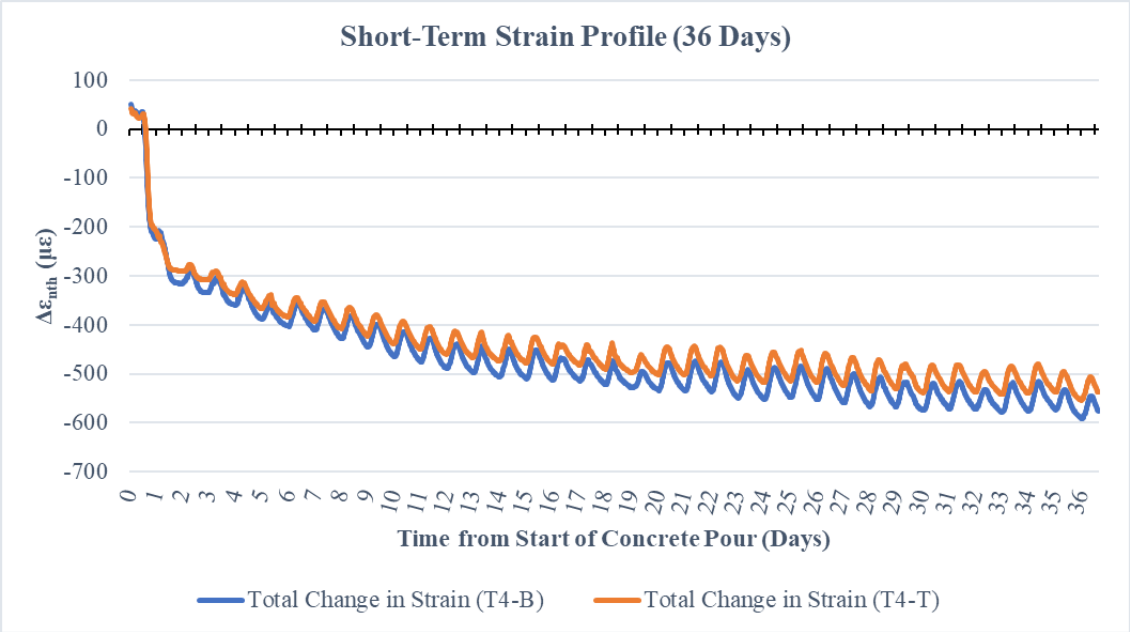

Figure A.11: Short-Term Strain Profile for Farwell Creek Bridge Gauges T4-B and T4-T

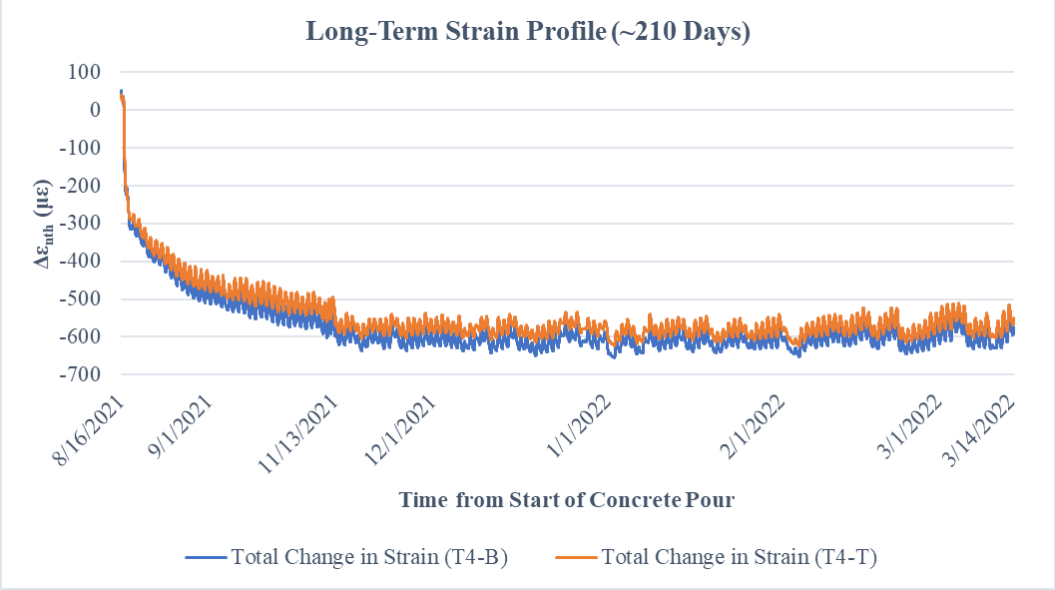

Figure A.12: Long-Term Strain Profile for Farwell Creek Bridge Gauges T4-B and T4-T

A.4 Farwell Creek Bridge NEXT Beam Short-Term and Long-Term Strain Data

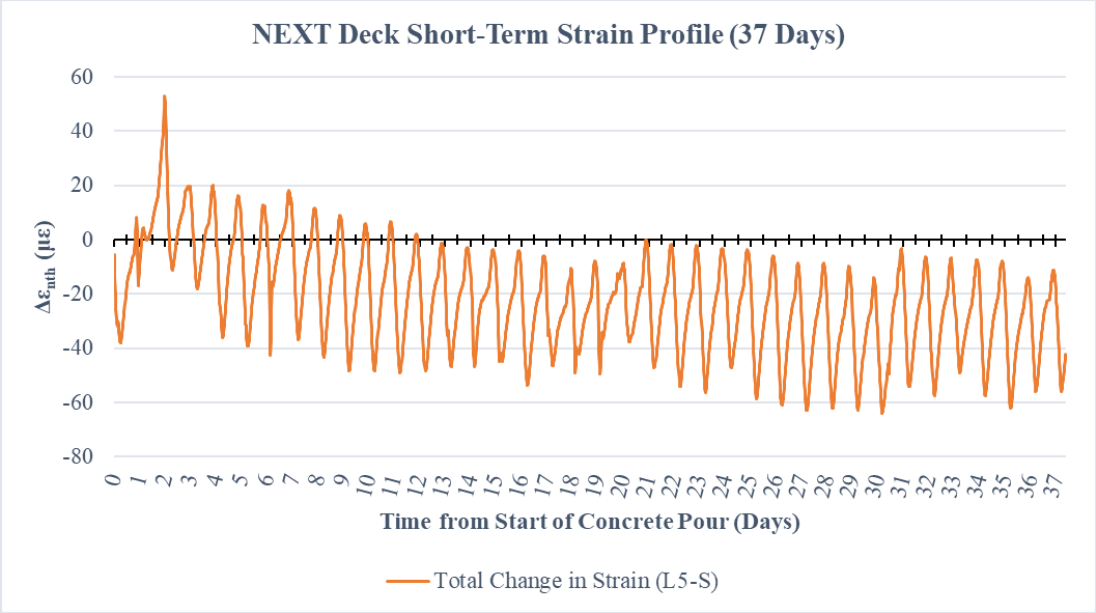

Figure A.13: Short-Term Strain Profile for Farwell Creek Bridge NEXT Beam Deck Gauge L5-S

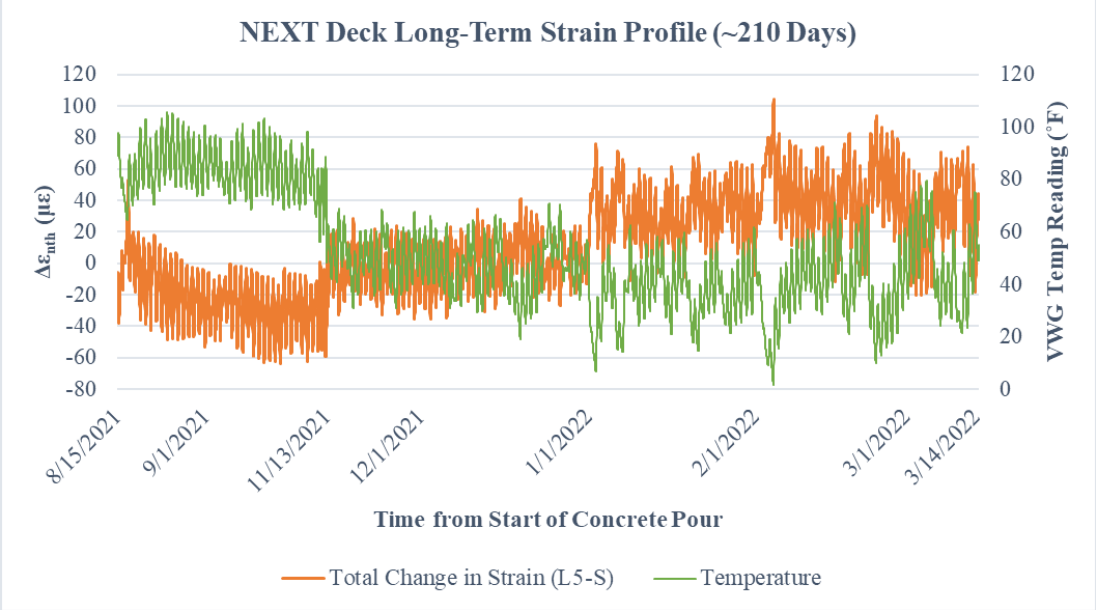

Figure A.14: Long-Term Strain Profile for Farwell Creek Bridge NEXT Beam Deck Gauge L5-S

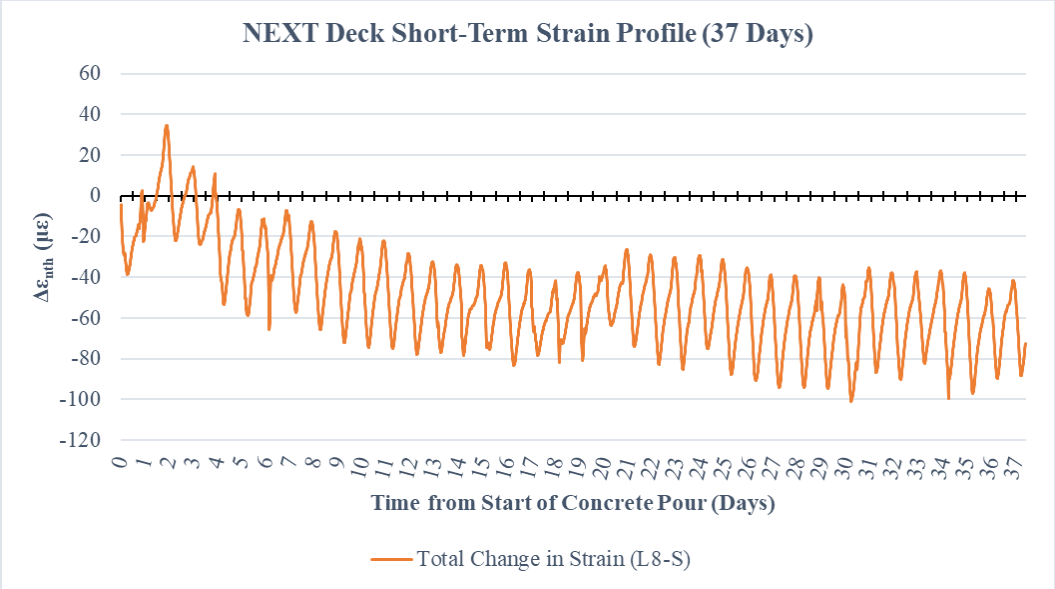

Figure A.15: Short-Term Strain Profile for Farwell Creek Bridge NEXT Beam Deck Gauge L8-S

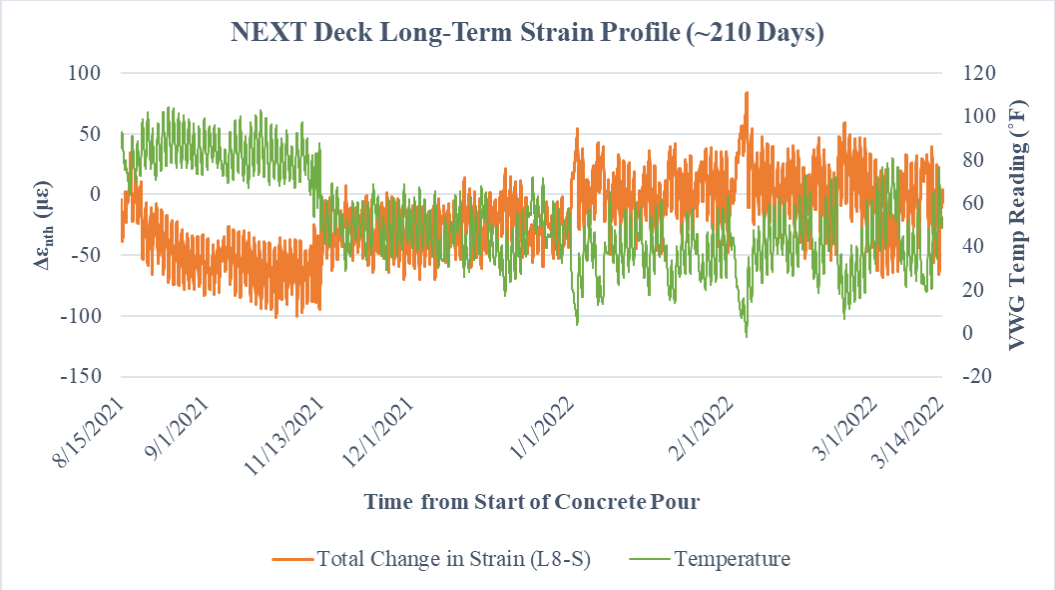

Figure A.16: Long-Term Strain Profile for Farwell Creek Bridge NEXT Beam Deck Gauge L8-S

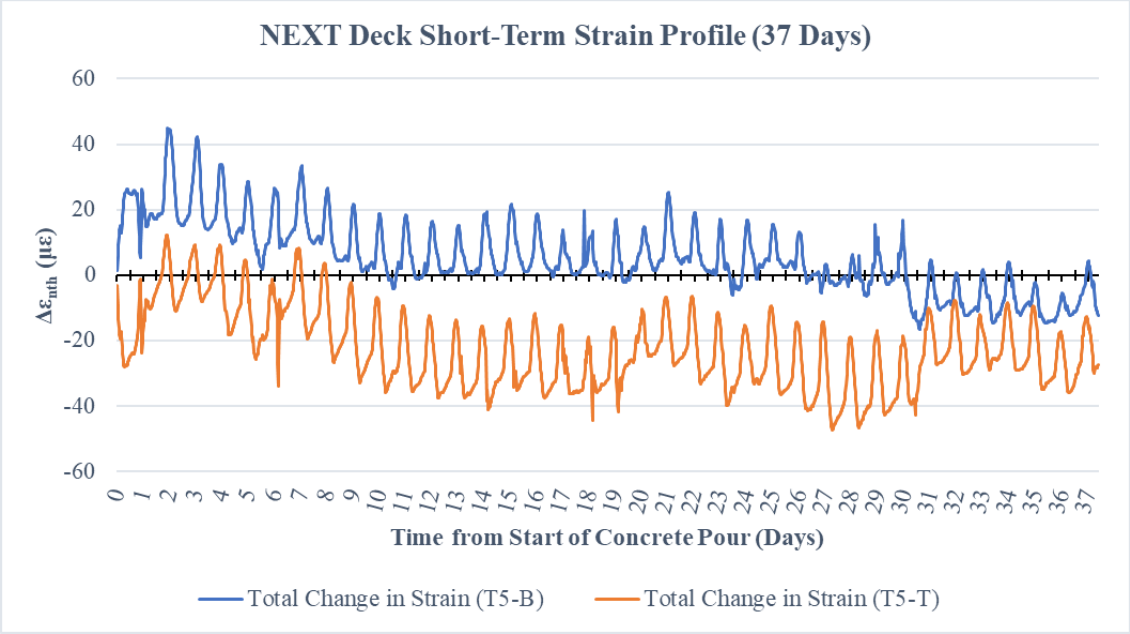

Figure A.17: Short-Term Strain Profile for Farwell Creek Bridge NEXT Beam Deck Gauges T5-B and T5-T

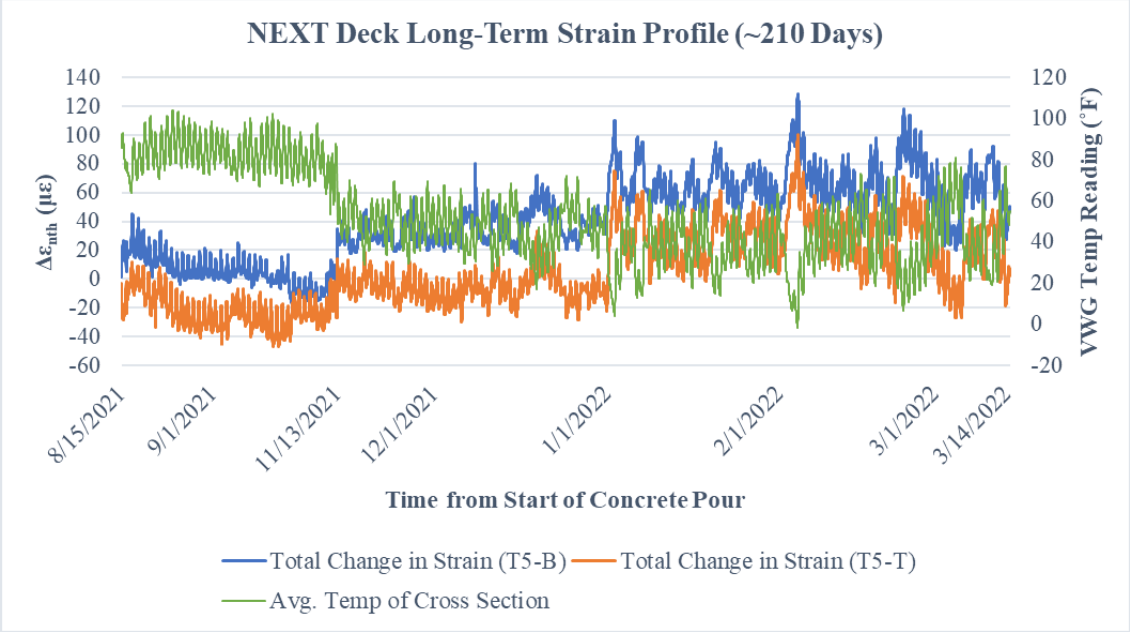

Figure A.18: Long-Term Strain Profile for Farwell Creek Bridge NEXT Beam Deck Gauges T5-B and T5-T

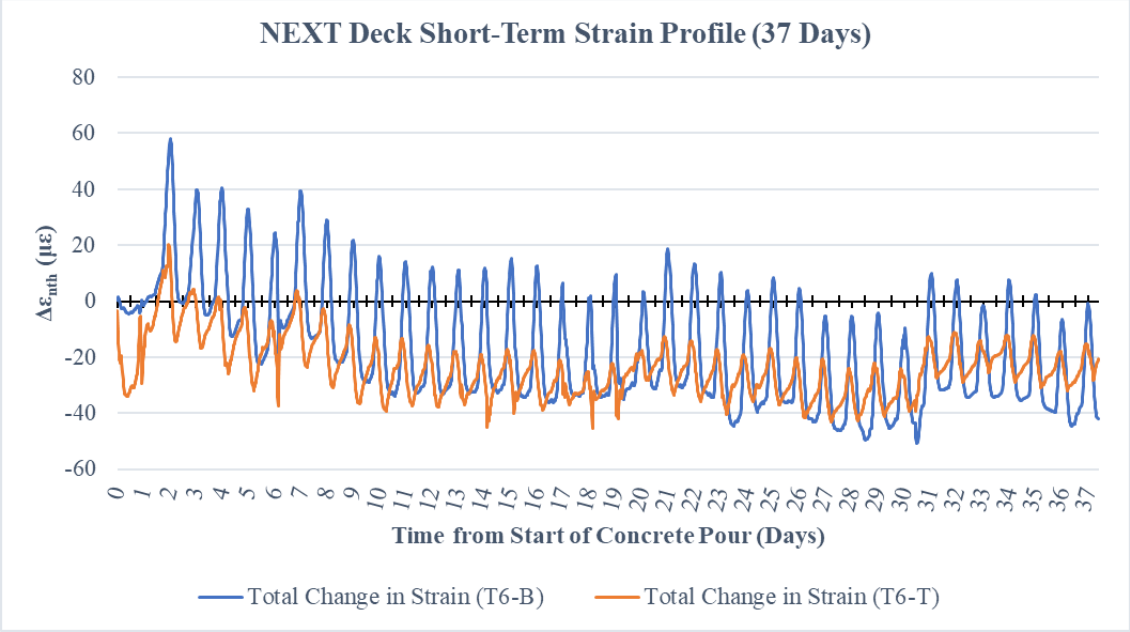

Figure A.19: Short-Term Strain Profile for Farwell Creek Bridge NEXT Beam Deck Gauges T6-B and T6-T

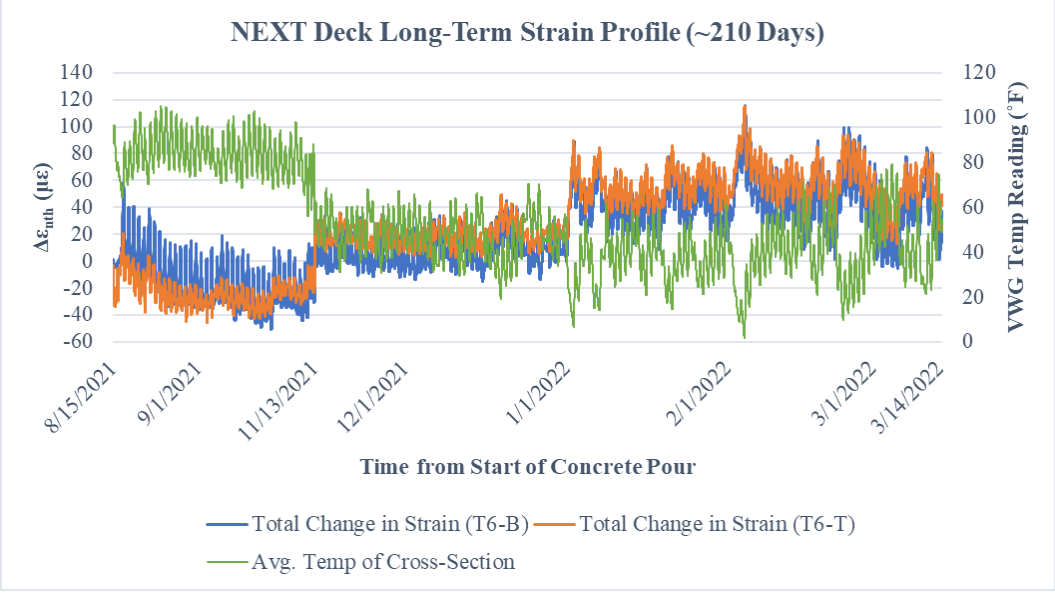

Figure A.20: Long-Term Strain Profile for Farwell Creek Bridge NEXT Beam Deck Gauges T6-B and T6-T

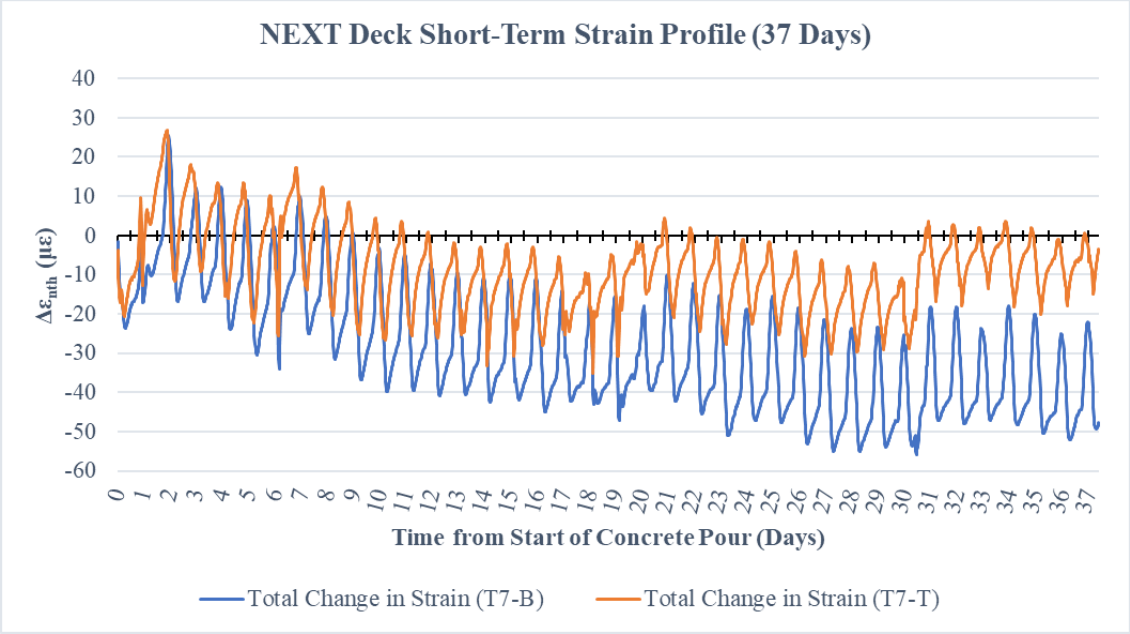

Figure A.21: Short-Term Strain Profile for Farwell Creek Bridge NEXT Beam Deck Gauges T7-B and T7-T

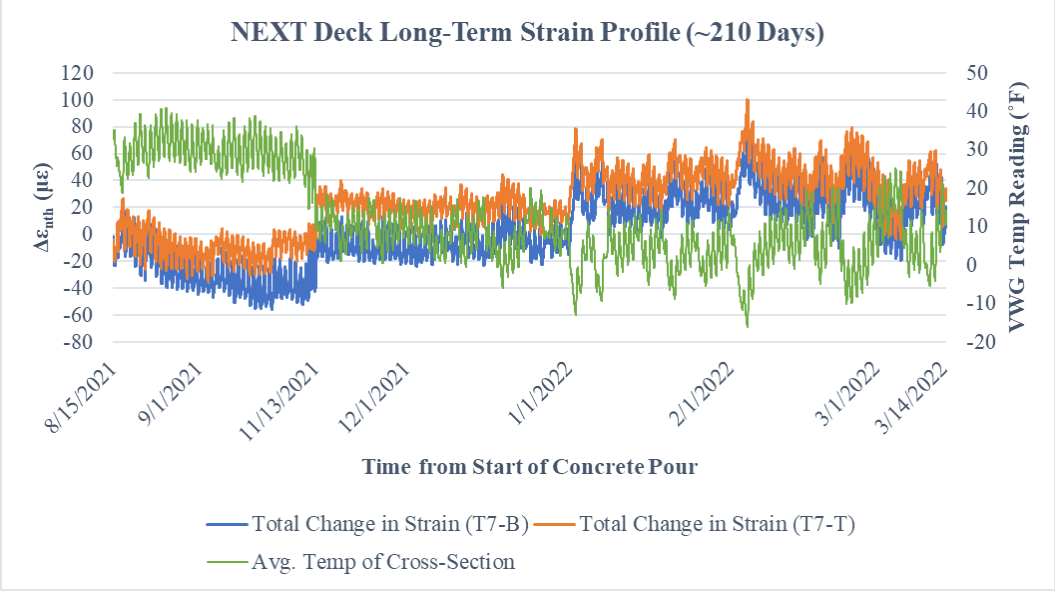

Figure A.22: Long-Term Strain Profile for Farwell Creek Bridge NEXT Beam Deck Gauges T7-B and T7-T

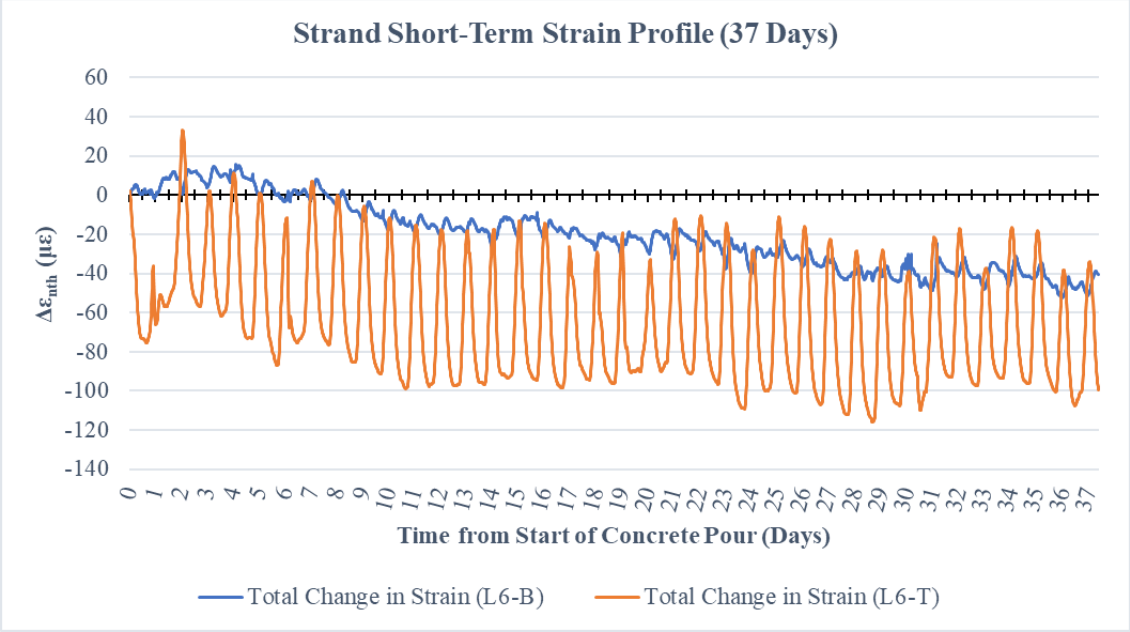

Figure A.23: Short-Term Strain Profile for Farwell Creek Bridge NEXT Beam Strand Gauges L6-B and L6-T

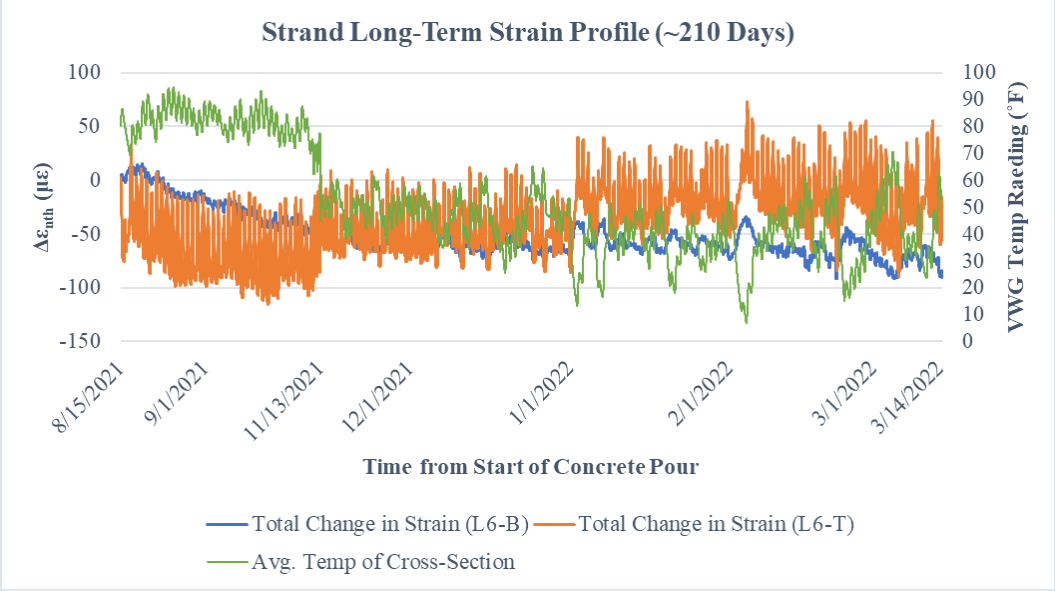

Figure A.24: Long-Term Strain Profile for Farwell Creek Bridge NEXT Beam Strand Gauges L6-B and L6-T

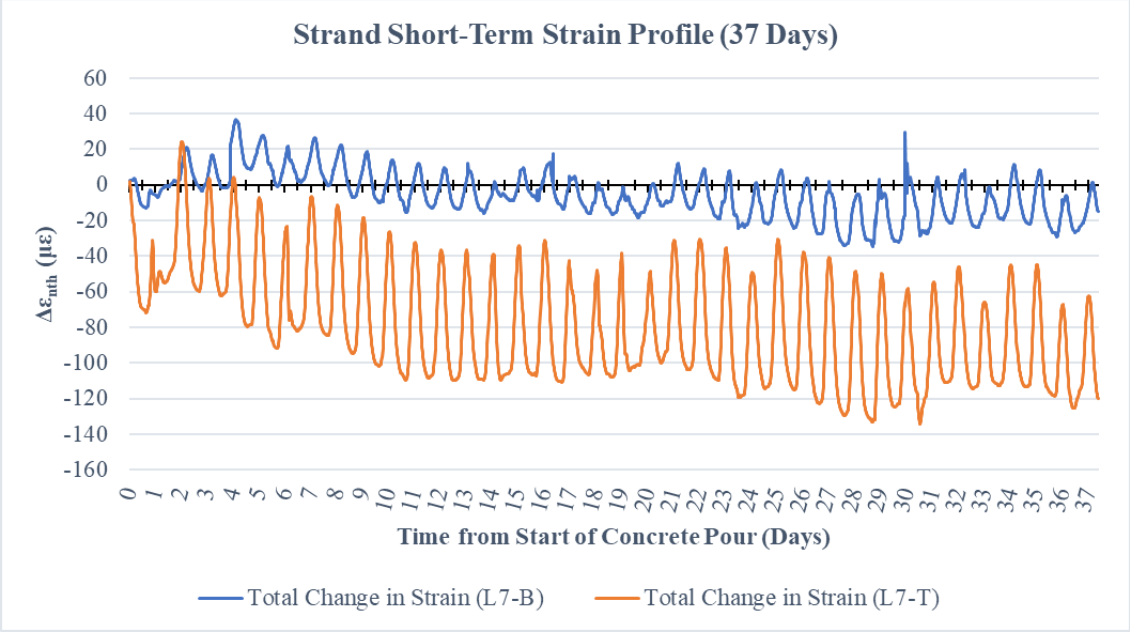

Figure A.25: Short-Term Strain Profile for Farwell Creek Bridge NEXT Beam Strand Gauges L7-B and L7-T

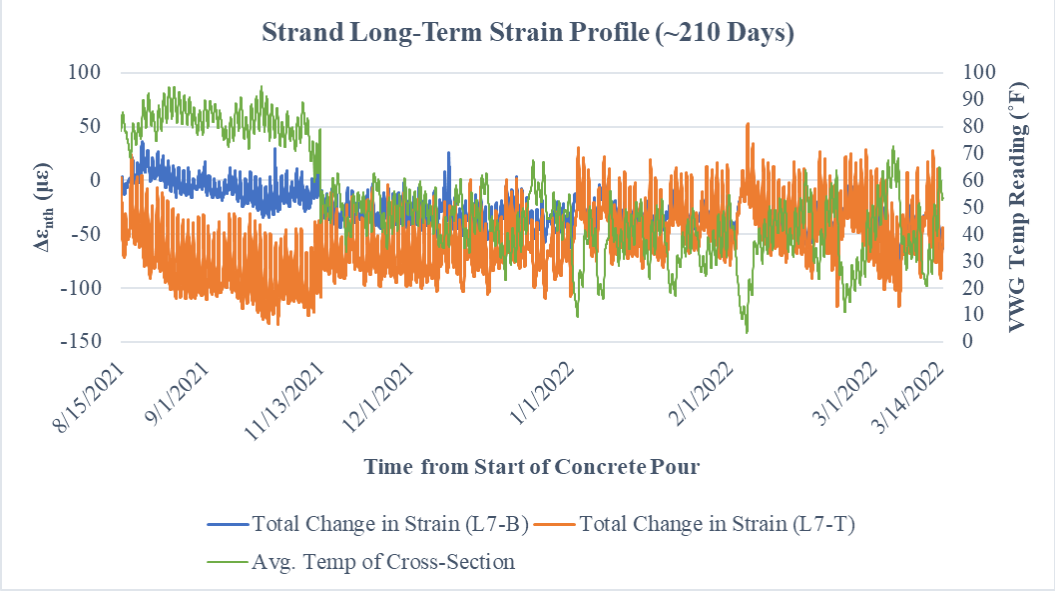

Figure A.26: Long-Term Strain Profile for Farwell Creek Bridge NEXT Beam Strand Gauges L7-B and L7-T

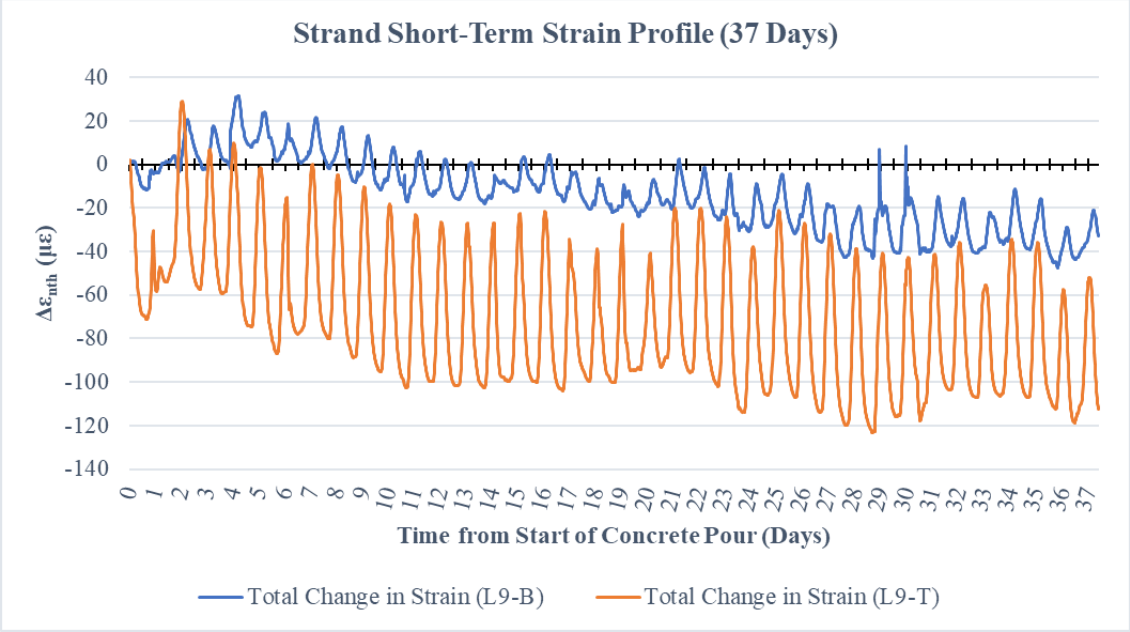

Figure A.27: Short-Term Strain Profile for Farwell Creek Bridge NEXT Beam Strand Gauges L9-B and L9-T

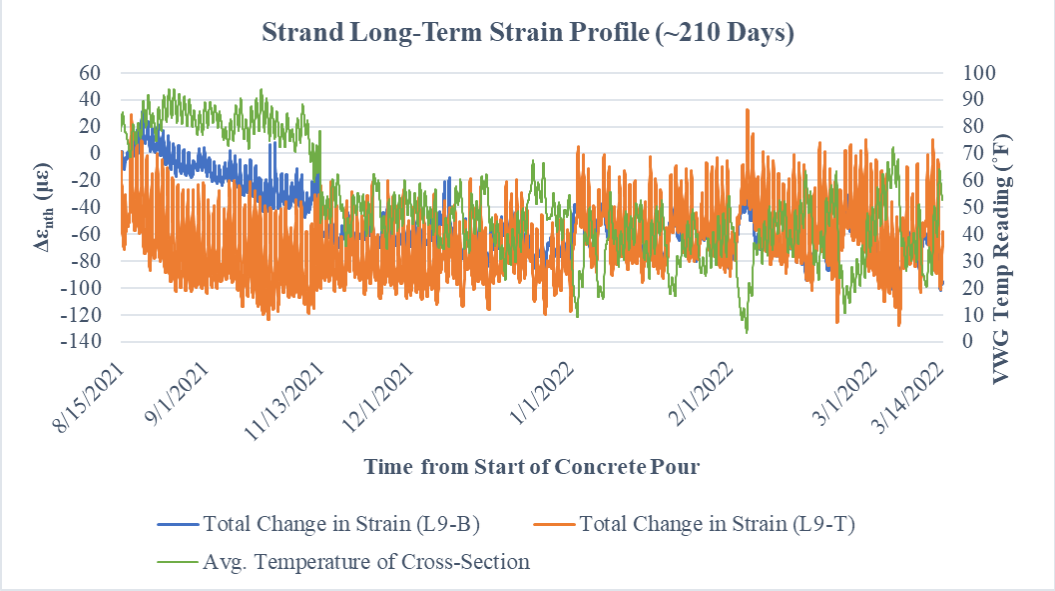

Figure A.28: Long-Term Strain Profile for Farwell Creek Bridge NEXT Beam Strand Gauges L9-B and L9-T

Appendix B. Crack Propagation Flexure Series Profiles

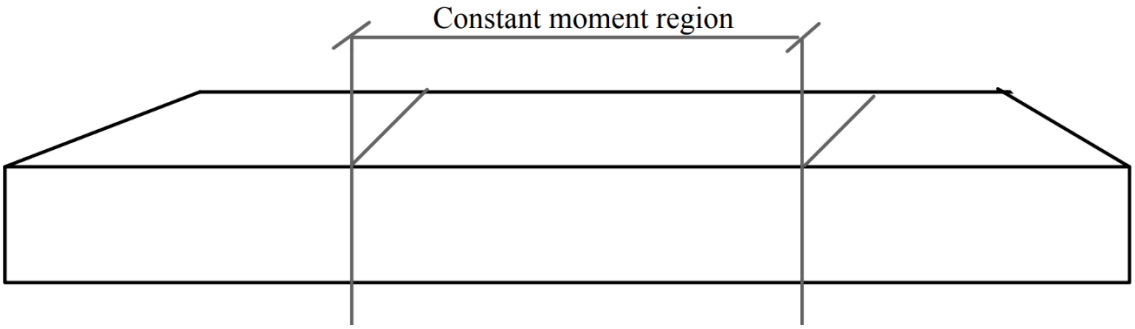

Figure B.1 Crack Propagation for Monolithic Control Specimen at 0 % of Final Load

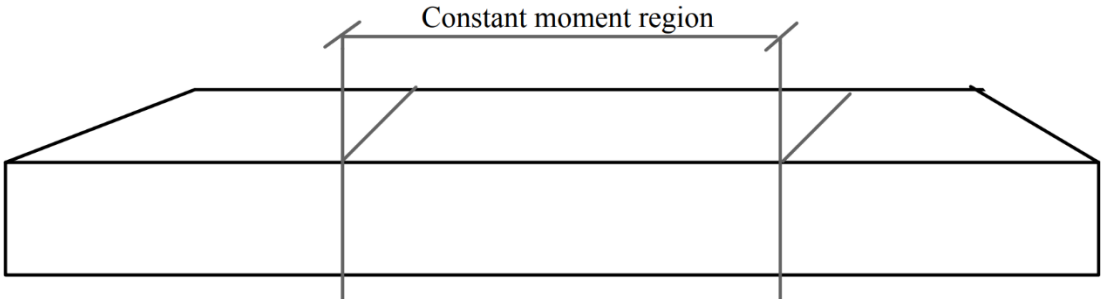

Figure B.2 Crack Propagation for Monolithic Control Specimen at 30 % of Final Load

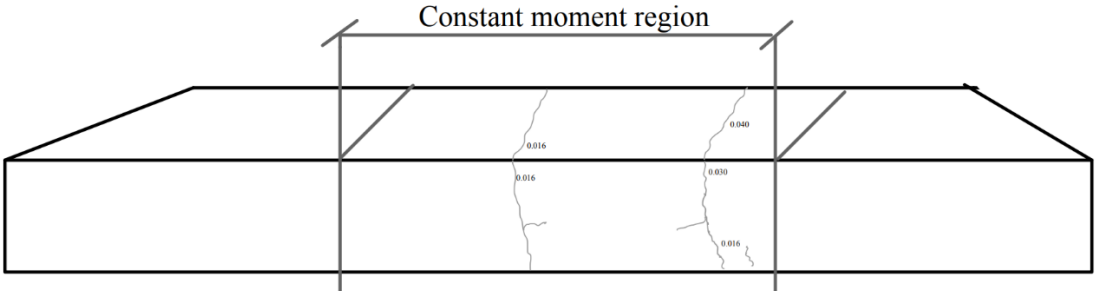

Figure B.3 Crack Propagation for Monolithic Control Specimen at 60 % of Final Load

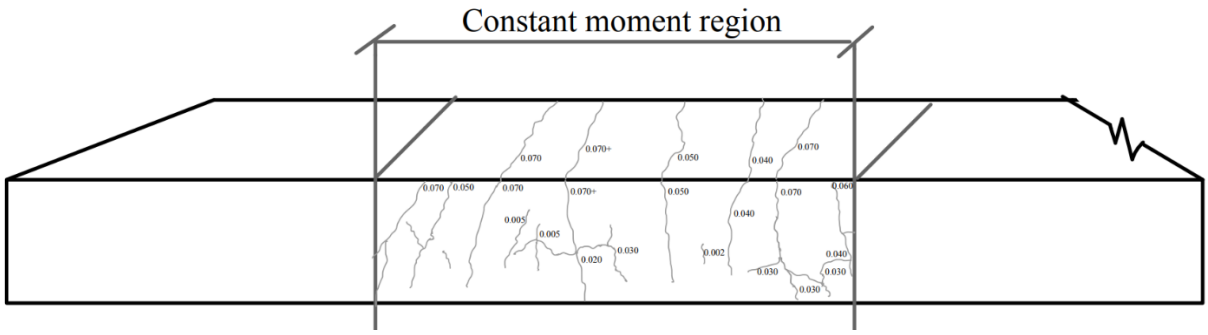

Figure B.4 Crack Propagation for Monolithic Control Specimen at 90 % of Final Load

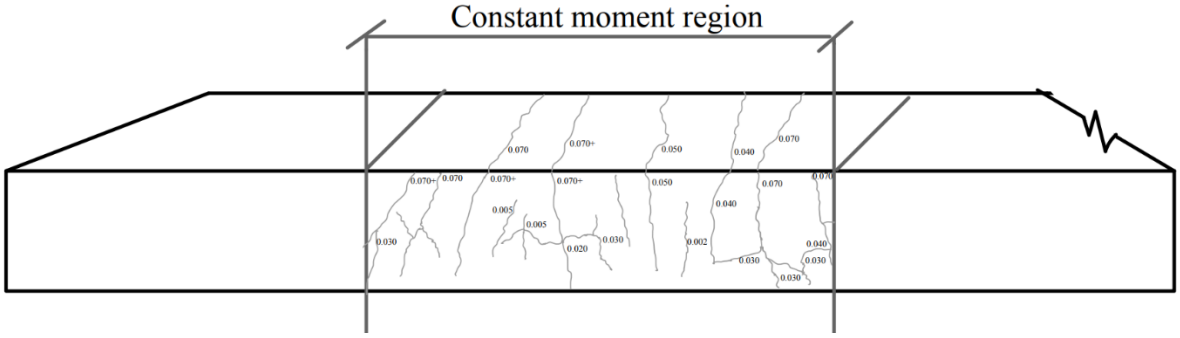

Figure B.5 Crack Propagation for Monolithic Control Specimen at Failure

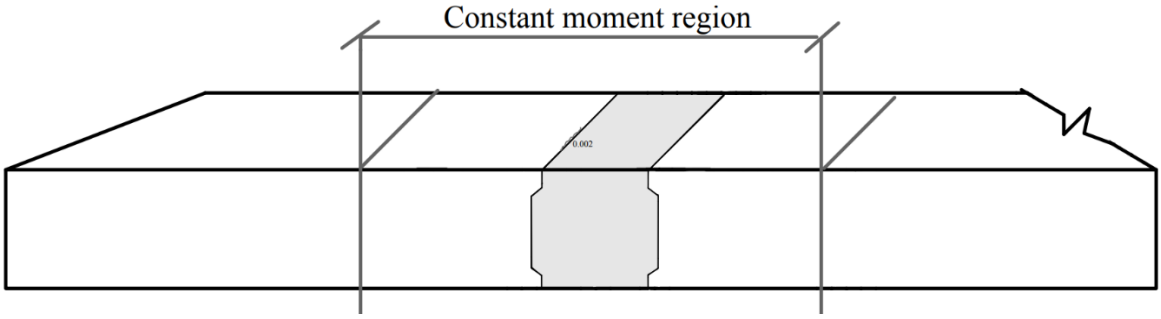

Figure B.6 Crack Propagation for Proprietary Short-Term Specimen at 0 % of Final Load

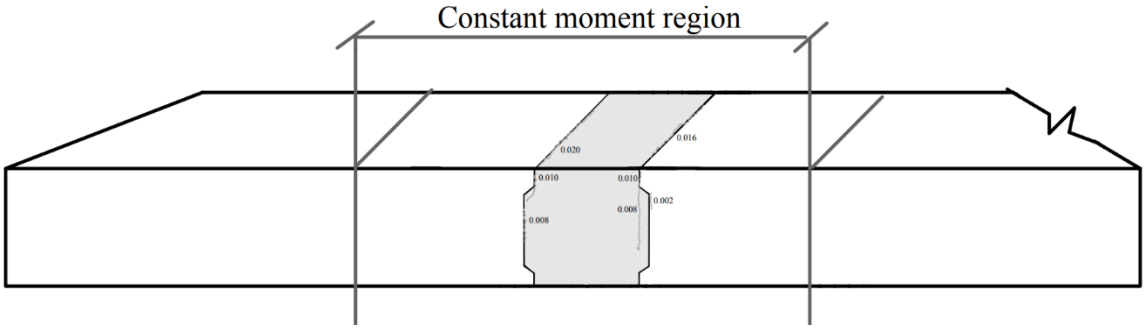

Figure B.7 Crack Propagation for Proprietary Short-Term Specimen at 30 % of Final Load

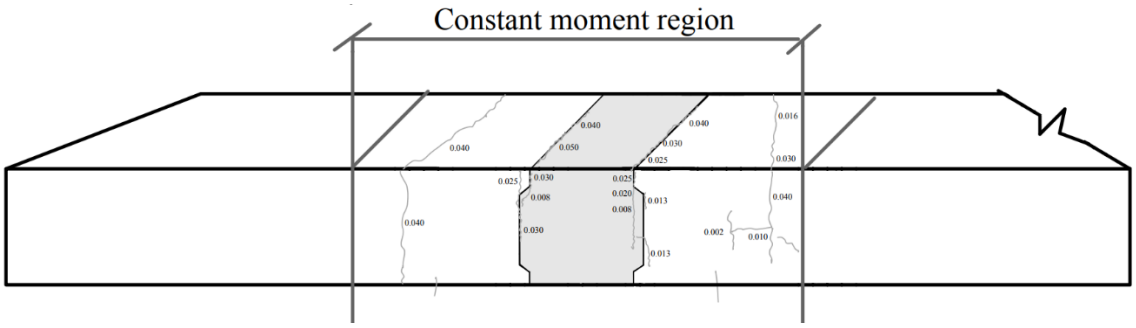

Figure B.8 Crack Propagation for Proprietary Short-Term Specimen at 60 % of Final Load

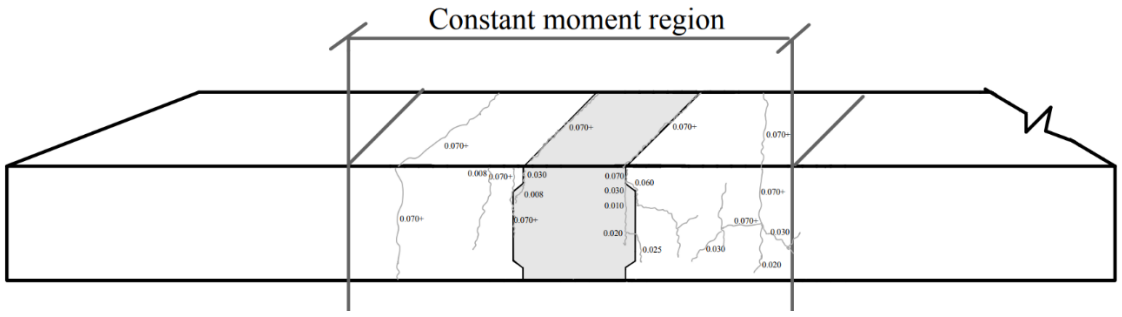

Figure B.9 Crack Propagation for Proprietary Short-Term Specimen at 90 % of Final Load

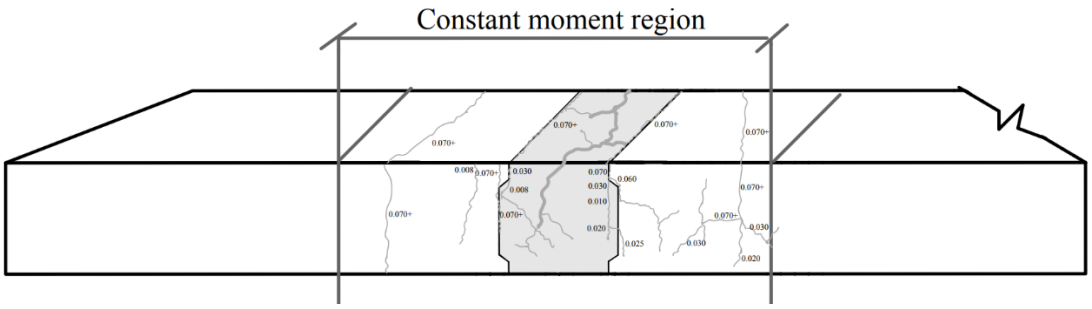

Figure B.10 Crack Propagation for Proprietary Short-Term Specimen at Failure

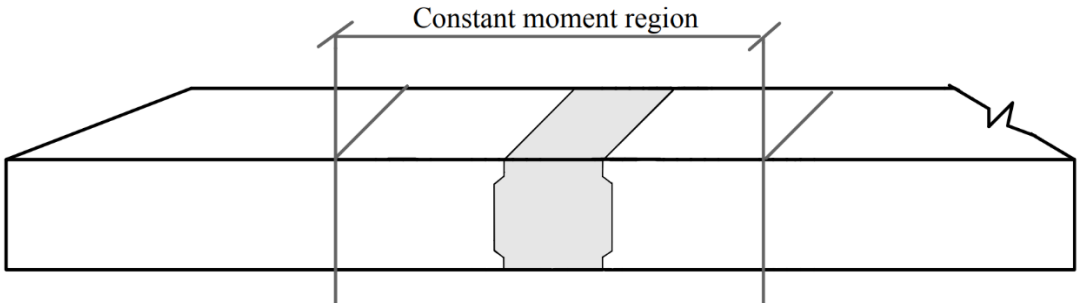

Figure B.11 Crack Propagation for Non-Proprietary Short-Term Specimen at 0 % of Final Load

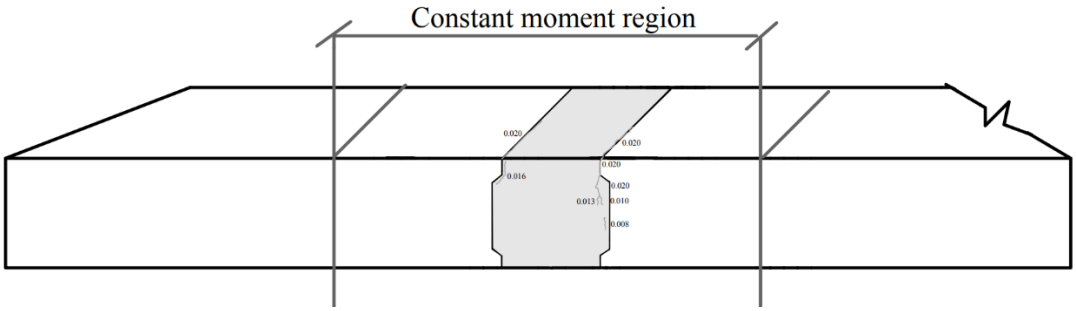

Figure B.12 Crack Propagation for Non-Proprietary Short-Term Specimen at 30 % of Final Load

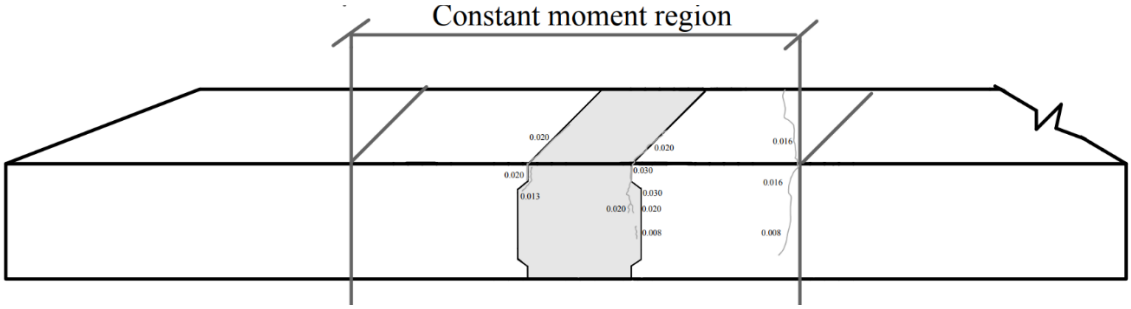

Figure B.13 Crack Propagation for Non-Proprietary Short-Term Specimen at 60 % of Final Load

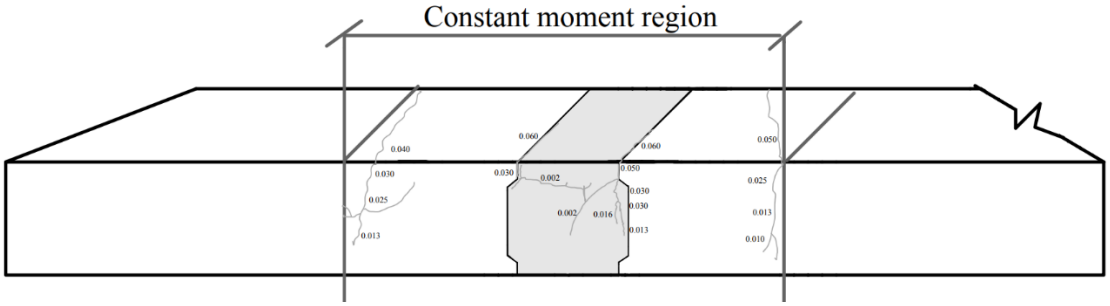

Figure B.14 Crack Propagation for Non-Proprietary Short-Term Specimen at 90 % of Final Load

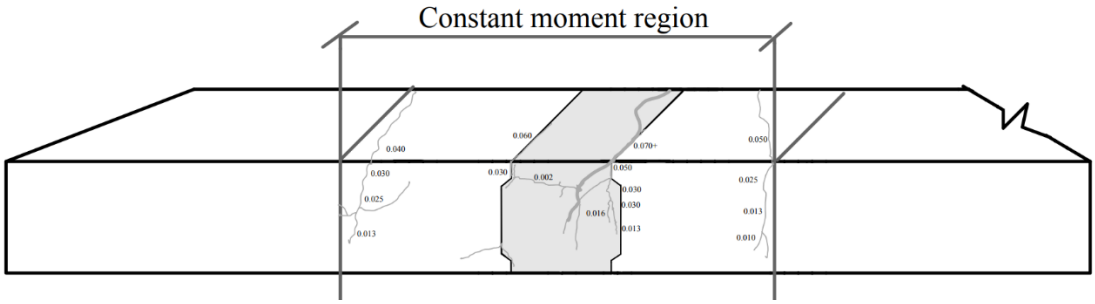

Figure B.15 Crack Propagation for Non-Proprietary Short-Term Specimen at Failure

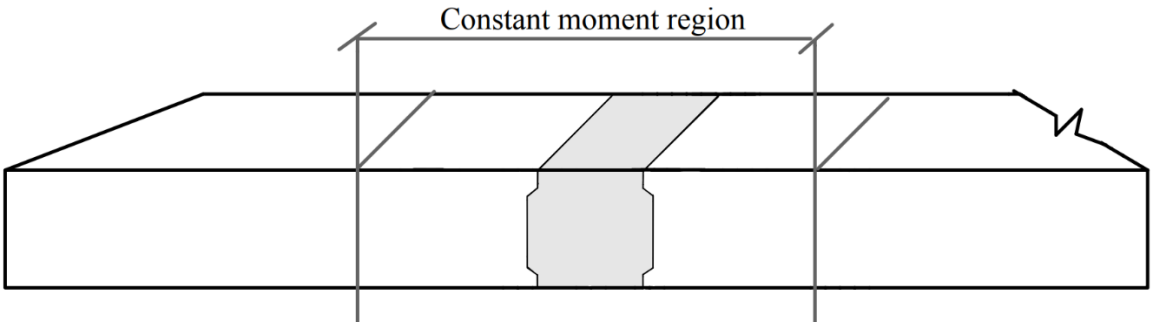

Figure B.16 Crack Propagation for Proprietary Long-Term Specimen at 0 % of Final Load

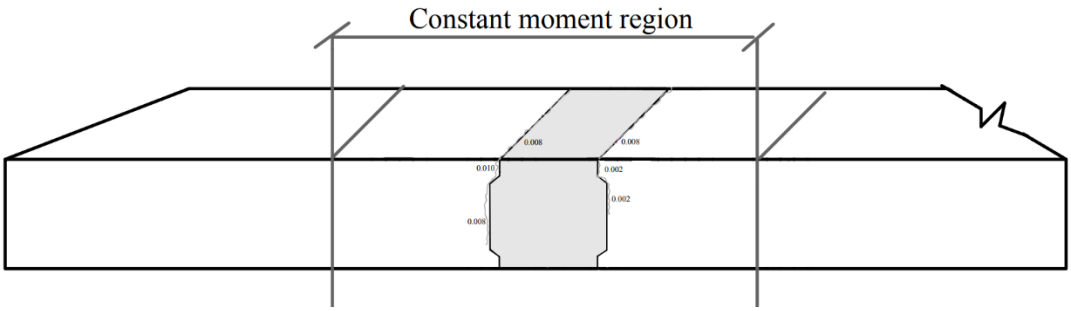

Figure B.17 Crack Propagation for Proprietary Long-Term Specimen at 30 % of Final Load

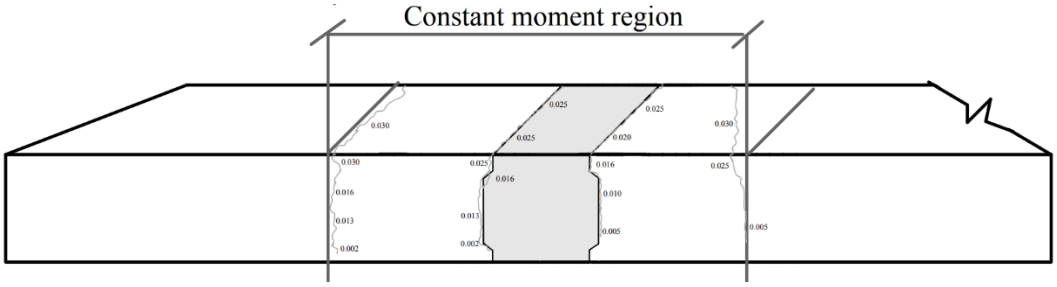

Figure B.18 Crack Propagation for Proprietary Long-Term Specimen at 60 % of Final Load

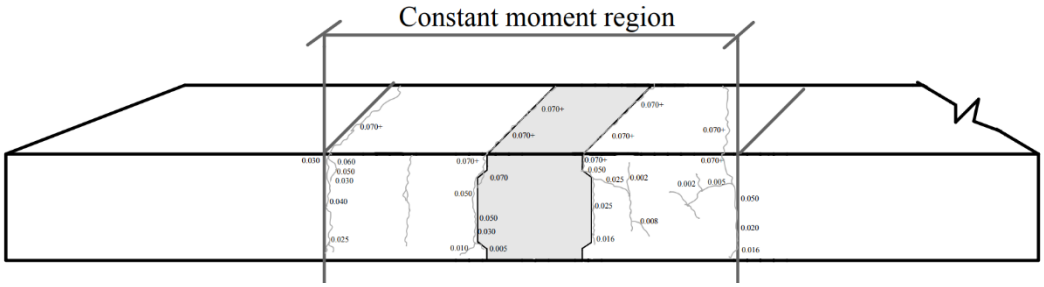

Figure B.19 Crack Propagation for Proprietary Long-Term Specimen at 90 % of Final Load

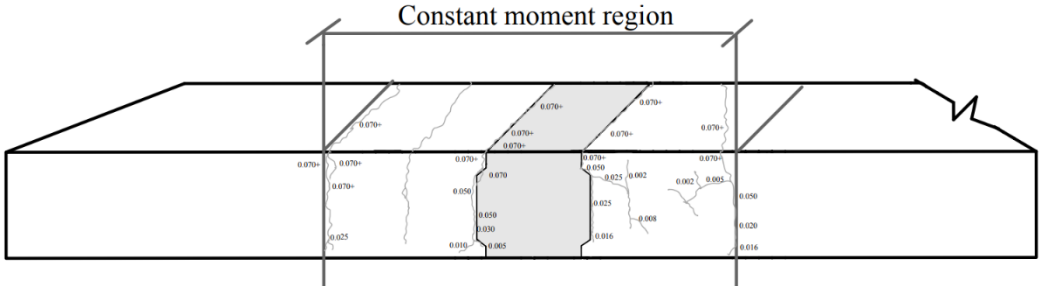

Figure B.20 Crack Propagation for Proprietary Long-Term Specimen at Failure

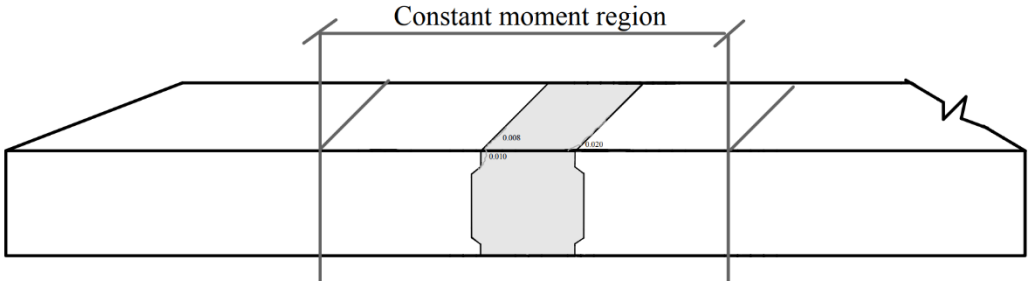

Figure B.21 Crack Propagation for Non-Proprietary Long-Term Specimen at 0 % of Final Load

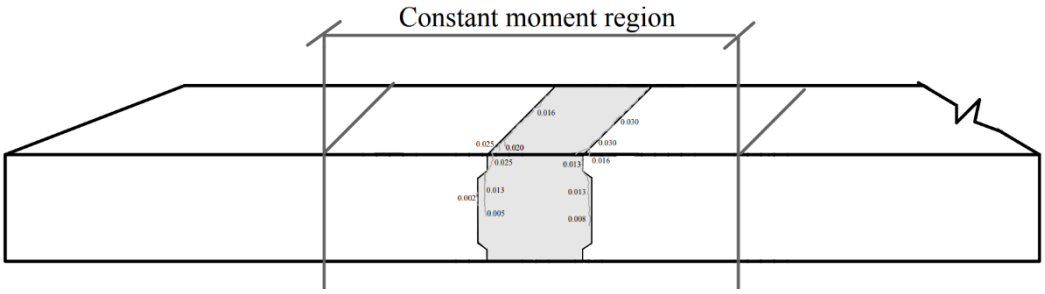

Figure B.22 Crack Propagation for Non-Proprietary Long-Term Specimen at 30 % of Final Load

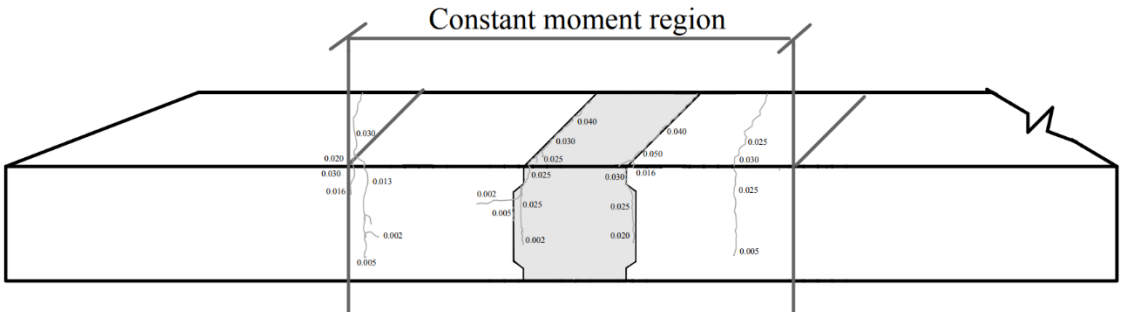

Figure B.23 Crack Propagation for Non-Proprietary Long-Term Specimen at 60 % of Final Load

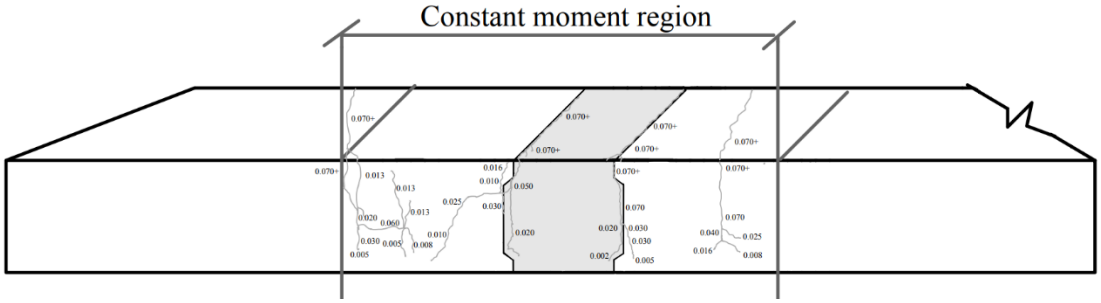

Figure B.24 Crack Propagation for Non-Proprietary Long-Term Specimen at 90 % of Final Load

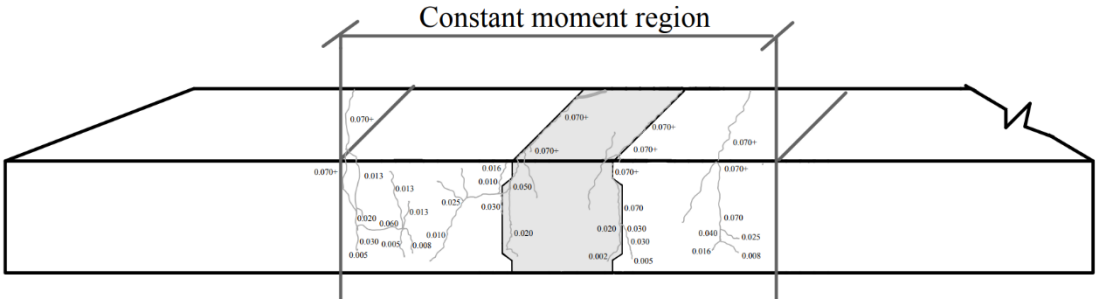

Figure B.25 Crack Propagation for Non-Proprietary Long-Term Specimen at Failure

Appendix C. Crack Propagation Shear Series Profiles

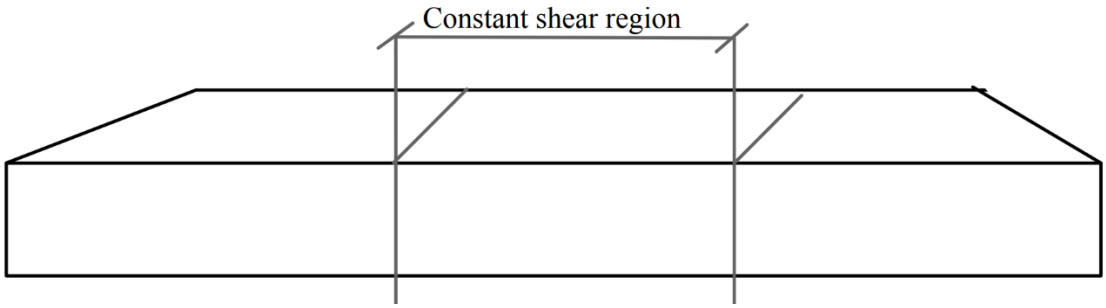

Figure C.1 Crack Propagation for Monolithic Control Specimen at 0 % of Final Load

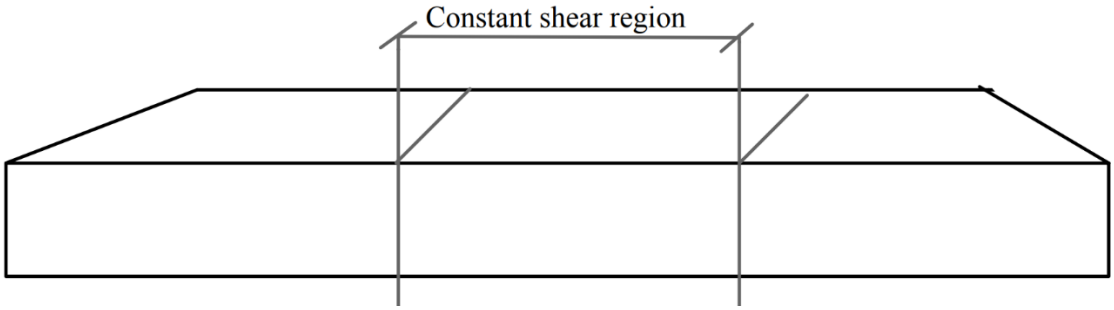

Figure C.2 Crack Propagation for Monolithic Control Specimen at 30 % of Final Load

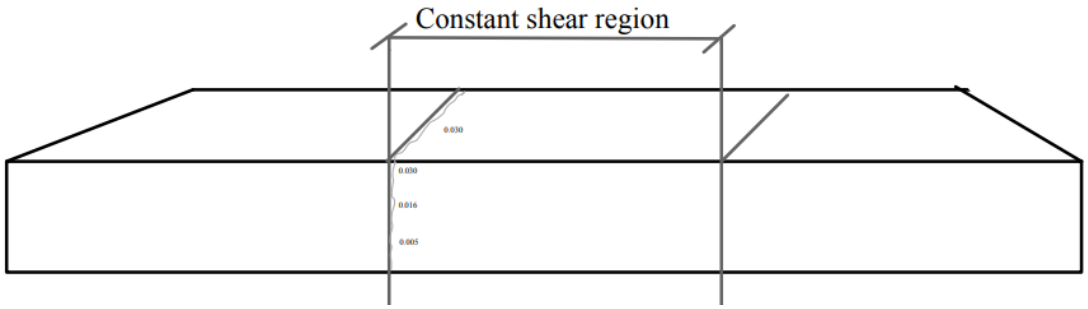

Figure C.3 Crack Propagation for Monolithic Control Specimen at 60 % of Final Load

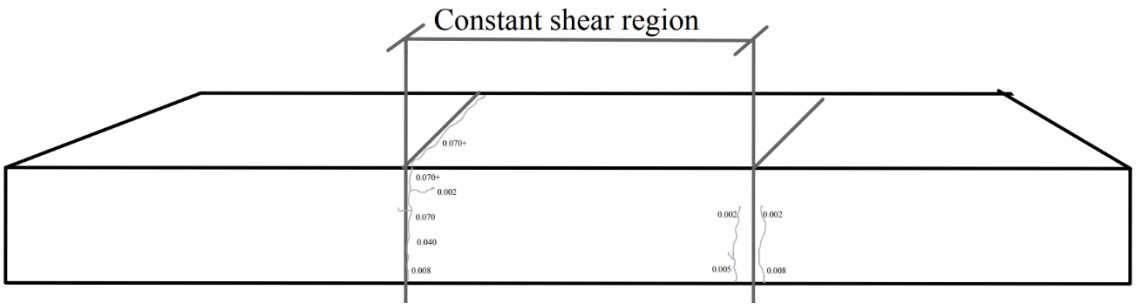

Figure C.4 Crack Propagation for Monolithic Control Specimen at 90 % of Final Load

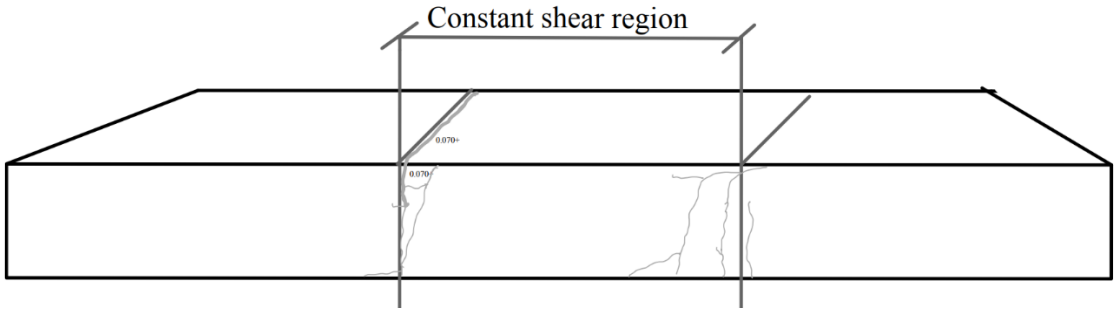

Figure C.5 Crack Propagation for Monolithic Control Specimen at Failure

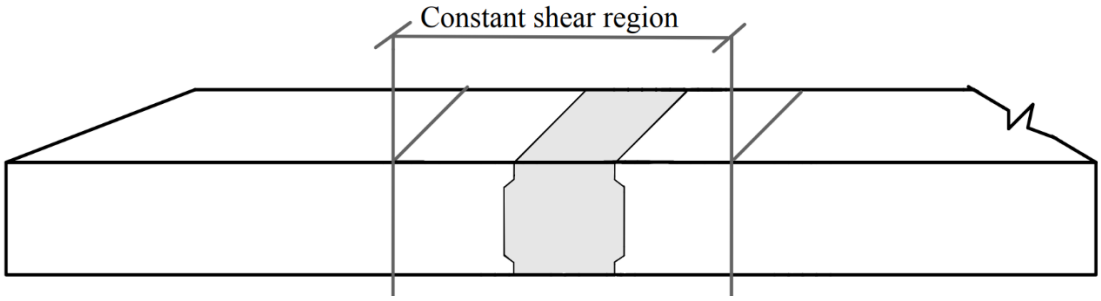

Figure C.6 Crack Propagation for Proprietary Short-Term Specimen at 0 % of Final Load

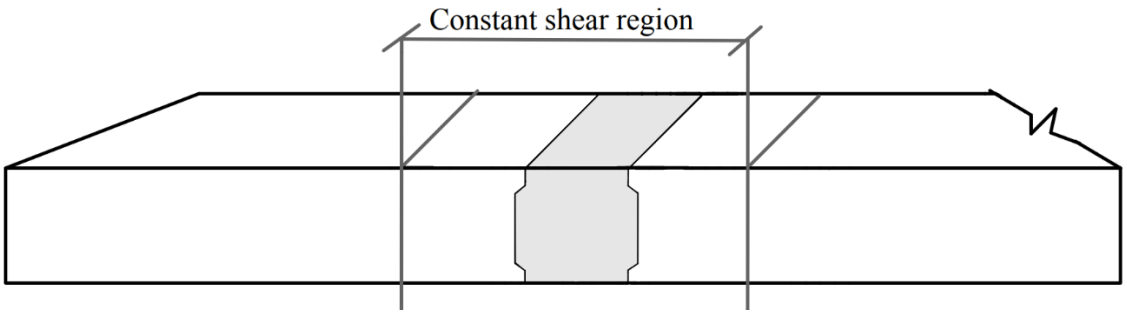

Figure C.7 Crack Propagation for Proprietary Short-Term Specimen at 30 % of Final Load

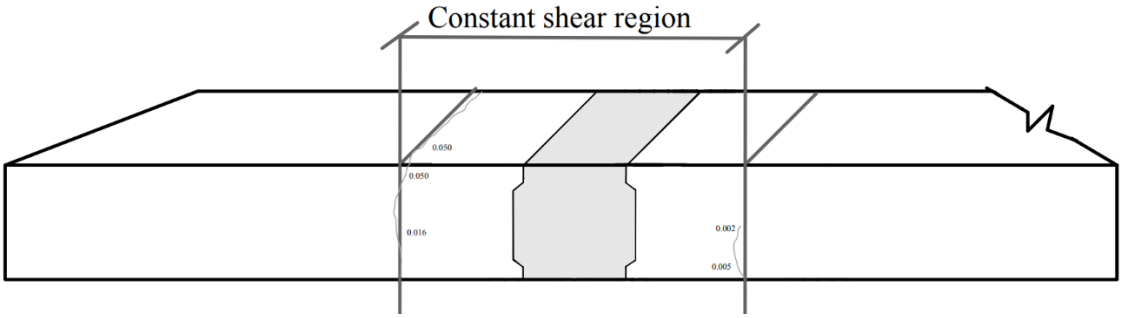

Figure C.8 Crack Propagation for Proprietary Short-Term Specimen at 60 % of Final Load

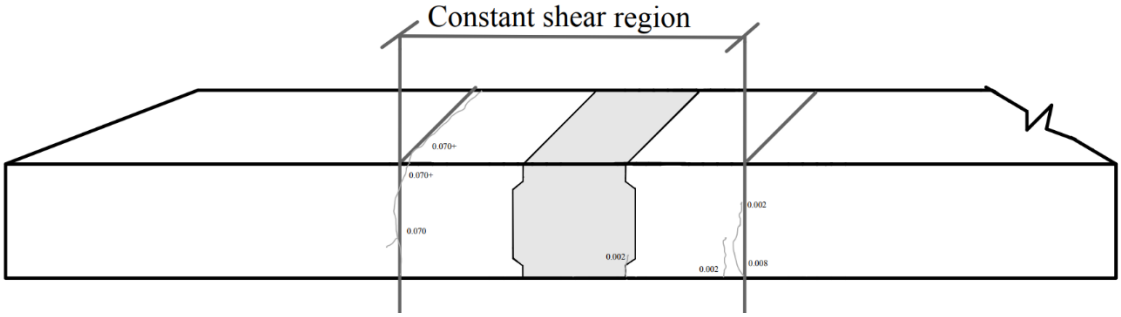

Figure C.9 Crack Propagation for Proprietary Short-Term Specimen at 90 % of Final Load

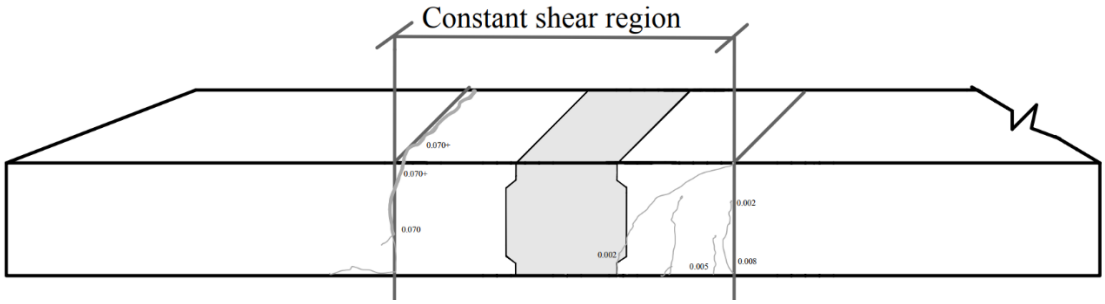

Figure C.10 Crack Propagation for Proprietary Short-Term Specimen at Failure

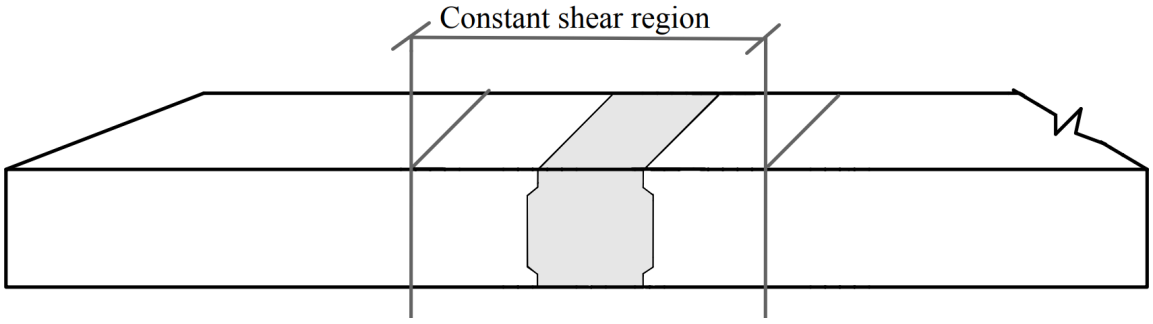

Figure C.11 Crack Propagation for Non-Proprietary Short-Term Specimen at 0 % of Final Load

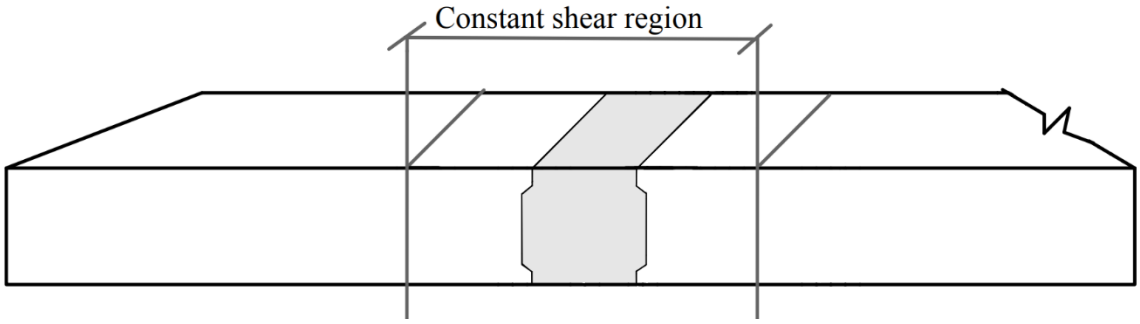

Figure C.12 Crack Propagation for Non-Proprietary Short-Term Specimen at 30 % of Final Load

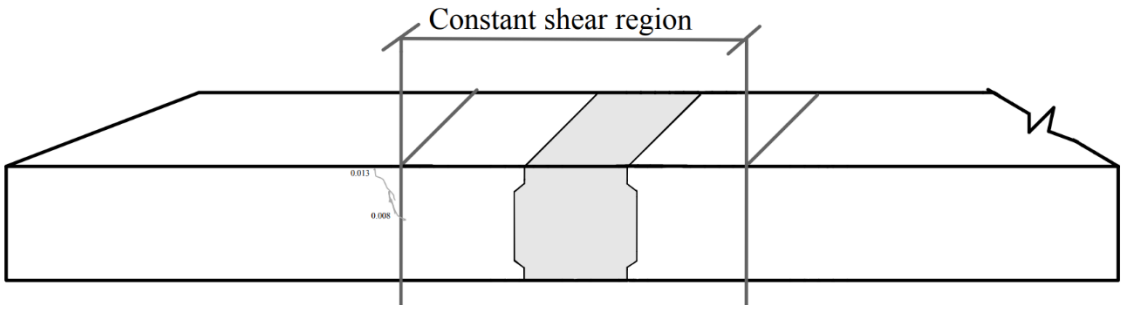

Figure C.13 Crack Propagation for Non-Proprietary Short-Term Specimen at 60 % of Final Load

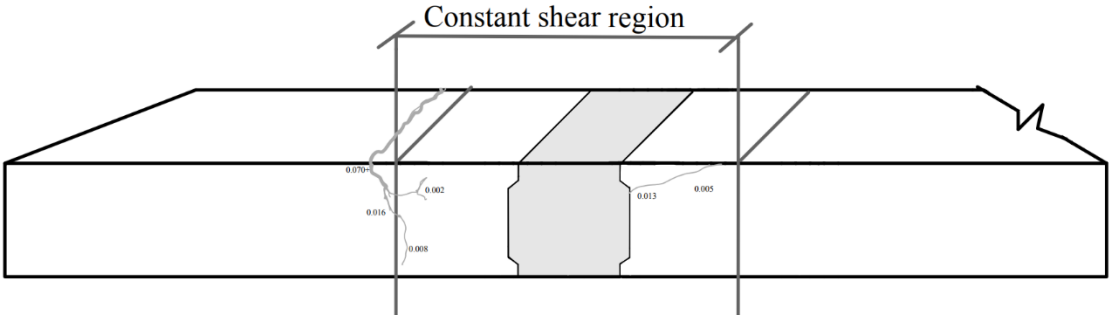

Figure C.14 Crack Propagation for Non-Proprietary Short-Term Specimen at 90 % of Final Load

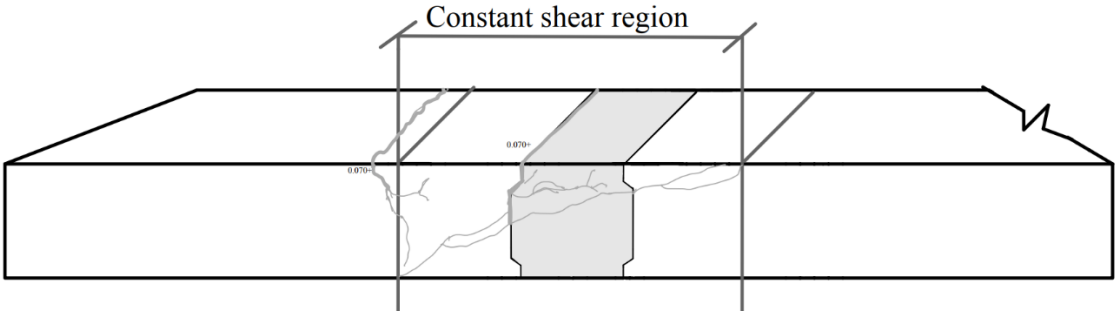

Figure C.15 Crack Propagation for Non-Proprietary Short-Term Specimen at Failure

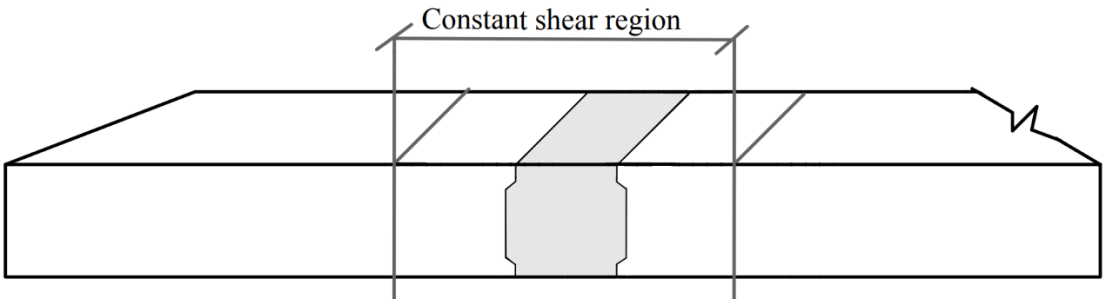

Figure C.16 Crack Propagation for Proprietary Long-Term Specimen at 0 % of Final Load

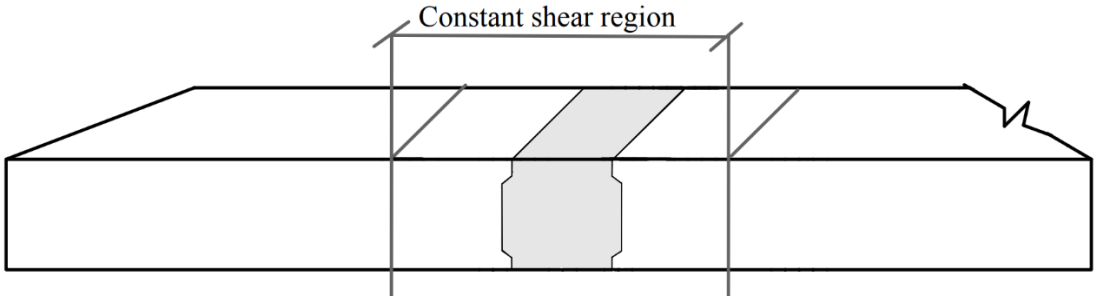

Figure C.17 Crack Propagation for Proprietary Long-Term Specimen at 30 % of Final Load

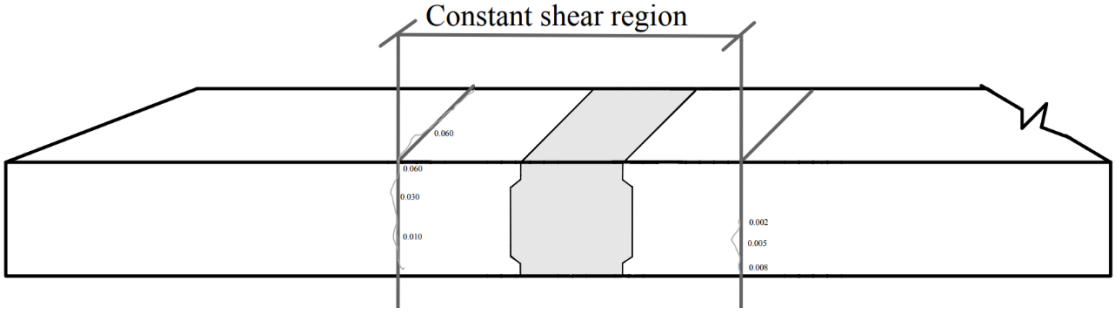

Figure C.18 Crack Propagation for Proprietary Long-Term Specimen at 60 % of Final Load

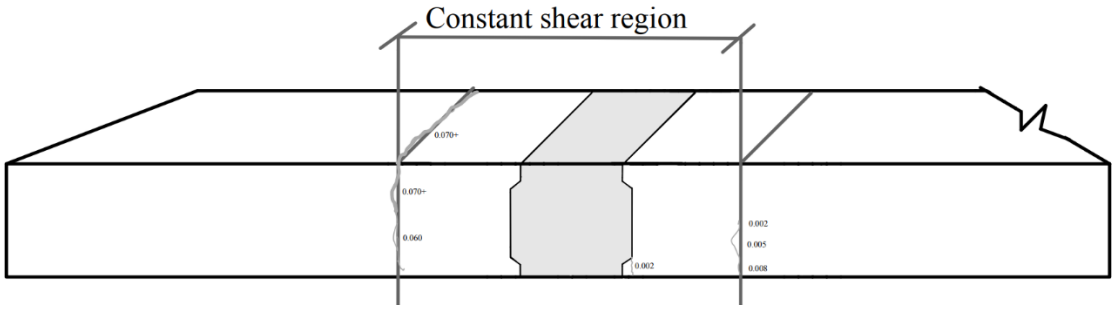

Figure C.19 Crack Propagation for Proprietary Long-Term Specimen at 90 % of Final Load

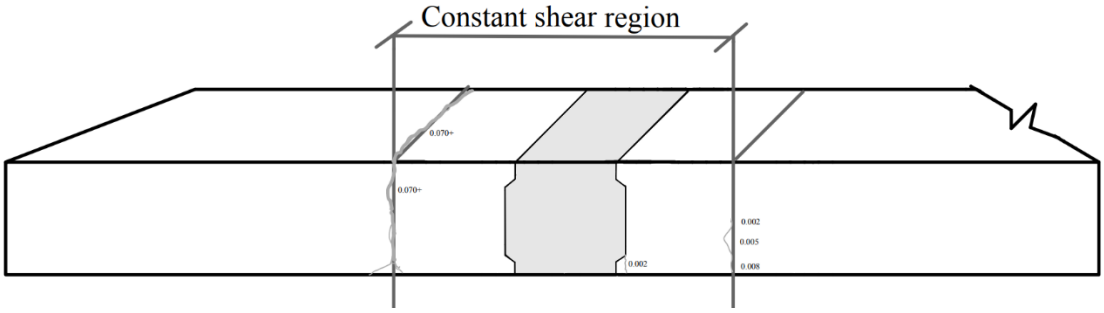

Figure C.20 Crack Propagation for Proprietary Long-Term Specimen at Failure

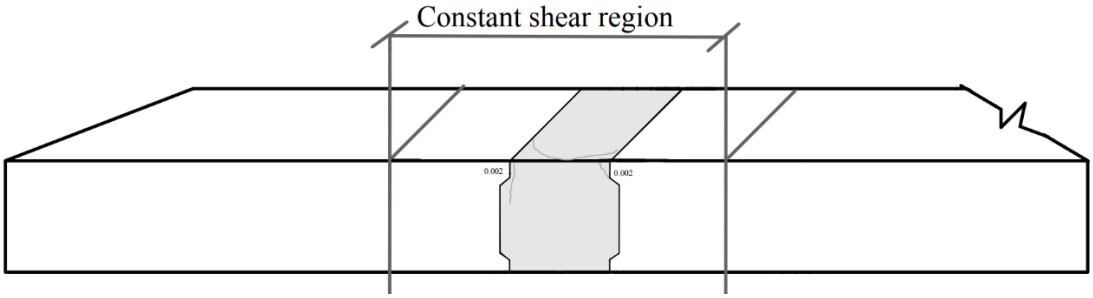

Figure C.21 Crack Propagation for Non-Proprietary Long-Term Specimen at 0 % of Final Load

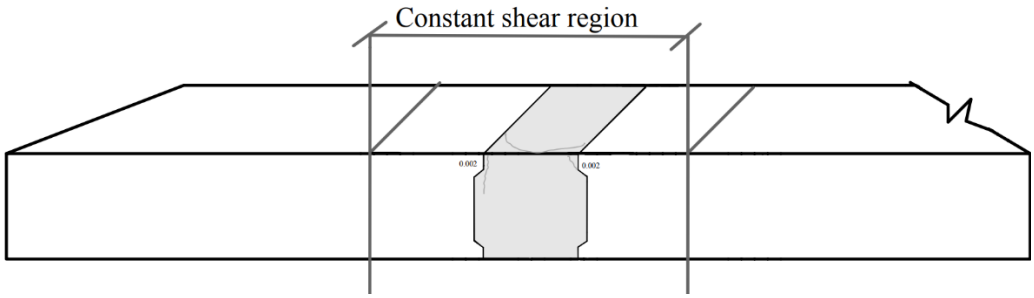

Figure C.22 Crack Propagation for Non-Proprietary Long-Term Specimen at 30 % of Final Load

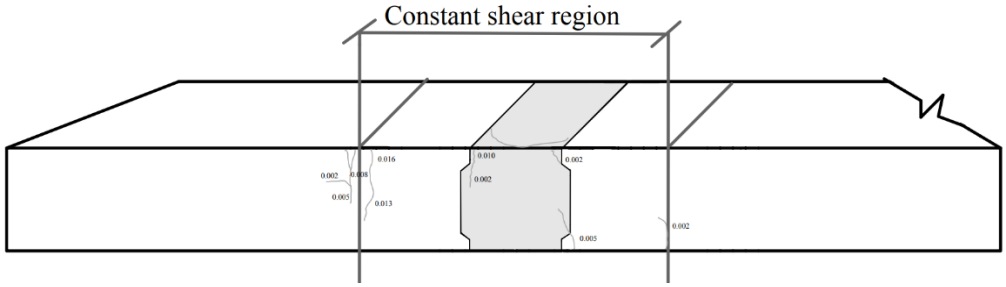

Figure C.23 Crack Propagation for Non-Proprietary Long-Term Specimen at 60 % of Final Load

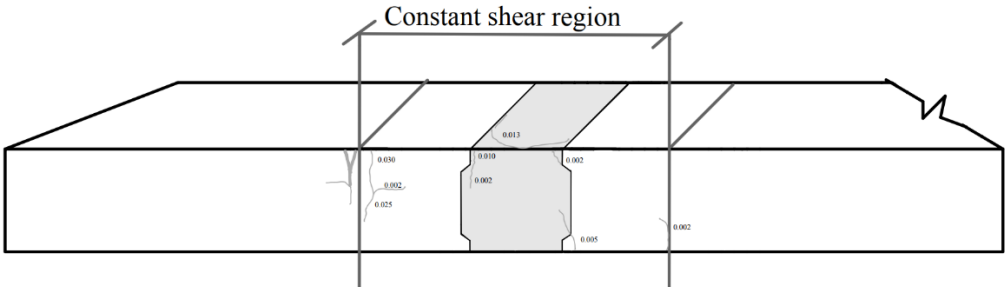

Figure C.24 Crack Propagation for Non-Proprietary Long-Term Specimen at 90 % of Final Load

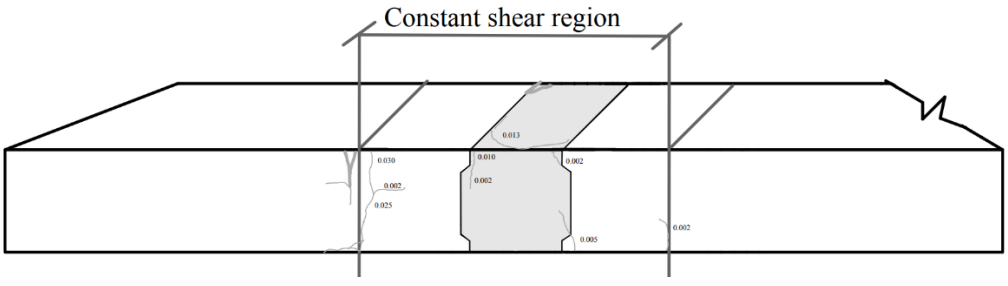

Figure C.25 Crack Propagation for Non-Proprietary Long-Term Specimen at Failure

Appendix D. Engineering Drawings of Specimens

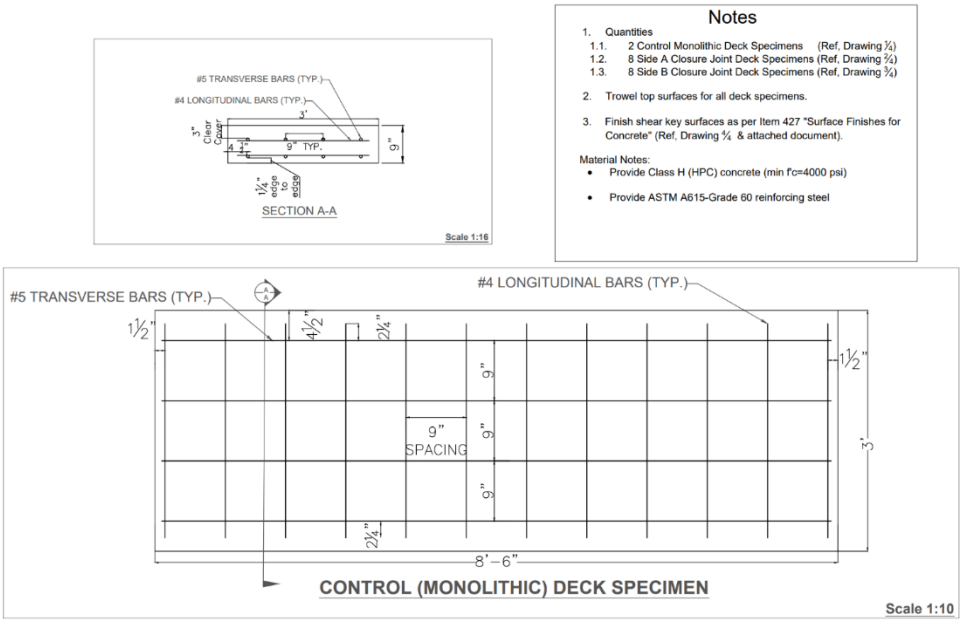

Figure D.1 Drawing of Monolithic Control Specimen (Scale altered due to formatting)

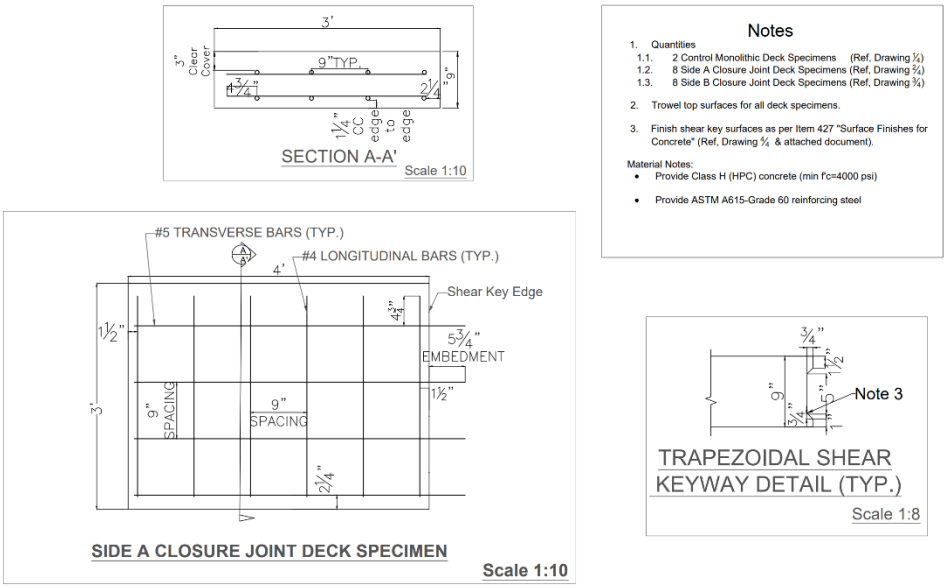

Figure D.2 Drawing of Side A Closure Joint Deck Specimen (Scale altered due to formatting)

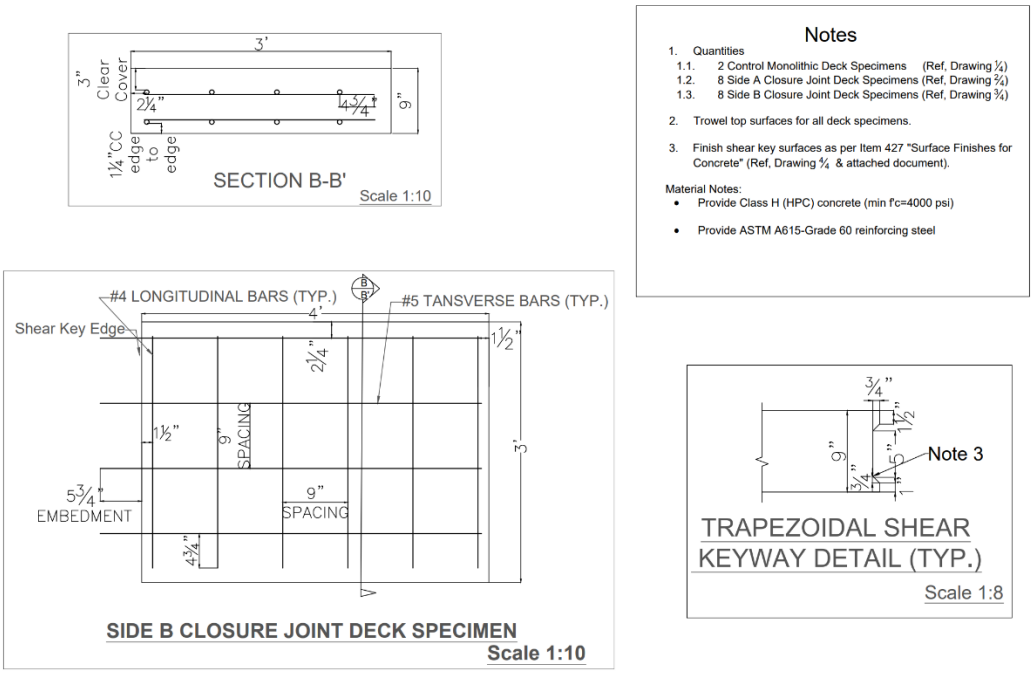

Figure D.3 Drawing of Side B Closure Joint Deck Specimen (Scale altered due to formatting)

Shear Key Surface Finish Notes

4.3.6. Exposed Aggregate Finish.

- Provide exposed aggregate finish as indicated on the plans. Provide a depth of finish between 3/8 in. and 1/2 in. unless directed otherwise.
- Apply a concrete surface retarder that penetrates approximately 1/4 in. into the forms or concrete surface to help achieve the desired finish. Apply 2 or 3 coats to wood forms to account for absorption if necessary.Tape or caulk form joints to prevent escape of the retarder during the placing operations. Protect the form surfaces from sun and rain while exposed to the atmosphere. Re-treat form surfaces with retarder if disturbed. Protect adjacent areas of concrete not requiring exposed aggregate finish from the retarder.
- Remove forms 12 to 15 hr. after concrete placement but not before concrete has gained sufficient strength to support the self-weight of the member unless directed otherwise. Expose the aggregate for the finish immediately after form removal. Remove the grout paste covering the aggregate to be exposed by an approved method. Do not loosen the aggregate by the grout removal operation. Maintain required curing on all surfaces except for the time while the aggregate is being exposed. Cure using wet mats or membrane after the aggregate is exposed.

Figure D.4 Shear Key Finish Notes

Appendix E. TxDOT Item 427 Surface Finishes For Concrete

4.3.6. **Exposed Aggregate Finish**. Provide exposed aggregate finish as indicated on the plans. Provide a depth of finish between 3/8 in. and 1/2 in. unless directed otherwise.

Apply a concrete surface retarder that penetrates approximately 1/4 in. into the forms or concrete surface to help achieve the desired finish. Apply 2 or 3 coats to wood forms to account for absorption if necessary. Tape or caulk form joints to prevent escape of the retarder during the placing operations. Protect the form surfaces from sun and rain while exposed to the atmosphere. Re-treat form surfaces with retarder if disturbed. Protect adjacent areas of concrete not requiring exposed aggregate finish from the retarder.

Remove forms 12 to 15 hr. after concrete placement but not before concrete has gained sufficient strength to support the self-weight of the member unless directed otherwise. Expose the aggregate for the finish immediately after form removal. Remove the grout paste covering the aggregate to be exposed by an approved method. Do not loosen the aggregate by the grout removal operation. Maintain required curing on all surfaces except for the time while the aggregate is being exposed. Cure using wet mats or membrane after the aggregate is exposed.

Repair defective areas as determined by the Engineer.

Re-clean exposed aggregate surfaces by an approved method. Apply a coat of clear Type II permanent anti-graffiti coating to cleaned exposed aggregate surface. Apply anti-graffiti coatings by spray, roller, or brush at the application rates recommended by the manufacturer and in accordance with Item 740, "Graffiti Removal and Anti-Graffiti Coating."

Figure E.1 Surface Finish Notes Referenced By Engineering Drawings

Appendix F. Value of Research (VoR)

In evaluating the value of research for this project, four qualitative benefits were identified, as shown in the table below and briefly described thereafter.

Benefit	Qualitative	Economic	Both	TxDOT	State	Both
Contribution to knowledge	✓			✓		
Improvement on engineering design	✓					✓
Cost-effectiveness	✓				✓	
Safety of structure	✓					✓

Contribution to Knowledge

This project contributed significantly to the body of knowledge regarding the use of ultra-high-performance concrete (UHPC) in bridge closure pours. Significant knowledge was gained and documented regarding materials and durability-related properties in the lab and on outdoor exposure sites. Large-scale structural testing was performed, and recommendations were made regarding the application of UHPC in closure pours. A particularly important contribution to knowledge involves the testing of UHPC closure pour/deck systems at early ages (24 hours), whereas most testing to date has been done on concrete at later ages. Lastly, long-term monitoring of closure pours has generated considerable data on strains within the closure pours, as well as visual crack surveys over the course of two years.

Improvement on Engineering Design

This project has contributed to the improvement of engineering design by validating and confirming the requisite UHPC properties and structural detailing requirements for UHPC closure pours, including guidance on early opening requirements. UHPC properties and test methods were recommended that can serve as the basis for future closure pours using UHPC or similar materials. Important information and guidance were also generated relative to UHPC placement properties and surface preparation requirements.

Cost-Effectiveness

Although not directly evaluated in this project, it is expected that when UHPC is used in closure pours in accelerated bridge construction (ABC) applications, significant cost savings may be realized. Cost savings could be derived from several aspects, including increased construction speed, reduced driver impact, improved long-term durability, and increased service life.

Safety of Structure

The use of UHPC in closure pours can improve the safety of structure by reducing the construction time (and hence the potential for construction-related incidents and accidents), by reducing the need for on-site superstructure construction (since precast elements are cast off site and erected prior to closure pour placement), and by enhancing the long-term structural performance and service life.